Aus dem Fachbereich Medizin
der Johann Wolfgang Goethe-Universität
Frankfurt am Main

betreut am
Zentrum der Pharmakologie
Institut für Allgemeine Pharmakologie und Toxikologie
Direktor: Prof. Dr. Josef M. Pfeilschifter

Elucidating the Role of the XCL1/XCR1 Chemokine Axis in Type 1 Diabetes Pathogenesis: Implications for Novel Therapeutic Interventions

Dissertation
zur Erlangung des Doktorgrades der theoretischen Medizin
des Fachbereichs Medizin
der Johann Wolfgang Goethe-Universität
Frankfurt am Main

vorgelegt von
Camilla Tondello

aus Padova, Italien

Frankfurt am Main, 2023

Aus dem Fachbereich Medizin

der Johann Wolfgang Goethe-Universität
Frankfurt am Main

betreut am
Zentrum der Pharmakologie
Institut für Allgemeine Pharmakologie und Toxikologie
Direktor: Prof. Dr. Josef M. Pfeilschifter

Elucidating the Role of the XCL1/XCR1 Chemokine Axis in Type 1 Diabetes Pathogenesis: Implications for Novel Therapeutic Interventions

Dissertation
zur Erlangung des Doktorgrades der theoretischen Medizin
des Fachbereichs Medizin
der Johann Wolfgang Goethe-Universität
Frankfurt am Main

vorgelegt von
Camilla Tondello

aus Padova, Italien

Frankfurt am Main, 2023

Dekan:	Prof. Dr. Stefan Zeuzem
Referent:	Prof. Dr. Urs Christen
Korreferent/in:	Prof. Dr. Dr. Gerd Geißlinger
Tag der mündlichen Prüfung:	01.03.2024

Parts of this project were submitted in:

The XCL1/XCR1 axis is activated in patients with type 1 diabetes and its disruption tips the T cell balance and ablates β-cell damage in a mouse model

Camilla Tondello, Christine Bender, Deborah Puppe, Elisa M. Blickberndt, Gregory J. Golden, Monika Bayer, Giulia Buchmann, Josef M. Pfeilschifter, Malte Bachmann, Edith Hintermann, Ralf P. Brandes, Michael R. Betts, Richard A. Kroczek, and Urs Christen

Submitted

Gene-expression profiling of laser-dissected islets and subsequent studies in deficient mice reveal a differential role of chemokines as a driving force of β-cell destruction during type 1 diabetes

Christine Bender[*], Peter Müller[*], Camilla Tondello[*], Jessica Horn, Martin Holdener, Stanley Lasch, Monika Bayer, Josef M. Pfeilschifter, Edith Hintermann, Frank Tacke, Andreas Ludwig, Martin-Leo Hansmann, Claudia Döring, and Urs Christen

Submitted

Table of Contents

I. List of abbreviation

Aab	Autoantibodies
AP	Alkaline phosphatase
APC	Antigen-presenting cell
ATAC	Activation-induced, T cell-derived, and chemokine-related cytokine
ATG	Anti-thymocyte globulin
BATF3	Basic transcription factor 3
BDCA-2	Blood dendritic cell antigen-2
BG	Blood glucose
BSA	Bovine serum albumin
C1	Channel 1
C2	Channel 2
CD	Cluster of differentiation
cDC	Conventional dendritic cells
cDC1	Conventional dendritic cells type 1
cDC2	Conventional dendritic cells type 2
CFSE	Carboxyfluorescein succinimidyl ester
CLEC9A	C-type lectin domain family 9 member A
C-pep.	C-peptide
CTL	Cytotoxic T lymphocyte
CTLA-4	Cytotoxic T-lymphocyte antigen 4
CYP	Cytochrome P
DAB	3,3′-Diaminobenzidine
DAPI	4′,6-Diamidino-2-Phenylindole
DBE	Dibenzyl ether
DC	Dendritic cell
DCM	Dichloromethane
DMSO	Dimethyl sulfoxide
EtOH	Ethanol
FACS	Fluorescence-activated cell sorting
FCS	Foetal Calf Serum
FDA	Food and Drug Administration

Flt-3L	FMS-like tyrosine kinase 3 ligand
FoxP3	Forkhead box protein 3
GAD65	Glutamic acid decarboxylase 65
GP	Glycoprotein
GrB	Granzyme B
HbA_{1C}	Glycated haemoglobin
HIRN	Human Islet Research Network
HLA	Human leukocytes antigen
HPAP	Human Pancreas Analysis Program
HRP	Horseradish peroxidase
i.p.	Intraperitoneal
i.v.	Intravenous
IA-2A	Insulinoma antigen-2 autoantibody
IAA	Insulin autoantibody
ICA	Islet cell autoantibody
ICCS	Intracellular cytokines staining
ID2	DNA-binding protein inhibitor 2
IDDM	Insulin-dependent diabetes mellitus
IFNγ	Interferon γ
IHC	Immunohistochemistry
IL	Interleukin
IL-1RA	Interleukin-1 receptor antagonist
IL-2RA	Interleukin-2 receptor antagonist
IP10	Interferon γ-induced protein 10 kDa
IRF	Interferon regulatory factor
IS	Immunological synapse
iTreg	Induced Treg
KLRG1	Killer-cell lectin like receptor G1
LC	Langerhans cells
LCMV	Lymphocytic choriomeningitis virus
LFA-1	Lymphocyte function-associated antigen 1
LYP	Lymphoid protein-tyrosine phosphatase
mDC	Monocyte derived DC
MeOH	Methanol

MHC	Major histocompatibility complex
mTEC	Thymic medullary epithelial cells
ND	Non-diabetic
NFIL3	Nuclear factor, interleukin 3 regulated
NK	Natural killer
NOD mouse	Non-obese diabetic mouse
nTreg	Natural Treg
P/S	Penicillin/Streptomycin
PBS	Phosphate buffered saline
PD-1	Programmed cell death protein-1
PDCA-1	Plasmacytoid dendritic cell antigen-1
PDLN	Pancreatic draining lymph nodes
Perf	Perforin
PFA	Paraformaldehyde
Pfu	Plaque forming units
PLP	PFA, Lysine, Periodate
PTPN22	Protein tyrosine phosphatase non-receptor type 22
PTwH	PBS/0.2% Tween-x with Heparin
RANTES	Regulated on activation, normal T cell expressed and secreted
RIP	Rat insulin promoter
RORγt	RAR-related orphan receptor gamma isoform t
RT	Room temperature
SCM-1	Single C motif-1
Sirpα	Signal regulatory protein α
STAT	Signal transducer and activator of transcription
T1D	Type 1 diabetes
TAE	Tris Acetate EDTA
T-bet	T-box expressed in T cells
Tc	T cytotoxic
TCR	T cell receptor
TGFβ	Transforming growth factor β
Th	T helper
TLR	Toll-like receptor

TNFα	Tumour necrosis factor α
TRAF6	Tumour necrosis factor receptor-associated factor 6
Treg	Regulatory T cells
XCL1	XC ligand 1
XCR1	XC receptor 1
ZnT8A	Zinc transporter 8 autoantibody

II. List of figures

III. List of tables

1. Summary

Type 1 diabetes (T1D) is an autoimmune disease that results from the progressive destruction of the β-cells in the islets of Langerhans. Even though the anti-CD3 antibody Teplizumab has recently been approved by the Food and Drug Administration (FDA), a cure for this disease has not been identified and new targets need to be found. Therefore, a laser dissection of the islet microenvironment during T1D was performed in our lab and the gene expression was analysed through gene array and qPCR, using the RIP-LCMV-GP mouse model. These mice express the glycoprotein (GP) of the lymphocytic choriomeningitis virus (LCMV) under the control of rat insulin promoter (RIP) and develop T1D only after being infected with LCMV. The results of the gene array showed that most chemokine ligand/receptor pairs are upregulated upon infection and some are maintained upregulated until the chronic phase of the disease. First, I further studied the expression of CXCL10/CXCR3, CCL5/CCR5, CXCL16/CCR6, and CX_3CL1/CX_3CR1 on T1D. CXCL10 was shown to play an important role in T1D pathogenesis. Both anti-CXCL10 antibody and CXCR3-antagonist were successfully used in combination with anti-CD3 antibody in two mouse models for T1D, with a better outcome than only anti-CD3. Our study confirmed that the CXCL10/CXCR3 axis is important in T1D and that CXCL10 is produced by β-cells and by islet infiltrating cells, as visible in both RNAscope *in situ* hybridization and immunohistochemistry (IHC). Although other chemokine axes, such as CCL5/CCR5, CXCL16/CCR6, CX_3CL1/CX_3CR1, and XCL1/XCR1 have also been found to be upregulated acutely and/or chronically, only some of them had an impact on T1D pathogenesis. We demonstrated that CCL5-deficiency does not impair T1D development, but in contrast deficiencies of either CXCR6 or CX_3CR1 leads to a reduced T1D progress.

The main focus of my thesis was however the XCL1/XCR1 chemokine axis. Both XCL1 and XCR1 were found persistently upregulated in diabetic RIP-GP mice. XCL1 is also elevated in the serum of T1D patients. XCL1 is a chemokine produced by CD8 and CD4 T cells, natural killer (NK), and NKT cells. Its receptor XCR1 is only expressed by resident and migratory conventional dendritic cells type 1 (cDC1). Such cDC1 are the most efficient cells in priming CD8 T cells. In my thesis, I first demonstrated with RNAscope duplex staining that XCL1 and

XCR1 expression is upregulated in the islets of RIP-GP mice upon infection and of non-obese diabetic (NOD) mice at different age and disease stage. Moreover, I showed that XCR1 is expressed in the islets of autoantibody-positive and T1D patients, underlying the possible involvement of the XCL1/XCR1 axis in T1D pathogenesis in humans. Therefore, I further investigated the role of this axis using first XCL1-deficient mice, in which the cDC1 migration to the islets is reduced as shown with IHC staining and with flow-cytometric analysis. The latter showed also a reduction of T cells, and in particular of islet autoantigen-specific T cells among the islet infiltrating cells. To investigate XCR1-deficiency, I used RIP-GP x XCR1$^{Venus/Venus}$ mice. Since these mice express the fluorescent Venus protein instead of XCR1, an immunofluorescent staining allowed to directly visualize the cDC1, that migrate to the islets even in absence of XCR1. In addition, I was able to demonstrate by flow cytometric analysis that migrated cDC1 lose their ability of priming T cells and therefore, the autoaggressive T cells get less activated. Interestingly, in both mouse lines, an increase of Treg cell frequencies among the islet infiltrating cells was visible and this, together with a reduction of autoaggressive T cells, corresponded to a shift in the immune balance towards a regulatory milieu. Most importantly, both XCL1- and XCR1-deficient mice showed a significantly reduced T1D incidence in comparison to regular RIP-GP mice. This corresponded to more intact islets as visible in pancreas sections stained for insulin. Moreover, a whole pancreas 3D-staining with anti-insulin antibody confirmed that in both XCL1- and XCR1-deficient mice the remaining insulin content after 8-12 weeks post-infection is still sufficient to maintain normoglycaemia. In conclusion, the XCL1/XCR1 axis plays an important role in the pathogenesis of T1D and might therefore be a promising target for T1D immunomodulation. A small molecule or an antibody to interfere with this axis needs to be tested alone or in a combination therapy.

2. Zusammenfassung

Typ-1-Diabetes (T1D) ist eine Autoimmunerkrankung, die durch die Zerstörung der Insulin-produzierenden β-Zellen in den Langerhans-Inseln entsteht. Obwohl der Anti-CD3-Antikörper Teplizumab vor kurzem von der Food and Drug Administration (FDA) zugelassen wurde, gibt es noch keine Heilung für diese Krankheit und es müssen neue Angriffspunkte gefunden werden. Deshalb wurde in unserem Labor die Mikroumgebung der Inselzellen mit Hilfe eines Lasers seziert und die Genexpression mittels Genarray und qPCR analysiert. Als Modell wurden RIP-LCMV-GP Mäuse verwendet, welche das Glykoprotein (GP) des lymphozytären Choriomeningitis-Virus (LCMV) unter der Kontrolle des Ratteninsulin-Promotors (RIP) exprimieren und erst nach einer Infektion mit LCMV einen T1D entwickeln. Die Ergebnisse zeigten, dass die meisten Chemokin-Liganden/Rezeptor-Paare bei der Infektion hochreguliert werden und einige bis in die chronische Phase der Krankheit hochreguliert bleiben. Zunächst habe ich die Expression verschiedener Chemokin-Achsen weiter untersucht. Durch RNAscope-in-situ-Hybridisierung als auch Immunhistochemie (IHC) konnte ich zeigen, dass CXCL10 von β-Zellen und inselinfiltrierenden Zellen produziert wird. Weiter zeigte sich, dass CXCL10 eine wichtige Rolle bei der T1D Pathogenese spielt, da eine Therapie mit einem Anti-CXCL10-Antikörper als auch einem CXCR3-Antagonisten vor allem in Kombination mit einem Anti-CD3-Antikörper in zwei Mausmodellen erfolgreich T1D vermindern konnte. Ich konnte auch die akut und/oder chronisch Expression anderer Chemokin-Achsen wie CCL5/CCR5, CXCL16/CCR6, CX_3CL1/CX_3CR1 und XCL1/XCR1 im Pankreas *in situ* bestätigen, allerdings hatten nicht alle einen Einfluss auf die T1D-Pathogenese. So beeinträchtigt ein CCL5-Mangel die Entwicklung von T1D nicht, aber im Gegensatz dazu führt ein Mangel an CXCR6 oder CX3CR1 zu einem geringeren Fortschreiten des T1D.

Das Hauptaugenmerk meiner Arbeit lag jedoch auf der XCL1/XCR1-Chemokin-Achse. Sowohl XCL1 als auch XCR1 sind bei Infektionen anhaltend hochreguliert. So ist XCL1 auch im Serum von T1D-Patienten erhöht. XCL1 ist ein Chemokin, das von CD8- und CD4-T-Zellen, natürlichen Killerzellen (NK) und NKT-Zellen produziert wird. Sein Rezeptor XCR1 wird dagegen nur von residenten und wandernden konventionellen dendritischen Zellen vom Typ 1

(cDC1) exprimiert. Diese cDC1 sind die effizientesten Primer von CD8-T-Zellen. In meiner Dissertation habe ich zuerst mit RNAscope-Duplex-Färbung gezeigt, dass die Expression von XCL1 und XCR1 in den Inseln von RIP-GP und NOD-Mäusen in verschiedenen Stufen der Pathogenese hochreguliert ist. Außerdem konnte ich zeigen, dass XCR1 in den Inseln von Autoantikörper-positiven Personen und T1D-Patienten exprimiert ist, was auf eine mögliche Beteiligung der XCL1/XCR1-Achse an der T1D-Pathogenese beim Menschen hindeutet. Daher habe ich die Rolle dieser Achse weiter untersucht, indem ich zunächst XCL1-defiziente Mäuse verwendete. Durch IHC-Färbung und durchflusszytometrische Analyse konnte ich zeigen, dass bei solchen Mäusen die cDC1-Migration zu den Inseln reduziert ist. Zusätzlich konnte ich auch eine Verringerung der T-Zellen und insbesondere der Inselautoantigen-spezifischen T-Zellen in den Inseln zeigen. Weiter habe ich RIP-GP x XCR1$^{Venus/Venus}$-Mäuse verwendet, welche das fluoreszierende Venus-Protein anstelle von XCR1 exprimieren. So konnten mit einer Immunfluoreszenzfärbung die cDC1 direkt sichtbar gemacht werden. Trotzdem konnten cDC1 auch ohne XCR1 zu den Inseln wandern, aber eine durchflusszytometrische Analyse hat ergeben, dass die eingewanderten cDC1 ihre Fähigkeit verlieren, T-Zellen effektiv zu primen. Interessanterweise war in beiden knock-out Mauslinien ein Anstieg der Treg-Zell-Frequenzen zu beobachten. Zusammen mit der Verringerung der autoaggressiven T-Zellen führt dies zu einer Verschiebung des Immungleichgewichts in Richtung eines regulatorischen Milieus. Dies hatte zur Folge, dass tatsächlich sowohl XCL1- als auch XCR1-defiziente Mäuse im Vergleich zu regulären RIP-GP-Mäusen eine deutlich geringere T1D-Inzidenz aufwiesen. Dies konnte ich auch mittels IHC von Pankreasschnitten, welche noch intakte Inseln aufwiesen, belegen. Darüber hinaus bestätigte eine 3D-Färbung des gesamten Pankreas mit einem Anti-Insulin-Antikörper, dass sowohl bei XCL1- als auch bei XCR1-defizienten Mäusen das verbleibende β-Zell Volumen nach 8-12 Wochen nach der Infektion noch ausreicht, um eine Normoglykämie aufrechtzuerhalten. Zusammenfassend lässt sich sagen, dass die XCL1/XCR1-Achse eine wichtige Rolle bei der Pathogenese von T1D spielt und daher ein vielversprechendes Ziel für deine Immunmodulation von T1D sein könnte. Ein kleines Molekül oder ein Antikörper, der in diese Achse eingreift, sollte allein oder in einer Kombinationstherapie getestet werden.

3. Introduction

3.1 Autoimmunity

The immune system can distinguish between self- and non-self-components. In a physiological state, the lymphocytes that are generated in the bone marrow migrate to the thymus where they go through a process of negative and positive selection, called central tolerance. If they are considered to be self-reactive, they get a negative signal that leads to their death or inactivation. Otherwise, they reach the secondary lymphoid organs where they are further controlled by peripheral tolerance mechanisms: in case of self-reactivity, they can be made anergic or suppressed by regulatory T cells.[1] In case one or more of these checkpoints fail, lymphocytes start to react against one or more organs and this leads to the outbreak of autoimmune diseases.

Nowadays, nearly 100 different autoimmune diseases have been identified and they affect at least 5% of the population, with type 1 diabetes (T1D), rheumatoid arthritis, and autoimmune thyroiditis being among the most common.[1,2] Autoimmune diseases differ for severity, involved tissues, and mechanisms. They are classified according to their target: some are organ-specific and therefore specific for only one organ, for example the central nervous system in multiple sclerosis and the pancreas in type 1 diabetes; and some are systemic, affecting many tissues, for example systemic lupus erythematosus and rheumatoid arthritis. Another way to classify them is to focus on the main cell population involved in their pathogenesis, either B cells or effector T cells.[2]

The causes of these diseases have not been fully understood yet. The breakdown of central tolerance does not derive only from a failure of the immune system but several factors contribute to the onset of autoimmunity. Among these factors, several studies have underlined the importance of a genetic predisposition, involving mainly the Human Leukocytes Antigen (HLA) gene. Moreover, also environmental factors can play a role in the pathogenesis of these diseases. For instance, low levels of vitamin D seem to be correlated with an augmented risk of developing an autoimmune disease. Infections can also rise the probability of autoimmune development with a mechanism called “molecular mimicry”: the immune system starts to react against the pathogen epitope and then cross-

reacts with a very similar self-molecule, breaking the tolerance. Some other factors which can play a role in the development of an autoimmune disease are diet, microbiome, stress, smoking, and exposure to pollution.[1–3]

3.2 Diabetes

Diabetes affects 537 million people worldwide.[4] Diabetes is a group of metabolic disorders characterized by loss of β-cell function and/or mass that leads to hyperglycaemia.[5,6] As a matter of fact, the pancreas consists of an endocrine and an exocrine part. In case of diabetes, the endocrine function is affected. The endocrine part is composed by millions of islets of Langerhans. Each of these islets contains α-cells which produce glucagon, β-cells that secrete insulin, and δ-cells for somatostatin generation. The main function of the islets of Langerhans is to regulate the blood glucose (BG) homeostasis reacting to the physiological changes, given by the food uptake but also external factors like stress. [7]

When the β-cell function is reduced like in diabetes, insulin secretion is altered and hyperglycaemia is the immediate consequence. Therefore, diabetes is diagnosed when the fasting BG level is higher than 7 mmol/l (126 mg/dl) and BG is more than 11.1 mmol/l (200 mg/dl) at any time. Another parameter is the glycated haemoglobin (HbA_{1C}), that is pathologic at concentrations higher than 6.5%. HbA_{1C} gives information about the mean BG concentration in the previous three months.[8] The main symptoms of the disease are polyuria, polydipsia, weight loss, polyphagia, and blurred vision. Diabetes can have long-term complications on a microvascular level such as nephropathy, retinopathy, neuropathy, and on a macrovascular level in case of cardiovascular diseases.[9,10]

Diabetes is divided in subtypes. T1D is an autoimmune disease which results from the progressive destruction of the β-cells in the islets of Langerhans. Usually, the first symptoms start during childhood or adolescence and patients need daily injections of insulin to survive, since there is yet no cure available. Type 2 diabetes is the most predominant form (75-80% of the cases) and it is caused by insulin resistance and inadequate compensatory response of insulin secretion. In this case, the risk is increased by age, obesity, and lack of physical activity. People affected by this form of diabetes do not need insulin treatment,

but some antidiabetic oral drugs are available to maintain their BG concentration under control.[11]

3.3 Type 1 diabetes

Type 1 diabetes affects 10% of all the patients with diabetes.[12] It is also called insulin-dependent diabetes mellitus (IDDM) and it is divided in two subgroups: type 1A, the autoimmune form, which represents the 70-90% of the cases and type 1B, an idiopathic form.[13] Type 1A diabetes (T1D) is an organ-specific autoimmune disease, characterized by the destruction of the β-cells in the islets of Langerhans performed by autoreactive T cells, which leads to a reduced insulin production.[6,13] T1D is divided in three main stages: at stage 1 two or more islet cell autoantibodies (ICA) are present in the blood, but the glycaemia values are still normal; at stage 2 the glucose intolerance starts, and at stage 3 the clinical manifestation with all the signs and symptoms appear.[9,14]

The precise immunologic events which start the process are not completely understood. A failure of the immune system causes the infiltration of dendritic cells in the islets of Langerhans. At the same time or immediately after, T cells start to migrate to the islets (peri-insulitis). This causes the expansion of autoreactive CD4 and CD8 T cells, the production of autoantibodies by the B cells, and the following activation of the innate immune system. Other cells are then involved in the inflammation process like natural killer (NK) cells and monocytes. CD8 T cells with the release of cytolytic granules containing perforin and granzyme B and with Fas/Fas ligand dependent interactions inducing apoptosis cause the destruction of the β-cells.[10,11,13]

T1D signs appear only when approximately 80% of the β-cells are destroyed. Before this point, the patients undergo a pre-diabetes/subclinical phase in which they have one to three ICA. The ICA do not seem to have a direct role in the disease but they are important markers to predict diabetes development, especially in children. Autoantibodies in T1D are predominantly directed against insulin (IAA), glutamic acid decarboxylase 65 (GAD65, GADA), insulinoma antigen 2 (IA-2A), and zinc transporter 8 (ZnT8A).[15–17]

Besides the screening for autoantibodies to try to predict T1D also the genome can be screened for risk factors, since T1D is correlated with several genetic

predispositions. In particular, T1D has a strong correlation with the HLA gene on chromosome 6p21. Some haplotypes of the HLA class II gene strongly increase the risk of developing T1D such as the DR3/4-DQ8 heterozygous haplotype (DR3 is DRB1*03-DQB1*0201, DR4 is DRB1*04-DQB1*0302, DQ8 is DQA1*0301, DQB1*0302); whereas some others can be protective against T1D, like the DRB1*1501-DQA1*0102-DQB1*0602 haplotype. Other genes that have been correlated with an increased risk of developing T1D are: the insulin gene on chromosome 11p5.5, cytotoxic T-lymphocyte antigen 4 (CTLA-4) gene on chromosome 2p33, protein tyrosine phosphatase non-receptor type 22 (PTPN22) gene which encodes the lymphoid protein-tyrosine phosphatase (LYP), and the interleukin (IL)-2 receptor-α gene (IL2RA).[11,18]

Genetic predisposition alone is not enough to start autoimmunity. Therefore, some external factors have been considered as triggers for this disease that might also explain the huge geographical variation. Among these factors, viral infections have been extensively studied. Viruses can induce anti-viral responses in several ways, for example expressing proteins which stimulate particular subtypes of T cells, upregulating pro-inflammatory cytokines, breaking self-tolerance and starting an epitope spreading process, or by molecular mimicry of host structures. The principal viral candidates are enteroviruses, in particular coxsackievirus and rotavirus, that have been correlated to T1D. However, there is still a controversial debate if they indeed start the disease, rather accelerate its course, or are just present by coincidence.[3,19,20]

Other environmental factors which have been associated with an increased risk of developing T1D are diet of the infants, toxins (N-nitroso derivatives), low levels of vitamin D, vaccine administration, and stress.[10,21]

3.4 T1D therapies

Patients with T1D are treated with daily subcutaneous injections of endogenous insulin to maintain glucose homeostasis. In 1922 the administration of insulin was life-changing for people diagnosed with T1D. Over the years, the treatment has been optimized: the dose of insulin has been increased, the pharmacokinetics improved, and the number of administrations decreased. Another important step was the switch from the isolation from animals to bacterial insulin cloning, which

allowed a scale up in the production. Nowadays, pumps are used to deliver insulin with an automatic dosing based on continuous glucose reading through a sensor.[22] Not only patients constantly need to be careful about hyperglycaemia, but the problem of insulin administration is also hypoglycaemia, especially the unawareness of a hypoglycaemic event. In this case, patients show symptoms like dizziness, fast heart beating, shaking, and can have short term problems or even mild cognitive impairments.

Whole pancreas transplantation followed by life-long immunosuppression is used in case of severe hypoglycaemia unawareness, of recurrent ketoacidosis, or of simultaneous kidney transplantation, but it can induce alloimmunity and autoimmunity can be evoked again because of the presence of memory T cells. Moreover, donors are limited.[10,12] Therefore, isolated pancreatic islet transplantation is also used with success with the application of the 'Edmonton protocol', introduced by Shapiro et al.[23] After islet transplantation, patients have at least one year of independence by insulin and their production of endogenous insulin is restored.[23] In this case, again, the therapy cannot be applied to many patients. Another approach is to induce pluripotent stem cell-derived β-cells, but the process cannot be performed in large scale and these cells are currently not able to restore also the α-cell function.[24]

Several studies and different approaches have been performed in the last three decades to try to find a cure which blocks the disease status, expand the regulatory T cell (Treg) subset, or succeed in regeneration of β-cell mass.[11]

The first drug which has been tested was Cyclosporine A in the 1980s. It inhibits calcineurin, which is involved in IL-2 transcription and is able to reduce the number of effector T cells and, at the same time, to increase the regulatory T (Treg) cells. The administration of this drug was however very dangerous for the patients, because it increased the risk for cancer and caused severe nephrotoxicity.[25,26]

Anti-thymocyte globulin (ATG) is also studied for its ability to suppress T cells and their precursors in the thymus. It is used in case of acute rejection of organ transplantation. In T1D, it was tested with prednisone, giving some positive results but the general immunosuppression derived from the treatment was too high.[13,27]

Another approach is to try to hit B cells: anti-CD20 antibody (Rituximab) was administrated to T1D patients even if B cells seem not to be implicated in the disease pathogenesis. The efficacy was limited and the effects did not last long.[28]
The attention has also been paid to costimulatory molecules such as CTLA-4. Abatacept is a CTLA-4-immoglobulin that interferes with the co-stimulation of the T cells via cluster of differentiation (CD) 28 and B7 interaction and it is used to treat patients with psoriasis or rheumatoid arthritis. It does not reduce effector T cells but can act on the Treg cell number. This however did not give promising results.[29–31]
Several cytokines have also been examined as targets. For example, interleukin-1 receptor antagonist (IL-1RA) was used in mice and reduced T1D incidence. Further, anti-tumor necrosis factor α (TNFα) therapy improved the insulin production, reducing the need for insulin; treatment with IL-2 increased Treg cell repertoire and decreased T1D incidence in mice, but not in humans.[11,32]
Cell-based therapy is also studied: phase I trial of isolated Treg cell infusion gave promising results, as well as the phase I trial with administration of autologous tolerogenic dendritic cells.[33,34]
Another idea was an antigen-based immunotherapy with administration of T1D antigens, for example oral and intranasal insulin, but the response was not successful, or GAD65 formulated with alum but the phase III trial results were not promising.[35,36]

3.4.1 Teplizumab

Since the main players of T1D are T cells, one of the main approaches in the research for T1D cure is to act against them. Therefore, a murine anti-CD3 antibody, OKT3, was studied. OKT3 was first approved as drug for acute graft rejection in 1985 by Food and Drug Administration (FDA). OKT3 is studied in T1D since 1993, as it showed remission of T1D in non-obese diabetic (NOD) mice: the effect was long-lasting, the T cell depletion was partial and transient, and the clinical remission was maintained.[37] However, OKT3 showed two main side effects: an important cytokine release syndrome soon after the first injection and immunogenicity with the insurgence of antibodies against OKT3 itself.[38,39]
Therefore, two humanized monoclonal antibodies without Fc region started to be

studied: Teplizumab, hOKT3y1(Ala/Ala), and Otelizumab, ChAglyCD3. Otelizumab reached phase III clinical trial. It can slow down the loss of functionality of β-cells in recent onset T1D patients but it has still side effects, like increased Epstein Barr virus reactivation in treated patients.[40,41]

Teplizumab is the first drug approved for T1D by the FDA in the United States in November 2022. Teplizumab (TZIELD™) is indicated for patients older than 8 years old with stage 2 T1D, meaning with two or more autoantibodies, dysglyceamia and no type 2 diabetes. The treatment consists in daily intravenous injections for 14 days.[42] Teplizumab binds to CD3 on CD4 and CD8 T cells and afterwards, the CD3/TCR complex is internalized. This has two effects: the direct action on effector T cells, reducing their number and their activation, and the induction of an immunomodulatory effect, through which Treg cells are expanded via transforming growth factor β (TGFβ).[42–44] This ensues a preserved β-cell functionality and a reduced need for insulin for at least two years after the treatment.[45,46] The problem is that some patients do not respond to the therapy. In contrast to the responders, the non-responders are usually individuals with a late disease onset and a sub-optimal glycaemic control at the beginning of the treatment.[27,45]

The approval of Teplizumab is only a starting point and since it showed to delay the onset of T1D, it also offers opportunities for combination therapies. For example, it has been tested in combination with anti-CXCL10 antibody in two mouse models and in both cases, the incidence of remission was higher with the combination therapy rather than with only Teplizumab.[47] In the same direction went the combination study of an antagonist for CXCR3 with Teplizumab, that showed an improved outcome in two different mouse models.[48] Moreover, a combination therapy with anti-CD3 and anti-CD20 antibodies was tested in NOD mice: diabetes was prevented and reverted with a Treg subset expansion.[49] Anti-CD3 was also tested in combination with antigen administration: for example both with the exedin-4, that mimes glucagon-like peptide 1 (GLP-1), and with nasal insulin the percentage of mice in remission was increased.[50,51]

Thus, there is still need for novel therapies focusing on new targets for immunotherapies, which can be used alone or in combination with anti-CD3. One group of target molecules are chemokines and their receptors that are orchestrating the migration of immune cells to the site of inflammation.

Chemokine receptors can be neutralized with antibodies and modified chemokines or small molecules can be used as antagonists.[52] Some elements which need to be considered in a chemokine therapy are type of administration and timing.[53] Moreover, another problem is the redundancy of the immune system: the blockade of one chemokine axis might have a small impact on the general immune system.[54] Therefore the target validation is critical and in this context the use of knock mice is important.[52]

3.5 Chemokines

Chemokines are small molecules characterized by a molecular weight usually between 8 and 12 kDa and are secreted by different cell types, like immune cells, endothelial cells, and cells involved in the immune response.[55] More than 50 different chemokines have been identified until now and they have been classified according to their structure. They are related by a conserved motif of four cysteine residues at the amino terminus. According to this, four different classes have been identified: CC chemokines with two consecutive cysteines at the N-terminus, for example CCL5 (or RANTES, regulated on activation, normal T cell expressed and secreted); CXC, which have the two cysteines separated by one amino acid, for example CXCL10 (or IP10, interferon gamma-induced protein 10); CX_3C, that is composed only by CX_3CL1 (or fraktaline), a chemokine with a domain fused with mucin-like branch; and C chemokine family, whose only representatives are XCL1 and XCL2, that lack 2 out of 4 cysteine residues.[56,57]
Chemokines are a subgroup of cytokines which act as chemoattractants. They attract leukocytes from the bloodstream to the site of inflammation in the so-called ‘leukocyte homing’ process. The chemokines direct the leukocyte migration by forming a gradient via binding to the glycosaminoglycans on the endothelium of the vessels. Once bound, they are not washed away by the bloodstream and they can interact with their receptors on the leukocytes. The leukocytes in the meantime start to slow down and roll along the vessel whereby the chemokine ligand-receptor interaction results in the expression of integrins at the surface of the leukocytes. In this way, the leukocytes can extravasate into the inflamed tissue.[58,59]

Chemokines are the first players of the innate immunity. They attract neutrophils, monocytes, NK cells, and immature dendritic cells. These cells then release further chemokines to attract T cells.[58] Chemokines also play an important role in T cell development, differentiation, and migration to secondary lymphoid organs. They can be involved in angiogenesis, fibrosis, proliferation, and apoptosis.[59,60]
According to their function, chemokines can be classified either as constitutive or homeostatic, or as inducible. Homeostatic chemokines, like CXCL12, are produced in healthy conditions in lymphoid organs to maintain the physiological traffic of the cells. Inducible chemokines, like CCL5 and CXCL10, are produced during acute and/or chronic inflammation in the target organ by both resident and infiltrating cells. There are also chemokines which might act in both states, called dual-function chemokines.[52,58,61]
Chemokine receptors are classified according to chemokines that bind to them (CCR, CXCR, and so on).[62] Currently there are more than 20 identified receptors and they can recognize several chemokines belonging to the same family. At the same time, many chemokines can bind to several receptors.[56,61] These receptors are seven-transmembrane structures coupled to G-proteins. They are composed by one chain which has three extracellular and three intracellular loops. The external amino-terminal region binds the ligand and the more conserved internal carboxy domain transfers the signal to the cell.[57,59] The signalling cascade leads to an increase of calcium concentration in the cell and to a following activation of protein kinases. The cell undergoes then processes of rearrangement, change of shape, and cytokine production.[57]

3.6 Chemokines in T1D

Chemokines play an important role during the infiltration process by immune cells in the islets of Langerhans.[54] T1D is a disease driven by interferon γ (IFNγ) production and many chemokines are produced after cell stimulation by this cytokine. T cells get activated in the pancreatic draining lymph nodes (PDLN) and then they extravasate to the islets where the inflammation increases and therefore, more chemokines are produced.[63] For example, CCL2 and CCL5 are involved in the recruitment of monocytes, dendritic cells, and mononuclear cells;

CCL19, CCL21, CXCL9, CXCL10, and CXCL11 recruit T cells in the lymph nodes; and CXCL13 plays a role in the recruitment of B cells.[63]

In the process, T cells become polarized according to the cytokines they get stimulated by. CD4 T cells can be distinguished in T helper 1 (Th1), Th2, Th17 and Treg cells (see paragraph 3.8). It has been shown in mice that an imbalance between a Th1 and a Th2 response can accelerate the disease. Th1 cells are pro-diabetic and destroy the β-cells, whereas Th2 cells have a more regulatory function and produce suppressive factors when they are stimulated by the antigen. The shift towards a Th1 response is necessary to start the disease. This has been shown in the RIP-LCMV-GP mouse model (see paragraph 3.9). After the infection, the resident antigen-presenting cells (APC) start to produce IFNγ and TNFα. This induces the β-cells and the endothelium to produce Th1 chemokines, such as CXCL10. At the same time, CXCR3 is upregulated on CD8 T cells. In parallel with the virus elimination, the activation of auto-aggressive CD4 and CD8T cells leads to the destruction of the β-cells.[53] β-cells themselves can produce CXCL10 and CXCL9 and attract CXCR3+ cells to the islets. These CXCR3+ cells are cytotoxic T cells that produce IFNγ.[62,64] CXCL10 appeared elevated in the serum of children which were newly diagnosed with T1D but after 16 months from the first observation, these levels decreased.[65]

Several studies have also been carried out on humans: in 2010, Chatzigeorgiou et al. found out that CCL2, CCL3, CCL4, and CCL5 are elevated in the serum of T1D patients and they could correlate this increase with the stage of the disease. In particular, the Th1 response and the CCL2 production were higher at the diagnosis than in the chronic stage.[66] Also Pan et al. saw an increase of CCL5 in the serum of T1D patients and could associate it with an increase of CCR5 in the islets.[67]

Studies have shown that mouse and human islets stimulated with IFNγ or TNFα produce high levels of CCL1, CCL4, CCL5, CXCL10, CX_3CL1, and XCL1.[54,68,69]

It seems that also the CXCR6/CXCL16 axis might play an important role since CXCR6 is located in the IDDM22 T1D risk locus in human and CXCL16 is expressed by dendritic cells (DC).[63]

3.6.1 XCL1 and its receptor XCR1

XCL1, also called lymphotactin or activation-induced T cell-derived and chemokine related molecule (ATAC) or single C mortif-1 (SCM-1), is a chemokine which has been discovered in 1994-1995 by several groups at the same time.[70–72] XCL1 is composed by 93 amino acids and it is located on the chromosome 1q23.[71,73] XCL1 is the only member of the C class of chemokines, having only 2 cysteine residues out of four.[70]

According to the temperature and the salt concentration, XCL1 can assume two different conformations. The first conformation is a monomeric structure that is very similar to the normal chemokine fold. It is able to bind to its receptor and to activate it, but it cannot bind to the glycosaminoglycans that are on the surface of the vessels. The second conformation is an atypical β-sandwich dimer which cannot interact with the receptor but binds to glycosaminoglycans and forms a gradient that can chemoattract the cells. Therefore, XCL1 is defined as a metamorphic protein. In physiological conditions both conformations can be found and this complicates the design of XCL1 antagonists.[74,75]

XCL1 is secreted mainly by activated CD8 T cells, CD4 T cells, γδ T cells, NK and NKT cells ,and thymic medullary epithelial cells (mTEC).[73] It is considered to promote differentiation towards a type 1 response in T cells. As a matter of fact, it is associated with the release of type 1 cytokines and chemokines like IFNγ, CCL2, CCL3, and CCL5.[76–78]

It has been shown that XCL1 production is elevated in both viral and bacterial infections but also in autoimmune diseases like rheumatoid arthritis and Crohn's disease.[79] Human XCL1 has a homologue in the mouse, which shares 60% of the aminoacidic sequence. In contrast to mice, humans also express XCL2 that differs from XCL1 only for 2 amino acids at the N-terminus and they have similar activation profiles.[79,80]

XCL1 has a chemotactic activity for cells bearing XC receptor 1 (XCR1) on their surface. XCR1 is a G protein coupled receptor that has been identified in 1998.[81] XCR1 is expressed by conventional dendritic cells type 1 (cDC1). In mice such XCR1+ cDC1 express either CD8α or CD103, whereas in humans they express CD141.[82] XCR1 can be found also on thymic DC and the XCL1/XCR1 axis is implied in the accumulation of thymic DC in the medullary area, where they can

contribute to the formation of self-tolerance.[83] XCR1 has two binding sites for XCL1 as most of the chemokine receptors. As a first contact, the N-terminus recognizes one region of XCL1. The second site, the main one, is an orthosteric pocket and is located in the transmembrane domain. After the first binding, the pocket changes conformation, in order to allow the second link with the N-terminus part of XCL1.[80] When this is completed, there is an increased calcium flux in the cytosol of the cell and a subsequent chemotactic response of the cell. IL12 and IFNγ are released by XCR1 DC and activated DC stimulate a type 1 differentiation in T cells.[70,82,83] Further, the XCL1/XCR1 axis seems to be important in the cross-presentation process (see paragraph 3.7.2). The XCL1/XCR1 axis is studied in formulating vaccines and gene therapies against cancer.[80,84]

We have shown in the RIP-LCMV-GP mouse model for T1D (see paragraph 3.9) that both the chemokine and the receptor are upregulated after the disease infection (Figure 1).

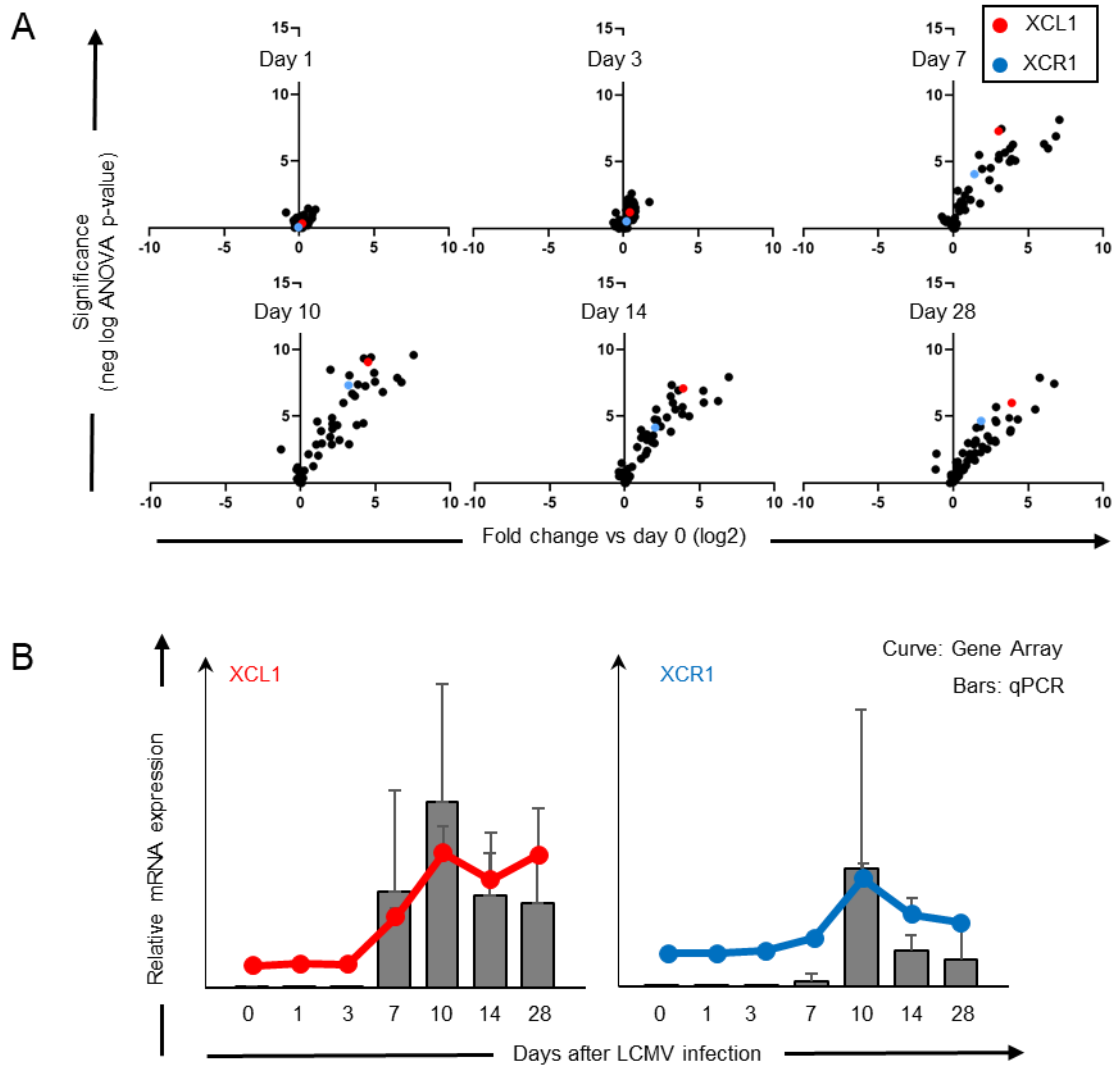

Figure 1. Results of the gene microarray of the islet microenvironment.
(A) Islets have been laser dissected from the pancreas of RIP-LCMV-GP mice at different time points after the infection. Gene expression profile of chemokines and their receptors from RIP-LCMV-GP mice at day 1, 3, 7, 10, 14, 28 after infection in comparison to uninfected mice. XCL1 and XCR1 have been highlighted in red and in blue, respectively. - (B) Graphs representing the quantification of XCL1 on the left and XCR1 on the right, obtained via quantitative PCR (bars) and via gene array (curves). Data are shown as mean ± SD.

3.7 Dendritic cells

DC are a heterogeneous family of APC that are involved in T cell responses and in tolerance.[85] Their name derives from the Greek word ‘dendron’ that means tree, since they have a stellate shape with dendrites that can bend and facilitate their main functions.[86] Their main function is to recognize the antigens and uptake them with different mechanisms, like phagocytosis, micropinocytosis, and adsorptive endocytosis. After this, DC mature upregulating major

histocompatibility complex class II (MHC-II), CD80, CD86, and CD40 and after processing the antigen, they transport it to the lymph nodes, where they can stimulate the T cell response.[86,87]

DC can be generally identified by the expression of CD11c and MHC-II, but they can be further classified in subgroups using several markers.[88] Plasmacytoid DC (pDC) are characterized by the expression of B220, plasmacytoid dendritic cell antigen-1 (PDCA-1), CD45RA, blood dendritic cell antigen 2 (BDCA-2) as well as toll-like receptor 7 (TLR7) and TLR9. They are similar to lymphoid cells and they express E2-2 (protein E2-2) and interferon regulatory factor 8 (IRF8) as transcription factors. They are activated during viral infections when they produce high amounts of type I IFN (IFNα and IFNβ). They have a unique mobility and are able to migrate to the viral site of infection. They can induce the activation of CD4+ CD25+ FoxP3+ regulatory T cells.[89–91]

A second subgroup is called conventional dendritic cells (cDC) and it is characterized by the expression of CD45, CD11c, and MHC-II. They derive from a common DC progenitor in the bone marrow and, as pre-conventional DC, they migrate to the lymphoid organs. Pre-cDC are characterized by the expression of the chemokine receptors CCR2 and CX_3CR1 that are important for their migration.[85,87]

Another DC type is called Langerhans cells (LC). These cells are present in the skin, where the play a role in both tolerance and T cell activation. Monocyte-derived DC (mDC) have been also identified. They are derived from the monocytes and are therefore different from other DC. Their main function is to facilitate CD4 T cell differentiation.[87,92]

3.7.1 Conventional dendritic cells

Conventional dendritic cells (cDC) can be found in two states: a resting state when they just circulate looking for antigens, and an activated state, after the recognition of the antigen, when they are able to interact with other cells and start to produce IL12, to activate CD8 T cells, or IL4 to activate CD4 T cells.[86] cDC can act also in immune tolerance and are able to convert CD4 T cells in regulatory T cells.[87]

cDC can be further divided in two subgroups: cDC type 1 and cDC type 2 (*Table 1*). cDC1 constitute 30% of DC in the periphery and 40% of DC in lymphoid organs. They differentiate when granulocyte-macrophage colony-stimulating factor (GM-CSF) and FMS-like tyrosine kinase 3 ligand (Flt-3L) are present.[85,87,93] In murine lymphoid organs, cDC1 can be divided in resident and migratory cells. The resident cells display MHC-II^{low} and CD11c^{high} and can also express CD8α or CD11b. The migratory cDC1 roam through the lymph vessels and display MHC-II^{high} and CD11c^{low}. They are characterized by the expression of CD103 and an upregulation of CD80 and CD86, as well as CCR7, which helps them in the migration process.[82] CD8α negative cDC1 can also express CD4, or can also be CD4 negative and are then called double negative cDC1.[88,94] Resident cDC1 can uptake antigens and present them locally to the T cells, whereas the migratory cDC1 uptake antigens in the periphery and bring them to the lymph nodes.[73]

All cDC1 express XCR1, C-type lectin domain family 9 member A (CLEC9A), CD205, and CD207 and they have a low expression of CD11b, signal regulatory protein α (Sirpα) and several macrophage markers. They are further characterized by the presence of some transcription factors like IRF8, basic transcription factor 3 (BATF3), nuclear factors, interleukin 3 regulated (NFIL3), and DNA-binding protein inhibitor 2 (ID2).[87] BATF3 is very important in the development of CD8α cDC1 and CD103 cDC1.[95] cDC1 also display high levels of TLR3, that is important for cross-priming, as well as TLR11 and TLR12, that are involved in IL12 production.[87] Once activated, cDC1 can also produce CXCL9 and CXCL10, important chemokines in the recruitment of aggressive T cells to the inflammation site.[96,97]

On the other hand, type 2 cDC (cDC2) are characterized in mice by the expression of CD11b and Sirpα and the absence of XCR1 and CLEC9A. Further, CD8α is absent and CD103 is present only on a small intestinal fraction. Their transcription factors are IRF4, IRF2, and tumour necrosis factor receptor-associated factor 6 (TRAF6).[87]

cDC1 and cDC2 can be found also in humans, where cDC1 are characterized by the expression of XCR1, CLEC9A, CD141, and the transcription factors BATF3 and IRF8 as well as high levels of TLR3 expression. They can produce IL12 but also CXCL10 that attracts more CXCR3+ lymphocytes in the area, creating a

positive loop for the activation of NK and CD8 T cells. In humans, cDC2 are characterized by the presence of CD1c and SIRPα.[87,98,99]

Table 1. Summary of the main characteristics of mouse and human cDC subtypes.

	cDC	Markers	TLR	Transcription factors
Mouse	Type 1	XCR1, CLEC9A, CD205, CD207 *Resident:* MHC-II^{low}, CD11c^{high}, CD8α or CD11b, CD4 (not always) *Migratory:* MHC-II^{low}, CD11c^{high}, CD103, CCR7, CD80^{high}, CD86^{high}	TLR3, TLR11, TLR12	IRF8, BATF3, NFIL3, ID2
	Type 2	CD11c, MHC-II, CD11b, Sirpα, CD103 (only in the intestine)		IRF4, IRF2, TRAF6
Human	Type 1	XCR1, CLEC9A, CD141	TLR3	BATF3, IRF8
	Type 2	CD1c, Sirpα		

3.7.2 Dendritic cell function and cross-presentation

The main function of DC is to uptake antigens and present them to T cells. In particular, endogenous proteins are presented via the MHC-I pathway to CD8 T cells and exogenous proteins are associated to MHC-II and therefore activate CD4 T cells. However, also exogenous antigens, like proteins, immune complexes, parasites, and cellular antigens, can be presented to CD8 T cells via MHC-I in a process called cross-priming.[100] The process is not completely understood yet, but one hypothesis is that the phagosomes containing the antigen fuse with the endoplasmic reticulum vesicles that contain the newly synthetized MHC-I. Upon antigen degradation in the phagosome antigen peptides are loaded into the MHC-I.[88] Moreover, it seems that CD4 T cells have an important role in cross-priming since they build a bridge between DC and CD8 T cells.[100,101] Plasmacytoid DC can as well contribute to cross-presentation, since they migrate to CD8 T cell during a cross-priming event in a CCR5-dependent manner and promote the cross-presentation by colocalization with XCR1 DC.[89] Resident CD8α cDC1 and their migratory counterpart CD103 cDC1, both

expressing XCR1 on their surface, are the most efficient cells in cross-priming. However, there are also other cells which are able to cross-present, such as B cells, endothelial cells, and macrophages.[88,100] For example, it has been shown that endothelial cells in the islets of Langerhans are able to cross-present the insulin antigen in T1D resulting in the attraction of insulin-specific CD8 T cells to the islets.[102]

3.8 T cells

Among the hemopoietic cells which arise from the bone marrow, there are also lymphocytes. The two main subgroups of lymphocytes are B and T cells. B cells are characterized by the presence of the B cell receptor on their surface and they are among the main players of the humoral immune response. Once activated, they proliferate and differentiate in plasma cells, that are cells able to produce large amounts of antibodies. T cells are characterized by the expression of the T cell receptor (TCR) and upon encountering the antigen they proliferate and differentiate. Naïve T cells can circulate between the different secondary lymphoid organs, searching for their cognate antigen on APC. After the encounter they undergo different phases. First, they start to expand and proliferate in the T cell zone in the secondary lymphoid organs. Then the antigen specific CD8 and CD4 T cells leave the lymph nodes and migrate to the inflammation site where they kill the pathogens. CD4 T cells which help B cell activation will move to the B cell zone in the secondary lymphoid organs. After 7-10 days from the beginning of the inflammation process, the contraction phase starts and 90% of the activated cells undergo apoptosis. The 5-10% of cells which remain alive constitute the memory T cell subset that keep on circulating. Such memory T cells ensure a much faster reaction in case of a second encounter with the same antigen.[103–105]

The interaction between T cells and DC forms the so-called immunological synapse (IS), which consists in three different signal types that have to be present to transmit the signal. The first signal is the interaction between the peptide-MHC complex and the antigen-specific TCR with CD4 or CD8 as co-receptor. The second signal is usually given by co-stimulatory molecules, such as CD80 and CD86, that are both members of the B7 family, and are expressed on DC. They

deliver the co-stimulation via CD28 on T cells to ensure an optimal clonal expansion. Other proliferative stimuli can derive from the interactions between CD137L and CD137, CD70 and CD27, and CD40 and CD40L. The interactions of B7 molecules on DC and CTLA-4 on T cells as well as PD-1 and PD-1L on hemopoietic cells or PD-2L on activated T cells inhibit T cell activation. The third signal is given by cytokines for example IL12 and type I IFN that are secreted by activated DC and are important for T cell survival.[105,106]

The main classes of T cells are cytotoxic T cells, helper T cells, and Treg cells. T cells orchestrate cell-immune mediated responses and are characterized by the presence of the co-receptor CD8 or CD4. CD8 is present on cytotoxic T cells and reacts with MHC-I that is expressed by most immune and tissue cells, usually in response to virus infections. CD4 is present on T helper cells and respond to antigens presented via MHC-II by APC. CD4 T cells can differentiate into different subtypes. T helper (Th) 1 cells, the aggressive phenotype, clear intracellular pathogens and act against bacterial infections. Th1 cells are stimulated by IL12 and produce IFNγ, TNFα, and IL2. They further express the chemokine receptors CXCR3 and CCR5. They are characterized by the expression of the transcription factor T-box expressed in T cells (T-bet). Th2 cells protect the tissue from parasite invasion and are involved in allergic reactions. They also counteract Th1 cell actions. Th2 cells are stimulated by IL4, IL25, and IL33 and produce IL4, IL5, IL6, IL10, and IL13. They express the chemokine receptors CCR3 and CCR4 and are characterized by the expression of signal transducer and activator of transcription 5 (STAT5) and STAT6, as well as the transcription factor GATA binding protein 3 (GATA-3).[107–109]

Th17 cells are stimulated by IL6 and TGFβ and express the chemokine receptor CCR6. They produce IL17A and IL17F, but also IL21. The transcription factor RAR-related orphan receptor gamma isoform t (RORγt) is characterizing this cell subtype. Their role is to act in case of extracellular bacteria or fungi infections or infections at mucosal surface.[110]

According to this classification, CD8 T cells have been also divided in the same way. Cytotoxic T cells 1 (Tc1 cells) are stimulated by the presence of IL12 that leads to the production of IFNγ, TNFα, and lymphotoxin. CD8 T cells can also differentiate to Tc2 cells that have a Th2-like profile, so they are stimulated by IL4 and produce mainly IL4 and IL5.[111,112]

Cytotoxic T cells can exploit their function in different ways. They can kill the infected cells by inducing apoptosis via the Fas/Fas ligand pathway, or in a calcium-dependent way, or they can release cytotoxic granules, containing perforin and granzymes (in humans also granulysin).[113] T cells can also be exhausted when exposure to the antigen is too strong in affinity and/or duration.[105]

Regulatory T cells are characterized by the expression of the transcription factor forkhead box protein 3 (FoxP3). They can express both CD4 or CD8 and can be subgrouped in natural Treg cells (nTreg) generated in response to self-antigens in the thymus and induced Treg cells (iTreg) in response to foreign- or self-antigens in the periphery. The latter are induced by TGFβ and are usually identified as a subset of CD4 T cells. IL2 is important for their homeostasis and for exploiting their functions. Treg cells are important to maintain the self-tolerance.[114] They act releasing anti-inflammatory cytokines for example IL10 and TGFβ. IL10 induces the downregulation of MHC-II, CD80, and CD86 on APC and decreases the release of proinflammatory cytokines by mast cells and macrophages. Some other mechanisms of suppression have been studied *in vitro*: for example, inhibition of perforin and granzyme B release, delivery of negative activation signals, physical impairment of the encounter between T cells and DC in a lymphocyte function-associated antigen 1 (LFA-1) dependent way, and alteration of CD80/CD86 expression in a CTLA-4 dependent way.[113,115,116]

T cells play an important role in type 1 diabetes. In humans, autoreactive CD8 T cells are the most predominant population in the infiltrates and also autoreactive CD4 T cells are involved in the pathogenesis of T1D.[117] CD4 T cells are important in maintaining the CD8 T cell effector function and are especially fundamental in the secondary cytotoxic T lymphocyte (CTL) expansion.[53,118]

3.9 Mouse models

There are several mouse models for T1D.[119] Widely used is the NOD mouse model. These mice were established in the Shionogi Research Lab in Japan in 1980 by Makino et al.[120] NOD mice spontaneously develop T1D usually between 10 and 30 weeks of age, with an incidence of 50-90% in the females and only 20% in the males.[10] They have many characteristics in common with humans, so

they allow an intensive study of T1D. For example, they show the main symptoms of T1D (polyuria, polydipsia, glucosuria, hyperglycaemia), with β-cell destruction and decreased insulin production.[120] Both insulin and GAD65 autoantibodies were found in NOD mice before the start of the disease. Through NOD mice, it was also possible to study the HLA-associated risk because also in NOD mice some MHC haplotypes are associated with higher risk to develop T1D.[121,122] The mechanism of pathogenesis of the disease is slightly different from the humans. Around the third week of age of the mice, dendritic cells, macrophages, and neutrophils start to infiltrate the islets of Langerhans, after a swelling of the blood vessels. At week 5-7 of age, both CD4 and CD8 T cells are also attracted to the islet microenvironment where they are the main players of β-cell destruction. If the infiltration is very intense, tertiary lymphoid structure may start to form. The disease seems to be more aggressive than in humans.[11,17,123] NOD mice are still a powerful tool to study T1D, but they have some limitations, for example the unknown starting point of the disease or the infiltration pattern which is different from the one found in the pancreas of T1D patients. Further, NOD mice display additional diseases, such as a Sjögren's syndrome-like disease.

Another model which is often used is the RIP-LCMV-GP inducible mouse model. Here, the mice express the glycoprotein (GP) of the lymphocytic choriomeningitis virus (LCMV) under the control of the rat insulin promoter (RIP) on the β-cells in the islets of Langerhans. This transgenic mouse model was developed by Oldstone et al.[124] in 1991, in parallel with a similar model called RIP-LCMV-NP. These mice express the nucleoprotein (NP) of the LCMV on the β-cells but also in the thymus.[124,125] RIP-LCMV mice have a viral gene (either GP or NP) that was inserted at the oocyte stage in the mice, so it is present in the islets as self-gene and the expressed self-protein is tolerated by the immune system. The model is based on the idea of molecular identity/mimicry, in which an environmental factor and a host component share one or more identical/similar antigen-epitopes.[126] This means that the mice do not develop T1D until they are infected with LCMV. With the infection, the immune system starts to react against the virus and subsequently also against the β-cells, since they both express the same GP or NP (Figure 2).[124,127] At this point, the mice start to show the first signs of T1D. The virus is usually cleared between 7 and 14 days after the infection.[124] There

are several advantages in using this mouse model, such as the known onset of the disease and the well-defined autoantigens and epitopes.[119]

The main difference between the two lines is that the RIP-LCMV-GP mice become diabetic between 7-14 days after the infection, whereas the RIP-LCMV-NP mice need 3 to 6 months.[125] Moreover, the GP mice have higher affinity for the H-2D^{b}-GP33 complex compared to H-2L^{d}-NP118 complex.[126] Another difference is that in the NP model, both CD4 and CD8 T cells are required for the onset of the disease, whereas in the GP mouse model, CD8 T cells are the main players of the process.[125]

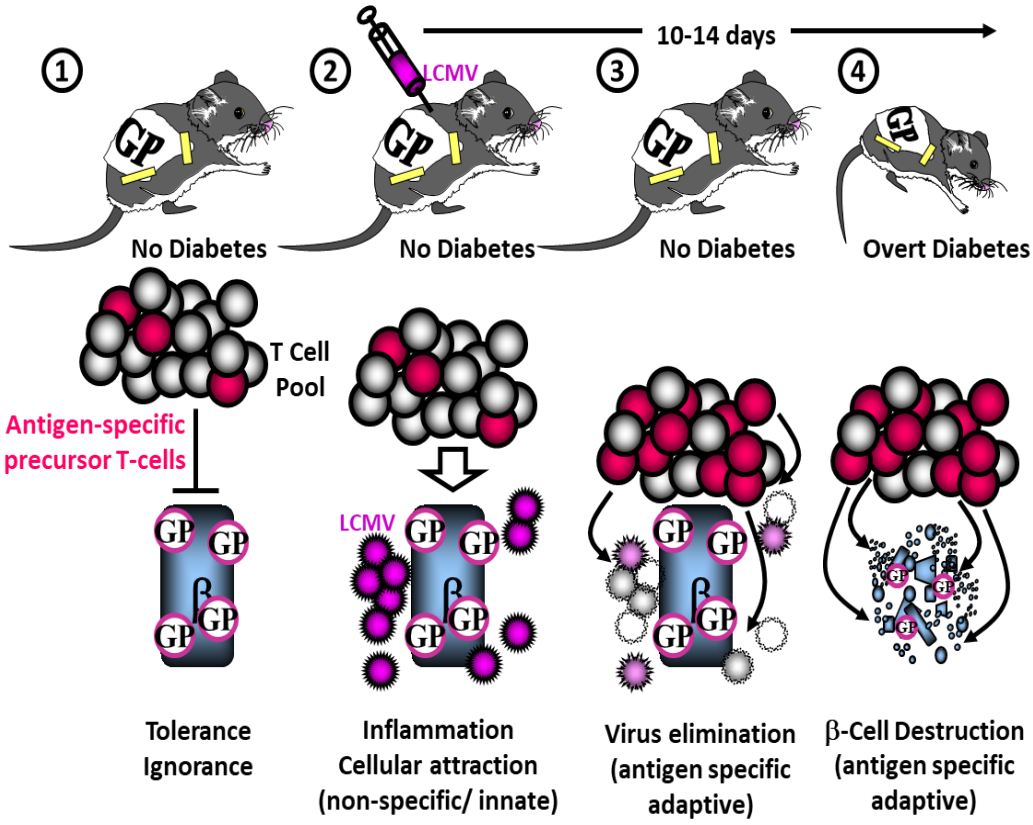

Figure 2: Schematic representation of the RIP-LCMV-GP mouse model.
(1) RIP-LCMV-GP transgenic mice do not show signs of T1D and are normoglycemic. The β-cells in the pancreas express the GP of the LCMV under the control of the RIP. T cells do not react towards the β-cells as long as the tolerance is still intact. - (2) As soon as LCMV is injected in the mice, the inflammation process starts and the cells are attracted towards the pancreas. - (3) The virus is eliminated by T cells in an LCMV-GP-specific adaptive response. - (4) The expansion of LCMV-GP-specific T cells causes the destruction of the β-cells as well. When most of the islets are destroyed, the mice turn diabetic, which occurs usually in between 10 and 14 days after the infection.

4. Aims of the study

Even if Teplizumab has recently been approved as a drug for T1D, the pathway to find a cure for this disease is still long. That is why this study is mainly focused on finding a new target for an immunotherapy for T1D or for a combination therapy with an anti-CD3 antibody or an anti-CXCL10 antibody.

It has previously been shown in our lab by Christine Bender that chemokine ligands and their receptors are upregulated during T1D pathogenesis. Among these, our attention focused on the following chemokine axes: CXCL10/CXCR3, CCL5/CCR5, CXCL16/CXCR6, CX_3CL1/CX_3CR1, and XCL1/XCR1. A particular focus was on the XCL1/XCR1 axis that has already been studied in other diseases, for example as a target in melanoma therapy.[128,129] Further, it was also found to be elevated in the serum of T1D patients,[68,69] but to date it has never been considered as a target in this context.

Therefore, the main goal of this work is to study
the role of the XCL1/XCR1 axis in T1D pathogenesis.

In particular, the aims are:

1) localize several chemokine-receptor axes in mouse pancreas sections.

2) localize XCL1 and XCR1 in the islets of patients with T1D, individuals with islet-autoantibodies, RIP-GP mice, and NOD mice, and confirm their upregulation during T1D pathogenesis.

3) study the effects of an absence of XCL1 or XCR1 on a cellular level and on T1D incidence and severity in mice.

4) study if an absence of XCL1 combined with an absence of CXCL10 further improves the positive effects of a CXCL10-deficiency in mice.

Aim 1: Localization of several chemokine-receptor axes in mouse pancreas sections.

The localization of CXCL10/CXCR3, CCL5/CCR5, CXCL16/CXCR6, and CX_3CL1/ CX_3CR1 will be done on murine pancreatic tissue with RNAscope *in situ* hybridization technique and immunohistochemistry (IHC). Slides of pancreas isolated at different time points after the infection will be used. Incidence studies interfering with these axes will be performed in our lab.

Aim 2: Localization of XCL1 and XCR1 and confirmation of their upregulation during T1D pathogenesis.

The localization of XCL1 and XCR1 will be done with RNAscope *in situ* hybridization technique since there is no reliable antibody for mouse XCR1 available for IHC. Sections of human pancreas from patients at different disease stages will be stained to see if XCL1 and XCR1 are upregulated during human T1D pathogenesis. Sections of pancreata obtained at different time points from infected RIP-GP mice will be used to confirm the gene array data. NOD mice will be used to verify that the upregulation is also occurring in a second mouse model for T1D.

Aim 3: Study of the effects of an absence of XCL1 or XCR1 on a cellular level and on T1D incidence and severity in mice.

RIP-GP mice will be crossed with $XCL1^{-/-}$ mice and with $XCR1^{Venus/Venus}$ mice (referred to as $XCR1^{-/-}$ mice) and the mice will be infected with LCMV to study the effects of an XCL1- or XCR1-deficiency on different cell populations. Moreover, I will study if XCL1- or XCR1-deficiency has an impact on T1D incidence and severity. Our hypothesis is that XCL1 and XCR1 are involved in the pathogenesis of T1D. The idea is that upon stress, infection, or insulitis, the β-cells start to release CXCL10, as previously demonstrated.[62] This chemokine attracts T cells, bearing CXCR3 on their surface. These T cells start to infiltrate the islets and to produce XCL1, which in turn attracts XCR1+ cDC1. These cells act on T cells in two ways. They attract even more CXCR3+ T cells to the islet microenvironment, being able to release CXCL10. Moreover, they are the most potent population of antigen-presenting cells able to prime T cells. The activated T cells initiate β-cell destruction resulting in T1D over time (Figure 3). Taken this in account, I would

like to see the impact of an interference with XCL1/XCR1 axis on the T1D pathogenesis.

Aim 4: Studying if an absence of XCL1 combined with an absence of CXCL10 further improves the positive effects of a CXCL10-deficiency in mice.

It has been shown that CXCL10-deficiency reduces T1D incidence in RIP-GP mice.[47] Moreover, it is known that DC and in particular cDC1 can produce CXCL10, contributing to the attraction of T cells to the islet microenvironment.[96–98] To improve further CXCL10-deficiency positive outcome, RIP-GP x $XCL1^{-/-}$ mice will be crossed with RIP-GP x $CXCL10^{-/-}$ mice. The idea is to act concomitantly on T cells and on DC to see if the blocked attraction of both cell types to the islet microenvironment can reduce T1D incidence and severity even more.

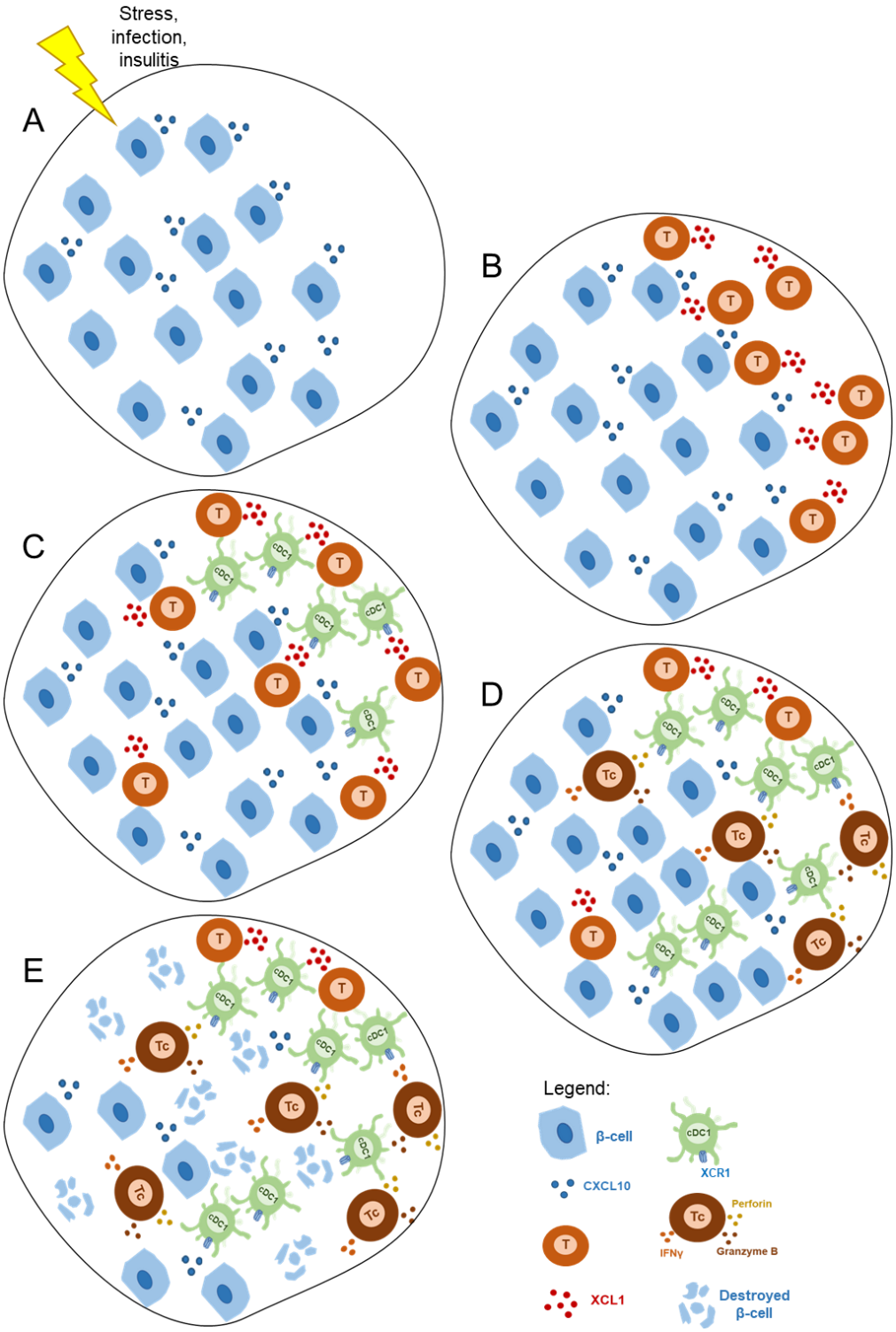

Figure 3. Schematic representation of the working hypothesis.
(A) Upon stress, infection, or insulitis the β-cells in the islets of Langerhans start to release CXCL10. - (B) CXCR3+ T cells are attracted to the islets and start to produce chemokines, such as XCL1. - (C) XCL1 attracts cDC1 expressing XCR1 to the islets. - (D) cDC1 start to produce cytokines and chemokines among which CXCL10 that attracts more T cells to the islets. They also activate T cells to cytotoxic T cells, which will start to release perforin and granzyme B. - (E) These effector molecules contribute to β-cell killing. When a critical mass of β-cells is destroyed (approximately 80-90%), BG homeostasis cannot be maintained anymore and T1D ensues. Note that to make the representation easier, other cells that compose the islets are not shown.

5. Materials and Methods

5.1 Materials

5.1.1 Antibodies

Table 2: Antibodies used for FACS-staining.

Antibody	Company
CD103 APC	BD Pharmingen; 562772
CD11b Alexa488	BioLegend; 101217
CD11b APCCy7	BioLegend; 101226
CD11c PeCy7	BioLegend; 117318
CD16/CD32	BioLegend; 101302
CD4 PeCy7	BD Pharmingen; 552775
CD8a APCCy7	BD Pharmingen; 557654
CD8a PerCp5.5	BioLegend; 100734
CD8b V510	BioLegend; 126631
FoxP3 PE	Invitrogen; 12-5773-82
Granzyme B PE	eBioscience; 12-8898-82
IFNγ V450	BD Pharmingen; 560661
IL12 PE	R&D; IC2191P
KLRG1 PerCp5.5	BioLegend; 138418
MHC-II V450	Invitrogen; 48-5321-82
PD-1 APCCy7	BioLegend; 135224
Perforin APC	BioLegend; 154304
XCR1 V510	BioLegend; 148218

Table 3: Primary antibodies for immunohistochemistry and immunofluorescence.

Antibody	Company
Biotinylated Armenian hamster anti-mouse CD11c	Invitrogen; 13-0114-82
Goat anti-mouse CD103	R&D; AF1990
Rabbit anti-mouse insulin	Abcam; ab181547

Rabbit anti-mouse CXCL10	PeproTech; 500-P129
Rabbit anti-mouse CXCR3	Zymed
Rabbit anti-mouse CX_3CL1	Abcam; ab25088
Rabbit anti-mouse CXCL16	Bioss; bs-1441R
Rabbit anti-GFP	Acris Antibodies; SP3005P
Goat anti-mouse CCL5	R&D Systems; AF478
Armenian hamster anti-mouse CCR5	BioLegend; 107008

Table 4: Secondary antibodies for immunohistochemistry and immunofluorescence.

Antibody	**Company**
Biotinylated anti-Armenian hamster	eBioscience; 13-4113-85
Biotinylated anti-goat	Vector; BA-5000
Biotinylated anti-rabbit	Vector; BA-1000
Donkey anti-goat Cy3	Jackson ImmunoResearch; 705-165-147
Goat anti-rabbit Cy3	Jackson ImmunoResearch; 111-165-003
Streptavidin FITC	BioLegend; 405201

Table 5: Antibodies for plaque assay.

Antibody	**Company**
Peroxidase – conjugate affiniPure goat anti-rat IgG (H+L) secondary antibody 1:400	Jackson ImmunoResearch Laboratories, Inc.112-035-033
VL-4 rat anti-LCMV (2 mg/ml)	In-house

5.1.2 Chemicals

Table 6: Chemicals.

Chemical	**Company**
10x buffer PCR	Peqlab
3,3′-Diaminobenzidine (DAB) powder	Roth; 231-018-9

4′,6-diamidino-2-phenylindole (DAPI)	Sigma-Aldrich; 28718-90-3
Acetic acid	Sigma-Aldrich; 33209-1L
Acetone	Sigma-Aldrich Chemie GmbH; 32201
Agarose Universal	VWR; 35-1020
Ammonium chloride	Sigma Aldrich; 213330
Ammonium sulphate	Fluka; 09980
Aquamount	Merck Chemicals KGaA; 1.08562
Bovine serum albumin (BSA)	Roth; T844.2
Brefeldin A	Sigma Aldrich Chemie GmbH; B6542
Bromophenol blue	Roth; A512.1
Carboxyfluorescein succinimidyl ester (CFSE)	Thermo Fisher; 65-0850-84
CD45 MicroBeads mouse	Miltenyi Biotec; 130-052-301
Chloroform	Fisher Scientific; C144960
Deoxycholic acid	Sigma; D6750
Dibenzyl ether (DBE)	Sigma Aldrich; 108014
Dichloromethane (DCM)	Sigma Aldrich; 270997
Dimethyl sulfoxide (DMSO)	Sigma Aldrich Chemie GmbH; D5879
Dipotassium hydrogen phosphate trihydrate	Merck; 1.05099.1000
Disodium hydrogen phosphate	VWR; 28029.292
DMEM + GlutaMax I	Gibco; 61965
DMEM powder	Gibco; 52100-021
dNTP for PCR	Roth
Donkey serum	Biorad; C06SB
Ethanol (EtOH) absolute	Sigma-Aldrich; 32221
Ethylenediamintetraacetic acid (EDTA)	AppliChem; A1103.1000
Fetal calf serum (FCS) heat inactivated	Sigma Aldrich; F7524
Ficoll-Paque PLUS	Cytiva; 17144003
Fluoromount G	Invitrogen; 00-4958-02
Formaldehyde	Roth; 6749-2

Gel Red	Biozum; 41003
Glycine	Sigma; G7126-1KG
Glycerol	Roth; 3783.1
Heparin	Sigma; H3149-25KU
Hydrochloric acid min. 37%	Kmf; KMF.08-721
Hydrogen peroxide	Roth; 8070.1
Isoflurane	Abbott; B506
L-Lysine monohydrochloride	Sigma; L5626-100G
MACS Quant calibration beads	Miltenyi Biotec; 130-093-607
MACSQuant Running buffer	Milteny Biotec; 130-092-747
MACSQuant Washing solution	Milteny Biotec; 130-092-749
MACSQuant/MACSima Storage solution	Milteny Biotec; 130-092-748
Mayer's Hematoxylin solution for clinical diagnosis	AppliChem A4840.1000
Methanol (MeOH)	Sigma-Aldrich; 32213
Methocel MC (methylcellulose)	Fluka; 64620
NP40	Sigma-Aldrich; 9016-45-9
NuSieve Agarose - low melting agarose	FCM Bio Products; 50080
OCT solution (Tissue-Tek)	Sakura; 4583
Paraformaldehyde	Merck; 1.04005.1000
PBS	Gibco; 14190-094
Penicillin-Streptomycin (P/S)	Gibco; 15140
Peroxidase substrate	Vector; SK-4100
Potassium acetate	Sigma Aldrich; 25059
Potassium chloride	Roth; 6781.1
Potassium dihydrogen phosphate	Roth; 3904.1
Primers (PCR)	Biomers
Proteinase K	Roth
RPMI 1640 + GlutaMax I	Gibco; 61870
Saponin	Sigma Aldrich Chemie GmbH; S7900
SDS Ultrapure	AppliChem; A1112,0500

Sodium (meta)periodate	Sigma; S1878-25G
Sodium azide	AppliChem; A1430
Sodium chloride	Sigma Aldrich Chemie GmbH; 31434
Sodium hydrogen carbonate	Merck; 1.06329.0500
Sodium hydroxide – pellet	Fisher Scientific; S/4920/60
Surgipath- Paarplast Plus (paraffin)	Leica; 39602004
Taq Polimerase	Paqlab
Triton X-100	Sigma; T8787
Trizma® base (Tris)	Sigma; T1503
Trypan Blue	Sigma; T8154
Trypsin	Sigma Aldrich; T3924
TWEEN 20 (Polyethylen-Sorbitan-Monolaureat)	Sigma Aldrich Chemie GmbH; P7949
VectaMount Permanent Mounting Medium	Vector Labs; H-5000
Xylol	Fisher Scientific; X/0200/17

5.1.3 Laboratory equipment and consumables

Table 7: Laboratory equipment and consumables.

Equipment or material	**Company**
70 µm / 100 µm nylon cell strainer	BD Falcon; 352350; 352360
96-well V-bottom plates	LifeScience Products; 781601
ACD EZ-Batch™ Slide Rack (20 slide capacity)	ACD Bio; 310017
Anesthesia unit 1200	Univentor
Autoclave v-150	Systec
Balance, CP 153	Sartorius
Capillary (Heparin coated)	Fisher scientific; 02-668-10
Cell culture flasks (25, 75, 175 cm^2)	Cellstar
Cell scraper	Sarstedt; 83.1830
Cellstar cell culture dishes 60 x 15 mm	Greiner Bio-One; 628160

Centrifuge Biofuge fresco Heraeus	Thermo Fisher Scientific
Centrifuge Multifuge 3 S-R	Thermo Fisher Scientific
Centrifuge, 5804	Eppendorf
CO_2 Incubator, Heraeus BBD6220	Thermo Fisher Scientific
Confocal Microscope LSM 510 META	Zeiss
Corning®Costar®Stripette®serological pipettes (5 ml, 10 ml, 25 ml, 50 ml)	Sigma-Aldrich Co
Coverslips (24x40 mm)	Carl Roth
Cryomolds (15 x 15 mm)	Thermo Fisher Scientific
Cryostat CM1850 UV	Leica
Cryotubes, Cryo pure (2 ml)	Sarstedt; 72.379.002
Electrophoresis apparatus	Biorad
Eppendorf tubes (0.5 ml, 1.5 ml, 2 ml)	Eppendorf
FACS (Fluorescence-activated cell sorting) tubes	Sarsted; 55.476.005
Falcon tubes (15, 50 ml)	Greiner Bio-One
Flowcytometer, MACS Quant Analyser 10	Miltenyi Biotec
Glassware	Schott AG
Gloves, Vasco Nitrile white	Braun
Glucometer SD Codefree	SD Biosensor
HybEZ™ Humidifying Paper	ACD Bio; 310015
HybEZ™ Humidity Control Tray (with lid)	ACD Bio; 310012
HybEZ™ Oven (110 VAC)	ACD Bio; 310010
ImmEdge™ Hydrophobic Barrier Pen	Vector Laboratory; H-4000
Incubator, Hybaid Shake'n'Stack	Thermo Fisher Scientific
Keyence fluorescence microscope BZ-9000	Keyence
Light-sheet microscope Olympus MVX10	LaVisionBiotec
Liquid Blocker Pap-Pen	Daido Sangyo Co
Microscope Axioscope 2	Zeiss

Microscope Axiovert 25C	Zeiss
Microscope Slides FischerbrandTM SuperfrostTM Plus	Fisher Scientific; J1800AMN
Microtome	Leica; RM2235
MS columns	Miltenyi Biotec; 130-042-201
Multichannel pipette, 12 channels (50-300 µL)	Labsystems Diagnostics Oy
Multichannel pipette, 8 channels (20-200 µL)	Gilson Inc.
Needles (23G, 27G, 30G)	Braun Melsungen AG
Omni Tissue Homogenizer	Omni International, Inc
Parafilm “M” Laboratory Film	Bemis
Pasteur pipettes	Mainz
PCR machine	Biorad
PCR markers	Roth; X902.1
PCR tubes	Life Science; 781340
pH-Meter	XS Instruments
Pipette tips (10 µl, 20 µl, 200 µl, 1000 µl)	Sarstedt AG & Co
Pipetting aid unit, Pipetboy acu	Integra Bioscience
Plastic Pasteur pipettes	VWR; 8112-1665
Plastic pipettes (5 mL, 10 mL, 25 mL), Costar	Corning
Pre-separation filters	Miltenyi Biotec; 130-041-407
Software BZ-II Analyzer	Keyence
Software FlowLogic	Inivai Technologies
Software Prism 5	GraphPad Software, Inc.
Sterile 96- well U- and V-bottom plates	Greiner; 650161 and 651161
Sterile Filter (50, 250, 500 ml)	Millipore
Stripes for glucometer SD Codefree	SD Biosensor
Surgical scissors	Roboz; RS-5913

Surgical forceps	Roboz; RS-5240
Syringe with needle, Omnican 100 (1 mL)	Braun
Syringes (0.5, 1, 3, 5, 10, 20 ml)	Braun
Tissue culture plates (6, 12, 24, 48, 96 wells)	Cellstar
Tissue Tek Cryomolds (10 x 10 mm)	Sakura; 4565
TP 1020 Tissue Processor	Laica
Transilluminator for agarose gel	Biorad
Vortex unit, MS2 Minishaker	IKA-Werke
Water bath, Isotemp 215	Fisher Scientific
Water Purification system	Merck
Whatman paper	Whatman International Ltd.

5.1.4 Enzymes, proteins, and peptides

Table 8: Enzymes, proteins, and peptides.

Protein	**Company**
Collagenase P	Sigma-Aldrich; 11213865001
LCMV-GP33 KAVYNFATM 1 mg/mL	GenScript Corp.
LCMV-GP61 GLKGPDIYKGVYQFKSVEFD 1 mg/mL	GenScript Corp.

5.1.5 Buffers, solutions, and culture media

Table 9: Composition of buffers, solutions, and culture media.

Solution	**Composition**
1% Triton X-100	1% Triton X-100 PBS
10x Phosphate buffered saline (PBS)	140 mM NaCl 10 mM KCl 6.4 mM Na_2HPO_4

	2 mM KH_2PO_4 ddH_2O pH 7.5
2% Methylcellulose	2% Methylcellulose ddH_2O
20x SSC	3.0 M NaCl 0.3 M Sodium citrate ddH_2O
2x DMEM	2.64% DMEM powder 0.74% $NaHCO_3$ ddH_2O pH 6.8
ABC reagent solution (Peroxidase Substrate Kit DAB)	2 drops of buffer 4 drops of DAB stock solution 2 drops of hydrogen peroxide solution 5 ml ddH_2O
Blocking buffer – whole pancreas staining	0.2% Triton X 100 10% DMSO 6% Donkey serum PBS Sterile filtered
Buffered PFA 4%	4% Paraformaldehyde 80 mM K_2HPO_4 20 mM KH_2PO ddH_2O pH = 7.3-7.4
DAB (plaque assay)	50 mg DAB powder 75 µl 37% HCl 5 ml ddH2O
DAB substrate for 3 plates (plaque assay)	0.6 ml aliquot of DAB in water 0.75 ml Tris (1M pH 7,5) 5.1 µL H_2O_2 (30 %) one drop of Nickel

	ddH_2O (final volume 15 ml)
DMEM (1x) + GlutaMAX-I	DMEM 2% FCS 1% Penicillin/Streptomycin
Erythrocyte lysis buffer for blood	0.74% NH_4Cl ddH_2O sterile filtered
Erythrocyte lysis buffer for spleen	0.83% NH_4Cl ddH_2O sterile filtered
FACS buffer	1% FCS 0.1% NaN_3 PBS pH 7.5
FACS/PFA buffer	1% FCS 0.1% NaN_3 1% PFA PBS pH 7.5
FACS/saponin buffer	1% FCS 0.1% NaN_3 0.1% Saponin PBS
First antibody buffer (whole pancreas staining)	5% DMSO 3% Donkey serum 0.2% Tween 20 10 µg/ml heparin PBS Sterile filtered
Loading gel buffer	30% Glycerol 70% ddH_2O Bromophenol blue

Lysine HCl 0.1 M	0.2 M Lysine HCl in ddH_2O pH 7.4 with Na_2HPO_4 1M Lysine to 0.1 M with 0.1 M sodium phosphate buffer
MACS buffer	0.5% BSA 1 mM EDTA PBS pH 7.2
MC57 culture medium	7% FCS 1% Penicillin/Streptomycin RPMI 1640 (1x) + GlutaMAX-I
Mouse tail buffer	20% SDS 4 M NaCl 1 M Tris PH 8.0 ddH_2O
NaN_3-H_2O_2 solution	0.3% H_2O_2 0.1% NaN_3 PBS
Permeabilization buffer – whole pancreas staining	0.2% Tween 20 5% DMSO 2.3% glycine 0.01% NaN_3 PBS
PFA/saponin buffer	0.1% saponin 4% PFA PBS pH 7.5
PLP (PFA, Lysine, Periodate) buffer	1 part 8% PFA 3 parts Lysine HCl 0.1M 0.01 M $NaIO_4$
Pre-treatment buffer 1 – whole pancreas staining	0.2% Triton X 20% DMSO 0.01% NaN3

	PBS
Pre-treatment buffer 2 – whole pancreas staining	0.1% Triton X 0.1% Deoxycholate 0.1% NP40 20% DMSO 0.01% NaN_3 PBS
Proteinase K stock	10 mg/ml Proteinase K 10 mM Tris-HCl ddH_2O pH 7.5
RPMI 1640 + GlutaMax I complete	1% Penicillin/Streptomycin (100u/ml) 10% FCS RPMI 1640 (+Glutamax-I)
Secondary antibody buffer (whole pancreas staining)	3% Donkey serum 0.2% Tween 20 10 µg/ml heparin PBS Sterile filtered
Sodium phosphate buffer 1M	77.4 ml Na_2HPO_4 1M 22.6 ml NaH_2PO_4 1M pH 7.4
TAE 50x	2 M Tris base 1 M Acetic acid 0.05 M EDTA pH 8.2 - 8.4
TE buffer	10 mM Tris pH 7,5 1 mM EDTA ddH_2O
Wash buffer (PTwH, whole pancreas staining)	0.2% Tween 20 10 µg/ml heparin PBS Sterile filtered

5.1.6 Kits

Table 10: Kits.

Kit	Company
ABC-Kit	Vector; PK-7100
Avidin/Biotin blocking kit	Vector; SP-2001
Peroxidase Substrate Kit DAB	Vector; SK-4100
RNAscope® H_2O_2 & Protease Plus reagents	ACD Bio; 322330
RNAscope® Target Retrieval Reagents	ACD Bio; 322000
RNAscope® 2.5 HD duplex detection kit	ACD Bio; 322500
Wash buffer kit	ACD Bio; 310091

5.1.7 RNAscope probes

Table 11: RNAscope probes.

Probes	Company
RNAscope® 2.5 Duplex positive control probe – Hs	ACD Bio; 321641
RNAscope® 2.5 Duplex positive control probe – Mm	ACD Bio; 321651
RNAscope® 2-plex Negative control probe	ACD Bio; 320751
RNAscope® Probe Hs-Xcl1-C2	ACD Bio; 562471-C2
RNAscope® Probe Hs-Xrc1-XMne	ACD Bio; 542041
RNAscope® Probe Mm-Ccl5-C2	ACD Bio; 469601-C2
RNAscope® Probe Mm-Ccr5	ACD Bio; 438651
RNAscope® Probe Mm-Cx3cl1	ACD Bio; 426211
RNAscope® Probe Mm-Cx3cr1-C2	ACD Bio; 314221-C2
RNAscope® Probe Mm-Cxcl10-C2	ACD Bio; 408921-C2
RNAscope® Probe Mm-Cxcl16-C2	ACD Bio; 466681-C2

RNAscope® Probe Mm-Cxcr3	ACD Bio; 402511
RNAscope® Probe Mm-Cxcr6	ACD Bio; 871991
RNAscope® Probe Mm-Xcl1-C2	ACD Bio; 507791-C2
RNAscope® Probe Mm-Xrc1	ACD Bio; 562371

5.1.8 Cell lines

Table 12: Cell lines.

Probes	**Company**
MC57	Supplied by Dr. von Herrath

5.2 Methods

5.2.1 Mice and virus

H-2b RIP-LCMV-GP (shortly, RIP-GP) transgenic mice were generated and screened by PCR as previously described.[124,125] XCL1$^{-/-}$ mice were generated as previously described by Dorner et al.[73] These mice have been backcrossed to C57BL/6 mice for more than 10 years and then crossed with H-2b RIP-LCMV-GP to obtain RIP-LCMV-GP x XCL1$^{-/-}$ mice (shortly, RIP-GP x XCL1$^{-/-}$).
XCR1$^{Venus/Venus}$ mice were generated as described[82] and crossed with the H-2b RIP-LCMV-GP mice to get RIP-LCMV-GP x XCR1$^{Venus/Venus}$ mice (referred to as RIP-GP x XCR1$^{-/-}$ mice).
CXCL10$^{-/-}$ mice were generated as previously described[130] and were crossed with the H-2b RIP-LCMV-GP mice to obtain RIP-LCMV-GP x CXCL10$^{-/-}$ mice. The latter were crossed with RIP-LCMV-GP x XCL1$^{-/-}$ mice to get RIP-LCMV-GP x CXCL10$^{-/-}$ x XCL1$^{-/-}$ mice (shortly, RIP-GP x CXCL10$^{-/-}$ x XCL1$^{-/-}$).
LCMV Armstrong clone 53b was produced as described previously.[125] Mice were infected with a concentration of 10^4 plaque-forming units (pfu) LCMV.
NOD (Non-obese diabetic) mice were purchased from The Jackson Laboratory.
Experiments were carried out with animals kept under specific pathogen free conditions, in accordance with German regulations. All animal experiments were conducted according to the protocols approved by the local Ethics Animal Review Board (Darmstadt, Germany).

5.2.2 T1D incidence study

Mice of different lines were intraperitoneally infected with 10^4 pfu of LCMV on day 0. Blood glucose (BG) concentration of the mice was measured with a SD Codefree glucometer on day 7, 10, 12, 14, 17, 21, and then on weekly intervals for three months. Mice were considered hyperglycaemic with a BG concentration higher than 200 mg/dl and diabetic with more than 300 mg/dl. Mice with BG concentration higher than 600 mg/dl for three weeks in a row were killed, according to the animal protocol.

5.2.3 Human samples

Human pancreas paraffin slides were provided by Prof. Dr. Michael Betts, who is a participant of the Human Islet Research Network (HIRN), which includes the Human Pancreas Analysis Program (HPAP). These samples were obtained by donors with different disease stages, in particular five of them were healthy donors (non-diabetic, ND), five of them were classified as islet autoantibodies (Aab+) positive since one or more islet autoantibodies could be found in their blood but HbA1c and C-Peptide (C-Pep.) values were normal, and five of them were affected by T1D. Detailed information about organ donors are reported in *Table 13*.

Table 13. Detailed information about organ donors, obtained through the HPAP programme.

Donor	Pancreas region	State	Age	Sex	Disease Duration	HbA_{1c}	C-Pep.	Aabs
HPAP-012	Body	ND	18	F		4.5	4.1	-
HPAP-034	Tail	ND	13	M		5.2	12.7	-
HPAP-095	Tail	ND	23	F		4.9	4.13	-
HPAP-099	Tail	ND	28	F		5	6.62	-
HPAP-110	Tail	ND	31	M			7.75	-
HPAP-016	Tail	AAb+	30	M		5	4.49	GAD, IA-2
HPAP-019	Tail	AAb+	22	M		5.2	8.82	GAD
HPAP-072	Tail	AAb+	19	M		5.6	4.37	GAD
HPAP-107	Tail	AAb+	15	M		5.3	5.49	GAD, IA-2, ZnT8
HPAP-114	Tail	AAb+	21	F		5.3	11.45	GAD
HPAP-020	Body	T1D	14	M	1	13.2	0.37	GAD, IA-2, IAA, ZnT8
HPAP-087	Tail	T1D	15	F	8	10.4	0.02	IAA
HPAP-102	Tail	T1D	18	M	6	6.7	0.07	IAA
HPAP-123	Tail	T1D	25	M	3	9.7	0.07	GAD, IAA, ZnT8
HPAP-135	Body	T1D	18	M	3	14.7	0.25	-

5.2.4 RNAscope *in situ* hybridization

Regular RIP-GP, RIP-GP x XCL1$^{-/-}$, and RIP-GP x XCR1$^{-/-}$ mice were infected and sacrificed at different time points after the infection (d0, d7, d10, d14, d28). NOD mice were sacrificed at determined age (week 6, 12, 22, 26). Mice were anesthetised with isoflurane and killed by cervical dislocation. Pancreata were dissected from the mice, with the pancreatic draining lymph nodes (PDLN), and, at once, immerged in a solution of 4% buffered paraformaldehyde (PFA). Samples were incubated overnight at room temperature (RT) on a horizontal shaker. The following day, the samples were dehydrated using Leica TP 1020 Tissue Processor and then embedded in paraffin. 4 µm slices were cut from the paraffin-embedded blocks of mouse pancreas. ACDBio RNAscope 2.5 HD Duplex Manual Assay kit was used on the obtained mouse sections and on the received human slides, following the company protocol. The time of “target retrieval” and “protease plus” incubations for mouse pancreas had to be reduced to 11 minutes and 15 minutes, respectively. For the human pancreas, the time of “target retrieval” incubation was 15 minutes and for the “protease plus” incubation was 30 minutes. The different probes could be detected in channel 1 (C1) through an enzymatic reaction via horseradish peroxidase (HRP) to develop a blue colour and in channel 2 (C2) through an alkaline phosphatase (AP) reaction, developing a red colour. The probes used on mouse samples are CCL5 (Cat No. 469601-C2, red) and CCR5 (Cat No. 438651, blue); CX$_3$CL1 (Cat No. 426211, blue) and CX$_3$CR1 (Cat No. 314221-C2, red); CXCL10 (Cat No. 408921-C2, red) and CXCR3 (Cat No. 402511, blue); CXCL16 (Cat No. 466681-C2, red) and CXCR6 (Cat No. 871991, blue); XCL1 (Cat No. 507791-C2, red) and XCR1 (Cat No. 562371, blue). For human samples, XCL1 (Cat No. 562471-C2, red) and XCR1 (Cat No. 542041, blue) were used. Images were acquired using a Axioscope 2 microscope (Zeiss) with a 40x and 63x oil objective.

5.2.5 Immunohistochemistry

After killing the mice as described before, the dissected pancreata were at once immerged in Tissue-Tek OCT and quick-frozen on dry ice. 7 µm tissue sections were cut, then fixed in ethanol (EtOH) or ethanol/acetone (1:1) at -20°C for 15

minutes. After removing the Tissue-Tek OCT, circles were drawn around the tissues with a wax pen. The slides were then washed two times for 2 minutes in PBS and incubated at RT for 10 minutes with 0.3% H_2O_2/0.1% Na-azide in PBS. The tissues were washed two times for 2 minutes in PBS and few drops of avidin (Avidin/Biotin Blocking Kit) were applied on them for 10 minutes at RT. After two washing steps, an incubation with few drops of biotin (Avidin/Biotin Blocking Kit) was performed for 10 minutes at RT. The tissues were then washed with PBS and blocked with FCS 10% in PBS for 30 minutes at RT. Without washing, a primary antibody (goat anti-CD103 antibody 1:300, rabbit anti-insulin antibody 1:4000, rabbit anti-CXCL10 1:100, rabbit anti-CXCR3 1:100, rabbit anti-CX_3CR1 1:100, rabbit anti-CXCL16 1:100, rabbit anti-GFP 1:100, goat anti-CCL5 1:200, Armenian hamster anti-CCR5 1:100) diluted in 10% FCS/PBS was applied on the slides for 2 hours at RT or overnight at 4°C in a humidified chamber. After tapping off the primary antibody, the samples were washed three times for 4 minutes and then incubated with the proper secondary antibody (biotinylated anti-goat antibody 1:400, biotinylated anti-rabbit antibody 1:500, biotinylated goat anti-Armenian hamster 1:400) for one hour at RT diluted in 10% FCS/PBS. The pancreata were then washed again three times for 4 minutes and incubated with ABC Reagent for 30 minutes at RT. After washing the slides, few drops of DAB solution (DAB kit) were added on the sections for 5 minutes at RT in the dark. The reaction was stopped by washing with PBS. The nuclei were counterstained with hematoxylin for 4 minutes, followed by two washing steps with PBS. One drop of Aquamount was added on the section and a coverslip was mounted on the slide. Slides were left to dry overnight. Images of pancreas sections were acquired with an Axioscope 2 microscope with a 40x objective (Zeiss). The software BZII Analyzer by Keyence was used for the quantification of the IHC pictures (Figure 4). Sections were also scanned with NanoZoomer S360 Digital slide scanner.

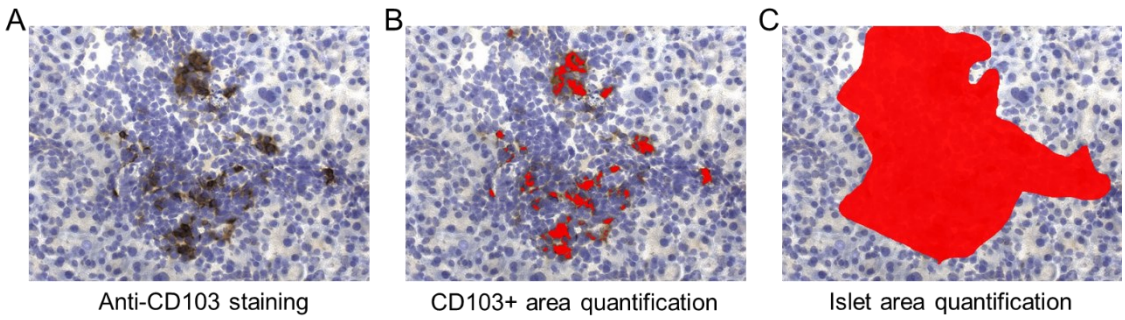

Figure 4. Example of staining quantification.
(A) Immunohistochemical staining with anti-CD103 antibody of one islet of Langerhans in one section of pancreas. - (B) Quantification of the CD103+ area (brown signal) in the islet with the Hue function of the BZII Analyzer software by Keyence. - (C) Islet area quantification with main function of the BZII Analyzer software by Keyence. The result is then expressed as percentage of positive CD103 area (B) per islet area (C).

5.2.6 Insulitis score

Insulitis quantification was done using pancreas sections stained for insulin as described above and scored according to the following system: Score 0: Very minor or no insulitis, only very few infiltrating cells; score 1: mild to moderate insulitis, 25-50% infiltrations, large parts with intact β-cells; score 2: considerable insulitis, 50-75% infiltrates, still some parts with intact β-cells; score 3: massive insulitis, 75-100% infiltrates, only few remaining β-cells producing insulin, islet scar.

5.2.7 Immunofluorescence

The pancreata were processed as described for immunohistochemistry. The sections of pancreas were fixed in EtOH or ethanol/acetone (1:1) at -20°C for 15 minutes. After removing the OCT, circles were drawn around the tissues with a wax pen. The slides were then washed two times for 2 minutes in PBS and incubated at RT for 10 minutes with 0.3% H_2O_2/0.1% Na-azide in PBS. The tissues were then washed and blocked with 10% FCS/PBS for 30 minutes at RT. Without washing, primary antibodies (goat anti-CD103 antibody 1:100 and Armenian-hamster anti-CD11c antibody 1:200) were diluted in 10% FCS/PBS and applied on the slides overnight at 4°C in a humidified chamber. After tapping off the primary antibodies, the samples were washed three times for 4 minutes in PBS and then incubated with the secondary antibodies (anti-goat Cy3 1:50,

biotinylated anti-Armenian hamster antibody 1:400) for one hour at RT diluted in 10% FCS/PBS, adding DAPI (1:5000) to stain for the nuclei. After washing the slides three times for 4 minutes in PBS, streptavidin-FITC was diluted 1:500 in 10% FCS/PBS and applied on the slides for 30 minutes. The slides were washed again 3 times for 4 minutes and one drop of Fluoromount G was added on each tissue and a coverslip was put on top. The sides of the coverslip were sealed off with some nail polisher. The slides were kept in the dark at 4°C and the images were acquired as soon as possible. Images of pancreas sections were acquired with confocal microscope LSM510 (Zeiss). The software BZII Analyzer by Keyence was used for the quantification of the immunofluorescent pictures with fluorescence function, as described in the previous paragraph.

5.2.8 Immunofluorescence – Venus signal

Once the pancreas was dissected from the mouse, it was immediately post-fixed in PFA, Lysine, Periodate (PLP) buffer for at least 3 hours, shaking at 4°C. It was then incubated first in sucrose 15% in water for 12 hours and then in sucrose 30% in water to dehydrate the sample. Finally, it was embedded in Tissue-Tek OCT and quick frozen on dry ice. The OCT blocks were stored at -80°C as well as the 7 µm slides once cut. The slides were fixed with EtOH 100% at -20°C for 15 minutes. OCT was removed, and a circle was drawn around each tissue with a wax pen. After washing two times for 2 minutes with PBS at RT, the unspecific reactions were blocked with 10% FCS/PBS for 30 minutes at RT. The samples were then incubated for 1 hour at room temperature with DAPI (1:5000) in 10% FCS/PBS. At the end, the slides were washed three times in PBS for 4 minutes and then one drop of Fluoromount G was added on the tissue. The coverslip was lied on top, and the sides were sealed off with some nail polisher. The images were acquired with confocal microscope LSM510 (Zeiss). BZII Analyzer by Keyence was used for the quantification of the immunofluorescent pictures, as previously described.

5.2.9 Whole pancreas 3D-staining

This protocol is a modified version of the iDISCO+ protocol.[131] The mouse was anesthetized with isoflurane and perfused through the heart with 10 ml 4% buffered PFA. The pancreas was then removed and incubated shaking for two hours at RT in 5 ml 4% buffered PFA. The sample was then washed with PBS/0.2% Tween-20 two times for one hour and incubated shaking overnight with the pre-treatment buffer 1 (PBS/0.2% Triton X/20% DMSO) at 37°C. The next day, the solution was changed to pre-treatment buffer 2 (PBS/0.1% Triton X/0.1% Deoxycholate/0.1% NP40/20% DMSO) for another overnight incubation, again shaking at 37°C. The pancreas was washed two times for one hour with PBS/0.2% Tween-20 and incubated with a permeabilization buffer (PBS/0.2% Tween 20/5% DMSO/2.3% glycine/0.02% NaN_3) for two days at 37°C shaking. Blocking was performed with a filtered blocking solution (PBS/0.2% Triton X-100/10% DMSO/6% donkey serum) for two days at 37°C shaking. Following this, the incubation with rabbit anti-insulin as first antibody started. The antibody was diluted in first antibody buffer (PBS/5% DMSO/3% donkey serum/0.2% Tween 20 with 10 µg/ml heparin) and the antibody concentration was increased every day (1:3200, 1:2000, 1:1600, 1:800). The sample was incubated shacking at 37°C during the day and centrifuged at 600 x g at RT overnight. The pancreas was then washed four times for one hour and one time overnight with PBS/0.2% Tween-20 with 10 µg/ml heparin (PTwH). The secondary antibody incubation was performed in the same way as the first one using an anti-rabbit Cy3 antibody at increased concentration of 1:800, 1:600, 1:400, 1:200 in secondary antibody buffer (PBS/3% donkey serum/0.2% Tween 20 with 10 µg/ml heparin). After washing again with PTwH as described above, the pancreas was embedded in a 1.3% low-melting agarose/H_2O solution. After the gel solidification, the sample was dehydrated, by incubating with tetrahydrofuran at increasing concentration in water, shaking: 50% overnight at 4°C, 70% two hours at RT, 80% two hours at RT, 100% two hours at RT, and 100% overnight at 4°C. The lipids were removed from the sample with dichloromethane with an incubation of 30 minutes at RT, shaking. The sample was then cleared with dibenzyl ether, overnight shaking and then stored in the same buffer until acquisition.

5.2.10 Whole pancreas acquisition and quantification

The whole stained pancreas was acquired in dibenzyl ether with the ultramicroscope Olympus MVX10, from LaVisionBiotec, with SuperKExtreme from NKTPhotonics as lasers and Neo 5.5 Coms as camera. The programme used for the acquisition is Imspector Pro. Once scanned, the images were analysed and quantified with Imaris 9.8.2. (Figure 5).

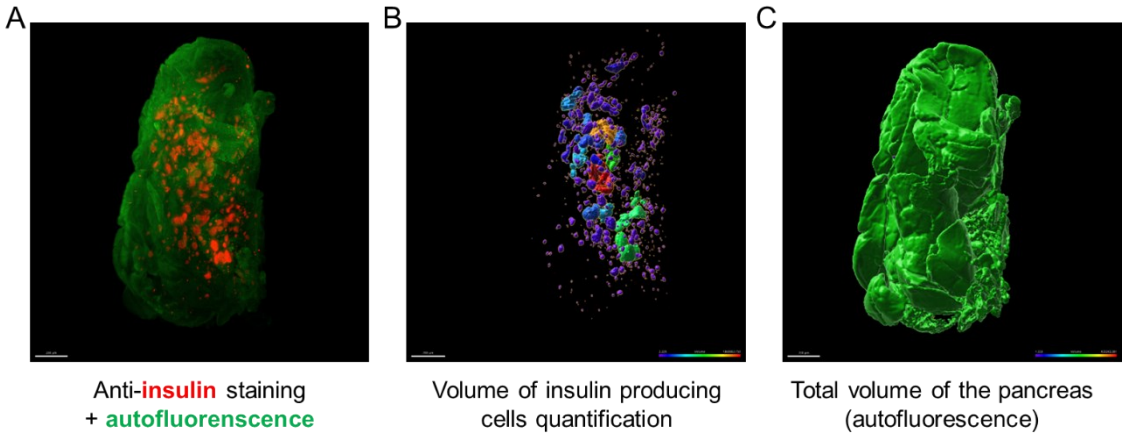

Figure 5. Example of quantification of 3D-pancreas staining with anti-insulin antibody. (A) Example of a 3D-staining of a healthy, uninfected murine pancreas with anti-insulin antibody (red) and the autofluorescence of the pancreas (green). - (B) Quantification of the insulin producing cell volume, reported in a colour code according to the islet volume size with Imaris 9.8.2 software. - (C) Total volume of the pancreas, quantified using the autofluorescence given by the pancreas with Imaris 9.8.2 software.

5.2.11 Isolation of islet infiltrating cells

Islets were isolated as previously described.[132] Briefly, pancreas was isolated, the PDLN were removed, and the pancreas was transferred to a falcon containing 5 ml RPMI. These 5 ml were then removed and the pancreas was injected with 1.2 U/ml collagenase P in 3 ml of RPMI and 7 ml of warm RPMI were added. The sample was digested for 30 minutes at 37°C. Digestion was stopped by removing the warm RPMI and adding 10 ml of cold RPMI. Pancreas was disaggregated by shaking the tube for 1 minute and then squeezing it through a kitchen sieve. After spinning down the sample for 2 minutes at 220 x g at RT, the pellet was resuspended in 10 ml of pre-warmed Ficoll-Paque and was overlayed by 5 ml of pre-warmed RPMI. The gradient was then centrifuged at 860 x g for 13 minutes at RT with both acceleration and break set at 1. Islets were isolated combining

the interface with the hand-picked islets from the pellet. Then they were centrifuged at 860 x g for 5 minutes at 4°C and resuspended with a tip to break them and get the cells in suspension. To avoid the exocrine part of the pancreas and isolate only the islet infiltrating cells, CD45 Microbeads (Miltenyi Biotec) were applied, following the company protocol. At the end, the cells were resuspended in FACS buffer for surface marker staining or in RPMI complete for intracellular cytokine staining (ICCS, see below).

5.2.12 Isolation of splenocytes

Spleen was isolated and collected in a 15 ml falcon tube with 5 ml RPMI complete. The spleen was then squeezed through a 70 µm strainer placed on a petri dish containing medium. The solution was washed 2-3 times through the strainer. The cell suspension was centrifuged at 550 x g for 5 minutes at 4°C and the supernatant was discarded. Erythrocyte lysis was performed adding 2 ml of 0.83% NH_4Cl/H_2O for 2 minutes. The lysis was stopped by filling the tube with ice-cold RPMI. The supernatant was transferred to new tubes avoiding the lysed cells. The sample was centrifuged at 550 x g for 5 minutes at 4°C. The supernatant was aspirated, the cells were resuspended and washed with 10 ml RPMI. The cell suspension was transferred to a new tube pipetting slowly with a 10 ml pipette kept horizontally, to avoid aggregated debris. The cells were centrifuged again with the same settings and were resuspended in the final volume of FACS buffer or RPMI complete according to the pellet size and to the assay that was following.

5.2.13 Isolation of leukocytes from pancreatic draining lymph nodes

PDLN were isolated while removing the pancreas. They were collected in a 15 ml falcon tube with 5 ml RPMI complete. The PDLN were then squeezed through a 70 µm strainer placed on a petri dish containing medium. The solution was washed 2-3 times through the strainer to remove any fat tissue left. The cells were centrifuged at 550 x g for 5 minutes at 4°C and the supernatant was discarded. The cells were resuspended in the final volume of FACS buffer or RPMI complete according to the assay that was following.

5.2.14 Surface marker staining for flow cytometry

Single-cell suspensions of islet infiltrating cells, PDLN cells, and splenocytes were plated in V-bottom plates and washed two times with FACS buffer. They were blocked with 10 µl/well of anti-CD16/CD32 diluted 1:10 in FACS buffer for at least 15 minutes at 4°C. Afterwards, cells were stained for surface expression: 50 µl/well of the different antibody mixes were applied for at least 30 minutes at 4°C. The plates were then washed with FACS buffer two times at 550 x g for 3 minutes at 4°C. Finally, the samples were fixed with FACS/PFA adding 200 µl/well and transferred to FACS tubes. Samples were acquired with a MACSQuant Analyzer 10 and the data were analysed with FlowLogic 7.3 (Inivai Technologies Pty Ltd.).

5.2.15 Intracellular cytokine staining (ICCS)

Single-cell suspensions of islet infiltrating cells, PDLN cells, and splenocytes were plated in U-bottom plates and stimulated overnight with the immunodominant LCMV peptides GP33 (10 µg/mL) for CD8 T cells and GP61 (10 µg/ml) for CD4 T cells in the presence of Brefeldin A (1 µg/mL) at 37°C with 5% CO_2. The day after, cells were first transferred to V-bottom plates and then washed two times with FACS buffer. They were blocked with 10 µl/well of anti-CD16/CD32 antibodies diluted 1:10 in FACS buffer for at least 15 minutes at 4°C. Afterwards, cells were stained for surface expression: 50 µl/well of the different antibody mixes were applied for at least 30 minutes at 4°C. The samples were then permeabilized with 100 µl/well of PFA/saponin for 10 minutes at RT in the dark. The plates were centrifuged at 550 x g for 6 minutes at 4°C and the supernatant was discarded. They were then washed two times with FACS/saponin and centrifuged at the same conditions. The cells were stained for intracellular cytokines, adding 50 µl/well of the mixture of antibodies and incubating for at least 30 minutes at 4°C. After adding 100 µl/well of FACS/saponin buffer, the plates were centrifuged at 550 x g for 5 minutes at 4°C. The plates were then washed two times with FACS/saponin and one time with FACS buffer. Finally, the samples were fixed adding 200 µl/well of FACS/PFA and transferred to FACS tubes. Samples were acquired with a MACSQuant

Analyzer 10 and the data were analysed with FlowLogic 7.3 (Inivai Technologies Pty Ltd.).

5.2.16 Cell culture

MC57 is a fibrosarcoma cell line established from a tumour arising in a C57BL/6 mouse after treatment with methylcholanthrene. This cell line is useful in the plaque assay because it can be quickly infected. Cells were kept in liquid nitrogen and thawed at least two weeks before the assay. Cells were cultivated with RPMI with 7% FCS and 1% penicillin/streptomycin (P/S). After taking them out from the liquid nitrogen, they were transferred to a falcon tube and spun down at 180 x g per 5 minutes. The cells were resuspended in their medium and split in 75 cm^2 flasks. Cells were cultured in the incubator at 37°C with 5% CO_2. Cells were split twice a week using RPMI with 7% FCS and 1% P/S.

5.2.17 Plaque assay

Plaque assay was performed as previously described.[133]

Spleens:

Spleens of different lines (RIP-GP, RIP-GP x $XCL1^{-/-}$, RIP-GP x $XCR1^{-/-}$, and RIP-GP x $CXCL10^{-/-}$ x $XCL1^{-/-}$ mice) were dissected from the mice at different time points (day 3 and day 7) after infection. The spleens were weighted and immediately frozen in liquid nitrogen. They were stored at -80°C until the day of the experiment. Spleens were then homogenized adding 1 ml of DMEM/2% FCS per 0.1 g of tissue. They were centrifuged at 300 x g for 5 minutes at 4°C. Then the supernatant was used for virus calculation. A round-bottom 96-well-plate was prepared by adding 130 µL of DMEM/1% P/S/2% FCS from column 2-11. 200 µL of each homogenized spleen sample were added to the first column of the plate. To obtain duplicates, each sample was added into four wells. Dilutions of the samples were performed with a multichannel pipette by taking 60 µL from the first column to the second and so on. In this way, in every third column the samples were diluted 10 times more.

MC57 cells:

In parallel, MC57 cells were removed from the flasks and centrifuged at 180 x g for 5 minutes at 4°C. Cells were resuspended in 10 ml of RPMI/7% FCS/1% P/S. They were stored on ice, while counting them with trypan blue. Cells were diluted to the concentration of 8 x 10^5 cells/ml with RPMI/7% FCS/1% P/S. Using a multi-channel pipette, 200 µL of MC57 cells were added to each well of a 24-well-plate and 200 µl of the diluted spleens were added to the cells, using only column 11, 9, 7, 5, 3, to have serial dilutions. To two wells per plate LCMV was added in two different dilutions as a positive control. To two wells per plate only medium was added as negative control.

Incubation and overlay:

After mixing the cells and the samples, the plates were placed in the incubator at 37°C with 5% CO_2 and 95% humidity for 4 hours, until the cells formed a monolayer. The cells were then overlayed using a 10 ml plastic pipette with four drops of a mix of DMEM 2x/2% P/S/20% FCS and 2% methylcellulose 1:1. The plates were incubated for 2 days at 37°C with 5% CO_2 and 95% humidity.

Staining:

After checking if the cells had formed a confluent monolayer, a staining of the plaques was performed. Once the supernatant was removed, 1.5 ml of 4% buffered PFA were added to each well to fix the cells and kill the virus and incubated for 30 minutes at RT. After PFA removal, 240 µL 1% Triton X-100 solution were applied for 20 minutes at RT. Triton X-100 was aspirated, and then 240 µL of a blocking solution (10% FCS/PBS) were added to each well for one hour at RT. The first antibody VL-4 rat anti-LCMV was diluted 1:2 in 1% FCS/PBS and incubated for 1 hour at RT. After washing 2 times for 5 minutes with 0.5 ml PBS per well, the secondary antibody peroxidase–conjugate AffiniPure goat anti-rat IgG (H+L) was added (240 µL per well; 1:400 in 1% FCS/PBS) for 1 hour at RT. The wells were washed again as described and 400 µL of DAB substrate were added and the plates were incubated for 5 minutes at RT in the dark. The DAB substrate for three plates was prepared using 0.6 ml aliquot of DAB in water (final volume 15 ml), adding 0.75 ml Tris (1M pH 7.5), 5.1 µL H_2O_2 (30%), one drop of Nickel (from the DAB kit by Vector Laboratories). DAB was flicked off and the plates were washed with water and let them dry.

The plaques were then counted, and this formula was applied:

$$Titer = \frac{(h*10)+l}{2} * (dilution\ factor\ of\ lower\ dilution) * 5\ [pfu/ml]$$

Where "*h"* is the number of foci with the higher dilution (less foci); *"l"* is the number of foci with the lower dilution (more foci); x 5 =200 µl were added→ /200 x 1000

5.2.18 *In vivo* cytotoxic T lymphocyte (CTL) assay

Here carboxyfluorescein succinimidyl ester (CFSE)-loaded target cells were injected into uninfected RIP-GP, infected RIP-GP, and RIP-GP x XCL1$^{-/-}$ recipient mice at day 28 post-infection.

Target cells:

On the day before the experiment, the spleens of the donor mice were collected and three of them were transferred to 15 ml falcon tubes with 10 ml of RPMI complete. Splenocytes were isolated as described above (see paragraph 5.2.12). After the lysis, the cells were resuspended in 20 ml of RPMI complete and counted with MACSQuant Analyzer 10, after diluting them 1:10 with FACS buffer. Cells were diluted to 5 x 10^6 cells/ml with RPMI complete. They were then split in two groups: one was labelled with GP33 at a concentration of 2 µg/ml (GP33+ fraction) and the other one was not labelled (GP33- fraction). The cells where then plated in big petri dishes in 10-11 ml/dish. They were placed overnight in the incubator at 37°C with 5% CO_2. On the day of the experiment, the cells were harvested, using a cell scraper and they were centrifuged at 550 x g for 5 minutes at 4°C. After discarding the supernatant, the cells were resuspended in 20 ml RPMI without FCS because it might interfere with the binding of CFSE. The cells were counted again with MACSQuant Analyzer 10 and diluted to a concentration of 5 x 10^6 cells/ml with RPMI. CFSE was added in a concentration of 5 µM to the GP33- cells ($CFSE^{hi}$) and of 0.5 µM to the GP33+ cells ($CFSE^{lo}$) and incubated for 10 minutes in the dark at RT. Tubes were filled with RPMI complete and centrifuged at 550 x g for 5 minutes at 4°C. After discarding the supernatant, cells were washed with 20 ml of RPMI complete and centrifuged at the same conditions than before. This washing step was repeated. Cells were counted and diluted to 5 x 10^7 cells/ml with RPMI without FCS since they needed to be injected.

Injection into recipient mice and flow cytometry:

The GP33+ and the GP33- fractions were mixed and 200 µl of this mixture were intravenously (i.v.) injected to each of the uninfected RIP-GP, infected RIP-GP, and infected RIP-GP x XCL1$^{-/-}$ recipient mice (0.5 x 10^7 cells GP33+ and 0.5 x 10^7 cells GP33-). Blood was collected after 10 minutes, 1 hour, 4 hours, 24 hours, and 48 hours after the injection and directly added to 10 ml of 0.74% NH_4Cl/H_2O in a 50 ml falcon. Cells were kept on ice up to 2 hours and the tubes were filled with cold RPMI to stop the lysis. The samples were then centrifuged at 550 x g for 5 minutes at 4°C. The supernatant was discarded, and the cells were resuspended in 200 µl of FACS/PFA. They were acquired with MACSQuant Analyzer 10 and the ratio between the % of CFSE low and high after 10 minutes after injection was used to normalize the data. All the consecutive points were calculated as % of this ratio.

5.2.19 Mouse genotyping: DNA extraction

The ear tag from the mouse was added with 550 µL of mouse tail buffer supplemented with Proteinase K (10 mg/ml stock) 1:100 diluted in the buffer, and it was incubated overnight at 55°C. The morning after, the tube was quickly spun down and the content was transferred to a safe-lock tube. 75 µl 8 M kalium acetate were added to the sample and after mixing, also 500 µL of chloroform were added. The sample was moved to a box, shaken, and put in the box at -80°C for at least 15 minutes. It was then taken out and spun at 16000 x g for 10 minutes at 4°C in a microcentrifuge. The supernatant was transferred to a non-safe lock tube and 1 ml 100% EtOH was added at RT. The sample was put in the fridge overnight and the following day, it was spun at 16000 x g for 10 minutes at 4°C. The supernatant was roughly removed with a blue tip without touching the pellet. 1 ml of 70% EtOH was added at RT and the tube was gently mixed and spun at 16000 x g for 10 minutes at 4°C. The supernatant was removed as much as possible, first using a blue tip and then a yellow tip, and the tube was left open, so that the pellet could dry. The DNA was resuspended in 200 µL TE buffer and stored at 4°C for short-term storage or -20°C for long-term storage.

5.2.20 Mouse genotyping: RIP-GP PCR

The PCR was used to amplify the expression of the RIP-GP gene in order to genotype the mice. 1 µl of extracted DNA was added to the master mix reported in *Table 14*.

Table 14: Master mix composition for one sample.

	1 x
Aqua dest.	15.5 µl
10 x Buffer	2.0 µl
10 mM dNTP - Mix	0.5 µl
10 µM GP - 3' - Primer	0.5 µl
10 µM GP - 5' - Primer	0.5 µl
TAQ -Polymerase	0.1 µl
DNA	1.0 µl
	20.1 µl

Primer Sequences:

GP - GP 3': 5' GGG AAA GCA GAA TCC TGG AC 3'

GP - GP 5': 5' GCA ATC TGA CCT CTG CCT TC 3'

C57BL/6 DNA was used as a negative control, whereas confirmed RIP-GP DNA was used as a positive control. The samples prepared as described were then put a PCR cycler. After the initialization phase (3 minutes at 94°C), 35 cycles were performed as following:

- Denaturation phase: 45 seconds at 94°C
- Annealing step: 45 seconds at 55°C
- Elongation phase: 1 minute at 72°C

At the end of the process, the samples were kept at 4°C.

5.2.21 Mouse genotyping: DNA agarose gel electrophoresis

Agarose 1% in TAE buffer was prepared and put in in the microwave until it was dissolved. 6 µL of Gel Red were added into the bottle of agarose. The chamber for the gel was prepared and the combs were inserted. The agarose was slowly poured into the chamber and left there at least one hour to solidify. The samples were prepared, adding 6 µL of Loading Gel buffer 6x to each of them. The gel was moved in the running system, covered with TAE 1x buffer and the combs were removed. In the first well, the marker solution was loaded, followed by all the samples. The gel was run with a voltage of 100 volt for at least 15 minutes. The image was acquired using a 300 nm transilluminator.

5.2.22 Statistical evaluations

The statistical analysis of the experiments was done using Mann Whitney t test, with the exception of BG mean values comparison that were analysed with 2way Anova with Bonferroni as post-test (Prismsoftware version 5.02 and version 10; GraphPad).

6. Results

In the present work, I first assessed the presence and the upregulation of selected chemokine ligands and their receptors in the islets of LCMV-infected RIP-GP mice to confirm the data that have been obtained earlier in our lab. These initial data had been generated via laser dissection of the islet microenvironment followed by expression analysis on gene arrays by Christine Bender. I used the RNAscope technology to localize upregulated chemokine axes in pancreas sections. Afterwards, I focused my attention on the main part of my PhD thesis, namely the investigation of the role of the XCL1/XCR1 chemokine axis, which was highly and persistently upregulated in T1D. To achieve my goal, I first evaluated the XCL1 and XCR1 expression in human pancreas sections obtained from individuals at different disease stages. Once determined the importance of this axis, I used either XCL1-deficient or XCR1-deficient RIP-GP mice to further investigate the role of this axis. Finally, I investigated the development of T1D in the RIP-GP x CXCL10$^{-/-}$ x XCL1$^{-/-}$ mice to see if a potential combination blockade of these two important chemokine axes might be beneficial as treatment for T1D.

6.1 Localization of several chemokine axes in RIP-GP mice islets

As already mentioned, a laser dissection of the islet microenvironment followed by gene array was performed by Christine Bender in our lab. The mice had been infected with 10^4 pfu of LCMV and the islets were analysed at day 1, 3, 7, 10, 14, and 28. The results can be visualized via volcano blots (Figure 6). The first element to highlight is that most of the genes were upregulated rather than downregulated during T1D progress in RIP-GP mice. These genes can be grouped in different ways, in this case the attention was focused on the expression kinetics of chemokine ligands and receptors. Almost all chemokine ligands and receptors were upregulated during T1D development. Most chemokines had a similar kinetics, with a peak of expression around day 7-10 after LCMV-infection. The expression of their receptors was slightly delayed. Importantly, some chemokines stayed elevated until day 28, meaning that they are important during the chronic phase of T1D. The focus was first moved on four different chemokine-receptor axes: CCL5/CCR1,3,5, CXCL10/CXCR3,

CXCL16/CXCR6, and CX_3CL1/CX_3CR1 (Figure 6*A*). Their expression was assessed by quantitative real-time PCR (qPCR), which confirmed the pattern seen with the gene array analysis (Figure 6*B*).

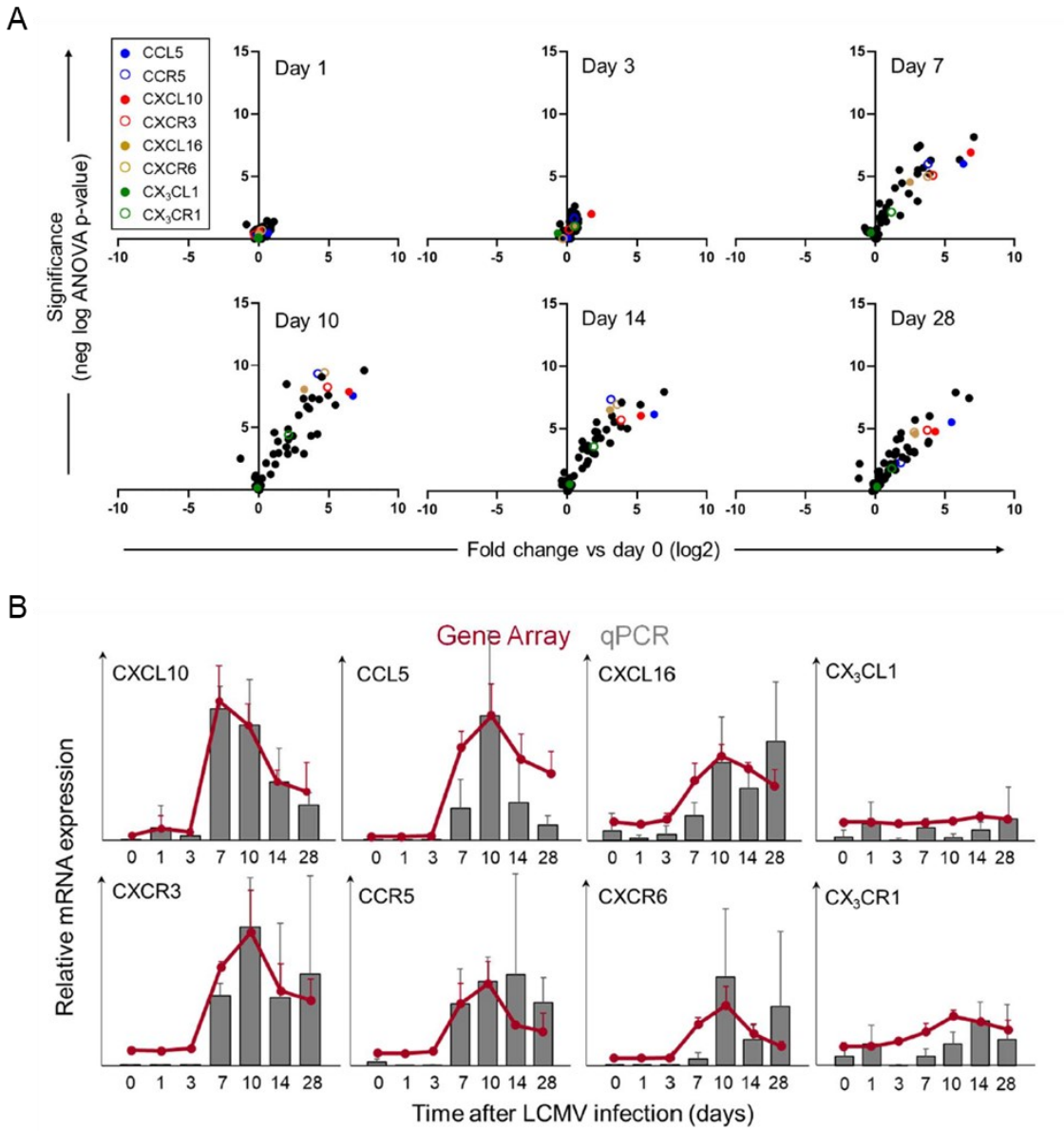

Figure 6. Expression of different chemokine axes in the islet microenvironment after LCMV-infection.

(A) Volcano blots of gene expression of chemokine ligands and receptors in the islet microenvironment of LCMV-infected mice at days 1, 3, 7, 10, 14, and 28 in comparison to uninfected mice. The chemokine axes CCL5/CCR5, CXCL10/CXCR3, CXCL16/CXCR6, and CX_3CL1/CX_3CR1 are highlighted in colour. Note that starting at day 7 post-infection the vast majority of chemokine ligands and receptors are upregulated and remain highly expressed during the chronic phase of T1D. - (B) Confirmation of the expression of the selected chemokine axes CCL5/CCR5, CXCL10/CXCR3, CXCL16/CXCR6, and CX_3CL1/CX_3CR1 by quantitative real-time PCR of the same islet microenvironment RNA that has been used for gene array analysis.

I performed then the duplex RNAscope technique to visualize both the chemokines and the receptors in the tissue. Finally, their expression was further assessed via IHC, which I contributed to perform. The duplex RNAscope *in situ* hybridization technique allows to stain for mRNA producing cells and it was used on pancreas slides of RIP-GP mice at day 0, day 10, and day 28 after infection (Figure 7). All four chemokine ligand/receptor pairs were stained. No or just a weak signal was detected at day 0, in uninfected mice. In contrast, at day 10 and day 28 all chemokines and receptors were localized in the islets. The kinetics confirmed the data obtained in the gene array analysis. In particular, CCL5 was highly upregulated at day 10 in the islets, both in the gene array and in the RNAscope staining. Moreover, the slow but persistent expression of CX_3CL1 and the upregulation of CXCL16 were evident in the stained tissue (Figure 7).

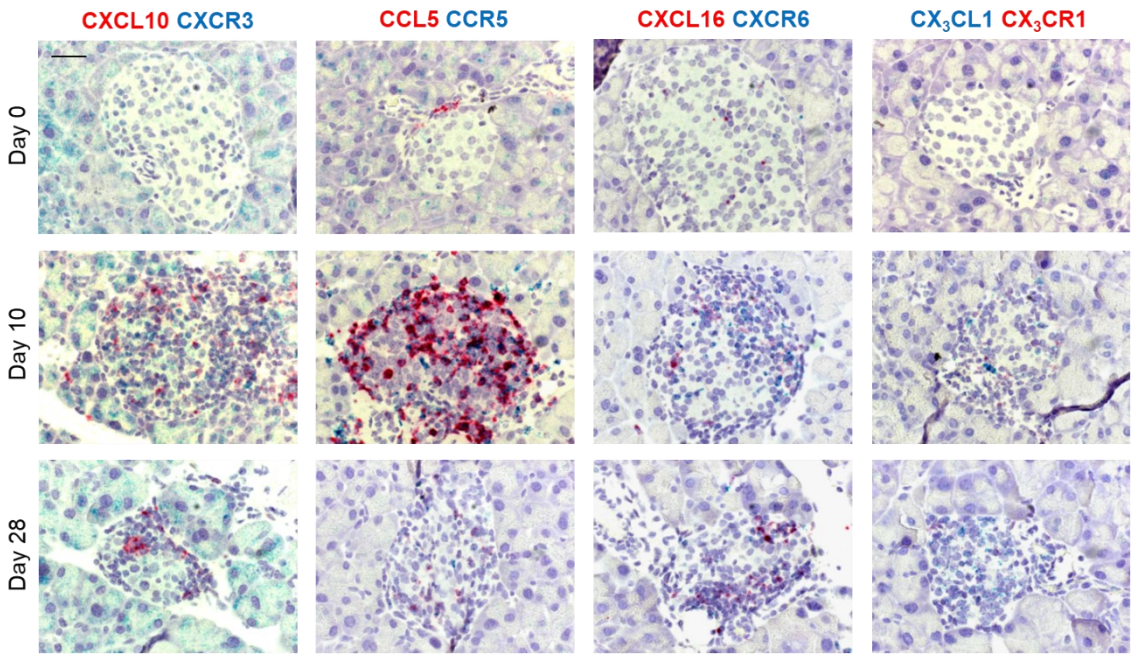

Figure 7. CCL5/CCR5, CXCL10/CXCR3, CXCL16/CXCR6, and CX_3CL1/CX_3CR1 are expressed in the RIP-GP islets upon infection.
Duplex RNAscope assay for CCL5/CCR5, CXCL10/CXCR3, CXCL16/CXCR6, and CX_3CL1/CX_3CR1 of tissue sections of pancreata of RIP-GP mice obtained at days 0, 10, and 28 after LCMV-infection. Note that the colours of the chemokine and the receptor are indicated and change among the different pairs. Original magnification 63x oil. Scale bar 20 µm.

In order to further confirm the expression on the protein level, IHC was performed with pancreas sections obtained at day 28 post-infection (Figure 8). CXCL10 was mainly localized in the β-cell region, confirming previous findings that β-cells

themselves can produce CXCL10.[62] In contrast, CCL5, CXCL16, and CX_3CL1, and all their receptors were expressed by infiltrating cells (Figure 8). Since it was not possible to find a good antibody for CXCR6, RIP-GP x CXCR6$^{gfp/+}$ mice were used. For IHC, an anti-GFP antibody was used.

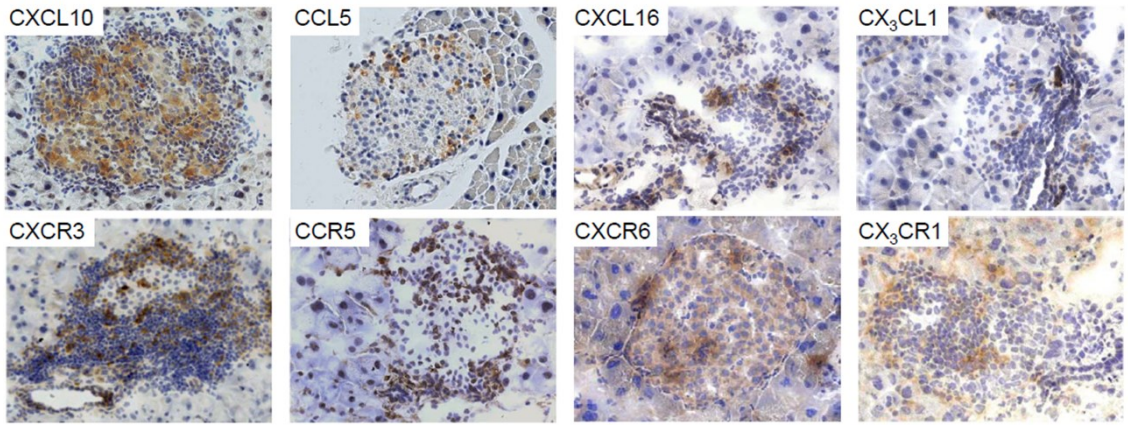

Figure 8. Localization of chemokine/receptor pairs on a protein level.
Immunohistochemistry for CCL5/CCR5, CXCL10/CXCR3, CXCL16/CXCR6, and CX_3CL1/CX_3CR1 protein expression on RIP-GP pancreas sections at day 28 post LCMV-infection. Note that due to the lack of an appropriate antibody, the expression of CXCR6 was demonstrated in RIP-GP x CXCR6$^{gfp/+}$ mice using an anti-GFP antibody.

To sum up the results obtained from these preliminary data that I contributed to obtain:

- The role of CXCL10/CXCR3 axis was already investigated by our group and described as important in the T1D pathogenesis. These new findings confirm its role. Moreover, it has been shown that the CXCL10/CXCR3 axis can be a useful target in establishing a therapy against T1D.[47,48,132]
- Surprisingly, the absence of CCL5 was not affecting T1D incidence in RIP-GP and RIP-NP mice.
- Both CXCR6- and CX_3CR1-deficient mice showed a decreased T1D incidence both in the RIP-GP and in the RIP-NP mouse model. Moreover, the CX_3CR1-deficient mice showed also reduced insulitis.

The submitted paper with these results can be found in the Appendix (see paragraph 10.4).

6.2 Localization of XCL1 and XCR1

6.2.1 XCL1 and XCR1 are upregulated in the islets of infected RIP-GP mice and pre-diabetic NOD mice

Among all the chemokines and receptors that are upregulated after LCMV-infection, another pair turned out to be particularly interesting. The data obtained from the gene array demonstrated that the chemokine XCL1 and its receptor XCR1 are increased from day 7 after infection and remain upregulated also at day 28 when the disease is already chronic. The peak of the expression of XCL1 is between day 7 and day 10 and of XCR1 at day 10 (Figure 1). To visualize and confirm that both XCL1 and XCR1 are in the islets of the RIP-GP mice, RNAscope *in situ* hybridization technique was used to stain the pancreas sections for XCL1 in red and XCR1 in blue (Figure 9). At day 0, neither XCL1 nor XCR1 mRNA producing cells were present in the islets. They started to appear at day 7, with an increasing production between day 10 and day 14. At day 28, the presence of both the ligand and the receptor was decreased but they were both still present in the islets. Importantly, they were produced by cells localizing among the infiltrating cells that migrated to the islets during T1D pathogenesis.

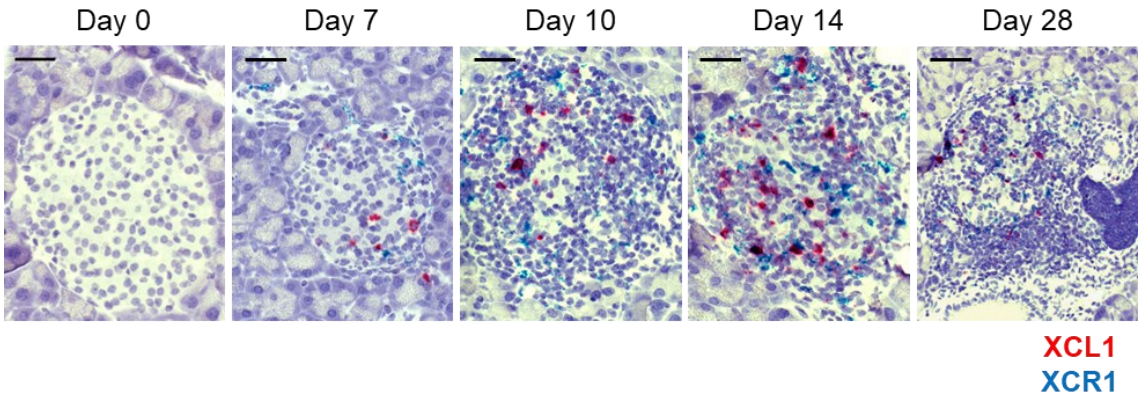

Figure 9. XCL1 and XCR1 are upregulated in the islets of RIP-GP mice upon infection. Duplex RNAscope *in situ* hybridization of XCL1 (red) and XCR1 (blue) on pancreas tissue slices from RIP-GP mice at day 0, 7, 10, 14, 28 after infection. Representative images are displayed per each time point. Original magnification 63x (oil). Scale bars represent 20 µm.

Sections of NOD mice were also stained with RNAscope *in situ* hybridization technique to demonstrate that XCL1 and XCR1 are also present in another mouse model of T1D, independently from virus infection. Representative images

of islets at different ages and stages of disease of NOD mice are shown (Figure 10). At week 6, when the mice were still young and not a lot of immune cells were infiltrating in the islets, only few cells produced XCR1 mRNA. At week 12, even when the mice were not diabetic, many infiltrating cells started to appear in the islets and, among these, both XCR1 and XCL1 mRNA producing cells were present. Some of them were also in close proximity to each other, which might indicate a possible interaction. Pancreata were then obtained from NOD mice at week 22, when they started to become diabetic. The comparison between diabetic and non-diabetic mice showed that in the islets of non-diabetic mice there were cells producing both XCL1 and XCR1 mRNA, whereas in diabetic mice, the infiltrating cells were mainly expressing XCR1.

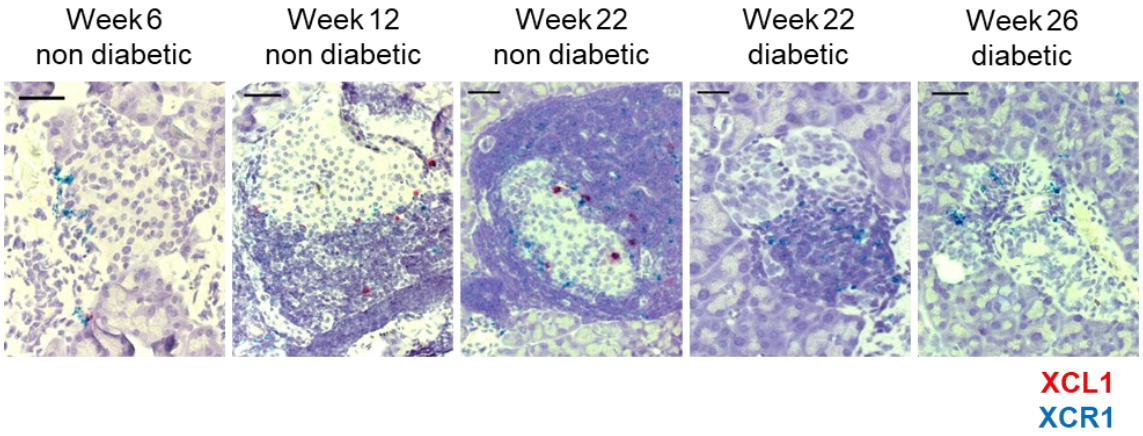

Figure 10. XCL1 and XCR1 are present in the islets of pre-diabetic and diabetic NOD mice. Duplex RNAscope *in situ* hybridization for XCL1 (red) and XCR1 (blue) of pancreas tissue slices from NOD mice obtained at different age and disease stage. Mice were considered diabetic with BG levels of >300 mg/dl. Original magnification 40x. Scale bars represent 25 µm.

6.2.2 XCL1 and XCR1 expression in human pancreas

Sections of human pancreas from individuals at different disease stages obtained through the HPAP programme were stained with RNAscope duplex technique for XCL1 and XCR1 producing cells. Pancreata from non-diabetic (ND), autoantibody-positive (Aab+), and patients with diagnosed T1D (T1D) were analysed (detailed information about the organ donors can be found in paragraph 5.2.3). Representative pictures of this staining are reported in Figure 11. Since the cells did show extensive signals, XCR1-expressing cells have been highlighted with an arrow. Tissue sections from Aab+ and T1D individuals

contained clearly more cells producing XCR1 mRNA compared to the pancreas of healthy controls. Interestingly these XCR1-positive cells were mostly found in or around the islets (black line). The XCL1-expressing cells have not been highlighted because only very few cells expressing XCL1 could be found in the analysed samples.

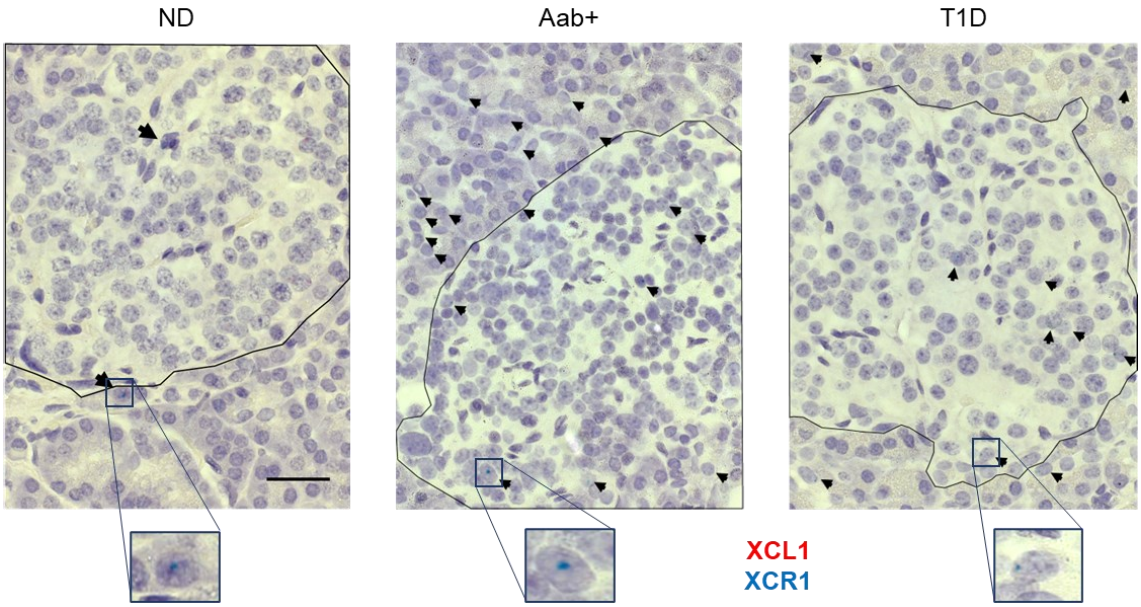

Figure 11. Representative pictures of XCL1 and XCR1 expression in human pancreas at different disease stage.
Duplex RNAscope *in situ* hybridization for XCL1 (red) and XCR1 (blue) of pancreas tissue slices from humans obtained through the HPAP programme. Human individuals were divided in non-diabetic (ND), autoantibody positive (Aab+), and diabetic (T1D) (see paragraph 5.2.3). XCR1-expressing cells are indicated with black arrows. Note that XCL1 expression is not indicated because only very few cells were found to be positive. In the square below the pictures, a zoom in for a positive cell is shown. The islets have been highlighted by the black line. Original magnification 63x. Scale bars represent 20 µm.

The XCR1-expressing cells were quantified, counting the positive cells in the islets and in the surrounding area. The mean for each tissue has been plotted and the results are shown in Figure 12*A*. Even though not significant due to the high variation of XCR1 cell numbers, in both Aab+ and T1D pancreata there were more XCR1+ cells per islet compared to ND control tissue. Moreover, in Aab+ and T1D patients most of the analysed islets had at least one cell expressing XCR1, contrary to the ND sections where the majority of islets do not contain any XCR1-positive cell at all. Surprisingly, almost no XCL1-positive cells were present in any pancreas, independently from the disease stage. This could be explained

both by a possible low number of CD8 T cells in the islets or by the transient RNA expression for the production of a chemokine. Therefore, the timing of the staining might be crucial to visualize the chemokine. In addition, the RNA stability over time in the collected tissue samples might also play a role, since I found that the expression of other chemokines, such as CXCL10, was clearly reduced in older samples.

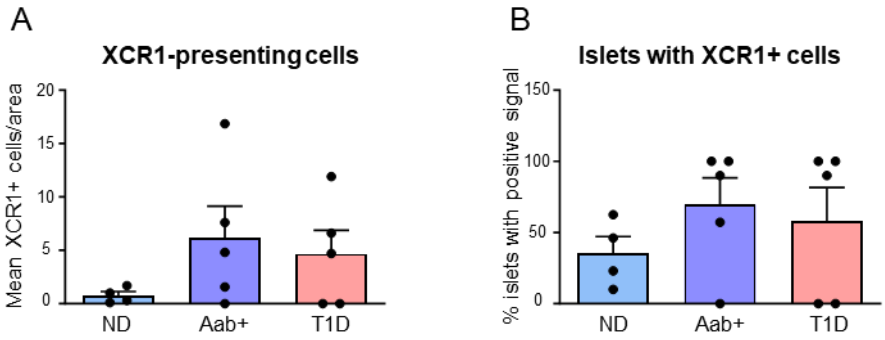

Figure 12. More cells express XCR1 in the islets of autoantibodies positive (Aab+) and T1D human samples.

Analysis of the RNAscope duplex staining. Human patients were divided in non-diabetic (ND), autoantibody positive (Aab+), and diabetic (T1D) (see paragraph 5.2.3). Number of islets analysed per section is 6-16. The mean for each patient is represented by each dot and the bars represent the mean ± SEM. (A) – Mean of XCR1-expressing cells per islet, including the surrounding area. (B) - Percentage of islets that show at least one cell expressing XCR1 per section. Note that one of the ND patients had to be excluded because of unclear designation of the disease stage.

6.2.3 XCL1 and XCR1 expression in XCL1- and XCR1-deficient mice

To investigate if the XCL1/XCR1 axis is important for the pathogenesis of T1D, XCL1-deficient RIP-GP mice were generated by crossing RIP-GP mice with $XCL1^{-/-}$ mice[73] and XCR1-deficient RIP-GP mice by crossing RIP-GP mice with $XCR1^{Venus/Venus}$ mice.[82] RIP-GP x $XCR1^{Venus/Venus}$ are here indicated as RIP-GP x $XCR1^{-/-}$ mice. To evaluate whether RIP-GP x $XCL1^{-/-}$ mice and RIP-GP x $XCR1^{-/-}$ mice were generally immunosuppressed, an LCMV plaque assay was performed. Spleens from regular RIP-GP mice and from both XCL1- and XCR1-deficient RIP-GP mice were isolated at day 3 and day 7 post-infection and after processing them, they were incubated with MC57 cells. After staining with anti-LCMV antibody, virus plaques were counted. The elimination of LCMV after infection was not altered neither in XCL1- nor in XCR1-deficient RIP-GP mice in

comparison with regular RIP-GP mice (Figure 13). These data also confirmed that the RIP-GP model as such is not influenced by an aberrant virus elimination neither in RIP-GP x XCL1$^{-/-}$ mice nor in RIP-GP x XCR1$^{-/-}$ mice. Note that at day 7 most of the virus was eliminated and in all the mouse lines the virus titre left was below the limit of detection of the assay.

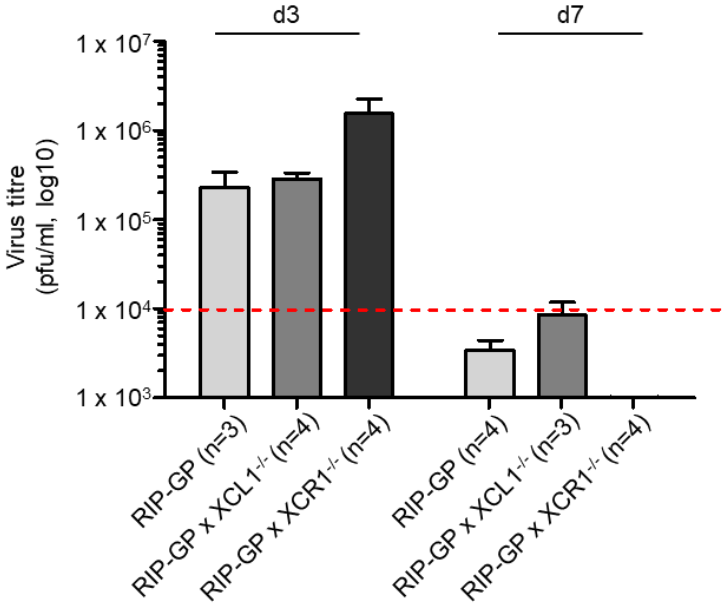

Figure 13. No differences in the virus elimination efficacy among the different mouse lines. Virus titre expressed in pfu/ml of LCMV left in spleens obtained via plaque assay. Spleens were collected from different mouse lines (RIP-GP, RIP-GP x XCL1$^{-/-}$, and RIP-GP x XCR1$^{-/-}$ mice) at day 3 and at day 7 after the infection. Results are displayed as mean ± SEM. Red dot line represents the limit of detection of this technique. Numbers of mice are indicated in brackets.

To further demonstrate the knock-out status of the RIP-GP x XCL1$^{-/-}$ and RIP-GP x XCR1$^{-/-}$ mice a duplex RNAscope *in situ* hybridization was performed, staining for both the chemokine and the receptor. In XCL1-deficient mice, the results showed that the chemokine was indeed not expressed in the islets, but that XCR1 was still expressed in the islets of the RIP-GP x XCL1$^{-/-}$ mice, starting from day 7 after infection (Figure 14). This indicates that XCR1+ infiltrating cells are also attracted to the islets in absence of XCL1.

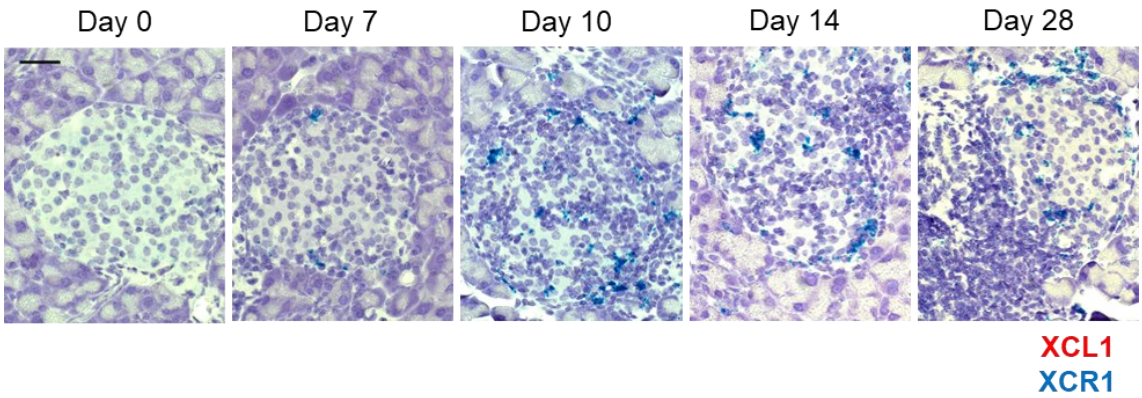

Figure 14. XCR1-expressing cells infiltrate the islets in absence of XCL1.
Duplex RNAscope *in situ* hybridization for XCL1 (red) and XCR1 (blue) of pancreas tissue sections obtained from RIP-GP x XCL1$^{-/-}$ mice at different time points after infection. Original magnification 63x (oil). Scale bar represents 20 µm.

In contrast, in XCR1-deficient mice it was possible to visualize the expression of XCL1, but not XCR1, in the islets. In fact, both XCL1- and XCR1-expressing cells were absent at day 0, before the infection. Once the mice had been infected, XCL1-expressing cells were present among the infiltrating cells, but there were no cells producing XCR1 mRNA (Figure 15).

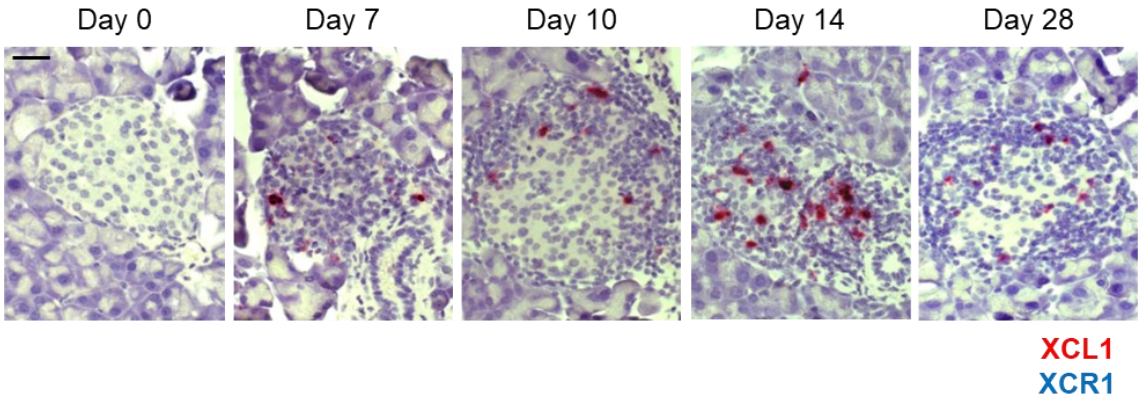

Figure 15. XCL1-expressing cells are present in the islets in absence of XCR1.
Duplex RNAscope *in situ* hybridization for XCL1 (red) and XCR1 (blue) of pancreas tissue sections obtained from RIP-GP x XCR1$^{-/-}$ mice at different time points after LCMV-infection. Original magnification 63x (oil). Scale bar represents 20 µm.

6.3 XCL1 absence

6.3.1 XCL1-deficient mice show reduced number of cDC1 in the islet microenvironment

XCR1 is expressed only on conventional dendritic cells type 1 (cDC1).[87] As mentioned, no good anti-XCR1 antibody is available for immunohistochemistry, therefore other markers for cDC1 were considered. In particular, pancreas sections obtained from RIP-GP and RIP-GP x XCL1$^{-/-}$ mice at day 7, 14, and 28 after infection were stained via IHC using anti-CD103 antibody. Quantification of the area of the positive signal per islet area was performed (Figure 16*A, B*). The results showed that, interestingly, at day 14 there were less CD103+ cells in the RIP-GP x XCL1$^{-/-}$ islets compared to regular RIP-GP.

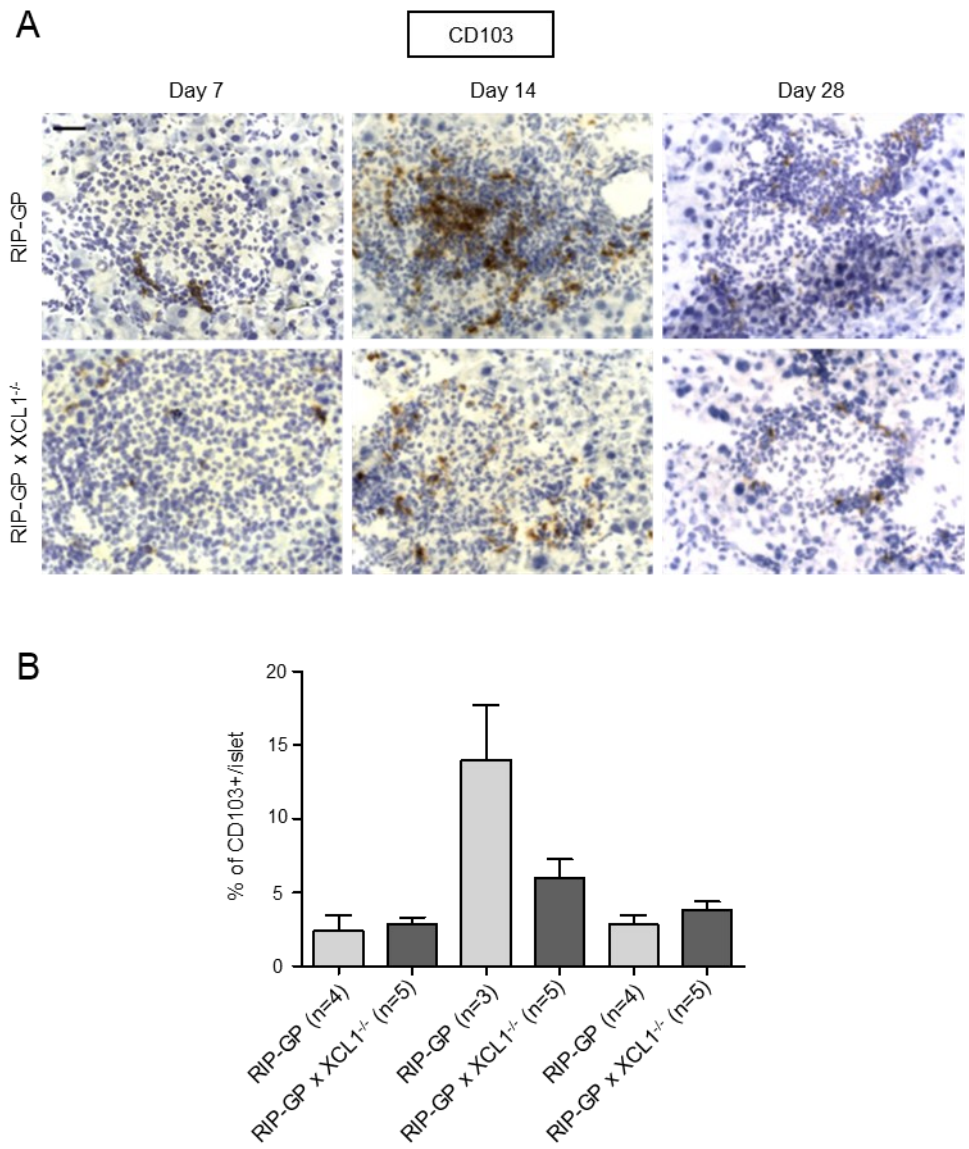

Figure 16. CD103+ cells are reduced in the islets of XCL1-deficient mice at day 14.
(A) Representative images of immunohistochemical staining with anti-CD103 antibody of quick-frozen pancreas sections at different time points after LCMV-infection, comparing RIP-GP with RIP-GP x XCL1$^{-/-}$ mice. Original magnification 40x. Scale bar represents 25 µm. - (B) Quantification of the CD103 stained area, expressed as percentage of the area of CD103+ signal per area of the islet. Numbers of mice per group are indicated. Data are shown as mean ± SEM.

However, since CD103 can also be expressed by a subset of T cells, an immunofluorescent double-staining using anti-CD103 and anti-CD11c antibodies was carried out to distinguish between T cells and DC. CD11c was used as a general marker for DC. I quantified the CD103+ CD11c+ double positive area per CD11c+ area (Figure 17*A*, *B*). These double positive cells tended to decrease at all time points. In particular, at day 14 they were reduced by 44% in the XCL1-deficient mice compared to the RIP-GP mice (p=0.022) (Figure 17*B*).

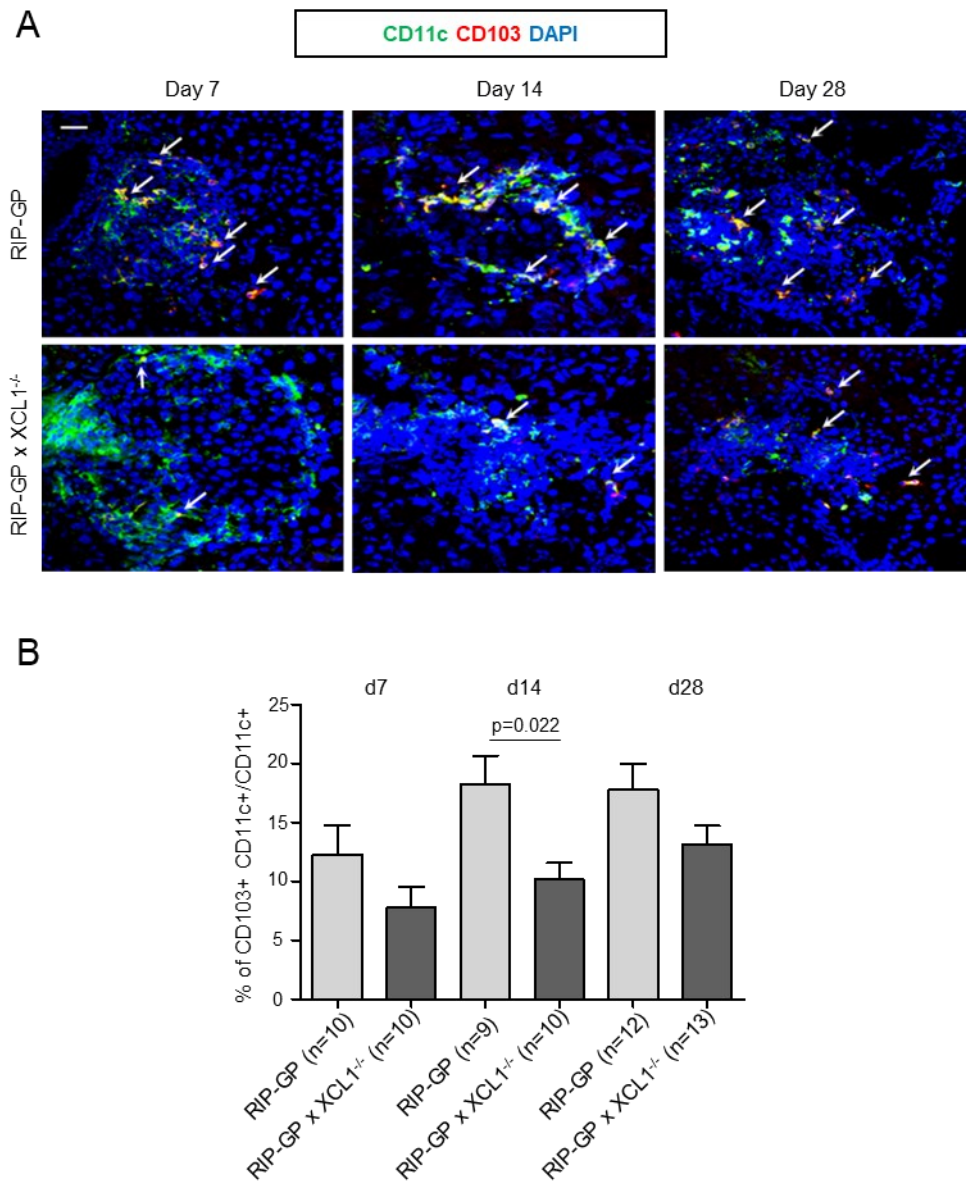

Figure 17. CD103+ CD11c+ cells are reduced in the islets of XCL1-deficient mice.
(A) Representative images of immunofluorescent double-staining for CD11c (green) and CD103 (red) of quick-frozen pancreas sections obtained at different time points after LCMV-infection, comparing RIP-GP with RIP-GP x XCL1$^{-/-}$ mice. Nuclei are stained with DAPI (blue). White arrows indicate the double positive cells (cDC1). Original magnification 40x. Scale bar represents 20 µm. - (B) Quantification of the CD103/CD11c double-staining shown in (A), expressed as percentage of the area of CD103/CD11c double-positive cells per CD11c positive area. Numbers of mice per group are indicated. Data are shown as mean ± SEM.

In order to confirm these data and to better investigate the consequences of XCL1-deficiency, flow-cytometric analysis was performed on splenocytes, cells isolated from PDLN, and islet infiltrating cells isolated from pancreas. The attention was focused on two time points after LCMV-infection: day 7, when the initial inflammation is still ongoing and the β-cells start to be destroyed, and day

28, when the disease is chronic. Total cell number per organ of RIP-GP mice and RIP-GP x XCL1$^{-/-}$ mice was calculated. First, CD11c+ MHC-II+ cells were identified as cDC, then a gate was set for XCR1+ CD11b- to pick out the cDC1. Finally, these were characterized for their expression of CD103, marker for migratory cDC1, and for their production of IL12, cytokine released once cDC1 are activated (Figure 18).

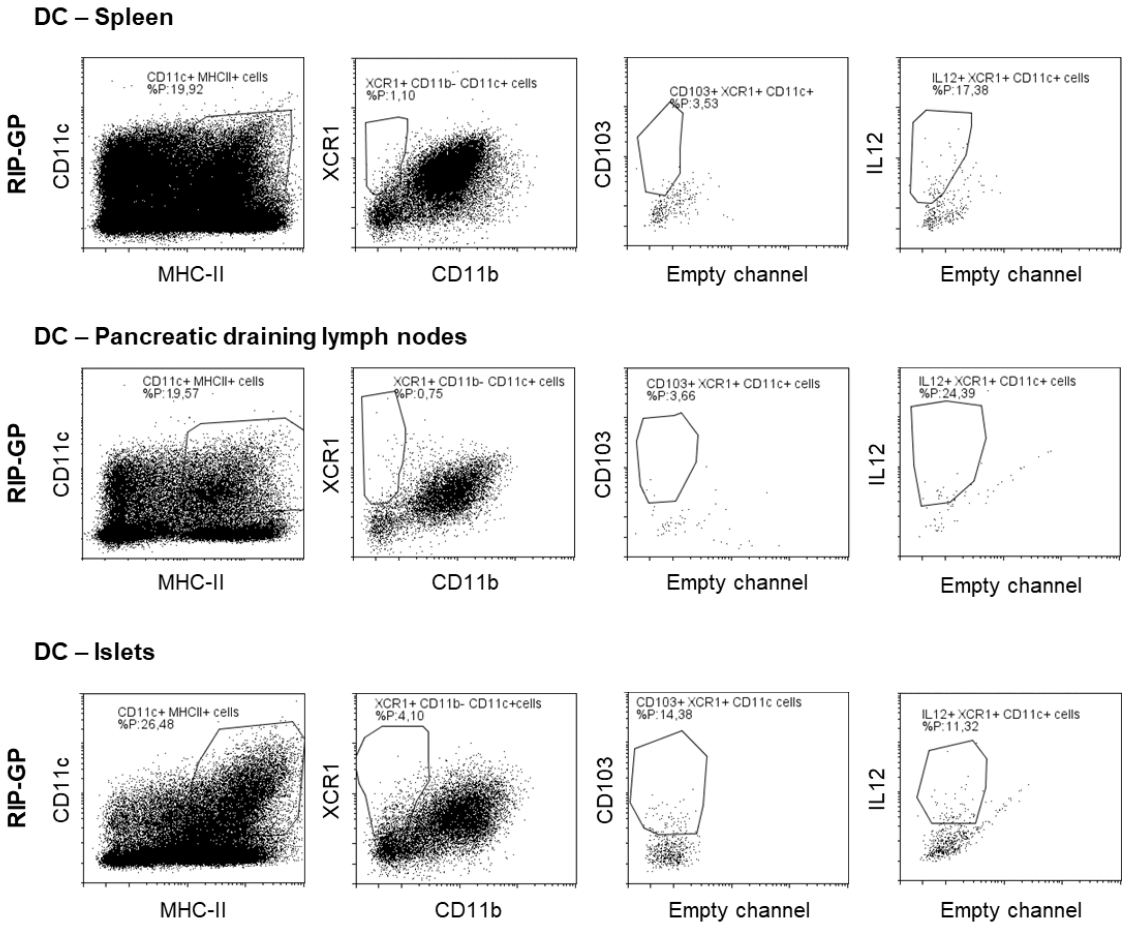

Figure 18. Gating strategy of DC in spleen, PDLN, and islet infiltrating cells (islets).
Representative DC analysis of dot plots obtained via flow cytometry. The analysis is shown for a RIP-GP mouse at day 7 post LCMV-infection.

At day 7, CD11c+ MHC-II+ cells did not show significant difference between the two lines in the spleen, but in the PDLN there were interestingly more CD11c+ MHC-II+ cells in the RIP-GP x XCL1$^{-/-}$ mice than in the regular RIP-GP mice ($p=0.002$). However, the opposite was observed in the pancreatic islets, where only one fourth of the cells was present in XCL1-deficient RIP-GP mice compared to regular RIP-GP mice ($p=0.011$). As described, the following step was to look at

cDC1 (CD11c+, MHC-II+, XCR1+, CD11b- cells). Here, a significant accumulation of cDC1 in the PDLN (p=0.021) corresponded to only a slight reduction of cells in the islets of XCL1-deficient RIP-GP mice. Therefore, migratory CD103+ cDC1 were analysed. As for total cDC, in the spleen there was not a detectable difference among the two lines and in the PDLN, there were more CD103+ cDC1 in the RIP-GP x XCL1$^{-/-}$ mice. In contrast, in the pancreatic islets, there were significantly less cells of this specific cell subtype in the RIP-GP x XCL1$^{-/-}$ mice (p=0.026). Finally, IL12 production of cDC1 was also evaluated. Again, in the XCL1-deficient PDLN there were more IL12 producing cDC1 (p=0.029) and, at the same time, among the islet infiltrating cells there were less cDC1 that produce IL12 (Figure 19).

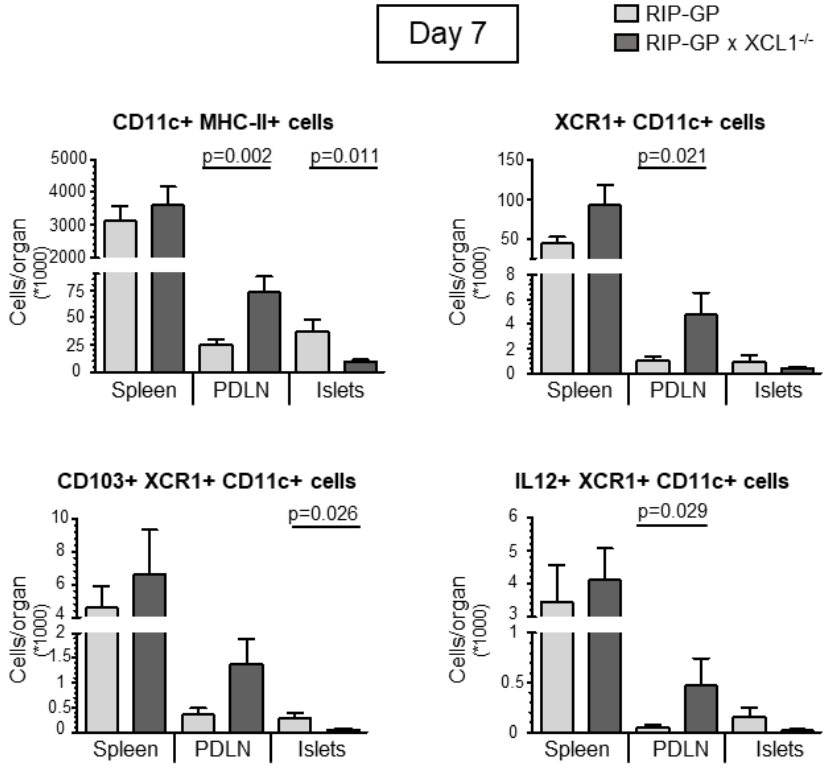

Figure 19. At day 7 cDC1 tend to accumulate in the PDLN of XCL1-deficient mice and not to migrate to the islets.

Absolute numbers of different DC subtypes per organ (spleen, PDLN, and islet infiltrating cells (islets)) obtained via flow cytometric analysis at day 7 after infection, comparing RIP-GP mice with RIP-GP x XCL1$^{-/-}$ mice. DC were first identified as CD11c+ MHC-II+ cells and then quantified for the entire organ and then the analysis was focused on cDC1 (XCR1+ CD11c+ cells). Finally, these were assessed for the peripheral subset (CD103+ XCR1+ CD11c+ cells) and for their activity (IL12+ XCR1+ CD11c+). Values are displayed as mean ± SEM and significant p-values are indicated (n=6-9, IL12+ XCR1+CD11c+ n=3-4).

At day 28, the tendency was similar to day 7. For all the investigated DC subsets the cell trend was to accumulate in the PDLN and to not migrate to the islets of RIP-GP x XCL1$^{-/-}$ mice as efficiently as in regular RIP-GP mice. However, the detected differences between RIP-GP x XCL1$^{-/-}$ and regular RIP-GP mice were not significant. IL12 producing cDC1 tended to be reduced in the islets of the XCL1-deficient RIP-GP mice, but it did not correspond to an accumulation in the PDLN (Figure 20).

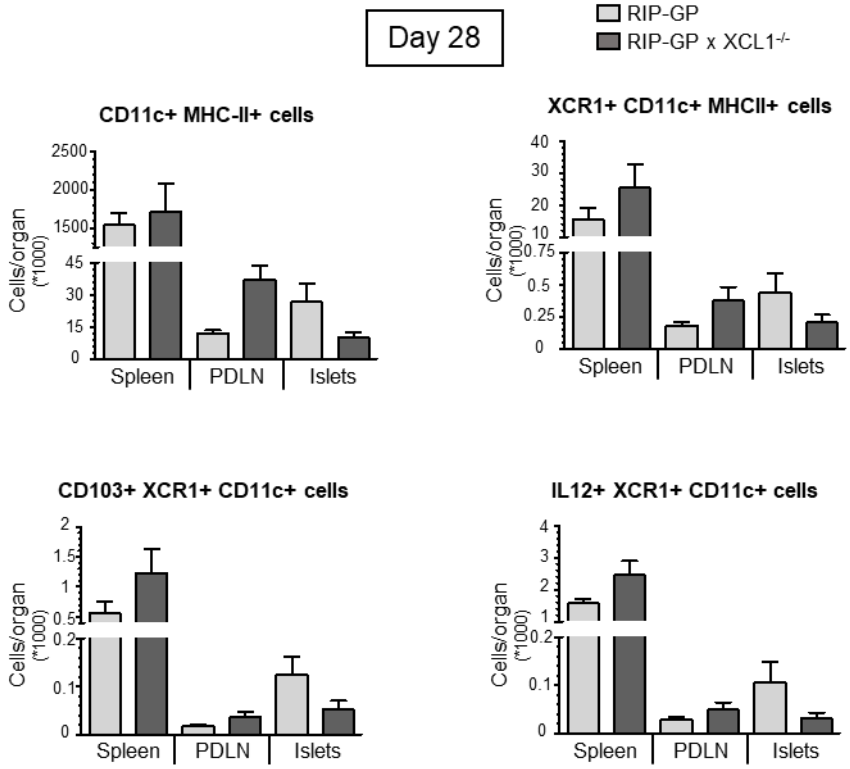

Figure 20. DC do not migrate to the islets of the XCL1-deficient mice at day 28.
Absolute numbers of different DC subtypes per organ (spleen, PDLN, and islet isolated cells (islets)) obtained via flow cytometric analysis at day 28 after infection, comparing RIP-GP mice with RIP-GP x XCL1$^{-/-}$ mice. DC were first identified as CD11c+ MHC-II+ cells and quantified for the entire organ and then the analysis was focused on cDC1 (XCR1+ CD11c+ cells). Finally, the cDC1 were assessed for the peripheral subset (CD103+ XCR1+ CD11c+ cells) and for their activity (IL12+ XCR1+ CD11c+ cells). Values are displayed as mean ± SEM and significant p-values are indicated (n=7-9).

6.3.2 In absence of XCL1 islet autoantigen-specific CD8 T cells are diminished

A similar approach was followed for T cells, performing flow cytometric analysis of leukocytes isolated from spleen, PDLN, and islets isolated from pancreata.

CD8b was used as a marker for T cells and islet autoantigen-specific T cells were identified through an intracellular staining for IFNγ after stimulation of the isolated cells with the immunodominant LCMV-GP epitope 33 peptide (Figure 21).

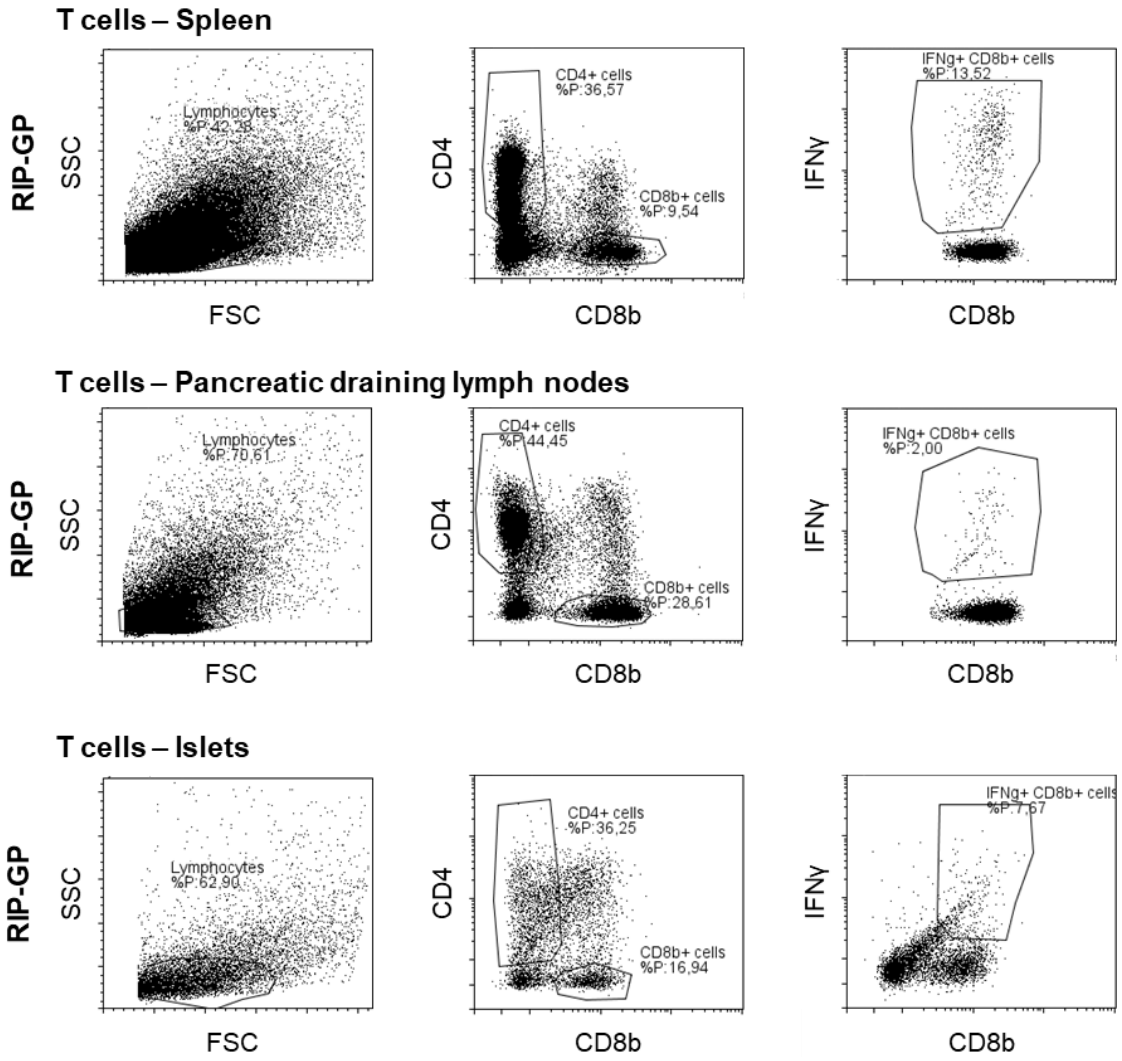

Figure 21. Gating strategy of T cells in spleen, PDLN, and islet infiltrating cells (islets). Representative T cell analysis of dot plots obtained via flow cytometry. The analysis is shown for a RIP-GP mouse at day 7 after LCMV-infection.

At day 7 after LCMV-infection, the CD8 T cell number did not differ in the spleen between the two mouse lines, but it was increased in the PDLN and decreased in the islets of the RIP-GP x XCL1$^{-/-}$ mice compared to the regular RIP-GP mice ($p=0.013$). Autoantigen-specific T cells behaved similarly in that. Indeed, there was an increased number of aggressive T cells in the PDLN and a significant reduction of IFNγ-producing cells in the islets of RIP-GP x XCL1$^{-/-}$ mice ($p=0.029$). At day 28 after infection, CD8 T cells were still increased in number in the PDLN

and also still decreased among the islet infiltrating cells of the RIP-GP x XCL1$^{-/-}$ mice. Importantly, the autoantigen-specific T cells in the RIP-GP x XCL1$^{-/-}$ mice were reduced to almost one fifth of the cells present in the islets of RIP-GP mice (p=0.091) (Figure 22).

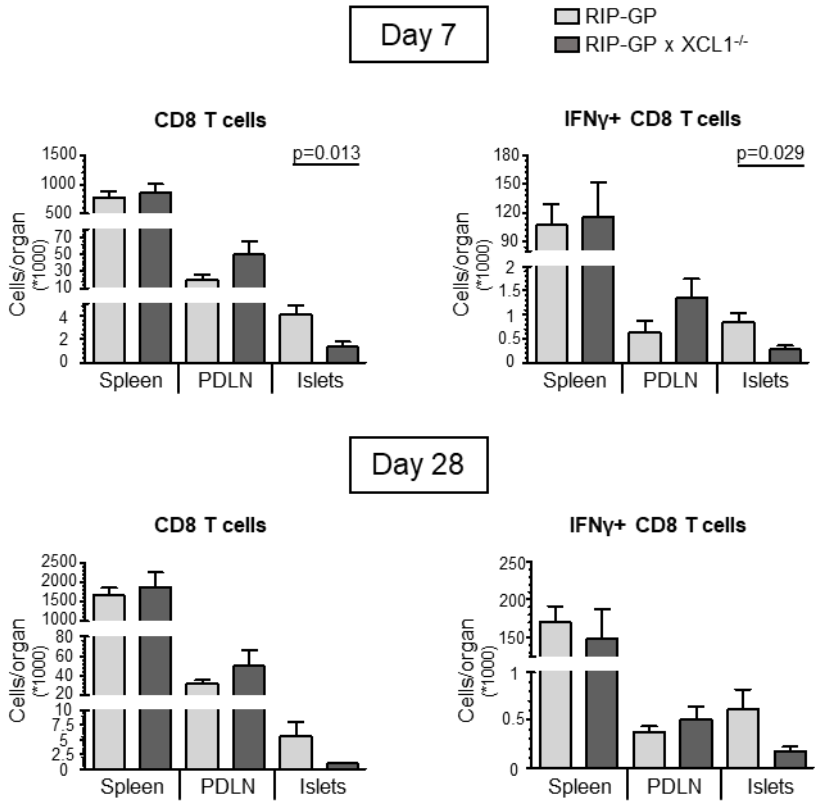

Figure 22. T cells show reduced migration to the islets of the XCL1-deficient mice.
Absolute numbers of different subtypes of T cells per organ (spleen, PDLN, and islet infiltrating cells (islets)) obtained via flow cytometric analysis at day 7 and day 28 after infection, comparing RIP-GP mice with RIP-GP x XCL1$^{-/-}$ mice. CD8 T cells were identified as CD8b+ cells and autoantigen-specific CD8 T cells as IFNγ-producing CD8 T cells upon stimulation with LCMV-specific peptides. Values are displayed as mean ± SEM and significant p-values are indicated (n=6-9).

6.3.3 Overall fitness of autoantigen-specific CD8 T cells is reduced in XCL1-deficient mice

Since the absence of XCL1 resulted in less cDC1 and less T cells, the focus was then moved to assess T cell activity and functionality, staining for perforin (Perf) and granzyme B (GrB), important factors in T cell killing activity, as well as programmed cell death protein-1 (PD-1) as a marker for T cell exhaustion and killer cell lectin-like receptor subfamily G member 1 (KLRG1) as a marker for T

cell senescence. These markers have been evaluated for both total CD8 T cells and islet autoantigen-specific CD8 T cells (Figure 23).

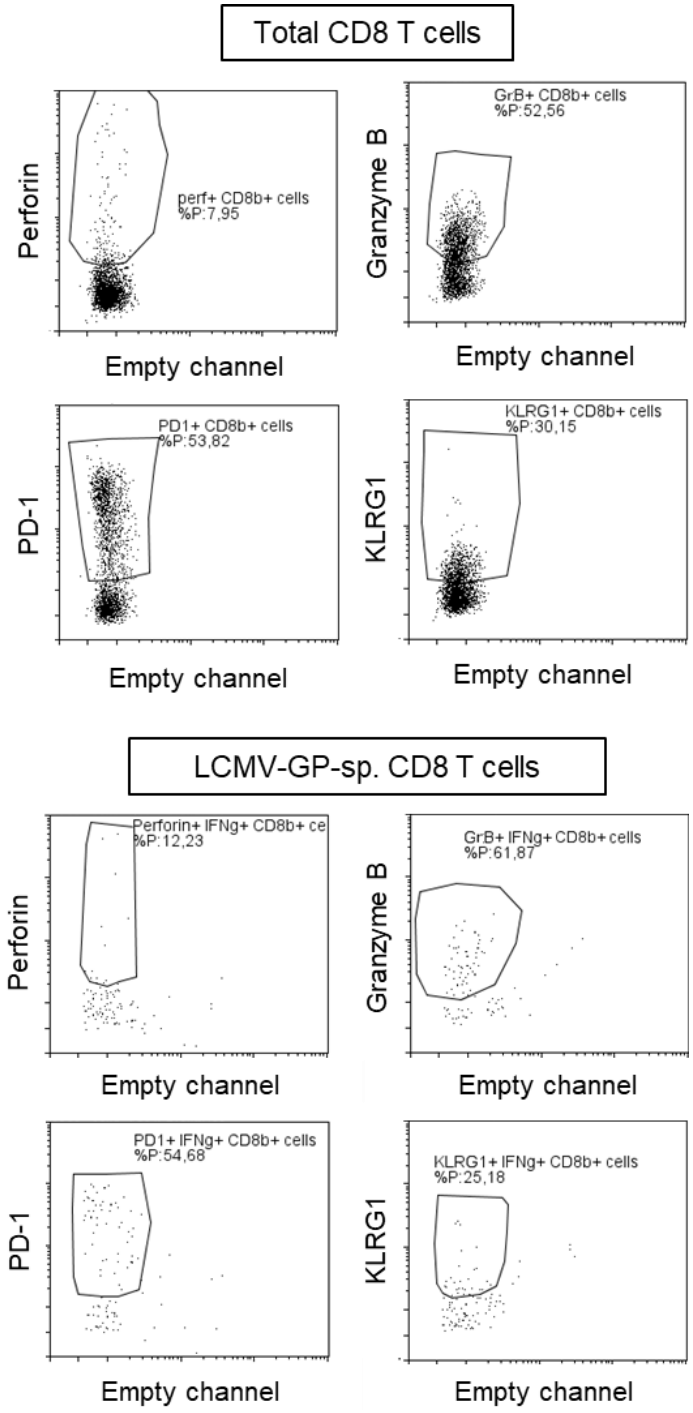

Figure 23. Gating strategy of T cell activity for islet infiltrating cells.
Dot plots representing perforin (perf), granzyme B (GrB), PD-1, and KLRG1 analysis both of total CD8 T cells and LCMV-GP-specific T cells isolated from the islets of a RIP-GP mouse at day 7 after infection.

The results are expressed as frequencies of these different cell subtypes on the total CD8 T cells and IFNγ-producing GP33-specific CD8 T cells (Figure 24), comparing the islet infiltrating cells isolated from pancreata of RIP-GP and XCL1-deficient RIP-GP mice both at day 7 and at day 28. Neither perforin producing cells nor KLRG1+ cells did significantly differ between the two lines. The main differences were visible at day 28: RIP-GP x XCL1$^{-/-}$ mice showed less GrB+ CD8+ T cells ($p=0.040$) and increased exhausted PD-1+ CD8+ T cells in the islets ($p=0.001$). In the case of IFNγ-producing GP33-specific T cells, at day 28 GrB+ islet autoantigen-specific CD8 T cells showed a tendency towards a lower frequency in the XCL1-deficient RIP-GP mice. At day 28 PD-1+ and KLRG1+ islet autoantigen-specific CD8 T cells were significantly higher in the islets of RIP-GP x XCL1$^{-/-}$ mice compared to RIP-GP mice (respectively, $p=0.012$ and $p=0.031$) (Figure 24).

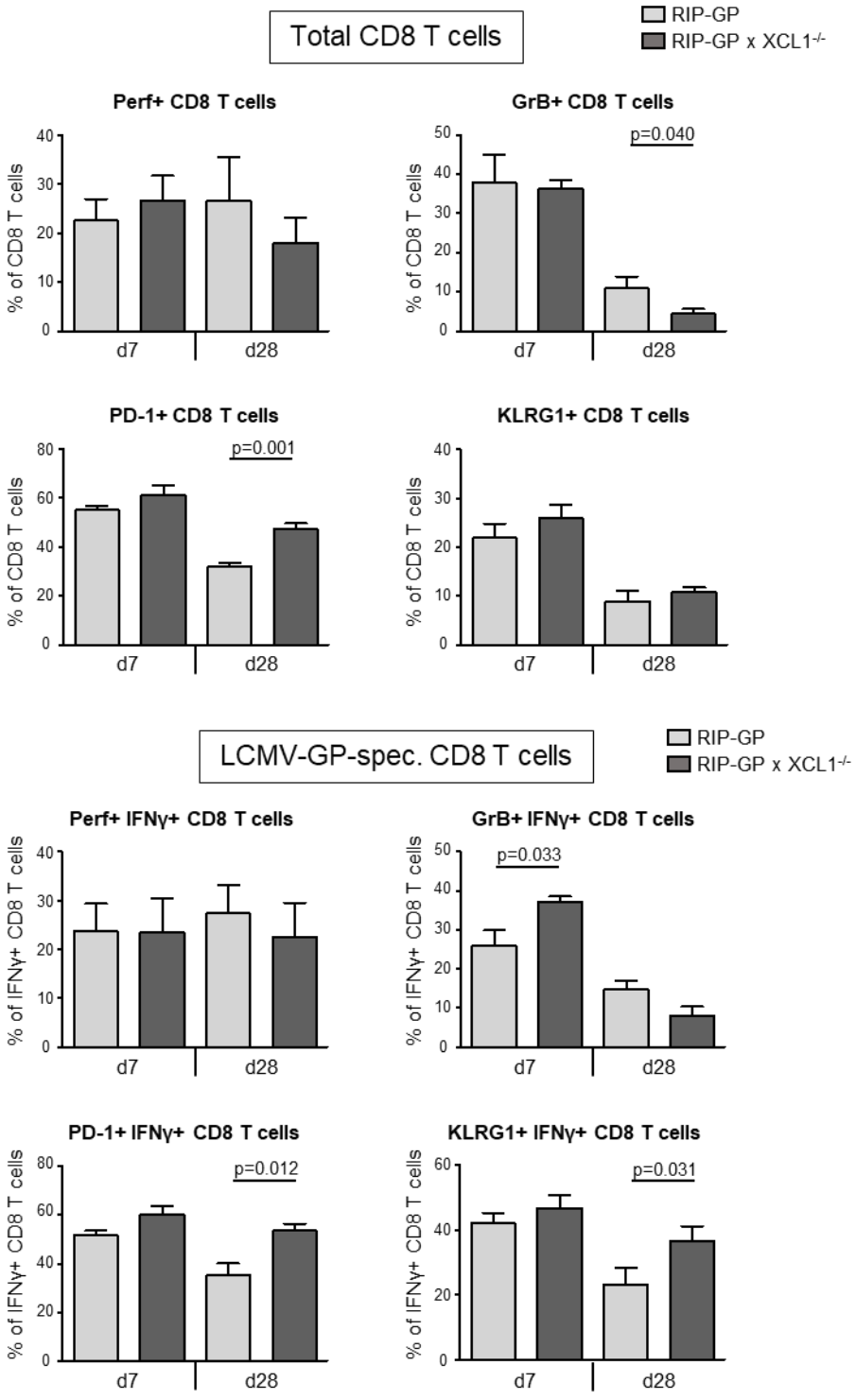

Figure 24. CD8 T cell activity is slightly decreased in XCL1-deficient mice.
Frequencies of CD8 T cells expressing perforin (Perf), granzyme B (GrB), PD-1, or KLRG1 of total CD8 T cells or LCMV-GP33-specific CD8 T cells. Data were obtained via flow cytometric analysis of islet infiltrating cells of RIP-GP mice and RIP-GP x XCL1$^{-/-}$ mice at day 7 and day 28 after infection. Results are shown as mean ± SEM and p-values are indicated when significant (n=7-9).

To further study the cytotoxicity of the islet autoantigen-specific T cells in presence or absence of XCL1, an *in vivo* CTL assay was carried out. Splenocytes were isolated from donor mice and were then split in two groups. Half of the cells were incubated with GP33 peptide and half of them were incubated without. The day after, these two groups were differently labelled with different concentrations of CFSE. GP33-loaded splenocytes were labelled with a low concentration of CFSE ($CFSE^{lo}$) and unloaded splenocytes were labelled with a high concentration of CFSE ($CFSE^{hi}$). These two groups were mixed at a 1:1 ratio and then i.v. injected into RIP-GP and RIP-GP x $XCL1^{-/-}$ recipient mice at day 28 after LCMV-infection. Uninfected RIP-GP were used as negative control. As expected, in the uninfected mice no specific killing of the GP33-loaded cells occurred. In both other groups, the GP33-loaded cells were specifically killed (Figure 25*A*). However, comparing the half-life of target cell elimination a slight delay in XCL1-deficient mice was detected (Figure 25*B*).

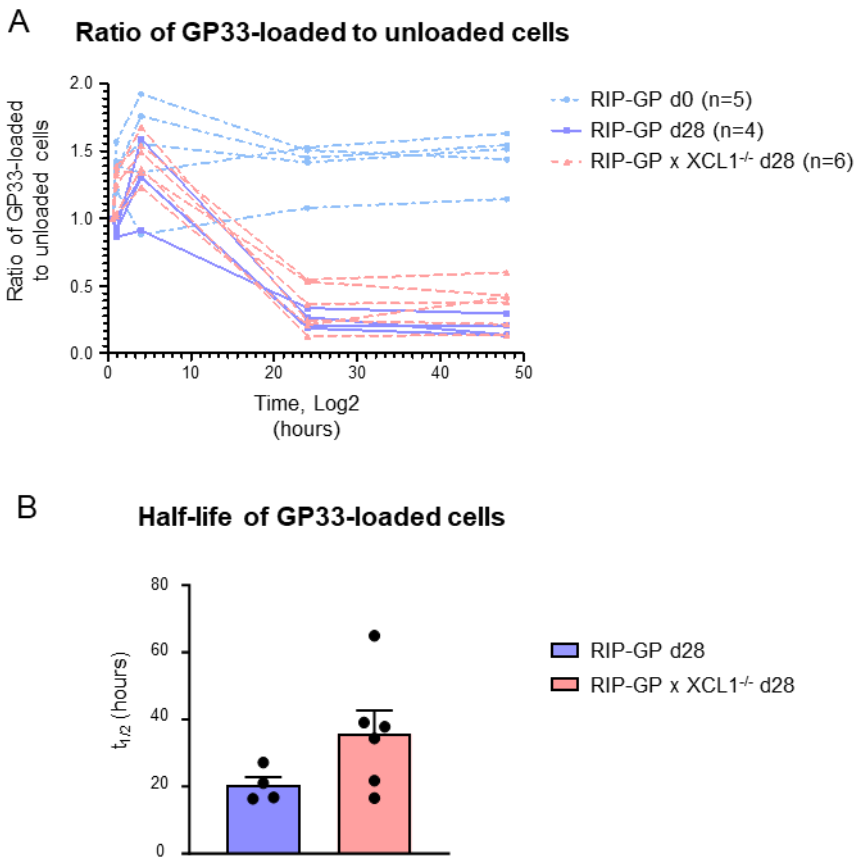

Figure 25. Slightly reduced *in vivo* cytotoxicity in XCL1-deficient mice.
(A) *In vivo* cytotoxic T lymphocyte (CTL) assay, comparing RIP-GP uninfected mice (d0) to RIP-GP and RIP-GP x XCL1$^{-/-}$ mice at day 28 after infection. CFSE differently labelled GP33-loaded and unloaded target splenocytes were i.v. injected at a 1:1 ratio. At 10 minutes and 1, 4, 24, and 48 hours after injection blood was taken and the ratio of GP33-loaded and unloaded target cells was determined by flow cytometry. The obtained data were normalized against the ratio at 10 minutes after the injection (baseline). - (B) Calculated half-life of GP33-loaded target cell turnover. Values are shown as mean ± SEM. Number of mice used is displayed in brackets.

6.3.4 Shift to a regulatory milieu in the islets of XCL1-deficient mice

Via flow cytometric analysis of the islet infiltrating cells, FoxP3 was also assessed as a marker for regulatory T cells both at day 7 and day 28 post-infection (Figure 26).

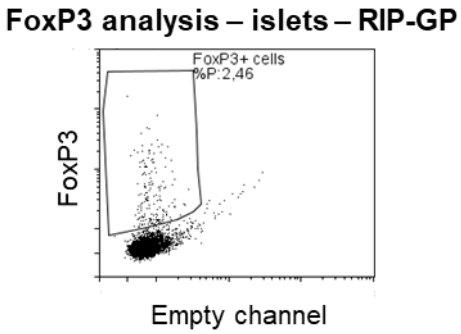

Figure 26. Gating strategy of regulatory T cells for islet infiltrating cells (islets).
FoxP3 cells dot plot analysis of a RIP-GP mouse at day 7 after the infection.

Interestingly, in contrast to total and IFNγ-producing islet autoantigen-specific CD8 T cells, more FoxP3+ T cells were detected among the islet infiltrating cells in the RIP-GP x XCL1$^{-/-}$ mice at both time points (Figure 27*A*). The ratio between the total FoxP3+ T cells (CD4 and CD8 Treg cells) and the total IFNγ-producing islet autoantigen-specific cells was calculated. Importantly, at day 28 the ratio was 3-fold higher in the islets of RIP-GP x XCL1$^{-/-}$ mice compared to the RIP-GP mice (p=0.005) (Figure 27*B*). These data indicate that in absence of a sufficient number of cDC1, the T cell balance is tipped towards a more regulatory phenotype.

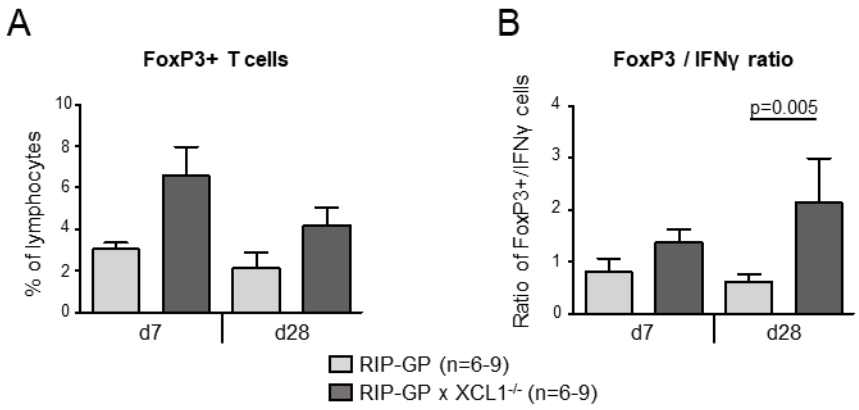

Figure 27. Switch to a regulatory T cell milieu in the islets of XCL1-deficient mice.
(A) Frequencies of FoxP3+ cells among all the lymphocytes obtained via flow cytometric analysis of islet infiltrating cells of RIP-GP and RIP-GP x XCL1$^{-/-}$ mice at day 7 and day 28 after infection. - (B) Ratio of total FoxP3+ T cells and total auto-aggressive (IFNγ+) T cells. Results are displayed as mean ± SEM. Numbers of mice and significant p-values are indicated.

6.3.5 XCL1-deficient mice have a reduced T1D incidence

XCL1-deficiency generates differences locally in the pancreas with a reduction of both cDC1 and aggressive T cells and, at the same time, an increase of Treg cells. Therefore, to see if this local immune shift has an impact on the overall disease, a T1D incidence study was conducted. After LCMV-infection of RIP-GP mice and RIP-GP x XCL1$^{-/-}$ mice, the BG concentration was measured at weekly intervals for 12 weeks. Mice with BG levels higher than 300 mg/dl were considered diabetic. Whereas, 80% of RIP-GP mice became diabetic, only 30% of RIP-GP x XCL1$^{-/-}$ mice was diabetic at day 17. Importantly, most of the XCL1-diabetic mice that became diabetic reverted their glycaemia to values lower than 300 mg/dl already 5-10 days after turning diabetic, indicating a milder form of T1D. Considering such remitting mice, at the end of the study only one out of twenty RIP-GP x XCL1$^{-/-}$ mice was still diabetic (Figure 28*A*). The mean BG concentration reflected the differences already visible in the percentage of mice that turned diabetic. The mean BG levels of RIP-GP mice were higher than 300 mg/dl already at day 14. XCL1-deficient mice always displayed a mean glycaemia below the non-diabetic value of 200 mg/dl, except between day 14-21 when there was a limited elevation (Figure 28*B*).

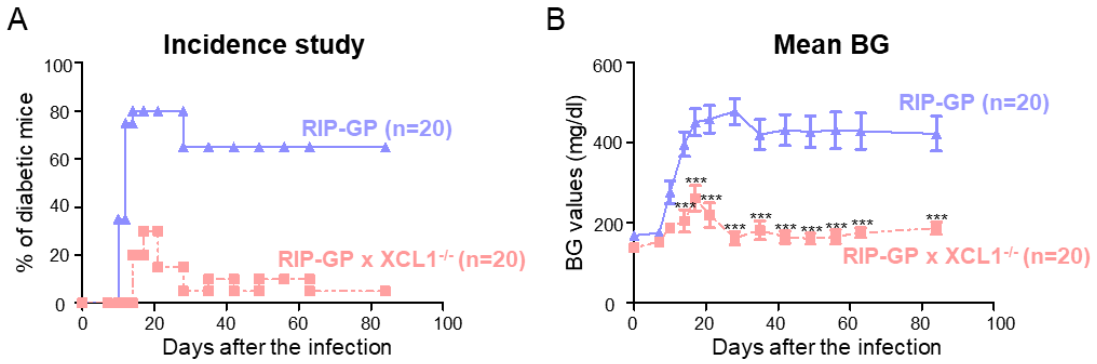

Figure 28. XCL1-deficient mice have reduced T1D incidence.
(A) T1D incidence study results, expressed as percentage of diabetic mice at each time point after infection. Mice with BG levels of >300 mg/dl were considered diabetic. Note that some mice reverted from a diabetic to a non-diabetic state over time. - (B) Mean BG levels over time ± SEM. Significant differences (* = p<0.05, ** = p<0.01, *** = p<0.001) and numbers of mice are indicated.

6.3.6 XCL1-deficient mice display largely intact islets in pancreas tissue sections

Immunohistochemical staining with anti-insulin antibody was performed on pancreas sections isolated from RIP-GP and RIP-GP x XCL1$^{-/-}$ mice at different time points after the infection. From the representative pictures (Figure 29), it is already possible to appreciate some differences. The RIP-GP islets were destroyed at day 28, completely infiltrated by immune cells with only few cells still producing insulin. Note that it was not possible to stain the regular RIP-GP mice at week 12 (endpoint of the incidence study), since they had to be killed before the end of the study due to animal welfare regulations. On the contrary, islets of RIP-GP x XCL1$^{-/-}$ mice showed only few infiltrating cell clusters and maintained insulin production throughout the whole observation time.

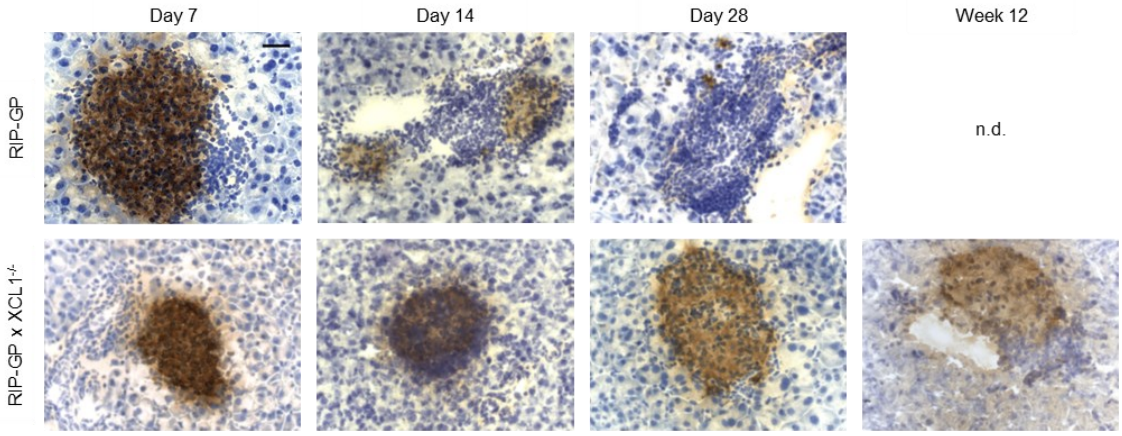

Figure 29. XCL1-deficient mice have more intact islets (representative pictures).
Representative images of immunohistochemical staining for insulin of quick-frozen pancreas sections of RIP-GP and RIP-GP x XCL1$^{-/-}$ mice at days 7, 14, and 28 as well as week 12 after infection. Original magnification 40x; scale bar represents 25 µm. Note that for RIP-GP mice it was not possible to acquire an image at week 12 (not done; n.d.), since all the mice had to be sacrificed earlier due to severe T1D.

To quantify the insulitis, a score was assigned to the islets according to the amount of infiltrated cells and the insulin producing β-cells left in the islet. More precisely, the score 0 is assigned when infiltrations are visible, score 1 when there is mild peri-insulitis, score 2 in presence of a moderate infiltrations, and score 3 in case of massive infiltrations with only islet scars left. At day 14 post-infection, there were more islets with moderate to massive infiltrations in the RIP-GP mice compared to RIP-GP x XCL1$^{-/-}$ mice. The same trend was maintained also at day

28. At week 12 after infection, it was not possible to quantify the islets of the RIP-GP mice since they had to be killed before. In contrast, in the RIP-GP x XCL1$^{-/-}$ mice most of the islets were still capable to produce insulin (Figure 30). However, this kind of analysis does not give complete information about the β-cell content in the entire pancreas since only one section of the pancreas is analysed. Moreover, in very diabetic mice where most of the islets are destroyed it is even more difficult to have an overview, since the insulin producing cells might not be evenly distributed throughout the pancreas. Therefore, 3D-staining of whole pancreas was performed with an antibody against insulin (see paragraph 6.5).

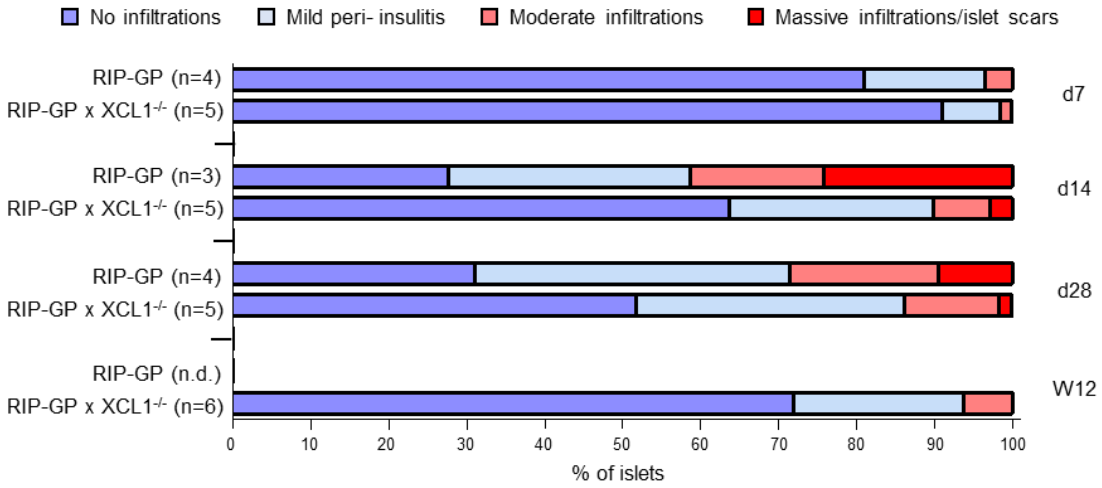

Figure 30. XCL1-deficient mice show reduced islet destruction.
Mean insulitis scores determined from the staining with anti-insulin antibody shown in Figure 29. Islets were scored as described in Materials and Methods. Insulitis in RIP-GP and RIP-GP x XCL1$^{-/-}$ mice was compared at days 7, 14, 28, and at week 12 after infection. Number of mice is displayed in brackets.

6.4 XCR1 absence

6.4.1 cDC are localized in the islets in absence of XCR1

To test if also the absence of XCR1 has an effect on T1D, RIP-GP x XCR1$^{-/-}$ mice were used. These mice are characterized by the insertion of the gene encoding for the Venus fluorescent protein in the XCR1 locus.[82] Therefore, RIP-GP x XCR1$^{+/-}$ mice which are heterozygotes express both XCR1 and Venus protein, whereas RIP-GP x XCR1$^{-/-}$ mice express the Venus protein instead of the receptor. These mice can be used to track the receptor on a protein level, since there is no reliable anti-XCR1 antibody available for IHC. RIP-GP x XCR1$^{+/-}$ and

RIP-GP x XCR1$^{-/-}$ mice have been therefore infected with LCMV and sacrificed at different time points (day 7, 14, 28, and week 12). After isolating the pancreata, the organs were processed by immerging them in PLP buffer, as described in the Materials and Methods section (See paragraph 5.2.8). After cutting some slides, the sections were just stained with DAPI to highlight the nuclei and localize the Venus protein. From the representative pictures (Figure 31*A*), it is visible that Venus positive cDC1 (in green) started to appear in the islets already at day 7 and they increased over time in both mouse lines. Importantly, this DC subtype remained in the islet until week 12 after the infection. The cDC1 were still attracted to the islets even though XCR1 was partially or completely missing (Figure 31*A*), indicating that other factors are also involved in the attraction of cDC1 to the islets. The area of Venus signal per total islet area was quantified and surprisingly, for most of the time points there were no differences among the two lines, except at week 12 when there was an even higher Venus signal in the islets of XCR1-deficient mice ($p=0.012$). Thus, in absence of the receptor Venus+ cells migrate in a similar way than when the receptor is only partially depleted. Note that these results should be considered with caution since the quantification is performed by measuring the area of the positive (green) signal rather than counting the number of green cells. Thus, in RIP-GP x XCR1$^{-/-}$ mice that contain the Venus gene in both alleles the green fluorescence turns out to be brighter than in the heterozygous RIP-GP x XCR1$^{+/-}$ mice. Subsequently, also the “green area” around the Venus+ signal might be larger in RIP-GP x XCR1$^{-/-}$ than RIP-GP x XCR1$^{+/-}$ mice leading to an overrepresentation of the signal in RIP-GP x XCR1$^{-/-}$ mice (Figure 31*B*).

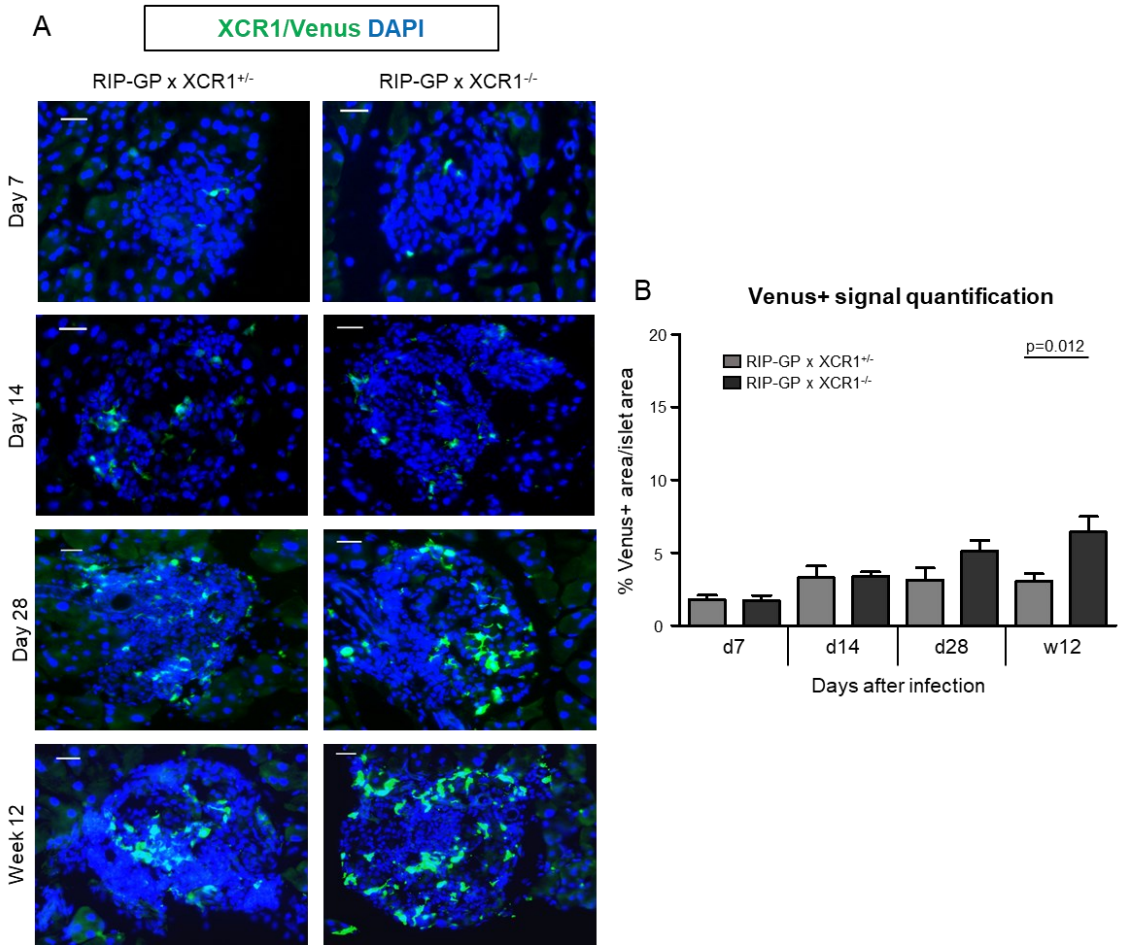

Figure 31. Venus+ cells infiltrate in the islets of XCR1-deficient mice.
(A) Representative pictures of RIP-GP x XCR1$^{+/-}$ and RIP-GP x XCR1$^{-/-}$ pancreatic islets at day 7, 14, 28, and week 12 after LCMV-infection. Tissues were treated with PLP buffer before embedding them in Tissue-Tek OCT. The Venus signal (green) is expressed in cDC1, since its gene is inserted in the locus for XCR1. DAPI was used to stain the nuclei. Original magnification 20x. Scale bars are 25 µm. - (B) Quantification of the Venus signal area per islet area of the staining in (A) comparing RIP-GP x XCR1$^{+/-}$ mice with RIP-GP x XCR1$^{-/-}$ mice. Values are displayed as mean ± SEM (n=4-5 at each time point, n=10 at week 12). P-values are indicated. Note that the increased signal in the RIP-GP x XCR1$^{-/-}$ mice could also be derived from the brighter signal given by the expression of the protein on both alleles.

6.4.2 XCR1-deficient mice do not show altered DC migration to the islets

To better investigate the effect of the absence of XCR1 on a cellular level and to quantify the Venus signal in the whole pancreas, cells were isolated from spleen, PDLN, and pancreatic islets and were analysed by flow cytometry. The attention was focused again on two time points: day 7, when the inflammation is still ongoing, and week 12, endpoint of the incidence study and chronic stage of the disease. RIP-GP x XCR1$^{+/-}$ mice were compared to RIP-GP x XCR1$^{-/-}$ mice. Here, the DC analysis was performed in a slightly different way. Since the XCR1-

deficient mice express the Venus protein in the XCR1 locus, the signal is visible in the green channel (B1 in MACSQuant). This means that Venus+ cells identify cDC1, since XCR1 and therefore Venus, is expressed only on cDC1. Thus, the gating strategy started with identifying directly Venus+ cells followed by selecting CD103+ Venus+ cells as peripheral cDC1 to see if there were some differences in the DC migration from the PDLN to the pancreas (Figure 32).

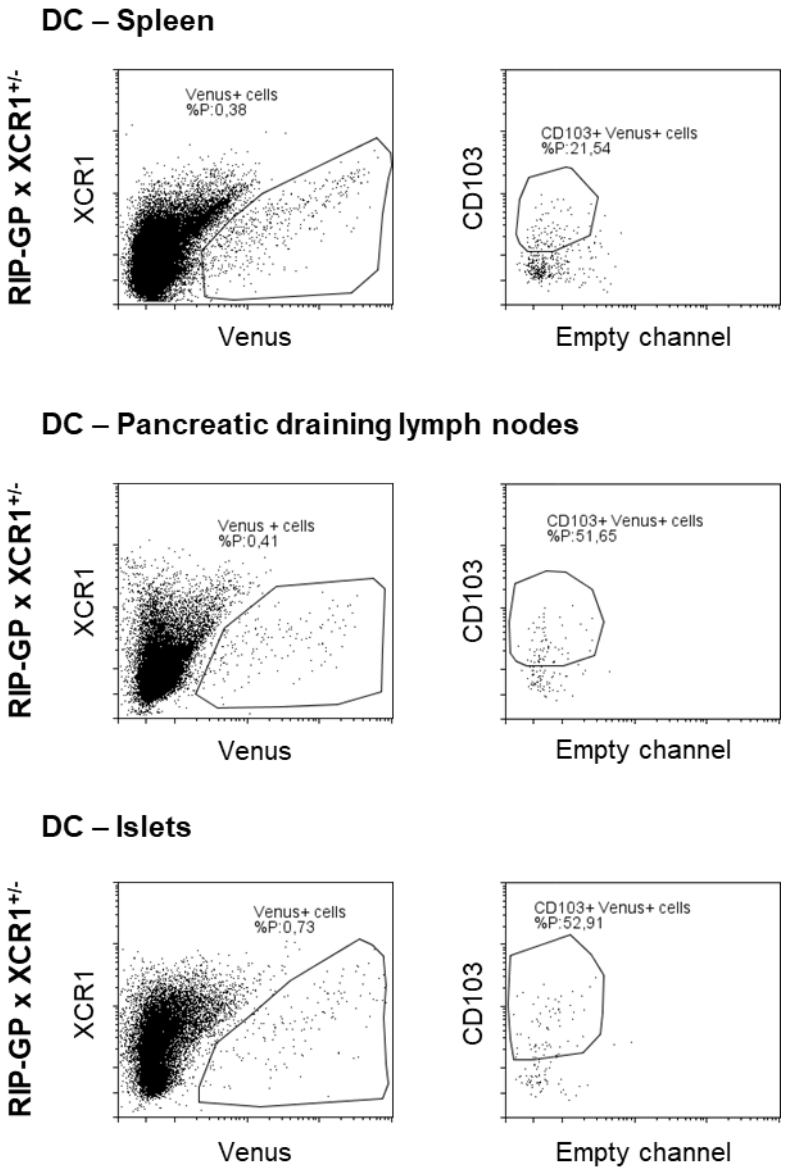

Figure 32. Gating strategy of DC in spleen, PDLN, and islet infiltrating cells (islets) in presence of the Venus signal.

Representative DC analysis of dot plots obtained via flow cytometry. The analysis is shown for a RIP-GP x XCR1$^{+/-}$ mouse at day 7 after LCMV-infection.

The absolute numbers per organ of the DC subsets were calculated for spleen, PDLN, and islet infiltrating cells at day 7 and week 12 after infection (Figure 33). In general, there were no significant differences among total cDC1 and peripheral cDC1 in all three organs at day 7 and at week 12. This stands in contrast with the data obtained with the immunofluorescent quantification, where at week 12 there were more Venus+ cells in the islets of XCR1-deficient mice. However, this confirms the hypothesis that the quantification of the green area in the immunofluorescent staining of the pancreas sections was flawed. Regarding CD103+ Venus+ cells, there was a slight tendency to decrease in the spleen and in the islet infiltrating cells in XCR1-deficient mice. However, the tendency was opposite at week 12, with an increase in both PDLN and islets of this DC subtype in XCR1-deficient mice compared to RIP-GP x XCR1$^{+/-}$ mice.

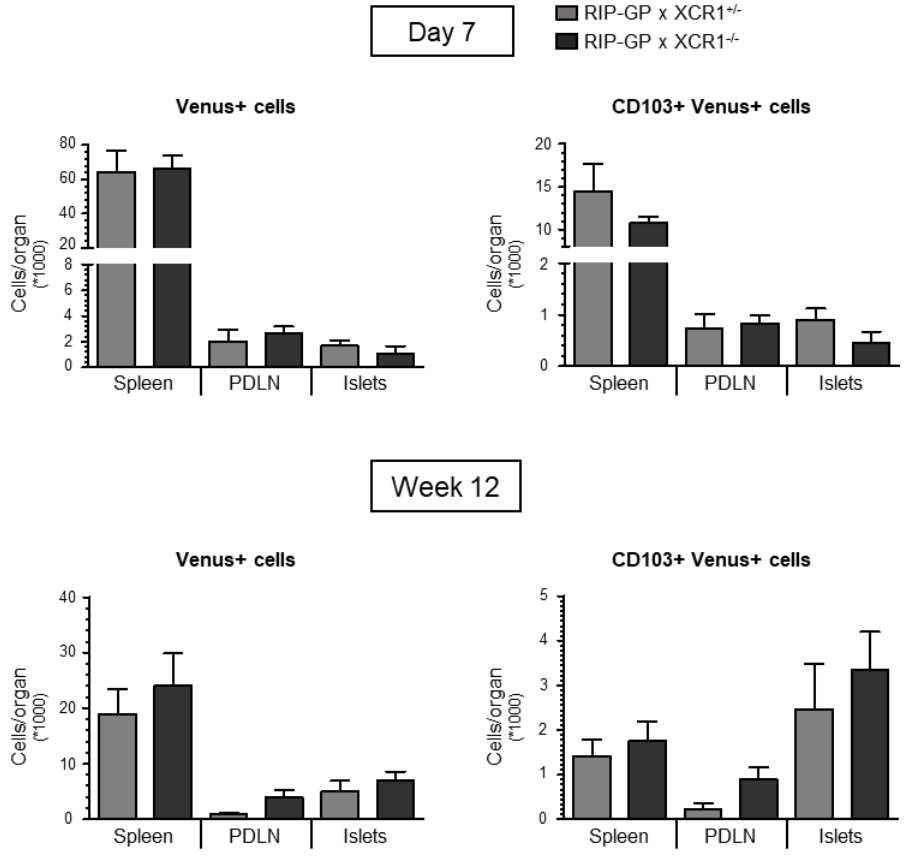

Figure 33. XCR1-deficient mice do not show altered migration of DC.
Absolute numbers of different subtypes of DC per organ (spleen, PDLN, and islets) obtained via flow cytometric analysis at day 7 and week 12 after infection. RIP-GP x XCR1$^{+/-}$ mice were compared with RIP-GP x XCR1$^{-/-}$ mice at day 7 and at week 12. cDC1 were first identified as Venus+ cells per organ and then as peripheral cDC1 (CD103+ Venus+ cells) per organ. Values are displayed as mean ± SEM and significant p-values are indicated (n=4-5 at day 7, n=4-7 at week 12).

6.4.3 XCR1-deficient mice display reduced number and activation of autoantigen-specific T cells in the islets

Analogous to the study with XCL1-deficient mice, the impact of the XCR1 deficiency on T cells was analysed. Therefore, flow cytometric analysis of leukocytes isolated from spleen, PDLN, and pancreatic islets was performed comparing RIP-GP mice with RIP-GP x XCR1$^{+/-}$ mice and RIP-GP x XCR1$^{-/-}$ mice at day 7 as well as RIP-GP x XCR1$^{+/-}$ mice with RIP-GP x XCR1$^{-/-}$ mice at week 12. T cells were analysed as previously described (see paragraph 6.3.2). CD8b was used to identify CD8 T cells, whereas islet autoantigen-specific T cells were identified as IFNγ-producing CD8 T cells, after overnight stimulation with the LCMV GP33 peptide. At day 7, the total number of CD8 T cells was lower in the spleen of XCR1-deficient mice compared to regular RIP-GP mice, but there were no differences in the other organs. Importantly, the total number of autoantigen-specific IFNγ-producing T cells was diminished in the islets of RIP-GP x XCR1$^{-/-}$ mice compared to regular RIP-GP mice ($p=0.032$). At week 12, both CD8 T cells and autoaggressive T cells increased in number in the PDLN of RIP-GP x XCR1$^{-/-}$ mice compared to RIP-GP x XCR1$^{+/-}$ mice. Similar to the number of cDC1 (as described in paragraph 6.4.2) there was no significant decrease of any of the CD8 T cell subsets in the pancreatic islets at week 12. However, week 12 constitutes an endpoint of the disease, which most regular RIP-GP mice do not reach and at which meaningful changes that might lead to a different T1D pathogenesis might be long gone. Thus, from these data, it is not possible to conclude that the migration of T cells to the islets is not impaired in absence of XCR1. However, the reduced autoantigen-specific CD8 T cells might lead to reduced β-cell destruction (Figure 34).

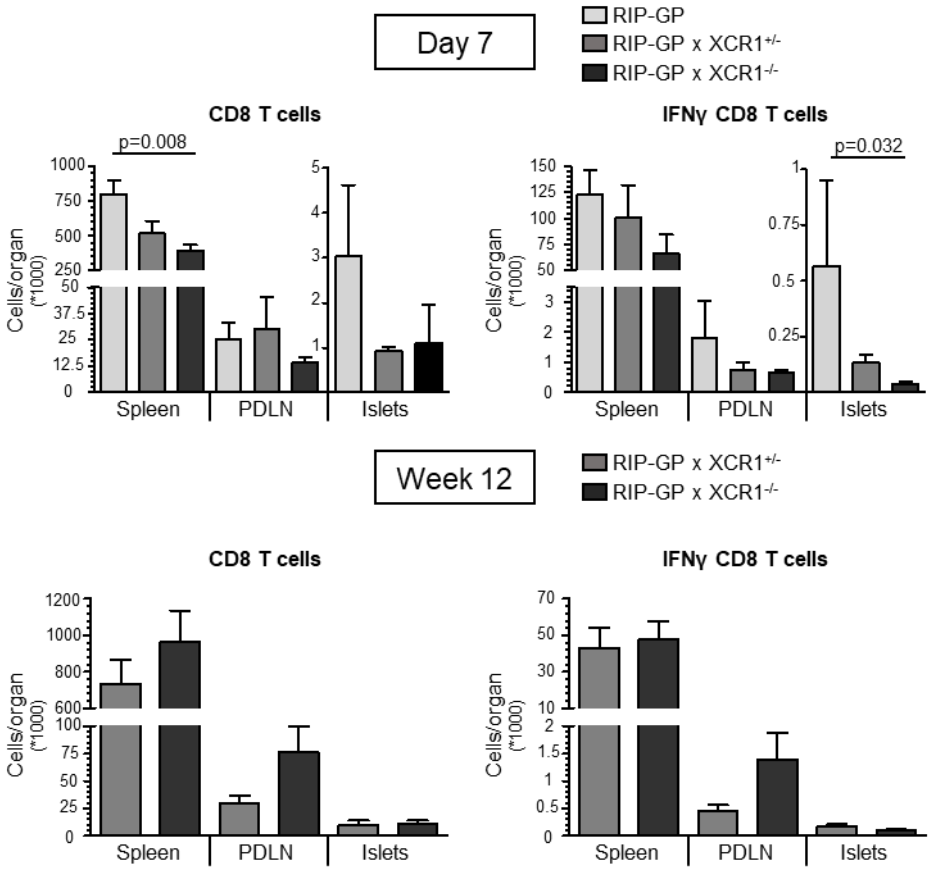

Figure 34. Autoantigen-specific T cells are reduced in the islets of XCR1-deficient mice. Absolute numbers of CD8 T cells and autoantigen-specific CD8 T cells per organ (spleen, PDLN, and islets) obtained via flow cytometric analysis at day 7 and week 12 after infection, comparing RIP-GP mice with RIP-GP x XCR1$^{+/-}$ and RIP-GP x XCR1$^{-/-}$ mice at day 7 and only RIP-GP x XCR1$^{+/-}$ mice and RIP-GP x XCR1$^{-/-}$ mice at week 12. T cells were first gated for CD8 T cells and then focused on IFNγ-producing CD8 T cells, obtained after overnight stimulation with the LCMV GP33 peptide. Values are displayed as mean ± SEM and significant p-values are indicated (n=4-5 at day 7, n=4-7 at week 12).

Since there was a reduction of IFNγ-producing CD8 T cells in the islets of RIP-GP x XCR1$^{-/-}$ mice at day 7 post-infection, the activation of T cells and of autoantigen-specific T cells was investigated, staining intracellularly for GrB and Perf, followed by flow cytometric analysis. Also, exhaustion with PD-1 and senescence with KLRG1 were assessed for both cell subsets. Here the gating strategy was applied as described in paragraph 6.3.3. Leukocytes were isolated from pancreatic islets of RIP-GP x XCR1$^{+/-}$ mice and RIP-GP x XCR1$^{-/-}$ mice at day 7 and at week 12 post-infection. Among CD8 T cells, there was a reduced frequency of GrB-producing cells in the islets of XCR1-deficient mice both at day 7 (p=0.032) and at week 12 (p=0.042). At week 12, a decreased number of Perf-producing cells was also detected (p=0.012). There were no significant

differences detected in the frequency of PD-1 and KLRG1 expressing cells. Importantly, at day 7 the frequency of islet autoantigen-specific CD8 T cells expressing Perf or GrB was also reduced in RIP-GP x XCR1$^{-/-}$ islets. Further, at week 12 the frequency of Perf-producing cells was significantly reduced in RIP-GP x XCR1$^{-/-}$ compared to RIP-GP x XCR1$^{+/-}$ islets ($p=0.012$). As for total CD8 T cells, there were no significant differences regarding the expression of PD-1 and KLRG1 in islet autoantigen-specific CD8 T cells (Figure 35). All this taken together suggests that in absence of XCR1 the activation of both CD8 T cells and of autoantigen-specific CD8 T cells, rather than their total number, is reduced.

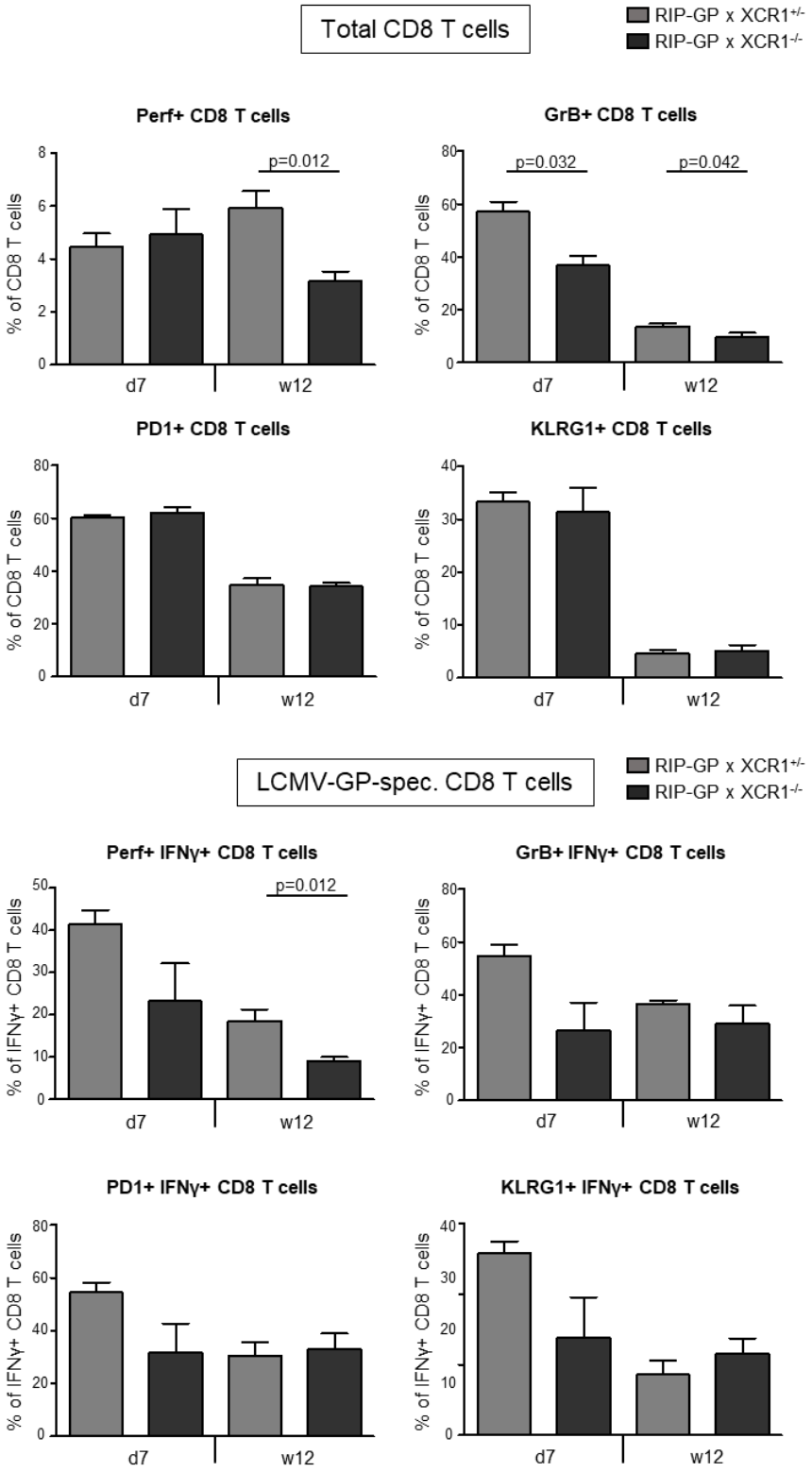

Figure 35. XCR1-deficient mice show reduced T cell activity in the islets.
Frequencies of CD8 T cells expressing perforin (Perf), granzyme B (GrB), PD-1, or KLRG1 of total CD8 T cells or LCMV-GP33-specific CD8 T cells. Data were obtained via flow cytometric analysis of islet infiltrating cells of RIP-GP x XCR1$^{+/-}$ and RIP-GP x XCR1$^{-/-}$ mice at day 7 and at week 12 post-infection. Results are shown as mean ± SEM and p-values are indicated when significant (n=4-5 at day 7, n=4-7 at week 12).

6.4.4 XCR1-deficient mice have more regulatory T cells in the islets

After finding differences in the T cell activity, flow cytometry of isolated cells from pancreatic islets was performed following an intracellular staining for FoxP3. Regulatory FoxP3+ cells were gated from the leukocyte gate as described in paragraph 6.3.4. RIP-GP, RIP-GP x XCR1$^{+/-}$, and RIP-GP x XCR1$^{-/-}$ mice were compared at day 7, whereas only the last two lines were analysed at week 12. Interestingly at day 7 there were significantly more FoxP3+ cells in the islets of RIP-GP x XCR1$^{-/-}$ mice than in regular RIP-GP mice (p=0.032). An increase was also visible when comparing the RIP-GP x XCR1$^{-/-}$ mice to the RIP-GP x XCR1$^{+/-}$ mice. However, this tendency was not significant. Such a difference was not detectable at week 12 after infection (Figure 36*A*). The ratio between all FoxP3+ T cells (CD4 and CD8), namely the Treg cells, and the IFNγ-producing T cells, autoaggressive T cells, was calculated. At day 7 post-infection this ratio was extremely high in the islets of RIP-GP x XCR1$^{-/-}$ mice in comparison to both regular RIP-GP mice, 18 times higher (p=0.016), and RIP-GP x XCR1$^{+/-}$ mice, with a 5-fold difference (p=0.032). Again, such a difference was not detectable at week 12 (Figure 36*B*).

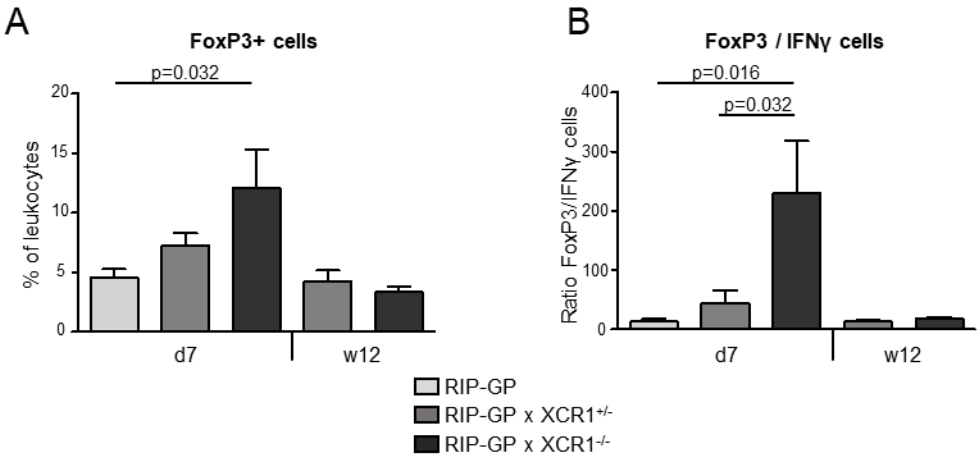

Figure 36. The immune balance is shifted towards a regulatory milieu in XCR1-deficient mice.
(A) Frequencies of FoxP3+ cells among all leukocytes isolated from islet infiltrating cells in the pancreas of RIP-GP mice, RIP-GP x XCR1$^{+/-}$ mice, and RIP-GP x XCR1$^{-/-}$ mice at day 7 and week 12 after infection. - (B) Ratio calculated of FoxP3+ (regulatory) cells and IFNγ-producing (autoaggressive) cells. Results are shown as mean ± SEM and p-values are indicated when significant (n=4-5 at day 7, n=4-7 at week 12).

6.4.5 XCR1-deficient mice are partially protected from developing T1D

To evaluate if the impaired T cell activation observed in XCR1-deficient mice had also a clinical impact on T1D, an incidence study was carried out comparing regular RIP-GP with RIP-GP x XCR1$^{+/-}$ and RIP-GP x XCR1$^{-/-}$ mice. Therefore, mice were infected with LCMV and BG concentration was measured at weekly intervals for 12 weeks. As already shown, 80% of RIP-GP mice developed T1D. The T1D incidence peaks in RIP-GP x XCR1$^{+/-}$ mice and RIP-GP x XCR1$^{-/-}$ mice were 60% and 50%, respectively. However, many mice reverted to a non-diabetic status and by the end of the study, there was a marked difference in T1D incidence between of RIP-GP x XCR1$^{-/-}$ mice (30%) and regular RIP-GP mice (65%) (Figure 37*A*). The mean BG levels reflected the data from the incidence study. The highest values were found in the group of regular RIP-GP mice, whereas the RIP-GP x XCR1$^{-/-}$ mice mainly had mean BG levels below 300 mg/dl (Figure 37*B*). These data indicate that XCR1-deficiency results in a lower T1D incidence and a milder form of the disease.

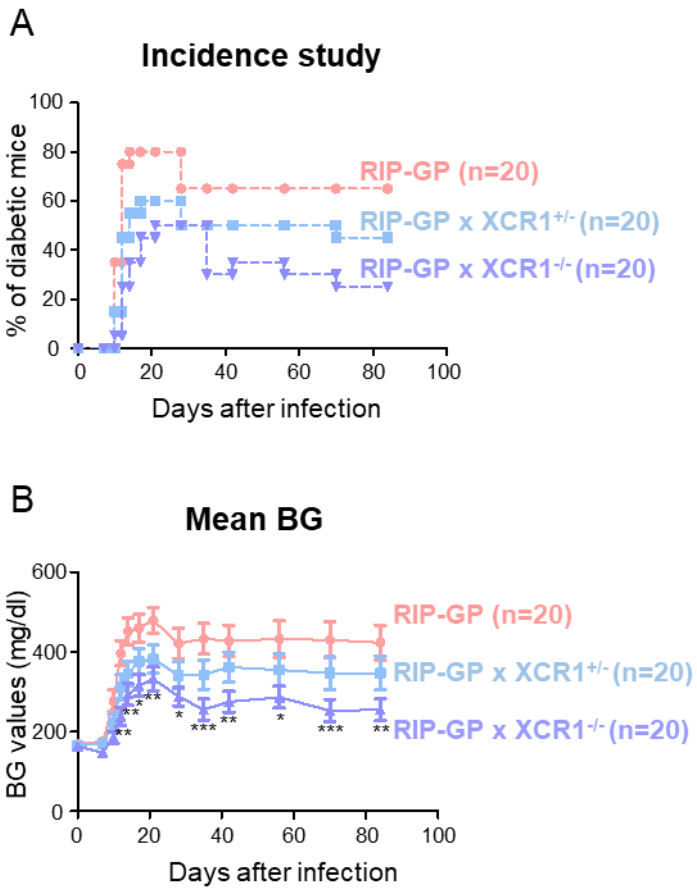

Figure 37. RIP-GP x XCR1$^{-/-}$ mice show reduced T1D incidence.
Mice have been infected and BG levels have been measured for 12 weeks after the infection. - (A) Frequencies of mice that developed T1D after the infection. Mice are considered diabetic when BG is >300 mg/dl. - (B) Mean BG per each line ± SEM. Significance is reported in the graph, comparing each line to regular RIP-GP mice. * = p<0.05, ** = p<0.01, *** = p<0.001. Number of mice is indicated in brackets. RIP-GP mice results are the same as in Figure 28.

6.4.6 XCR1-deficient mice have more intact islets

To check the status of the pancreas, immunohistochemistry with anti-insulin antibody was performed on pancreas sections of RIP-GP mice, RIP-GP x XCR1$^{+/-}$ mice, and RIP-GP x XCR1$^{-/-}$ mice at week 12 post-infection, endpoint of the incidence study. Note that half of the RIP-GP mice had to be killed before the endpoint because they were too sick (5 to 12 weeks after the infection). They were anyway included in this quantification. From the representative pictures (Figure 38*A*), it is visible that both RIP-GP and RIP-GP x XCR1$^{+/-}$ mice had destroyed islets, where only few cells were able to produce insulin. Many islets in RIP-GP x XCR1$^{-/-}$ mice were still intact and β-cells were still producing insulin at week 12 after infection. Note that the morphology of the tissue looks somewhat

different from traditional immunohistochemistry because the organs had to be processed in PLP buffer before embedding in Tissue-Tek OCT. Insulitis was quantified as previously described, assigning a score according to the islet damage. RIP-GP x XCR1$^{-/-}$ mice had more intact islets (score 0 and score 1) compared to the other two groups of mice (Figure 38*B*). However, staining of only one section of pancreas does not give a comprehensive information about the whole pancreas. Therefore, 3D-staining of the whole pancreas was performed (see next paragraph).

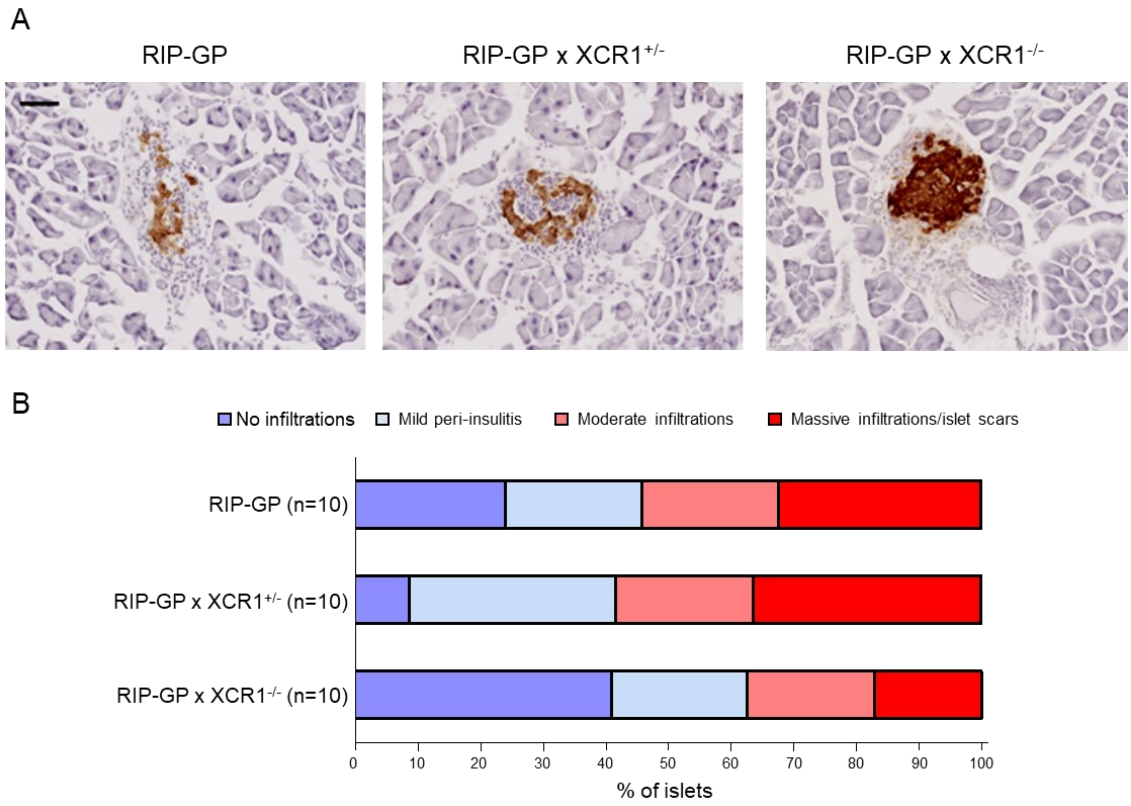

Figure 38. XCR1-deficient mice show less destroyed islets.
(A) Representative pictures of insulin-stained pancreas sections of RIP-GP mice, RIP-GP x XCR1$^{+/-}$ mice, and RIP-GP x XCR1$^{-/-}$ mice at week 12 after infection (endpoint of incidence study). Note that most of the RIP-GP mice had to be killed before the endpoint, resulting in time range of 5 to 12 weeks for this group. Note that the morphology of the tissue looks somewhat different from traditional immunohistochemistry because the tissue was treated with PLP buffer before embedding in OCT. Images were taken with Nanozoomer Digital Pathology after scanning them with NanoZoomer S360 Digital slide scanner. Digital magnification is 20x and scale bar is 50 µm. - (B) Islet damage score assigned to the islets. The score system is describe in Materials and Methods section. Number of mice is indicated in brackets.

6.5 XCL1- and XCR1-deficient mice have more functional islets compared to regular RIP-GP mice

The quantification of the islet damage from only one slide of pancreas per mouse can be ambiguous. As a matter of fact, the location of the one slide used for IHC might be derived from a region of the pancreas that displays islets with more or less insulitis. Therefore, whole pancreas isolated from uninfected RIP-GP mice as control and RIP-GP, RIP-GP x XCL1$^{-/-}$, and RIP-GP x XCR1$^{-/-}$ mice at the endpoint of their incidence study (week 8-12 accordingly to their disease stage) after LCMV-infection was stained with anti-insulin antibody. Shortly, after perfusing the whole mouse with buffered PFA and fixation of the isolated pancreas, some permeabilization steps were carried out. Unspecific signal was blocked with a blocking solution containing DMSO and donkey serum. As primary antibody an anti-insulin antibody was diluted in first antibody buffer and the pancreas was incubated in this solution for 4 days. Each day the concentration of the antibody was increased and the sample was incubated at 37°C shaking over the day and centrifuged at 600 x g overnight. After some washing steps, a fluorescent secondary antibody incubation followed using the same conditions as the first, but diluted in secondary antibody buffer. Finally, the pancreas was embedded in low-melting agarose 1.3%, dehydrated with tetrahydrofuran, and cleared with dibenzyl ether. The stained pancreas was acquired with an ultramicroscope Olympus MVX10, from LaVisionBiotec. For more detailed protocol, see Materials and Methods section. Representative pictures of the whole pancreas staining are shown in Figure 39.

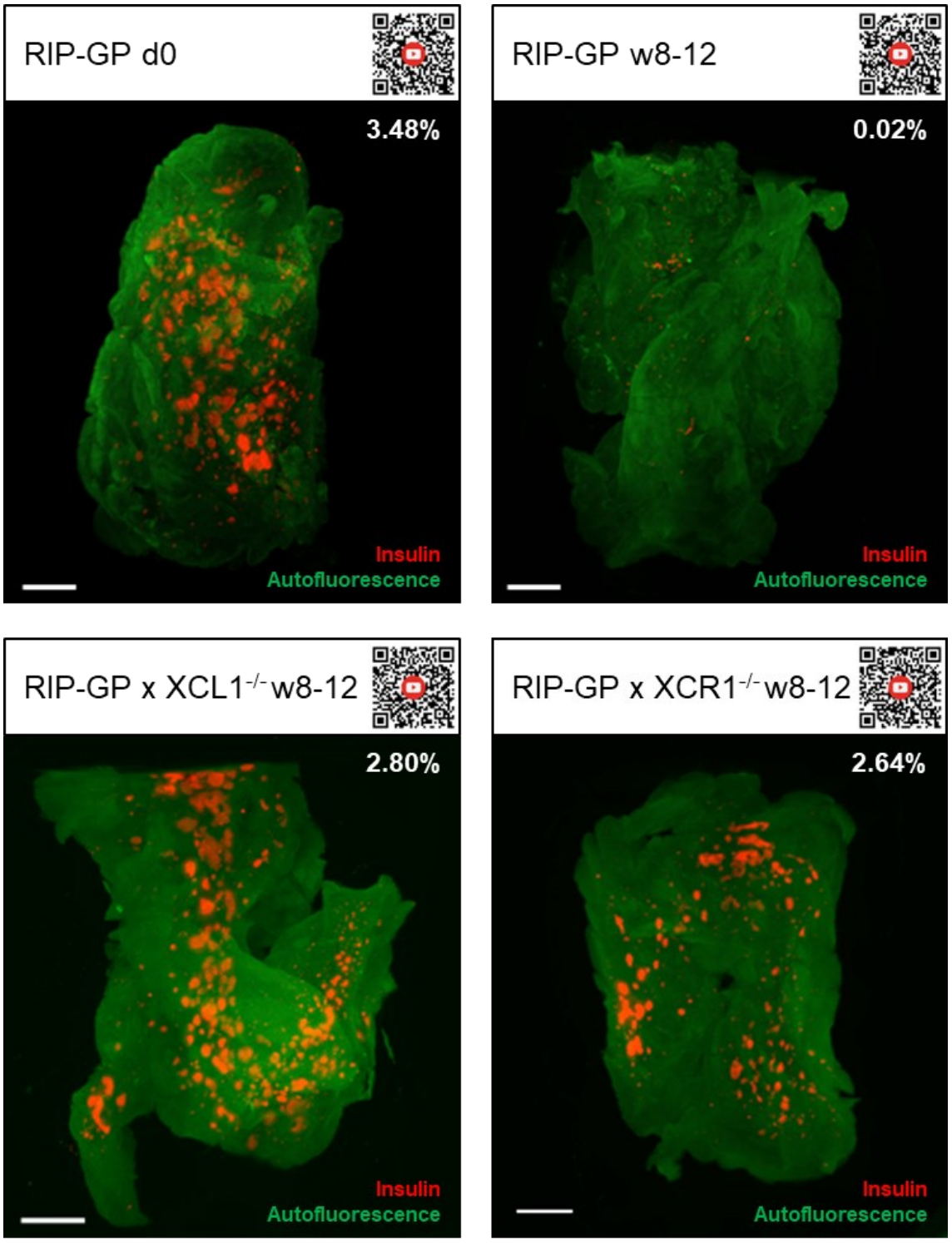

Figure 39. Representative pictures of the 3D-fluorescent staining of the whole pancreas. 3D pancreas representative pictures of uninfected, healthy RIP-GP pancreas and infected RIP-GP, RIP-GP x XCL1$^{-/-}$, and RIP-GP x XCR1$^{-/-}$ pancreata at week 8-12 after LCMV-infection. Insulin producing cells are stained in red with an antibody against insulin and the structure of the pancreas is given by its autofluorescent signal in green. The QR codes inserted next to the image titles are connected to YouTube videos showing the 3D movie of each pancreas. The insulin producing cell volume per pancreas volume is calculated and indicated for each pancreas. Scale bars indicate 200 µm.

With this technique, the quantification of the volume of insulin producing cells per pancreas volume was possible (Figure 40*A*). The uninfected, healthy RIP-GP mice had on average 2.33% of their entire pancreas volume occupied by insulin producing cells. In the infected RIP-GP mice, the volume of the remaining insulin producing cells was dramatically reduced to 0.29%. If only diabetic mice are considered (7 out of 8 in this case), the β-cell volume would even be decreased to 0.02%. In contrast, XCL1- and XCR1-deficient RIP-GP mice at the same time point showed a mean insulin-producing cell volume of respectively 0.91% and 1.5% of the total volume (Figure 40*A*). The size of the individual islets was also analysed. Islets were divided in 4 groups according to their volume (fragments, <25 μm^3; small, 25-100 μm^3; intermediate, 100-500 μm^3; and large, >500 μm^3) (Figure 40*B*). In general, the total number of islets detected in infected RIP-GP mice was decreased compared to uninfected RIP-GP mice (Figure 40*C*). At the same time, there were more islets in the XCL1- and XCR1-deficient mice compared to uninfected regular RIP-GP mice. One reason for this might be that uninfected mice contain a higher proportion of large islets. As a matter of fact, an initially large islet that now contains large volumes of infiltrating cells after disease onset might be separated into several islet fractions that appear as two or more medium/small islets. As shown in Figure 40*B* and *C*, RIP-GP mice contained about 64% large islets (>500 μm^3). Importantly, infected RIP-GP mice had not only reduced numbers of islets, but also only a small quantity of large islets (31%). In contrast, RIP-GP x $XCL1^{-/-}$ mice as well as RIP-GP x $XCR1^{-/-}$ mice presented many islets, and an intermediate fraction of islets with a large volume (41% for the XCL1-deficient mice and 37% for the XCR1-deficient mice). These data indicate that in absence of XCL1 or XCR1 the diabetogenic process is massively constrained resulting in a sustained content of functional islets.

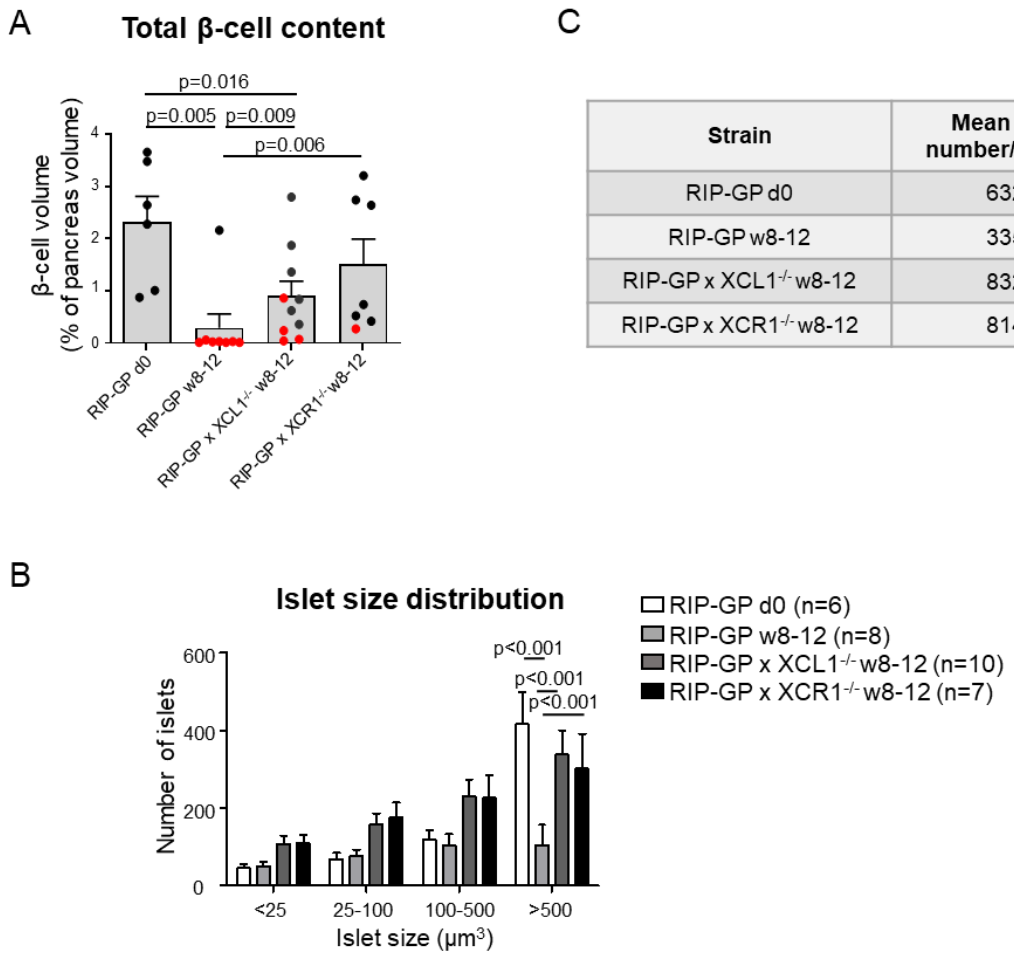

Strain	Mean islet number/mouse
RIP-GP d0	632
RIP-GP w8-12	335
RIP-GP x XCL1$^{-/-}$ w8-12	832
RIP-GP x XCR1$^{-/-}$ w8-12	814

Figure 40. XCL1- and XCR1-deficient mice show higher content of insulin compared to RIP-GP mice.
(A) Total β-cell content per pancreas of uninfected RIP-GP mice and infected RIP-GP, RIP-GP x XCL1$^{-/-}$, and RIP-GP x XCR1$^{-/-}$ mice at week 8-12 after LCMV-infection, calculated as percentage of the insulin producing cell volume per pancreas total volume. Each dot indicates insulin content of one mouse. In red, diabetic mice have been highlighted. - (B) The islets have been grouped according to their volume size in fragments (<25 µm^3), small (25-100 µm^3), intermediate (100 - 500 µm^3), and large (>500 µm^3). - (C) The table shows the mean number of islets per mouse of each line. Results are displayed as mean ± SEM. Number of mice and p-values are indicated in the figure.

6.6 CXCL10 and XCL1 deficiency

6.6.1 RIP-GP x CXCL10$^{-/-}$ x XCL1$^{-/-}$ mice show reduced T1D incidence compared to CXCL10-deficient mice

Since both the XCL1- and XCR1-deficient mice showed that the XCL1/XCR1 axis plays a role in the pathogenesis of the disease but their absence did not completely prevent T1D, we crossed the RIP-GP x XCL1$^{-/-}$ mice to the RIP-GP x

CXCL10$^{-/-}$ mice. CXCL10 was already identified as a good target and anti-CXCL10 antibody seems to be a useful therapy for T1D[134], especially in combination with anti-CD3 antibody.[47] Further, CXCL10-deficient RIP-GP mice, similar to XCL1-deficient RIP-GP mice, were partially, but not completely protected from T1D.[47] Moreover, CXCL10 is also produced by cDC1 once they are activated to attract more T cells to the inflammation site.[96–98] Therefore, blocking CXCL10 acts both on the recruitment of T cells and on one of the functions of cDC1.

First a plaque assay was performed to be sure that the double deficiency did not affect the virus elimination. Also in this case, no differences were detected among the regular RIP-GP mice, RIP-GP x CXCL10$^{-/-}$ x XCL1$^{+/-}$ mice, and RIP-GP x CXCL10$^{-/-}$ x XCL1$^{-/-}$ mice both at day 3 and at day 7 after infection (Figure 41).

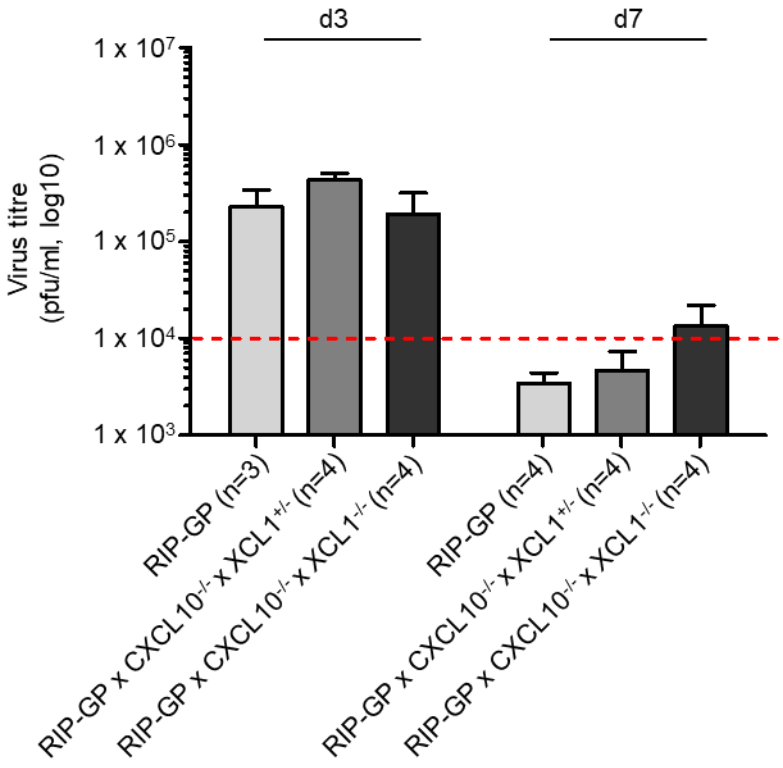

Figure 41. RIP-GP x CXCL10$^{-/-}$ x XCL1$^{-/-}$ mice do not show differences in virus elimination compared to regular RIP-GP mice.

Virus titre expressed in pfu/ml of LCMV left in spleens obtained with plaque assay. Spleens were collected from different mouse lines (RIP-GP, RIP-GP x CXCL10$^{-/-}$ x XCL1$^{+/-}$, and RIP-GP x CXCL10$^{-/-}$ x XCL1$^{-/-}$ mice) at day 3 and at day 7 after the infection. Results are shown as mean ± SEM. Red dot line represents the limit of detection of this technique. Number of mice is indicated in brackets.

A T1D incidence study was performed to find out if XCL1-deficiency would improve CXCL10-deficiency results. CXCL10-deficient mice were therefore compared with or without XCL1 expression. RIP-GP x CXCL10$^{-/-}$ x XCL1$^{+/-}$ and RIP-GP x CXCL10$^{-/-}$ x XCL1$^{-/-}$ mice were infected with LCMV and their BG levels were measured for 16 weeks in weekly intervals. RIP-GP x CXCL10$^{-/-}$ x XCL1$^{+/-}$ mice developed T1D in the 50% of the cases, but this was reduced to 15% by the end of the incidence study including some remitting mice. RIP-GP x CXCL10$^{-/-}$ x XCL1$^{-/-}$ mice had an incidence of 16.6% between day 17 and 21, and for the rest of the time was only 8.33%: only one mouse was diabetic for the whole study (Figure 42*A*). When comparing the mean BG values of these mice, no big differences were evident. The mean values of both lines were below 300 mg/dl at all time points and no significant difference was visible between the two groups (Figure 42*B*).

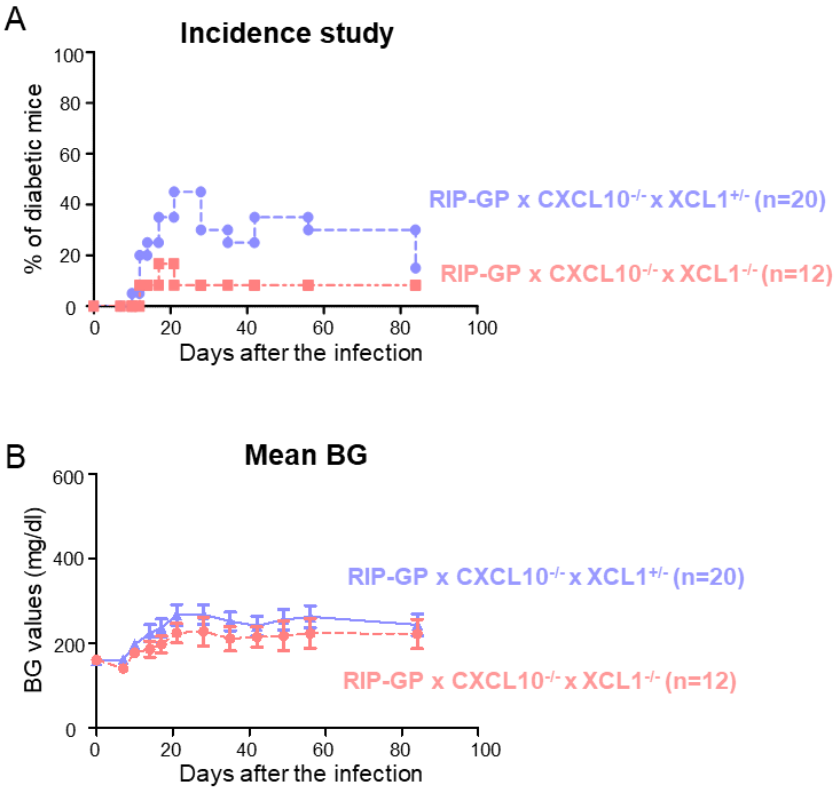

Figure 42. RIP-GP x CXCL10$^{-/-}$ x XCL1$^{-/-}$ mice are more protected from developing T1D than CXCL10-deficient mice.

(A) Percentage of mice that turned diabetic after LCMV-infection. The incidence study was performed for 16 weeks, comparing RIP-GP x CXCL10$^{-/-}$ x XCL1$^{+/-}$ mice with RIP-GP x CXCL10$^{-/-}$ x XCL1$^{-/-}$ mice. Mice with BG > 300 mg/dl were considered diabetic. - (B) Mean BG levels of the mice in (A). Values are reported as mean ± SEM. Note that in both cases the average is below the threshold of 300 mg/dl at any time point.

6.6.2 CXCL10- and XCL1-deficient mice show reduced insulitis at the endpoint of the incidence study

To see if RIP-GP x CXCL10$^{-/-}$ mice show a difference in the status of the pancreas in presence or absence of XCL1, quantification of the insulitis in the insulin-stained pancreas sections was performed by Deborah Puppe during her internship under my supervision. Pancreas sections were stained at day 7, 14, 28, and week 16 (endpoint of the incidence study) with anti-insulin antibody and then quantified as previously described. From the representative images, no obvious differences were visible at the different time points (Figure 43*A*). However, a careful quantification revealed a difference among the two lines at week 16 in that RIP-GP x CXCL10$^{-/-}$ x XCL1$^{-/-}$ mice had less insulitis compared to RIP-GP x CXCL10$^{-/-}$ x XCL1$^{+/-}$ mice (Figure 43*B*).

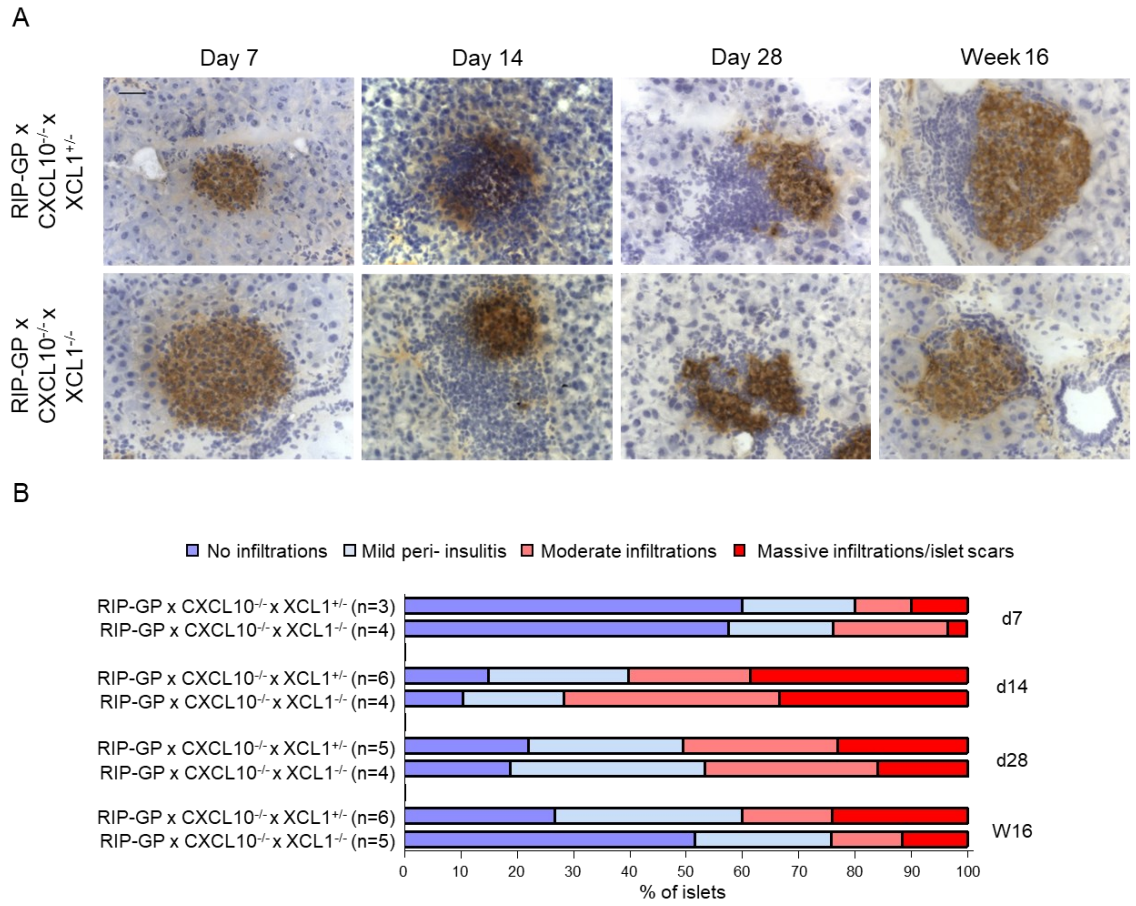

Figure 43. RIP-GP x CXCL10$^{-/-}$ x XCL1$^{-/-}$ mice show more intact islets at the endpoint of the incidence study.

(A) Representative images of immunohistochemical staining of pancreas slides with anti-insulin antibody comparing RIP-GP x CXCL10$^{-/-}$ x XCL1$^{+/-}$ mice with RIP-GP x CXCL10$^{-/-}$ x XCL1$^{-/-}$ mice at day 7, 14, 28, and week 16 after infection. Original magnification 40x. Scale bar represents 25 µm. - (B) Islet damage score applied to the staining with anti-insulin antibody. The score system is described in Materials and Methods section. Number of mice is indicated in brackets. Note that at day 14 most of the islets have moderate to massive infiltrations, and this is not the case at day 28 and at week 16. The mice at day 14 were mostly diabetic mice.

7. Discussion

In November 2022, the first drug for T1D has been approved by the FDA.[42] Teplizumab can be prescribed for stage 2 diabetic patients and can reduce the need for insulin up to at least 4 years. Unfortunately, an anti-CD3 therapy with Teplizumab can result in side effects, such as cytokine release syndrome and Epstein-Barr virus reactivation.[135] Moreover, some patients do not respond to treatment for yet unknown reasons.[27] Finally, treatment with anti-CD3 is an immunomodulation which delays the development of the disease but it is not a cure for T1D. That is why there is still urgent need for new targets to attack separately or in combination with Teplizumab.

7.1 CXCL10/CXCR3, CCL5/CCR5, CX_3CL1/CX_3CR1, and CXCL16/CXCR6

Chemokines have been studied in the context of T1D for a long time. They are among the major players in the disease pathogenesis. It has been demonstrated that CD8 T cell released chemokines have a role in T1D development and characterize not only the early stages of the disease,[69] but also the later ones due to a chemokine release by memory T cells.[68] However, such data have been often obtained by analysing patient sera or total pancreas homogenates in animal models. In order to better characterize their expression in the islets of Langerhans at several stages of the disease, in our lab Christine Bender performed a laser dissection of the islet microenvironment followed by a gene array analysis. She used the RIP-GP mouse model and dissected the islets at days 1, 3, 7, 10, 14, and 28 after LCMV-infection. Thereby, the focus was primarily on chemokine and receptor gene expression. Interestingly, almost all chemokines and receptors were upregulated after infection in comparison with healthy, uninfected controls. Among these, some chemokine-receptor pairs remained upregulated at least until day 28, when T1D became chronic in the RIP-GP mice (Figure 1).

We first focused our attention on CXCL10 and its receptor CXCR3. They resulted upregulated around day 7-10 after the infection. CXCL10 has already been shown as an important factor in T1D pathogenesis. It was demonstrated to be released directly by β-cells upon stress or external stimuli [62] and its neutralization

in combination with anti-CD3 treatment reduced T1D incidence.[47] With RNAscope *in situ* hybridization technique and with immunohistological staining using anti-CXCL10 antibody or anti-CXCR3 antibody, I was able to visualize that CXCL10 is expressed throughout the islet, also by β-cells, whereas CXCR3 positive signal is mainly localized among the infiltrating cells (Figure 8).

Our attention was then moved on CCL5/CCR5, CX_3CL1/CX_3CR1, and CXCL16/CXCR6. CCL5 is mainly expressed by T cells and monocytes and can bind to several protein-G coupled receptors, like CCR1, CCR3, and with highest affinity CCR5. Besides CCL5, CCR5 can also bind CCL3 and CCL4 and is expressed on T cells and smooth muscle endothelial cells.[136] CCL5 is involved in many inflammatory processes, chronic diseases, and fibrosis. The CCL5/CCR5 axis has been studied in the context of viral infections. As a matter of fact, anti-CCR5 antibody is useful in particular in the treatment of HIV infections.[137] CCL5 is studied in the context of T1D and found to be higher in the serum of T1D patients in the initial phase of the disease.[66] It has been shown that CCL5 concentration is high at T1D diagnosis and decreases over time. Moreover, CCL5 decreases in the serum of patients in remission.[138] It was therefore not surprising to see the impressive upregulation of CCL5 and of its receptor, CCR5, in the gene array from RIP-GP mice between day 7 and day 10. However, when we studied T1D incidence in RIP-GP x $CCL5^{-/-}$ mice we could not see any difference in comparison to regular RIP-GP mice. This could be explained by the redundancy of the axis that could react to the absence of CCL5 by upregulating the other chemokines.

CX_3CL1 is the only chemokine of the CX_3C family. It can be found as a soluble or a membrane-bound chemokine in neurons and in epithelial cells. Its receptor CX_3CR1 is present on monocytes, NK cells, T cells, and muscle smooth cells.[139] CX_3CL1 has been found to be expressed in human islet cultures and in some human pancreas sections, and it seems to be involved in T1D pathogenesis.[140] Thus, we generated CX_3CL1-deficient mice and they showed a reduced T1D incidence both in RIP-GP and RIP-NP mice.

CXCL16 is released by CD11c+ cells and its receptor CXCR6 is expressed by T cells.[141] As shown in the gene array both are upregulated upon infection and they are found to be correlated with T1D since CXCR6 is located in the IDDM22 T1D risk locus in humans and CXCL16 was found on the Idd4 locus, which is

correlated with T1D in NOD mice.[142,143] Also in this case, we used CXCR6-deficient mice and we saw a reduction in T1D incidence compared to regular mice.

7.2 XCL1/XCR1 axis

The main part of my thesis focused on another chemokine/receptor pair which turned out to be upregulated between day 7 and day 10 and maintained at high levels at least up to day 28, when the disease is chronic. This is the XCL1/XCR1 axis. XCL1 is the only chemokine belonging to the X-C family. It was discovered in the late 1990s[70–72] and its only known receptor is XCR1.[81] XCL1 is found to be produced in spleen, thymus, intestine, blood, lung, colon, and prostate gland. It is produced by CD8+ T cells, CD4- CD8- TCRαβ+ T cells, γδ T cells, CD4+ T cells, NK cells, and NK T cells.[79] It is secreted by T cells in a dose-dependent manner 8-36 hours after encountering the antigen, presented by DC.[73] Stievano et al.[144] found that constitutive and activation-induced XCL1 are expressed in the blood of healthy patients mainly by CD8 T cells. In particular, CD8+ CD5- T cells and γδ T cells are the major sources for this chemokine.[144] XCL1 has been described as a type 1 (Th1/Tc1) chemokine, since it is secreted together with CCL3, CCL4, CCL5, and IFNγ. T cells and NK cells are stimulated by IL2, IL12, IL15, and IL18 to produce this type of response. Type 1 chemokines work as chemoattractant, but also as coactivators of macrophages and they form a bridge between NK cells and T cells to close the gap between innate and adaptive immunity.[77,78] Eberlein at al.[69] and Davenport et al.[68] demonstrated that both effector and memory CD8 T cells produce a high number of different chemokines. In particular, CCL3, CCL4, and CCL5 are produced by most CD8 T cells, whereas XCL1 is produced by a smaller fraction, followed by CCL1 and CCL9/10 which are generated only by few CD8 T cells.[68,69]

XCL1 has only one receptor, XCR1. It is expressed only by cDC1, which are a particular subset of DC. cDC1 are characterized by the expression of CD11c, MHC-II, CD8α and/or CD103 in mice; by the presence of CD141 in humans.[82,87] Given the exclusivity of the receptor and the importance of cDC1 in priming T cells, the XCL1/XCR1 axis has been already studied in other diseases. Therapies that improve XCR1+ cell migration are studied related to melanoma. In particular,

XCL1 based treatments are used via injection within the dermis to increase T cell response against the tumour.[128] XCL1-fusion vaccines against influenza virus are also studied to improve the immune response.[129]

With the RNAscope *in situ* hybridization technique (Figure 9), we could demonstrate that prior infection neither XCL1- nor XCR1-expressing cells were present in the islets of RIP-GP mice. Once the mice were infected, both XCL1- and XCR1-producing cells were found in the islets, increasing over time and persisting to day 28. It is interesting to notice that these XCR1+ cells are localized among the infiltrating cells confirming that they are mainly part of leukocytes. The upregulation of XCL1 and XCR1 was also visible in the NOD mouse (Figure 10). Importantly, the highest expression was in the pre-diabetic stage indicating that XCL1- and XCR1-expressing cells are actively involved in the initiation of the autodestructive process. Once the NOD mice became diabetic, mainly XCR1-expressing cells remained in the islets. Thus, the XCL1/XCR1 axis is particularly attractive, since the T cells play a dominant role in T1D pathogenesis and XCL1 is involved in the Th1-type response.[77,117]

To further investigate the importance of the XCL1/XCR1 axis, also some human pancreas sections obtained from individuals at different disease stage were assessed with RNAscope *in situ* hybridization. Interestingly, the number of cells producing XCR1 was increased in Aab+ and T1D pancreata in comparison to ND sections (Figure 12). Unfortunately, almost no cells producing XCL1 mRNA were detected in any section. This could be explained by the fact that not so many CD8+ cells might be present in the islets at the moment of investigation. Another possible explanation could be that since XCL1 is a chemokine, its production could be just transient and therefore difficult to see. Moreover, not only the XCL1 signal was not present but also the XCR1 signal was quite weak. This could be that since the samples have been stored for more than one year, the mRNA signal got weaker. Anyhow, it is important for the purpose of this study that an increased number of XCR1-expressing cells is present in the islets of Aab+ and T1D patients. It is planned to further investigate the XCL1 and XCR1 expression in human pancreas samples in more detail with fresh samples that will be obtained via the Network for Pancreatic Organ Donors with Diabetes (nPOD).

Since it seems that the XCL1/XCR1 is involved in T1D pathogenesis, in order to closely study its role, we used both XCL1-deficient as well as XCR1-deficient mice that we crossed with the RIP-GP mice.

7.3 XCL1 absence or XCR1 absence

7.3.1 DC behaviour

In absence of XCL1 or XCR1, we saw that some cDC1 still migrate to the pancreas. With RNAscope *in situ* hybridization we demonstrated that in XCL1-deficient mice, there were still XCR1-expressing cells among the infiltrating cells (Figure 14). At the same time, using the XCR1-deficient mice which express the Venus gene instead of the XCR1 gene, Venus+/+ cells (cDC1) were still able to infiltrate the islets starting from day 7 and were still present at week 12 (Figure 31). This migration behaviour of cDC1 in absence of a functional XCL1/XCR1 axis might be explained by the presence of redundant migration factors. One of these could be CCR6, which is expressed by immature DC, that are attracted to the site of inflammation via CCL20. Upon their arrival, they can encounter the antigen and maturate into cDC1.[145] Another possible pathway might be the CCL21/CCR7 axis. CCR7 is present on migratory CD103+ DC that have encountered the antigen. Following a CCL21 gradient, CCR7 allows cDC1 to migrate to the lymph nodes to prime CD8+ T cells.[87,146] Further, to migrate to the tumour microenvironment, mature cDC1 follow CCL5 and XCL1 gradients, thanks to their expression of CCR5 and XCR1.[96] In absence of one of the components of the XCL1/XCR1 axis, the CCL5/CCR5 axis might be responsible for the presence of some cDC1 in the pancreas.

However, we could demonstrate via IHC and flow cytometry that even if still present, CD103+ cDC1 are reduced in the islets of XCL1-deficient mice (Figure 16, Figure 17). At the same time such mice show an accumulation of this cell type in the pancreatic draining lymph nodes, suggesting that their migration to the islets is indeed reduced. In this context, it has been demonstrated that Batf3-deficient NOD mice are protected from developing T1D.[147] This is interesting because Batf3 is an important transcription factor that characterizes XCR1+ DC[94] and the lack of Batf3 has been correlated to a lower number of CD103+ DC and

a reduced number of effector T cells in the islets.[147] However, it has been demonstrated that CD103 itself does not have a role in T1D pathogenesis. When RIP-GP mice have been used to demonstrate the impact of CD103 deficiency, this did not result in a beneficial effect in T1D effect, showing less importance for CD103 in T1D pathogenesis.[148] CD103 is expressed not only on cDC. In the pancreas of healthy patients CD103 is expressed also by CD4 and CD8 T cells.[149] In this case the redundancy between adhesion molecules such as E-cadherin results in only a small impact on cDC1 and T cell migration in absence of CD103. On the contrary, XCR1-deficient mice did not show changes in the migration of cDC1 to their islets via flow cytometric analysis (Figure 33). Moreover, in the IHC quantification of the Venus signal XCR1-deficient mice seemed to show an even higher Venus+ signal/islet area compared to RIP-GP x XCR1$^{+/-}$ mice at week 12 after the infection (Figure 31). However, here the measured fluorescent cell area might appear larger, due to the brighter green fluorescent signal in the XCR1-deficient mice that express the Venus protein on both alleles, compared to the heterozygous mice, which contain the Venus gene on only one allele.

7.3.2 T cell behaviour

CD8 T cells have been demonstrated to be the major players in T1D pathogenesis in the RIP-LCMV-GP mouse model.[125] IFNγ-producing cells, the so-called effector T cells, have an active role in killing β-cells and IFNγ itself is a very important cytokine in the development of the disease.[150,151] LCMV-GP33 peptide autoantigen-specific CD8 T cells can be stimulated overnight with GP33 LCMV-specific protein to release IFNγ. After an intracellular cytokine staining, we identified these cells as autoantigen-specific CD8 T cells, the most aggressive CD8 T cell phenotype.

Indeed, in XCL1-deficient mice a decreased amount of autoantigen-specific CD8 T cells was found in the islets which corresponded to a diminished cDC1 number. In contrast with that, there was an increase of autoantigen-specific CD8 T cells in the PDLN (Figure 22). This result fits very well to the fact that cDC1 are the best cell-type in cross-presenting the exogenous antigen to CD8 T cells and starting the (auto)immune reaction.[96] Thus, the reduced number of cDC1 could not

sufficiently prime CD8 T cells, explaining not only the decreased number of specific CD8 T cells, but also their reduced activity.

XCR1-deficient mice also showed less IFNγ-producing cells among their infiltrating cells compared to regular RIP-GP mice, in particular at day 7. In contrast to XCL1-deficient mice, the increase of this cell subtype in the PDLN was not visible (Figure 34). A hypothesis might be that in absence of XCR1, T cells can still migrate to the islets but they are less active. In order to investigate this, we checked the aggressive phenotype of T cells for perforin and granzyme B production. Perforin and granzymes together are one of the main mechanisms which causes β-cell death.[152] Perforin is required to create holes in the target cell membrane and thereby facilitate the entrance of the different granzymes in the cell to cause its death. It has been shown that perforin-deficient NOD mice and perforin-deficient RIP-GP mice had reduced T1D incidence but no reduced insulitis, meaning that perforin is important for cell death but not for cell infiltration in the islets.[153–155] Similarly, Sutton et al. demonstrated that granzyme B-deficient T cells were not able to kill the β-cells.[156] Several studies have also demonstrated that this is only one of many different mechanisms that act on β-cells, as it is shown with perforin-deficient mice, where T1D incidence is not completely reduced to zero because other mechanisms, like Fas/FasL induced apoptosis, tumour necrosis factors, and IL1, can also kill β-cells.[152,157,158] We studied the release of both perforin and granzyme B by CD8 T cells and LCMV-specific CD8 T cells. In absence of XCL1, there are less islet autoantigen-specific T cells and a decreased frequency of granzyme B producing T cells at day 28 after infection, confirming a reduced killing activity of these cells (Figure 24). In absence of XCR1, the frequency of both perforin and granzyme B releasing T cells is decreased (Figure 35). This reduced cytotoxic potential can be explained by a suboptimal T cell activation in absence of a suitable number of cDC1.

Furthermore, the cytotoxic potential T cells of XCL1-deficient mice seem to display an additional impairment in their overall fitness. T cell exhaustion and senescence are two different stages of T cell development. Exhaustion-like profile in T cell expression markers was found in the islets of slow T1D progress patients.[159] Moreover, in chronic viral infections and cancer, the continuous exposure to the antigen exhausts the T cells in their function.[160] Exhaustion is controlled by three different mechanisms: cell surface inhibitory receptors,

soluble factors, and regulatory cells. Among the first category, PD-1 has been identified to inhibit T cell activity together with other factors, like CTLA-4 and LAG-3.[161] Once PD-1 is bound to one of its ligands, PD-1L and PD-2L, it causes the downregulation of the TCR. Subsequently the T cell undergoes a series of steps that first ceases the production of IFNγ and then induces programmed-cell death.[161–163] Senescent T cells have low proliferation capacity but they can still produce high amounts of proinflammatory cytokines, even if they reduce their release of perforin and granzyme B.[164] With the progression of aging, T cells downregulate the expression of CD28 and upregulate KLRG1.[165]

Therefore, we looked at PD-1 and KLRG1 expression for both total CD8 T cells and LCMV-specific CD8 T cells and we found that XCL1-deficient mice display a higher frequency of exhausted and senescent total CD8 T cells, compared to regular RIP-GP mice (Figure 24). This is significant at day 28 and it is therefore unlikely that the observed exhaustion is connected with the initial virus exposure. At the same time, it means that in XCL1-deficient mice the islet autoantigen-specific cells that infiltrate the islets have a less aggressive phenotype. In order to confirm this, we performed an *in vivo* CTL-assay to highlight a difference in the islet autoantigen-specific T cell killing between regular RIP-GP and XCL1-deficient RIP-GP mice. Although, there was no obvious difference in the killing profiles in the two mouse lines, looking at the half-life of GP33-labelled targets cells, it seemed that in the XCL1-deficient mice the killing was slowed down (Figure 25).

XCR1-deficient mice did not show a more exhausted or senescent phenotype compared to the RIP-GP x XCR1$^{+/-}$ mice. On the contrary, there was a slight reduction of the expression of these markers (Figure 35). This might be due to the fact that the T cells are in general less active in this case and therefore they do not become exhausted/senescent.

Among the different subsets of T cells, we also focused on regulatory T cells since a reduced activation of aggressive T cells might locally result in a shift in the immune balance in the islets. Opposite to most of the other analysed cell types, the frequency of Treg cells was increased in the islets of both XCL1-deficient mice and XCR1-deficient mice (Figure 27, Figure 36). In XCL1-deficient mice the increase was significant both at day 7 and at day 28, whereas in the XCR1-deficient mice the increase was present only at day 7. Interestingly, the ratio

between regulatory and autoantigen-specific T cells was increased at these time points for both mouse lines compared to the RIP-GP mice, suggesting a shift in the immune balance towards a regulatory milieu. This was not completely expected since, according to previous studies, CD103+ cDC1 have been reported to be also responsible for the induction of Treg in the intestine.[166] However, the observation might be specific for the intestine, since another study showed that CD103+ cDC1 can induce Treg cells specifically in the intestine, with a retinoic acid-dependent mechanism.[167] In contrast, several groups have shown that the Treg cells are more likely predominantly activated by immature DC, whereas mature, activated DC rather stimulate effector T cell.[168,169] In addition, also other DC subtypes are able to effectively activate Treg, as it has been shown for plasmacytoid DC (pDC) and dysfunctional myeloid DC (mDC) in cancer.[170,171] Thus, in our model a Treg stimulation by immature DC as well as pDC and dysfunctional mDC might outrun the suboptimal stimulation of aggressive T cells by insufficient numbers of cDC1. Alternatively, cDC1 in absence of XCL1 or XCR1 might remain in a somewhat immature form and would therefore preferentially activate Treg cells rather than aggressive T cells.

7.3.3 T1D incidence and insulitis

After finding differences at a cellular level in the pancreatic islets, the following step was to investigate the actual impact of an absence of XCL1 or XCR1 on the T1D pathogenesis. Indeed, there was a rather massive impact on T1D incidence and severity on both XCL1- and XCR1-deficient mice. In XCL1-deficient mice only 30% of the mice developed T1D at any given time after disease initiation with LCMV, compared to 80% of the regular RIP-GP mice (Figure 28). Interestingly, the XCL1-deficient mice had a milder form of T1D with a lower mean BG value over time. In addition, most of the diabetic mice reverted to a non-diabetic state after 5-10 days after the disease onset. At the end of the study only one mouse was diabetic. In XCR1-deficient mice the protective effect of an impaired XCL1/XCR1 axis was not as pronounced as in absence of XCL1 (Figure 37). 50% of XCR1-deficient mice developed T1D and thereof 40% went into remission, resulting in final incidence of 30%. Interestingly, the T1D onset is delayed in

XCR1-deficient mice. The peak of T1D incidence in the regular RIP-GP mice was at day 12, whereas in the XCR1-deficient mice was at day 21.

The pancreas status was also analysed with an anti-insulin staining of pancreas tissue sections to quantify the insulitis. First, traditional IHC revealed that the overall insulitis was indeed reduced in XCL1-deficient mice already at day 28 (Figure 30). Similarly, in XCR1-deficient mice the insulitis was less pronounced compared to both RIP-GP x XCR1$^{+/-}$ and regular RIP-GP mice (Figure 38). Second, to avoid inconsistencies due to the position of the two-dimensional pancreas section used for IHC, we performed a 3D-fluorescent staining of the whole pancreas. Such a staining was achieved by extended exposure of the entire pancreas to an anti-insulin antibody and a fluorescent secondary antibody, followed by the clearing of the tissue, and the acquisition of a 3D-image of the pancreas by a light sheet fluorescence microscope. Both XCL1- and XCR1-deficient mice showed a reduced total β-cell content compared to uninfected RIP-GP mice of 39% and 64%, respectively (Figure 40). Such a still rather large β-cell content is sufficient to maintain the BG homeostasis. The difference among these two lines might be due to the fact that among the analysed XCR1-deficient mice only one mouse was diabetic, compared to the 4 diabetic XCL1-deficient mice. Importantly, infected regular RIP-GP mice displayed only 12% of the β-cell content of an uninfected mouse. These findings align well with the fact that in patients the signs of clinical diabetes appear when more than 80% of the islets is destroyed.[12] In addition, infected RIP-GP mice had roughly half of the islets of uninfected RIP-GP mice. On the contrary, both the XCL1- and the XCR1-deficient mice have even more islets than the uninfected RIP-GP mice. This might be explained by the results obtained by the islet size distribution analysis. Both XCL1- and XCR1-deficient mice have a smaller fraction of large islets compared to uninfected RIP-GP mice, but at the same time they have a larger fraction of intermediate islets. This might result from the presence of infiltrates which somehow split the large islets in two or more intermediate ones, thus resulting in a higher mean number of islets.

7.4 Other possible therapies and combinations

The next critical step in this research would be the development of an antibody or small molecule which selectively modulates the operation of the XCL1/XCR1 axis, without completely blocking it. This approach aims to achieve a delicate balance, reducing T1D incidence while minimizing potential side effects. In patients, T1D is usually discovered when the autoimmune process has already started.[12] By that time critical factors driving the early steps in the pathogenesis might already been downregulated again. Therefore, a possibility would be to deplete the DC before interfering with the XCL1/XCR1 axis. Specifically, depleting DC using anti-CD103 antibody before interfering with XCL1/XCR1 could create an optimal environment for starting a therapy targeting this axis. This combined approach may better prepare the immune system for modulation, leading to more significant and sustainable outcomes.

A distinct perspective combines the interference of the XCL1/XCR1 axis with the administration of tolerogenic DC pulsed with proinsulin peptide. Tolerogenic DC have demonstrated their ability to reduce the autoimmune response in T1D and induce Treg cells without directly impacting T cells.[172] By coupling this approach with the interference of XCL1/XCR1, a combination strategy is formed, addressing both DC and T cell components of the autoimmune response. This could potentially yield synergistic effects, resulting in improved outcomes and an increase in Treg.

Another intriguing approach could be to act on DC migration, interfering with both XCL1/XCR1 axis and CCL5/CCR5 axis. As discussed in paragraph 6.1, the absence of CCL5 did not reduce T1D incidence. But from the RNAscope staining we saw a marked increased expression of this chemokine upon infection. Since CCL5 plays a role in cDC1 attraction,[173] it could be a valuable option to work on both chemokines at the same time. Simultaneously working on both chemokines may lead to a cumulative effect, further modulating DC recruitment and enhancing the therapeutic potential.

The interference with the XCL1/XCR1 axis may also be successfully employed in other combination therapies, such as with an anti-CXCL10 therapy. As already mentioned, CXCL10 is an important chemokine in T1D pathogenesis,[62,134] and preliminary investigations in CXCL10 and XCL1 double knockout mice showed

promising results. In fact, in absence of a small molecule or antibody to interfere with the XCL1/XCR1 axis, we decided to generate RIP-GP x CXCL10$^{-/-}$ x XCL1$^{-/-}$ mice and to compare them with RIP-GP x CXCL10$^{-/-}$ x XCL1$^{+/-}$ mice, in order to evaluate whether the absence of XCL1 in addition to CXCL10-deficiency would have been beneficial. The T1D incidence study (Figure 42) showed that only one mouse turned diabetic in the double deficient mice (8.33%) compared to the only CXCL10-deficient mice where the incidence was 50% at the peak. These findings need to be further investigated to fully comprehend the potential benefits of this combination therapy.

Considering the use of anti-CD3 in the treatment of T1D, it is known that the effects may wane over time, leading to re-infiltration of T cells in the pancreas. However, the repetitive administration of Teplizumab has not been considered for safety reasons. Thus, anti-CD3 administration could be employed as a starting point in combination therapies, as it effectively reduces the number of T cells in the short term.[42,44] Coupled with the interference of the XCL1/XCR1 axis, which acts on both DC and T cells, this combination could potentially yield long-lasting effects, preventing the re-infiltration of T cells. Similarly, a depletion of T cells with anti-CD3 antibody combined with a T cell re-infiltration blockade with anti-CXCL10 antibody has already been shown to be more successful in two mouse models for T1D compared to the treatment with only anti-CD3.[47]

In conclusion, among the various approaches discussed, the combination therapy involving the interference with the XCL1/XCR1 axis and the administration of tolerogenic DC pulsed with proinsulin peptide stands out as the most promising and potentially successful one. Its strategy addresses different aspects of T1D pathogenesis, potentially yielding additive or synergistic effects for improved outcomes. However, all the proposed approaches need to be further investigated to evaluate their potential.

8. Conclusions

Taken all the results together, we could confirm our initial hypothesis that the XCL1/XCR1 axis plays an important role in the pathogenesis of T1D. Thus the following scenario seems feasible: initially, upon stress, infections, or insulitis, the β-cells start to produce CXCL10.[62] T cells migrate to the islets following the CXCL10 gradient and start releasing XCL1. This attracts cDC1 to the islet microenvironment, where further activation enables them to prime T cells. Moreover, cDC1 can release CXCL10 as well, attracting even more T cells to the islet microenvironment. Autoaggressive T cells get activated and start to destroy the β-cells. Treg infiltrate the islets as well but possibly not in a sufficient number to impair the start of the autoimmune process.

I was able to demonstrate that XCL1 and XCR1 are upregulated and localized in the islets of RIP-GP mice upon infection and in the islets of NOD mice in a pre-diabetic stage. In order to investigate the role of XCL1/XCR1 axis in T1D, I used XCL1- and XCR1-deficient RIP-GP mice. By preventing XCL1 expression, the number of cDC1 and T cells migrating to the islets was reduced. Importantly, also the number of the aggressive islet autoantigen-specific CD8 T cells was significantly reduced. At the same time an increased number of FoxP3+ Treg cells was found in the islets. This represents a shift in the immune balance towards a more regulatory milieu in the islet microenvironment that strongly decreases the β-cell destruction resulting in a greatly reduced T1D incidence.

Similarly, XCR1-deficient mice showed a reduced T1D incidence. In this case, we could not see a significant difference in the number of cDC1 migrating to the islets. Therefore, we hypothesized that cDC1 lacking XCR1 are less able to prime T cell compared to XCR1+ cDC1, leading to a reduced T cell activation. Indeed, in absence of XCR1, there was a decrease of islet autoantigen-specific CD8 T cells. As for XCL1-deficient RIP-GP mice, there was also an increased number of Treg cells in the islets of XCR1-deficient mice. Thus, there was again a shift of the immune balance towards a more regulatory milieu, which correlated with a reduced β-cell destruction. This is schematized in Figure 44.

Thus, the findings presented in my thesis suggest that the XCL1/XCR1 axis is a promising target for future T1D therapies, as also confirmed by the increased number of XCR1-expressing cells that are present in the islets of Aab+ and T1D

patients. In humans XCL1 and XCR1 are found to be correlated to T1D and seem to play a similar role compared to mice.[79,80] Therefore, we plan to further investigate the role of XCR1 and XCL1 in T1D pathogenesis in humans with additional stainings focusing in more detail on cluster formation between XCL1- and XCR1-positive cells. Moreover, it would be interesting to study which cell types interact with the XCR1-expressing cells. In addition, our next important goal is to bring our findings closer to a possible therapy of T1D in patients. We intend to produce an antibody or a small molecule to interfere with the XCL1/XCR1 axis in both the RIP-GP and NOD mice.

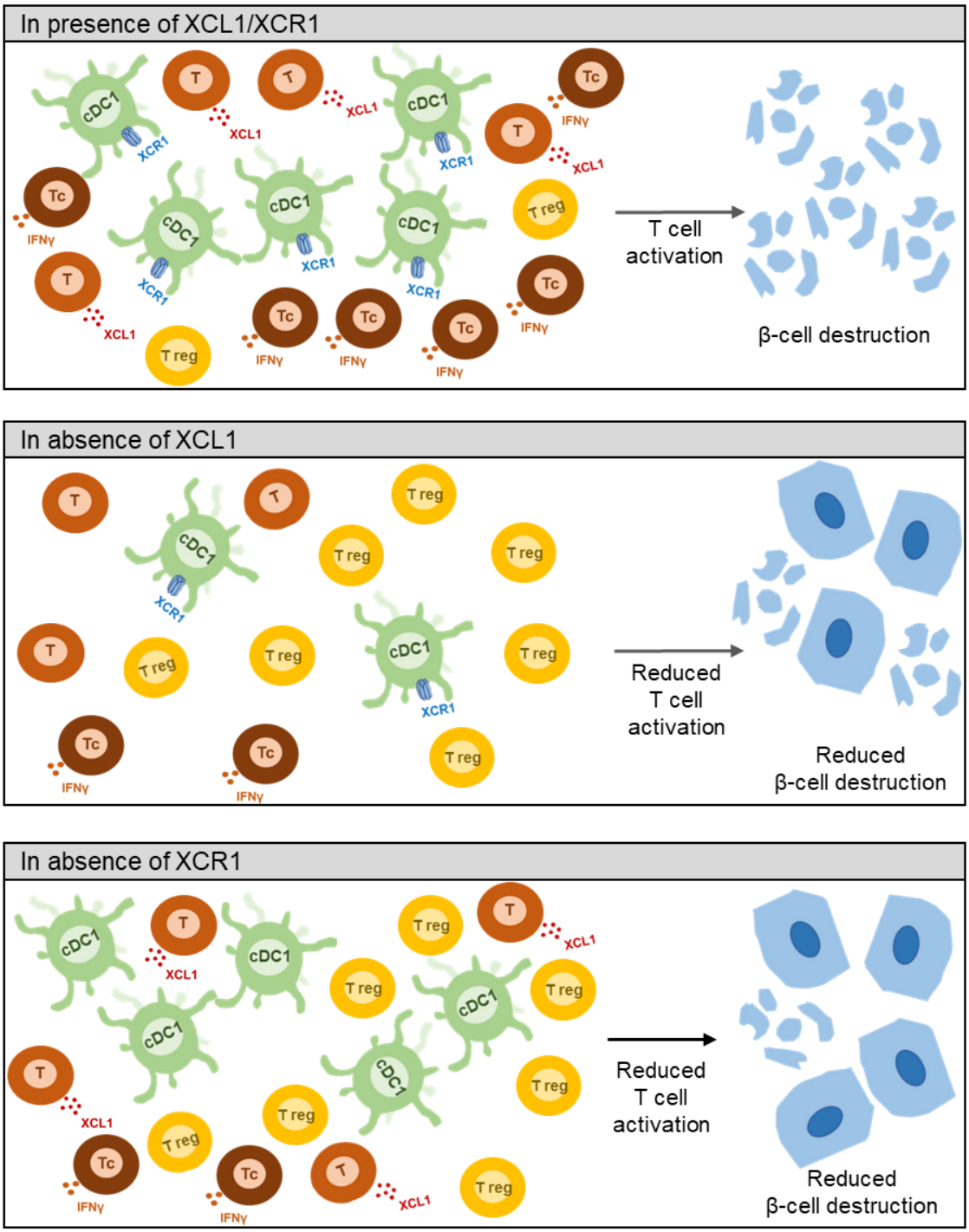

Figure 44. Schematic representation of the consequences of an absence of XCL1 or XCR1. In presence of both XCL1 and XCR1, T cells producing XCL1 attract XCR1+ cDC1 which activate T cells. Islet autoantigen-specific CD8 T cells destroy the β-cells, starting T1D. In absence of XCL1, T cells which migrate to the islet cannot produce XCL1 and therefore the number of cDC1 attracted to the islet is reduced. As a consequence, cDC1 produce less CXCL10 and less additional T cells migrate to the islet. Moreover, T cells are less activated and T1D incidence is reduced. In absence of XCR1, T cells migrate to the islet and produce XCL1. Even though the cDC1 do not express XCR1, they migrate to the islet along other chemokine gradients but they are not able to effectively prime the T cells. Reduced T cell activation leads to reduced β-cell destruction and subsequently reduced T1D incidence.

9. References

1. Wang L, Wang FS, Gershwin ME. Human autoimmune diseases: A comprehensive update. *J Intern Med*. 2015;278(4):369-395. doi:10.1111/joim.12395

2. Bieber K, Hundt JE, Yu X, et al. Autoimmune pre-disease. *Autoimmun Rev*. 2023;22(2). doi:10.1016/j.autrev.2022.103236

3. Christen U. Pathogen infection and autoimmune disease. *Clin Exp Immunol*. 2019;195(1):10-14. doi:10.1111/cei.13239

4. Sun H, Saeedi P, Karuranga S, et al. IDF Diabetes Atlas: Global, regional and country-level diabetes prevalence estimates for 2021 and projections for 2045. *Diabetes Res Clin Pract*. 2022;183:109119. doi:10.1016/j.diabres.2021.109119

5. Tuomi T. What Do They Have in Common? *Diabetes*. 2005;54(December):S40-S45. http://diabetes.diabetesjournals.org/cgi/content/abstract/54/suppl_2/S40

6. Ahlqvist E, Prasad RB, Groop L. Towards improved precision and a new classification of diabetes mellitus. *J Endocrinol*. 2022;252(3):R59-R70. doi:10.1530/JOE-20-0596

7. Dolenšek J, Rupnik MS, Stožer A. Structural similarities and differences between the human and the mouse pancreas. *Islets*. 2015;7(1):2-9. doi:10.1080/19382014.2015.1024405

8. Atkinson MA, Eisenbarth GS, Michels AW. Type 1 diabetes. *Lancet*. 2014;383(9911):69-82. doi:10.1016/S0140-6736(13)60591-7

9. Daneman D. Type 1 diabetes. *Lancet*. 2006;391(10138):2449-2462. doi:10.1016/S0140-6736(18)31320-5

10. Burrack AL, Martinov T, Fife BT. T cell-mediated beta cell destruction: Autoimmunity and alloimmunity in the context of type 1 diabetes. *Front Endocrinol (Lausanne)*. 2017;8(DEC):1-15. doi:10.3389/fendo.2017.00343

11. Van Belle TL, Coppieters KT, Von Herrath MG. Type 1 diabetes: Etiology, immunology, and therapeutic strategies. *Physiol Rev*. 2011;91(1):79-118. doi:10.1152/physrev.00003.2010

12. Gillespie KM. Type 1 diabetes: Pathogenesis and prevention. *C Can Med Assoc J*. 2006;175(2):165-170. doi:10.1503/cmaj.060244

13. Bluestone JA, Herold K, Eisenbarth G. Genetics, pathogenesis and clinical interventions in type 1 diabetes. *Nature*. 2010;464(7293):1293-1300.

14. Insel RA, Dunne JL, Atkinson MA, et al. Staging presymptomatic type 1 diabetes: A scientific statement of jdrf, the endocrine society, and the American diabetes association. *Diabetes Care*. 2015;38(10):1964-1974. doi:10.2337/dc15-1419

15. Ziegler AG, Rewers M, Simell O, et al. Seroconversion to multiple islet autoantibodies and risk of progression to diabetes in children. *Jama*. 2013;309(23):2473-2479. doi:10.1001/jama.2013.6285

16. Achenbach P, Warncke K, Naserke HE, et al. Islet Autoantibody Characteristics. *Seven*. 2004;(July 2003).

17. Miao D, Yu L, Eisenbarth GS. Role of Autoantibodies in Type 1 Diabetes. *Front Biosci*. Published online 2007:1889-1898.

18. Noble JA. Immunogenetics of type 1 diabetes: A comprehensive review. *J Autoimmun*. 2015;64:101-112. doi:10.1016/j.jaut.2015.07.014

19. Oldstone MBA. Molecular mimicry and immune-mediated diseases. *FASEB J*. 1998;12(13):1255-1265. doi:10.1096/fasebj.12.13.1255

20. Christen U, Edelmann KH, McGavern DB, et al. A viral epitope that mimics a self antigen can accelerate but not initiate autoimmune diabetes. *J Clin Invest*. 2004;114(9):1290-1298. doi:10.1172/JCI200422557

21. Atkinson MA, Eisenbarth GS. Type 1 diabetes: New perspectives on disease pathogenesis and treatment. *Lancet*. 2001;358(9277):221-229. doi:10.1016/S0140-6736(01)05415-0

22. Sims EK, Carr ALJ, Oram RA, DiMeglio LA, Evans-Molina C. 100 Years of Insulin: Celebrating the Past, Present and Future of Diabetes Therapy. *Nat Med*. 2021;27(7):1154-1164. doi:10.1038/s41591-021-01418-2

23. Shapiro AMJ, Ricordi C, Hering BJ, et al. International Trial of the Edmonton Protocol for Islet Transplantation. *N Engl J Med*. 2006;355(13):1318-1330. doi:10.1056/nejmoa061267

24. Pagliuca FW, Millman JR, Gürtler M, et al. Generation of functional human pancreatic β cells in vitro. *Cell*. 2014;159(2):428-439. doi:10.1016/j.cell.2014.09.040

25. Feutren G, Assan R, Karsenty G, et al. CYCLOSPORIN INCREASES THE RATE AND LENGTH OF REMISSIONS IN INSULIN-DEPENDENT DIABETES OF RECENT ONSET. Results of a Multicentre Double-blind Trial. *Lancet*. 1986;328(8499):119-124. doi:10.1016/S0140-6736(86)91943-4

26. Parving H, Tarnow L, Nielsen FS, et al. Cyclosporine Nephrotoxicity in Type 1 Diabetic Patients. *Diabetes Care*. 1999;22(3):1-6.

27. Daifotis AG, Koenig S, Chatenoud L, Herold KC. Anti-CD3 clinical trials in type 1 diabetes mellitus. *Clin Immunol*. 2013;149(3):268-278. doi:10.1016/j.clim.2013.05.001

28. Pescovitz MD, Greenbaum CJ, Krause-steinrauf H, et al. Rituximab, B-Lymphocyte Depletion, and Preservation of Beta-Cell Function. 2019;361(22):2143-2152. doi:10.1056/NEJMoa0904452.Rituximab

29. Orban T, Bundy B, Becker DJ, et al. Co-stimulation modulation with abatacept in patients with recent-onset type 1 diabetes: A randomised, double-blind, placebo-controlled trial. *Lancet*. 2011;378(9789):412-419. doi:10.1016/S0140-6736(11)60886-6

30. Orban T, Bundy B, Becker DJ, et al. Costimulation modulation with abatacept in patients with recent-onset type 1 diabetes: Follow-up 1 year aftercessation of treatment. *Diabetes Care*. 2014;37(4):1069-1075. doi:10.2337/dc13-0604

31. Abrams JR, Lebwohl MG, Guzzo CA, et al. CTLA4Ig-mediated blockade of T-cell costimulation in patients with psoriasis vulgaris. *J Clin Invest*. 1999;103(9):1243-1252. doi:10.1172/JCI5857

32. Bluestone JA, Buckner JH, Herold KC. Immunotherapy: Building a bridge to a cure for type 1 diabetes. *Science (80-)*. 2021;373(6554):510-516. doi:10.1126/science.abh1654

33. Bluestone JA, Buckner JH, Fitch M, et al. Type 1 diabetes immunotherapy using polyclonal regulatory T cells. *Sci Transl Med*. 2015;7(315):498-503. doi:10.1126/scitranslmed.aad4134

34. Giannoukakis N, Phillips B, Finegold D, Harnaha J, Trucco M. Phase I (safety) study of autologous tolerogenic dendritic cells in type 1 diabetic patients. *Diabetes Care*. 2011;34(9):2026-2032. doi:10.2337/dc11-0472

35. Warshauer JT, Bluestone JA, Anderson MS. New Frontiers in the Treatment of Type 1 Diabetes. *Cell Metab*. 2020;31(1):46-61. doi:10.1016/j.cmet.2019.11.017

36. Ludvigsson J, Krisky D, Casas R, et al. GAD65 antigen therapy in recently diagnosed type 1 diabetes mellitus. *Diabetes Technol Ther*. 2013;15(SUPPL.1):433-442. doi:10.1089/dia.2013.1510

37. Chatenoud L, Thervet E, Primo J, Bach JF. Anti-CD3 antibody induces long-term remission of overt autoimmunity in nonobese diabetic mice. *Proc Natl Acad Sci U S A*. 1994;91(1):123-127. doi:10.1073/pnas.91.1.123

38. Gaglia J, Kissler S. Anti-CD3 Antibody for the Prevention of Type 1 Diabetes: A Story of Perseverance. *Biochemistry*. 2019;58(40):4107-4111. doi:10.1021/acs.biochem.9b00707

39. Chatenoud L. CD3-specific antibody-induced active tolerance: From bench to bedside. *Nat Rev Immunol*. 2003;3(2):123-132. doi:10.1038/nri1000

40. Keymeulen B, Vandemeulebroucke E, Ziegler AG, et al. Insulin Needs after CD3-Antibody Therapy in New-Onset Type 1 Diabetes. *N Engl J Med*. 2005;352(25):2598-2608. doi:10.1056/nejmoa043980

41. Aronson R, Gottlieb PA, Christiansen JS, et al. Low-dose otelixizumab anti-CD3 monoclonal antibody DEFEND-1 study: Results of the randomized phase III study in recent-onset human type 1 diabetes. *Diabetes Care*. 2014;37(10):2746-2754. doi:10.2337/dc13-0327

42. Keam SJ. Teplizumab : First Approval. *Drugs*. 2023;(0123456789). doi:10.1007/s40265-023-01847-y

43. von Herrath MG, Coon B, Wolfe T, Chatenoud L. Nonmitogenic CD3 Antibody Reverses Virally Induced (Rat Insulin Promoter-Lymphocytic Choriomeningitis Virus) Autoimmune Diabetes Without Impeding Viral Clearance. *J Immunol*. 2002;168(2):933-941. doi:10.4049/jimmunol.168.2.933

44. You S, Candon S, Kuhn C, Bach JF, Chatenoud L. Chapter 2 CD3 Antibodies as Unique Tools to Restore Self-Tolerance in Established Autoimmunity. Their Mode of Action and Clinical Application in Type 1 Diabetes. *Adv Immunol*. 2008;100(08):13-37. doi:10.1016/S0065-2776(08)00802-X

45. Herold KC, Gitelman SE, Ehlers MR, et al. Teplizumab (Anti-CD3 mAb) treatment preserves C-peptide responses in patients with new-onset type 1 diabetes in a randomized controlled trial: Metabolic and immunologic features at baseline identify a subgroup of responders. *Diabetes*. 2013;62(11):3766-3774. doi:10.2337/db13-0345

46. Herold KC, Gitelman SE, Masharani U, et al. A single course of anti-CD3 monoclonal antibody hOKT3γ1(ala-ala) results in improvement in C-peptide responses and clinical parameters for at least 2 years after onset of type 1 diabetes. *Diabetes*. 2005;54(6):1763-1769. doi:10.2337/diabetes.54.6.1763

47. Lasch S, Müller P, Bayer M, et al. Anti-CD3/Anti-CXCL10 antibody combination therapy induces a persistent remission of type 1 diabetes in two mouse models. *Diabetes*. 2015;64(12):4198-4211. doi:10.2337/db15-0479

48. Christen U, Pouzol L, Tunis M, et al. Combination treatment of a novel CXCR3 antagonist ACT-777991 with an anti-CD3 antibody synergistically increases persistent remission in experimental models of type 1 diabetes. *Clin Exp Immunol*. 2023;0(0):000. doi:10.1093/cei/uxad083

49. Hu C, Ding H, Zhang X, Wong FS, Wen L. Combination treatment with anti-CD20 and oral anti-CD3 prevents and reverses autoimmune diabetes. *Diabetes*. 2013;62(8):2849-2858. doi:10.2337/db12-1175

50. Bresson D, Togher L, Rodrigo E, et al. Anti-CD3 and nasal proinsulin combination therapy enhances remission from recentonset autoimmune diabetes by inducing Tregs. *J Clin Invest*. 2006;116(5):1371-1381. doi:10.1172/JCI27191

51. Sherry NA, Chen W, Kushner JA, et al. Exendin-4 improves reversal of diabetes in NOD mice treated with anti-CD3 monoclonal antibody by enhancing recovery of β-cells. *Endocrinology*. 2007;148(11):5136-5144. doi:10.1210/en.2007-0358

52. Proudfoot AEI. Chemokine receptors: Multifaceted therapeutic targets. *Nat Rev Immunol*. 2002;2(2):106-115. doi:10.1038/nri722

53. Christen U, Von Herrath MG. Manipulating the type 1 vs type 2 balance in type 1 diabetes. *Immunol Res*. 2004;30(3):309-325. doi:10.1385/IR:30:3:309

54. Christen U, Kimmel R. Chemokines as Drivers of the Autoimmune Destruction in Type 1 Diabetes: Opportunity for Therapeutic Intervention in Consideration of an Optimal Treatment Schedule. *Front Endocrinol (Lausanne)*. 2020;11(October):1-12. doi:10.3389/fendo.2020.591083

55. Zlotnik A, Yoshie O. Chemokines: A new classification system and their role in immunity. *J Cult Herit*. 2000;1(2):121-127.

56. Rot A, von Andrian UH. Chemokines in Innate and Adaptive Host Defense: Basic Chemokinese Grammar for Immune Cells. *Annu Rev Immunol*. 2004;22(1):891-928. doi:10.1146/annurev.immunol.22.012703.104543

57. Charo IF, Ransohoff RM. The Many Roles of Chemokines and Chemokine Receptors in Inflammation. *N Engl J Med*. 2006;354(6):610-621. doi:10.1056/nejmra052723

58. Oo YH, Shetty S, Adams DH. The Role of Chemokines in the Recruitment of Lymphocytes to the Liver. *Dig Dis*. 2010;28(1):31-44. doi:10.1159/000282062

59. Mantovani A, Bonecchi R, Locati M. Tuning inflammation and immunity by chemokine sequestration : decoys and more. 2006;6(December):907-918. doi:10.1038/nri1964

60. Campbell DJ, Kim CH, Butcher EC. Chemokines in the systemic organization of immunity. *Immunol Rev*. 2003;195:58-71. doi:10.1034/j.1600-065X.2003.00067.x

61. Nomiyama H, Osada N, Yoshie O. The evolution of mammalian chemokine genes. *Cytokine Growth Factor Rev*. 2010;21(4):253-262. doi:10.1016/j.cytogfr.2010.03.004

62. Frigerio S, Junt T, Lu B, et al. β cells are responsible for CXCR3-mediated T-cell infiltration in insulitis. *Nat Med*. 2002;8(12):1414-1420. doi:10.1038/nm792

63. Sandor AM, Jacobelli J, Friedman RS. Immune cell trafficking to the islets during type 1 diabetes. *Clin Exp Immunol*. 2019;198(3):314-325. doi:10.1111/cei.13353

64. Uno S, Imagawa A, Saisho K, et al. Expression of chemokines, CXC chemokine ligand 10 (CXCL10) and CXCR3 in the inflamed islets of patients with recent-onset autoimmune type 1 diabetes. *Endocr J*. 2010;57(11):991-996. doi:10.1507/endocrj.K10E-076

65. Antonelli A, Fallahi P, Ferrari SM, et al. Serum Th1 (CXCL10) and Th2 (CCL2) chemokine levels in children with newly-diagnosed type 1 diabetes: a longitudinal study. *Diabet Med*. 2008;25(11):1349-1353. doi:10.1111/j.1464-5491.2008.02577.x

66. Chatzigeorgiou A, Harokopos V, Mylona-Karagianni C, Tsouvalas E, Aidinis V, Kamper E. The pattern of inflammatory/anti-inflammatory cytokines and chemokines in type 1 diabetic patients over time. *Ann Med*. 2010;42(6):426-438. doi:10.3109/07853890.2010.495951

67. Pan X, Kaminga AC, Kinra S, et al. Chemokines in Type 1 Diabetes Mellitus. *Front Immunol*. 2022;12(February):1-15. doi:10.3389/fimmu.2021.690082

68. Davenport B, Eberlein J, Nguyen TT, et al. Chemokine Signatures of Pathogen-Specific T Cells II: Memory T Cells in Acute and Chronic Infection. *J Immunol*. 2020;205(8):2188-2206. doi:10.4049/jimmunol.2000254

69. Eberlein J, Davenport B, Nguyen TT, et al. Chemokine Signatures of Pathogen-Specific T Cells I: Effector T Cells. *J Immunol*. 2020;205(8):2169-2187. doi:10.4049/jimmunol.2000253

70. Kelner GS, Kennedy J, Bacon KB, et al. Lymphotactin: A cytokine that represents a new class of chemokine. *Science (80-)*. 1994;266(5189):1395-1399. doi:10.1126/science.7973732

71. Müller S, Dorner B, Korthäuer U, et al. Cloning of ATAC, an activation-induced, chemokine-related molecule exclusively expressed in CD8+ T lymphocytes. *Eur J Immunol*. 1995;25(6):1744-1748. doi:10.1002/eji.1830250638

72. Yoshida T, Imai T, Kakizaki M, Nishimura M, Yoshie O. Molecular cloning of a novel C or γ type chemokine, SCM-1. *FEBS Lett*. 1995;360(2):155-159. doi:10.1016/0014-5793(95)00093-O

73. Dorner BG, Dorner MB, Zhou X, et al. Selective Expression of the Chemokine Receptor XCR1 on Cross-presenting Dendritic Cells Determines Cooperation with CD8+ T Cells. *Immunity*. 2009;31(5):823-833. doi:10.1016/j.immuni.2009.08.027

74. Kuloglu ES, McCaslin DR, Kitabwalla M, Pauza CD, Markley JL, Volkman BF. Monomeric solution structure of the prototypical “C” chemokine

lymphotactin. *Biochemistry*. 2001;40(42):12486-12496. doi:10.1021/bi011106p

75. Tuinstra R, Peterson F, Kutlesa S, Elgin ES, Kron M, Volkman B. Interconversion between two unrelated protein folds in the lymphotactin native state. *Chemtracts*. 2008;21(3):94-95.

76. Bachem A, Güttler S, Hartung E, et al. Superior antigen cross-presentation and XCR1 expression define human CD11c+CD141+ cells as homologues of mouse CD8+ dendritic cells. *J Exp Med*. 2010;207(6):1273-1281. doi:10.1084/jem.20100348

77. Dorner BG, Scheffold A, Rolph MS, et al. MIP-1α, MIP-1β, RANTES, and ATAC/lymphotactin function together with IFN-γ as type 1 cytokines. *Proc Natl Acad Sci U S A*. 2002;99(9):6181-6186. doi:10.1073/pnas.092141999

78. Dorner BG, Smith HRC, French AR, et al. Coordinate Expression of Cytokines and Chemokines by NK Cells during Murine Cytomegalovirus Infection. *J Immunol*. 2004;172(5):3119-3131. doi:10.4049/jimmunol.172.5.3119

79. Lei Y, Takahama Y. XCL1 and XCR1 in the immune system. *Microbes Infect*. 2012;14(3):262-267. doi:10.1016/j.micinf.2011.10.003

80. Fox JC, Thomas MA, Dishman AF, et al. Structure-function guided modeling of chemokine-GPCR specificity for the chemokine XCL1 and its receptor XCR1 Jamie. *Sci Signal*. 2020;12(597):1-30. doi:10.1126/scisignal.aat4128.Structure-function

81. Yoshida T, Imai T, Kakizaki M, Nishimura M, Takagi S, Yoshie O. Identification of single C motif-1/lymphotactin receptor XCR1. *J Biol Chem*. 1998;273(26):16551-16554. doi:10.1074/jbc.273.26.16551

82. Yamazaki C, Sugiyama M, Ohta T, et al. Critical Roles of a Dendritic Cell Subset Expressing a Chemokine Receptor, XCR1. *J Immunol*. 2013;190(12):6071-6082. doi:10.4049/jimmunol.1202798

83. Lei Y, Ripen AM, Ishimaru N, et al. Aire-dependent production of XCL1

mediates medullary accumulation of thymic dendritic cells and contributes to regulatory T cell development. *J Exp Med*. 2011;208(2):383-394. doi:10.1084/jem.20102327

84. Kroczek RA, Henn V. The role of XCR1 and its ligand XCL1 in antigen cross-presentation by murine and human dendritic cells. *Front Immunol*. 2012;3(FEB):1-5. doi:10.3389/fimmu.2012.00014

85. Bedoui S, Whitney PG, Waithman J, et al. Cross-presentation of viral and self antigens by skin-derived CD103+ dendritic cells. *Nat Immunol*. 2009;10(5):488-495. doi:10.1038/ni.1724

86. Banchereau J, Steinman RM. Dendritic cells and the control of immunity. [Review] [103 refs]. *Nature*. 1998;392(6673):245-252.

87. Cabeza-Cabrerizo M, Cardoso A, Minutti CM, Pereira Da Costa M, Reis E Sousa C. Dendritic Cells Revisited. *Annu Rev Immunol*. 2021;39:131-166. doi:10.1146/annurev-immunol-061020-053707

88. Heath WR, Belz GT, Behrens GMN, et al. Cross-presentation, dendritic cell subsets, and the generation of immunity to cellular antigens. *Immunol Rev*. 2004;199:9-26. doi:10.1111/j.0105-2896.2004.00142.x

89. Brewitz A, Eickhoff S, Dähling S, et al. CD8+ T Cells Orchestrate pDC-XCR1+ Dendritic Cell Spatial and Functional Cooperativity to Optimize Priming. *Immunity*. 2017;46(2):205-219. doi:10.1016/j.immuni.2017.01.003

90. Wylie B, Seppanen E, Xiao K, et al. Cross-presentation of cutaneous melanoma antigen by migratory XCR1+CD103− and XCR1+CD103+ dendritic cells. *Oncoimmunology*. 2015;4(8):1-11. doi:10.1080/2162402X.2015.1019198

91. Waisman A, Lukas D, Clausen BE, Yogev N. Dendritic cells as gatekeepers of tolerance. *Semin Immunopathol*. 2017;39(2):153-163. doi:10.1007/s00281-016-0583-z

92. Ness S, Lin S, Gordon JR. Regulatory Dendritic Cells, T Cell Tolerance, and Dendritic Cell Therapy for Immunologic Disease. *Front Immunol*.

2021;12(March). doi:10.3389/fimmu.2021.633436

93. Ginhoux F, Liu K, Helft J, et al. The origin and development of nonlymphoid tissue CD103+ DCs. *J Exp Med*. 2009;206(13):3115-3130. doi:10.1084/jem.20091756

94. Bachem A, Hartung E, Güttler S, et al. Expression of XCR1 characterizes the Batf3-dependent lineage of dendritic cells capable of antigen cross-presentation. *Front Immunol*. 2012;3(JUL):1-12. doi:10.3389/fimmu.2012.00214

95. Edelson BT, Wumesh KC, Juang R, et al. Peripheral CD103+ dendritic cells form a unified subset developmentally related to CD8α+ conventional dendritic cells. *J Exp Med*. 2010;207(4):823-836. doi:10.1084/jem.20091627

96. Böttcher JP, Reis e Sousa C. The Role of Type 1 Conventional Dendritic Cells in Cancer Immunity. *Trends in Cancer*. 2018;4(11):784-792. doi:10.1016/j.trecan.2018.09.001

97. Dähling S, Mansilla AM, Knöpper K, et al. Type 1 conventional dendritic cells maintain and guide the differentiation of precursors of exhausted T cells in distinct cellular niches. *Immunity*. 2022;55(4):656-670.e8. doi:10.1016/j.immuni.2022.03.006

98. Haniffa M, Shin A, Bigley V, et al. Human Tissues Contain CD141 hi Cross-Presenting Dendritic Cells with Functional Homology to Mouse CD103 + Nonlymphoid Dendritic Cells. *Immunity*. 2012;37(1):60-73. doi:10.1016/j.immuni.2012.04.012

99. Crozat K, Guiton R, Contreras V, et al. The XC chemokine receptor 1 is a conserved selective marker of mammalian cells homologous to mouse CD8α+ dendritic cells. *J Exp Med*. 2010;207(6):1283-1292. doi:10.1084/jem.20100223

100. Den Haan JMM, Lehar SM, Bevan MJ. CD8+ but not CD8- dendritic cells cross-prime cytotoxic T cells in vivo. *J Exp Med*. 2000;192(12):1685-1695. doi:10.1084/jem.192.12.1685

101. Kurts C, Robinson BWS, Knolle PA. Cross-priming in health and disease. *Nat Rev Immunol*. 2010;10(6):403-414. doi:10.1038/nri2780

102. Savinov AY, Wong FS, Stonebraker AC, Chervonsky A V. Presentation of antigen by endothelial cells and chemoattraction are required for homing of insulin-specific CD8+ T cells. *J Exp Med*. 2003;197(5):643-656. doi:10.1084/jem.20021378

103. Castellino F, Germain RN. Cooperation between CD4+ and CD8+ T cells: When, where, and how. *Annu Rev Immunol*. 2006;24:519-540. doi:10.1146/annurev.immunol.23.021704.115825

104. Krueger PD, Osum KC, Jenkins MK. CD4+ Memory T-Cell Formation during Type 1 Immune Responses. *Cold Spring Harb Perspect Biol*. 2021;13(12). doi:10.1101/CSHPERSPECT.A038141

105. Arens R, Schoenberger SP. Plasticity in programming of effector and memory CD8+ T-cell formation. *Immunol Rev*. 2010;235(1):190-205. doi:10.1111/j.0105-2896.2010.00899.x

106. Williams MA, Bevan MJ. Effector and memory CTL differentiation. *Annu Rev Immunol*. 2007;25:171-192. doi:10.1146/annurev.immunol.25.022106.141548

107. Sallusto F, Lenig D, Mackay CR, Lanzavecchia A. Flexible programs of chemokine receptor expression on human polarized T helper 1 and 2 lymphocytes. *J Exp Med*. 1998;187(6):875-883. doi:10.1084/jem.187.6.875

108. Szabo SJ, Kim ST, Costa GL, Zhang X, Fathman CG, Glimcher LH. A novel transcription factor, T-bet, directs Th1 lineage commitment. *Cell*. 2000;100(6):655-669. doi:10.1016/S0092-8674(00)80702-3

109. Zhu J, Paul WE. CD4 T cells : fates , functions , and faults ASH 50th anniversary review CD4 T cells : fates , functions , and faults. *Immunobiology*. 2009;112(5):1557-1569. doi:10.1182/blood-2008-05-078154.BLOOD

110. Ivanov II, McKenzie BS, Zhou L, et al. The Orphan Nuclear Receptor RORγt Directs the Differentiation Program of Proinflammatory IL-17+ T Helper Cells. *Cell*. 2006;126(6):1121-1133. doi:10.1016/j.cell.2006.07.035

111. Mosmann TR, Li L, Sad S. Functions of CD8 T-cell subsets secreting different cytokine patterns. *Semin Immunol*. 1997;9(2):87-92. doi:10.1006/smim.1997.0065

112. Carter LL, Dutton RW. Type 1 and Type 2: A fundamental dichotomy for all T-cell subsets. *Curr Opin Immunol*. 1996;8(3):336-342. doi:10.1016/S0952-7915(96)80122-1

113. Gravano DM, Hoyer KK. Promotion and prevention of autoimmune disease by CD8+ T cells. *J Autoimmun*. 2013;45:68-79. doi:10.1016/j.jaut.2013.06.004

114. Von Herrath MG, Harrison LC. Antigen-induced regulatory T cells in autoimmunity. *Nat Rev Immunol*. 2003;3(3):223-232. doi:10.1038/nri1029

115. Raphael I, Nalawade S, Eagar TN, Forsthuber TG. T cell subsets and their signature cytokines in autoimmune and inflammatory diseases. *Cytokine*. 2015;74(1):5-17. doi:10.1016/j.cyto.2014.09.011

116. Sakaguchi S, Wing K, Onishi Y, Prieto-Martin P, Yamaguchi T. Regulatory T cells: How do they suppress immune responses? *Int Immunol*. 2009;21(10):1105-1111. doi:10.1093/intimm/dxp095

117. Bender C, Rajendran S, von Herrath MG. New Insights Into the Role of Autoreactive CD8 T Cells and Cytokines in Human Type 1 Diabetes. *Front Endocrinol (Lausanne)*. 2021;11(January):1-6. doi:10.3389/fendo.2020.606434

118. Espinosa-Carrasco G, Le Saout C, Fontanaud P, et al. CD4+ T helper cells play a key role in maintaining diabetogenic CD8+ T cell function in the pancreas. *Front Immunol*. 2018;8(JAN). doi:10.3389/fimmu.2017.02001

119. Van Belle TL, Taylor P, von Herrath MG. Mouse models for Type 1 Diabetes. *Drug Discov Today Dis Model*. 2009;6(2):41-45.

doi:10.1016/j.ddmod.2009.03.008

120. Makino S, Kunimoto K, Muraoka Y, Mizushima Y, Katagiri K, Tochino Y. Breeding of a Non-Obese, Diabetic Strain of Mice. *Exp Anim*. 1980;29(1):1-13. doi:10.1538/expanim1978.29.1_1

121. Pearson JA, Wong FS, Wen L. The importance of the Non Obese Diabetic (NOD) mouse model in autoimmune diabetes. *J Autoimmun*. 2016;66:76-88. doi:10.1016/j.jaut.2015.08.019

122. Delovitch TL, Singh B. The nonobese diabetic mouse as a model of autoimmune diabetes: Immune dysregulation gets the NOD. *Immunity*. 1998;8(4):530. doi:10.1016/S1074-7613(00)80557-9

123. Jansen A, Homo-Delarche F, Hooijkaas H, Leenen PJ, Dardenne M, Drexhage HA. Immunohistochemical characterization of monocytes-macrophages and dendritic cells involved in the initiation of the insulitis and β-cell destruction in NOD mice. *Diabetes*. 1994;43(5):667-675. doi:10.2337/diabetes.43.5.667

124. Oldstone MBA, Nerenberg M, Southern P, Price J, Lewicki H. Virus infection triggers insulin-dependent diabetes mellitus in a transgenic model: Role of anti-self (virus) immune response. *Cell*. 1991;65(2):319-331. doi:10.1016/0092-8674(91)90165-U

125. von Herrath MG, Dockter J, Oldstone MBA. How virus induces a rapid or slow onset insulin-dependent diabetes mellitus in a transgenic model. *Immunity*. 1994;1(3):231-242. doi:10.1016/1074-7613(94)90101-5

126. Christen U, Hintermann E, Holdener M, von Herrath MG. Viral triggers for autoimmunity: Is the ‘glass of molecular mimicry’ half full or half empty? *J Autoimmun*. 2010;34(1):38-44. doi:10.1016/j.jaut.2009.08.001

127. Ohashi PS, Oehen S, Buerki K, et al. Ablation of “tolerance” and induction of diabetes by virus infection in viral antigen transgenic mice. *Cell*. 1991;65(2):305-317. doi:10.1016/0092-8674(91)90164-T

128. Terhorst D, Fossum E, Baranska A, et al. Laser-Assisted Intradermal

Delivery of Adjuvant-Free Vaccines Targeting XCR1 + Dendritic Cells Induces Potent Antitumoral Responses . *J Immunol*. 2015;194(12):5895-5902. doi:10.4049/jimmunol.1500564

129. Tesfaye DY, Bobic S, Lysén A, et al. Targeting Xcr1 on Dendritic Cells Rapidly Induce Th1-Associated Immune Responses That Contribute to Protection Against Influenza Infection. *Front Immunol*. 2022;13(February):1-13. doi:10.3389/fimmu.2022.752714

130. Dufour JH, Dziejman M, Liu MT, Leung JH, Lane TE, Luster AD. IFN-γ-Inducible Protein 10 (IP-10; CXCL10)-Deficient Mice Reveal a Role for IP-10 in Effector T Cell Generation and Trafficking. *J Immunol*. 2002;168(7):3195-3204. doi:10.4049/jimmunol.168.7.3195

131. iDisco Protocol. iDisco protocol, https://idisco.info/idisco-protocol/. Accessed Janaury 13, 2023. Published 2016. Accessed January 13, 2023. https://idisco.info/

132. Bender C, Christen S, Scholich K, et al. Islet-expressed CXCL10 promotes autoimmune destruction of islet isografts in mice with type 1 diabetes. *Diabetes*. 2017;66(1):113-126. doi:10.2337/db16-0547

133. Battegay M, Cooper S, Althage A, Bänziger J, Hengartner H, Zinkernagel RM. Quantification of lymphocytic choriomeningitis virus with an immunological focus assay in 24- or 96-well plates. *J Virol Methods*. 1991;33(1-2):191-198. doi:10.1016/0166-0934(91)90018-U

134. Christen U, McGavern DB, Luster AD, von Herrath MG, Oldstone MBA. Among CXCR3 Chemokines, IFN-γ-Inducible Protein of 10 kDa (CXC Chemokine Ligand (CXCL) 10) but Not Monokine Induced by IFN-γ (CXCL9) Imprints a Pattern for the Subsequent Development of Autoimmune Disease. *J Immunol*. 2003;171(12):6838-6845. doi:10.4049/jimmunol.171.12.6838

135. Keymeulen B, Walter M, Mathieu C, et al. Four-year metabolic outcome of a randomised controlled CD3-antibody trial in recent-onset type 1 diabetic patients depends on their age and baseline residual beta cell mass.

Diabetologia. 2010;53(4):614-623. doi:10.1007/s00125-009-1644-9

136. Zeng Z, Lan T, Wei Y, Wei X. CCL5/CCR5 axis in human diseases and related treatments. *Genes Dis*. 2022;9(1):12-27. doi:10.1016/j.gendis.2021.08.004

137. Marques RE, Guabiraba R, Russo RC, Teixeira MM. Targeting CCL5 in inflammation. *Expert Opin Ther Targets*. 2013;17(12):1439-1460. doi:10.1517/14728222.2013.837886

138. Pfleger C, Kaas A, Hansen L, et al. Relation of circulating concentrations of chemokine receptor CCR5 ligands to C-peptide, proinsulin and HbA1c and disease progression in type 1 diabetes. *Clin Immunol*. 2008;128(1):57-65. doi:10.1016/j.clim.2008.03.458

139. White GE, Greaves DR. Fractalkine: A survivor's guide chemokines as antiapoptotic mediators. *Arterioscler Thromb Vasc Biol*. 2012;32(3):589-594. doi:10.1161/ATVBAHA.111.237412

140. Sarkar SA, Lee CE, Victorino F, et al. Expression and regulation of chemokines in murine and human type 1 diabetes. *Diabetes*. 2012;61(2):436-446. doi:10.2337/db11-0853

141. Kim CH, Kunkel EJ, Boisvert J, et al. Bonzo/CXCR6 expression defines type 1-polarized T-cell subsets with extralymphoid tissue homing potential. *J Clin Invest*. 2001;107(5):595-601. doi:10.1172/JCI11902

142. Sandor AM, Lindsay RS, Dyjack N, et al. CD11c+ cells are gatekeepers for lymphocyte trafficking to infiltrated islets during type 1 diabetes. *Front Immunol*. 2019;10(JAN):1-17. doi:10.3389/fimmu.2019.00099

143. Ivakine EA, Gulban OM, Mortin-Toth SM, et al. Molecular Genetic Analysis of the Idd4 Locus Implicates the IFN Response in Type 1 Diabetes Susceptibility in Nonobese Diabetic Mice. *J Immunol*. 2006;176(5):2976-2990. doi:10.4049/jimmunol.176.5.2976

144. Stievano L, Tosello V, Marcato N, et al. CD8 + αβ + T Cells That Lack Surface CD5 Antigen Expression Are a Major Lymphotactin (XCL1) Source

in Peripheral Blood Lymphocytes . *J Immunol*. 2003;171(9):4528-4538. doi:10.4049/jimmunol.171.9.4528

145. Dieu MC, Vanbervliet B, Vicari A, et al. Selective recruitment of immature and mature dendritic cells by distinct chemokines expressed in different anatomic sites. *J Exp Med*. 1998;188(2):373-386. doi:10.1084/jem.188.2.373

146. Roberts EW, Broz ML, Binnewies M, et al. Critical Role for CD103+/CD141+ Dendritic Cells Bearing CCR7 for Tumor Antigen Trafficking and Priming of T Cell Immunity in Melanoma. *Cancer Cell*. 2016;30(2):324-336. doi:10.1016/j.ccell.2016.06.003

147. Ferris ST, Carrero JA, Mohan JF, Calderon B, Murphy KM, Unanue ER. A Minor Subset of Batf3-Dependent Antigen-Presenting Cells in Islets of Langerhans Is Essential for the Development of Autoimmune Diabetes. *Immunity*. 2014;41(4):657-669. doi:10.1016/j.immuni.2014.09.012

148. Fousteri G, Dave A, Juntti T, von Herrath M. CD103 is dispensable for anti-viral immunity and autoimmunity in a mouse model of virally-induced autoimmune diabetes. *J Autoimmun*. 2009;32(1):70-77. doi:10.1016/j.jaut.2008.12.001

149. Radenkovic M, Uvebrant K, Skog O, et al. Characterization of resident lymphocytes in human pancreatic islets. *Clin Exp Immunol*. 2017;187(3):418-427. doi:10.1111/cei.12892

150. von Herrath MG, Oldstone MBA. Interferon-γ Is Essential for Destruction of β Cells and Development of Insulin-dependent Diabetes Mellitus. *J Exp Med*. 1997;185(3):531-540. doi:10.1084/jem.185.3.531

151. Seewaldt S, Thomas HE, Ejrnaes M, et al. Virus-Induced Autoimmune Diabetes. *Diabetes*. 2000;49(11):1801-1809.

152. Kägi D, Ledermann B, Bürki K, et al. Cytotoxicity mediated by T cells and natural killer cells is greatly impaired in perforin-deficient mice. *Nature*. 1994;369(6475):31-37. doi:10.1038/369031a0

153. Kägi BD, Odermatt B, Seiler P, Zinkernagel RM, Mak TW, Hengartner H. Perforin-deficient Nonobese Diabetic Mice. *J Exp Med*. 1997;186(7):989-997.

154. Kägi D, Odermatt B, Ohashi PS, Zinkernagel RM, Hengartner H. Development of insulitis without diabetes in transgenic mice lacking perforin-dependent cytotoxicity. *J Exp Med*. 1996;183(5):2143-2152. doi:10.1084/jem.183.5.2143

155. Amrani A, Verdaguer J, Anderson B, Utsugi T, Bou S, Santamaria P. Perforin-independent β-cell destruction by diabetogenic CD8+ T lymphocytes in transgenic nonobese diabetic mice. *J Clin Invest*. 1999;103(8):1201-1209. doi:10.1172/JCI6266

156. Sutton VR, Estella E, Li C, et al. A critical role for granzyme B, in addition to perform and TNFα, in alloreactive CTL-induced mouse pancreatic beta cell death. *Transplantation*. 2006;81(2):146-154. doi:10.1097/01.tp.0000191939.68451.d9

157. Thomas HE, Trapani JA, Kay TWH. The role of perforin and granzymes in diabetes. *Cell Death Differ*. 2010;17(4):577-585. doi:10.1038/cdd.2009.165

158. Christen U, Darwiche R, Thomas HE, et al. Virally Induced Inflammation Triggers Fratricide of Fas-Ligand-Expressing β-Cells. *Diabetes*. 2004;53(3):591-596. doi:10.2337/diabetes.53.3.591

159. Wiedeman AE, Muir VS, Rosasco MG, et al. Autoreactive CD8+ T cell exhaustion distinguishes subjects with slow type 1 diabetes progression. *J Clin Invest*. 2020;130(1):480-490. doi:10.1172/JCI126595

160. Wherry EJ, Kurachi M. Molecular and cellular insights into T cell exhaustion. *Nat Rev Immunol*. 2015;15(8):486-499. doi:10.1038/nri3862

161. Wherry EJ. T cell exhaustion. *Nat Immunol*. 2011;12(6):492-499. doi:10.1038/ni.2035

162. Sandu I, Cerletti D, Claassen M, Oxenius A. Exhausted CD8+ T cells

exhibit low and strongly inhibited TCR signaling during chronic LCMV infection. *Nat Commun*. 2020;11(1):1-11. doi:10.1038/s41467-020-18256-4

163. Keir ME, Francisco LM, Sharpe AH. PD-1 and its ligands in T-cell immunity. *Curr Opin Immunol*. 2007;19(3):309-314. doi:10.1016/j.coi.2007.04.012

164. Zhao Y, Shao Q, Peng G. Exhaustion and senescence: two crucial dysfunctional states of T cells in the tumor microenvironment. *Cell Mol Immunol*. 2020;17(1):27-35. doi:10.1038/s41423-019-0344-8

165. Badowski M, Shultz CL, Eason Y, Ahmad N, Harris DT. The influence of intrinsic and extrinsic factors on immune system aging. *Immunobiology*. 2014;219(6):482-485. doi:10.1016/j.imbio.2014.02.008

166. Joeris T, Gomez-Casado C, Holmkvist P, et al. Intestinal cDC1 drive cross-tolerance to epithelial-derived antigen via induction of FoxP3+CD8+ Tregs. *Sci Immunol*. 2021;6(60). doi:10.1126/sciimmunol.abd3774

167. Coombes JL, Siddiqui KRR, Arancibia-Cárcamo C V., et al. A functionally specialized population of mucosal CD103+ DCs induces Foxp3+ regulatory T cells via a TGF-β -and retinoic acid-dependent mechanism. *J Exp Med*. 2007;204(8):1757-1764. doi:10.1084/jem.20070590

168. Mahnke K, Johnson TS, Ring S, Enk AH. Tolerogenic dendritic cells and regulatory T cells: A two-way relationship. *J Dermatol Sci*. 2007;46(3):159-167. doi:10.1016/j.jdermsci.2007.03.002

169. Jonuleit H, Schmitt E, Schuler G, Knop J, Enk AH. Induction of interleukin 10-producing, nonproliferating CD4+ T cells with regulatory properties by repetitive stimulation with allogeneic immature human dendritic cells. *J Exp Med*. 2000;192(9):1213-1222. doi:10.1084/jem.192.9.1213

170. Wei S, Kryczek I, Zou L, et al. Plasmacytoid dendritic cells induce CD8+ regulatory T cells in human ovarian carcinoma. *Cancer Res*. 2005;65(12):5020-5026. doi:10.1158/0008-5472.CAN-04-4043

171. Zou W. Regulatory T cells, tumour immunity and immunotherapy. *Nat Rev*

Immunol. 2006;6(4):295-307. doi:10.1038/nri1806

172. Nikolic T, Suwandi JS, Wesselius J, et al. Tolerogenic dendritic cells pulsed with islet antigen induce long-term reduction in T-cell autoreactivity in type 1 diabetes patients. *Front Immunol*. 2022;13(November):1-13. doi:10.3389/fimmu.2022.1054968

173. Böttcher JP, Bonavita E, Chakravarty P, et al. NK Cells Stimulate Recruitment of cDC1 into the Tumor Microenvironment Promoting Cancer Immune Control. *Cell*. 2018;172(5):1022-1037.e14. doi:10.1016/j.cell.2018.01.004

10. Appendix

10.1 Acknowledgments

First of all, I would like to thank Urs Christen for giving me the possibility to do my PhD in his lab. Working alongside him was an absolute honour, and I am indebted to him for sharing with me his vast knowledge of immunology. I am deeply appreciative of the exceptional project he entrusted me with, as well as of the collaborative side projects that expanded my perspectives.

I am deeply thankful to Edith Hintermann for her contributions to the experiments, her insightful suggestions for the project, the great organization of the lab, and her exceptional support throughout. She has been an amazing listener, problem solver, and a source of continuous encouragement.

I thank Monika Bayer for the help in the lab and I especially thank her for always talking to me in English.

I extend my sincere gratitude to all the students (Deborah Puppe, Elisa Blickberndt, and Maren Später), who worked in the lab during this period, for the scientific discussions and the funny moments we had in the lab. I am particularly thankful to Urs Christen for giving me the opportunity to guide them through various experiments and to provide some help in the supervision. This experience has significantly enriched my own knowledge.

I would like to thank all my friends, both longstanding and newfound, for their unwavering encouragement and companionship throughout this journey.

A great thank you also to my family and my family friends for their unconditional love, support, and for being always my number one fan.

I am deeply thankful to my boyfriend for his continuous understanding and encouragement that have been fundamental in these years.

I am profoundly grateful to my parents and my brother for their unending love, guidance, and sacrifices. Your belief in me has been a driving force, and your unwavering support meant a lot to me.

The collective influence of each of you has left an indelible mark on my PhD experience, therefore from the bottom of my heart, thank you.

10.2 Curriculum vitae

Personal information:

Name:	Camilla Tondello
Place of birth:	Padova (Italy)
Nationality:	Italian

Education and qualifications:

Sep 2019 – present	PhD at Pharmazantrum *Faculty of Medicine, Goethe University Frankfurt* Supervisor: Prof. Dr. Urs Christen
Oct 2013 - Dec 2018	M.Sc. Chemistry and Pharmaceutical Techniques *University of Padua* (Final Mark: 110 cum laude/110) Thesis research project about drug delivery with nanoparticles. Supervisor: Prof. Dr. Margherita Morpurgo

Work experience:

Jun 2019 - Aug 2019	Research Assistant *University of Padua* Scholarship “Development of a nanoparticle-based pharmacological approach for amyotrophic lateral sclerosis”
Jan 2019 - May 2019	Research Assistant – Erasmus+ for Traineeship *Goethe University Frankfurt* In vivo analysis of CD103 receptor expression in a mouse model for primary sclerosing cholangitis (PSC).
Aug 2017 - Oct 2017	Pharmacist Trainee *Pharmacy Meltias Sanfiori, Padua - Italy*
May 2017 - Jul 2017	Pharmacist Trainee in Hospital *Veneto Institute of Oncology IOV – IRCCS, Padua – Italy*

10.3 Presentations and publications

10.3.1 Presentations

nPOD Scientific Meeting 2023 — Poster presentation
Amelia Island, USA, February 2023

Immunology of Diabetes Society Meeting — Poster presentation
Paris, France, May 2023

10.3.2 Publications

Tondello C., Bender C., Puppe D., Blickberndt E. M., Golden G. J., Bayer M., Buchmann G., Pfeilschifter J. M., Bachmann M., Hintermann E., Brandes R. B., Betts M. R., Kroczek R. A., Christen U. *Submitted, 2023.* "The XCL1/XCR1 axis is activated in patients with type 1 diabetes and its disruption tips the T cell balance and ablates β-cell damage in a mouse model"

Hintermann E., **Tondello C.**, Fuchs S., Bayer M., Taubert R., Pfeilschifter J. M., Manns M. P., Christen U. *Submitted, 2023.* "Blockade of neutrophil extracellular trap components ameliorates cholestatic liver disease in Mdr2 (Abcb4) knockout mice"

Bender C., Müller P., **Tondello C.**, Horn J., Holdener M., Lasch S., Bayer M., Pfeilschifter J. M., Tacke F., Ludwig A., Hansmann M. L., Döring C., Hintermann E., Christen U. *Submitted, 2023.* "Gene-expression profiling of laser-dissected islets and studies in deficient mice reveal chemokines as differential driving force of type 1 diabetes"

Christen U., Pouzol L., Tunis M., Sassi A., **Tondello C.**, Bayer M., Hintermann E., Strasser D. S., Schuldes S., Mentzel U., Martinic M. M. "Combination treatment of a novel CXCR3 antagonist ACT-777991 with an anti-CD3 antibody synergistically increases persistent remission in experimental models of type 1 diabetes, *Clinical and Experimental Immunology*, 2023 uxad083, https://doi.org/10.1093/cei/uxad083

Violatto M. B., Pasetto L., Casarin E., **Tondello C**., Schiavon E., Talamini L., Marchini G., Cagnotto A., Morelli A., Lanno A., Passoni, A., Bigini P., Morpurgo M., Bonetto V. "Development of a Nanoparticle-Based Approach for the Blood-Brain Barrier Passage in a Murine Model of Amyotrophic Lateral Sclerosis" *Cells.* 2022 Dec 10;11(24):4003. doi:10.3390/cells11244003.

Violatto M. B., Casarin E, Talamini L., Russo L., Baldan S., **Tondello C.**, Messmer M., Hintermann E., Rossi A., Passoni A., Bagnati R., Biffi S., Toffanin C., Gimondi S., Fumagalli S., De Simoni M. G., Barisani D., Salmona M., Christen U., Invernizzi P., Bigini P., Morpurgo M. "Dexamethasone Conjugation to Biodegradable Avidin-Nucleic-Acid-Nano- Assemblies Promotes Selective Liver Targeting and Improves Therapeutic Efficacy in an Autoimmune Hepatitis Murine Model" *ACSNano,* 2019, 13, 4, 4410–4423. doi:10.1021/acsnano.8b09655.

10.4 Bender, Müller, Tondello et al., submitted manuscript

Gene-expression profiling of laser-dissected islets and studies in deficient mice reveal chemokines as differential driving force of type 1 diabetes

Christine Bender[1,*], Peter Müller[1,*], Camilla Tondello[1,*], Jessica Horn[1], Martin Holdener[1], Stanley Lasch[1], Monika Bayer[1], Josef M. Pfeilschifter[1], Frank Tacke[2], Andreas Ludwig[3], Martin- Leo Hansmann[4], Claudia Döring[4], Edith Hintermann[1], and Urs Christen[1,#]

[1]Institute for Pharmacology and Toxicology Pharmazentrum Frankfurt / ZAFES, Goethe University Frankfurt, Frankfurt am Main, Germany, [2]Charité - Universitätsmedizin Berlin, Department of Hepatology and Gastroenterology, Campus Virchow-Klinikum (CVK) and Campus Charité Mitte (CCM), Berlin, Germany, [3]Institute of Molecular Pharmacology, University Hospital, RWTH Aachen, Aachen, and [4]Dr. Senckenberg Institute of Pathology, University Hospital Frankfurt, Frankfurt am Main, Germany
* equal contribution

Abstract

Although type 1 diabetes (T1D) results from the autoimmune destruction of the insulin-producing β-cells, its treatment is largely restricted to exogenous insulin administration. Only few therapies targeting the autoaggressive immune system have been introduced into clinical practice or are considered in clinical trials. Here, we provide a gene expression profile of the islet microenvironment obtained by laser-dissection microscopy in an inducible mouse model. Thereby, we have identified novel targets for immune intervention. Increased gene expression of most inflammatory proteins was apparent at day 10 after T1D induction and largely paralleled the observed degree of insulitis. We further focused on genes involved in leukocyte migration, including chemokines and their receptors. Besides the critical chemokine CXCL10, we found several other chemokines upregulated locally in temporary or chronic manner. Localization of the chemokine ligand/receptor pairs to the islet microenvironment has been confirmed by RNAscope. Interference with the CXCL16-CXCR6 and CX_3CL1-CX_3CR1 axes, but not the CCL5-CCR1/3/5 axis, resulted in reduced insulitis and lower T1D incidence. Further, we found that the receptors for the differentially expressed chemokines CXCL10, CXCL16 and CX_3CL1 are distributed unevenly among islet autoantigen-specific T cells, which explains why the interference with just one chemokine axis cannot completely abrogate insulitis and T1D.

Keywords:
T1D roadmap, chemokine axis, islet microdissection, gene array, RNAscope

List of abbreviations:
T1D – type 1 diabetes
LCMV – lymphocytic choriomeningitis virus
GP – glycoprotein
NP - nucleoprotein
RIP – rat insulin promoter
LCM – laser capture dissection microscopy
CXCL10 – C-X-C motif chemokine ligand 10
CXCR3 – C-X-C motif chemokine receptor 3
CCL5 – C-C motif chemokine ligand 5
CCR5 – C-C motif chemokine receptor 5
CXCL16 – C-X-C motif chemokine ligand 16
CXCR6 – C-X-C motif chemokine receptor 6
CX3CL1 – C-X3-C motif chemokine ligand 1
CX3CR1 – C-X3-C motif chemokine receptor 1
GFP - green fluorescent protein
PDLN – pancreatic draining lymph node
ADAM10 - a disintegrin and metalloproteinase 10
ADAM17 - a disintegrin and metalloproteinase 17

1. Introduction

In type 1 diabetes (T1D) the insulin-producing β-cells of the islets of Langerhans in the pancreas are attacked by the dysregulated immune system. Conventional treatment of T1D with exogenous insulin is indispensable and lifesaving but is not a cure for the disease and does not completely prevent long-term complications [1]. Many additional treatments for T1D include glucose lowering drugs that are often used to treat type 2 diabetes but are only moderately successful and do not target the autoaggressive immune system [2]. Alternative strategies aim at a tolerization by administration of oral/nasal β-cell antigens or by infusion with in vitro expanded regulatory T cells (Treg) or tolerogenic dendritic cells (DC) [3-5]. Further, several clinical trials have been conducted to evaluate a restoration of a healthy immune balance by anti-CD3 antibody administration [6-9]. Recently, the anti-CD3 antibody teplizumab has been approved by the FDA for the treatment of stage 2 T1D. Unfortunately, efficacies of such immunoregulatory regimen are often only short-lived and many patients do not respond to the treatment [7]. Only few clinical trials target critical inflammatory factors, such as cytokines and chemokines. One reason might be a certain redundancy in the cytokine/chemokine network, which makes it difficult to single out key factors driving the disease. To identify such key factors, we mapped the gene expression during the pathogenesis of T1D locally in the islets of Langerhans. Since this endeavour demands for a precise knowledge of the beginning and the progress of the pathogenesis, we used an inducible T1D model. The RIP-LCMV model uses transgenic mice that express the glycoprotein (GP) or the nucleoprotein (NP) of the lymphocytic choriomeningitis virus (LCMV) under control of the rat insulin promoter (RIP). Upon LCMV-infection RIP-LCMV mice develop T1D within 10-14 days (fast-onset RIP-GP mice) or 1-6 months (slow-onset RIP-NP mice) [10, 11]. We used laser-dissection microscopy to collect the local islet microenvironment at several times before and after LCMV-infection. Expression mapping of the obtained mRNA by gene-array revealed a multitude of genes that are up- or down-regulated during T1D pathogenesis. Expectedly, we found that gene products related to autoimmunity, including inflammatory factors and their receptors as well as leukocyte surface markers, were increased in the islet microenvironment, whereas genes associated with β-cell function were

downregulated. For further investigations, we focused on chemokines and their receptors. We have previously demonstrated that the CXCL10/CXCR3 chemokine axis plays an important role in the attraction of autoaggressive T cells to the islets. Blockade of CXCL10 alone and in particular after treatment of diabetic mice with an anti-CD3 antibody, reduced insulitis and T1D incidence radically [12, 13]. Here, we found that besides CXCL10/CXCR3, other previously somewhat neglected chemokines and their receptors might also play a crucial role. We took a closer look at the CCL5/CCR1/3/5, CXCL16/CXCR6, and CX_3CL1/CX_3CR1 axes and crossed our RIP-LCMV mice with either CCL5, CXCR6, or CX3CR1 deficient mice. Whereas no significant difference was detected between RIP-LCMV and RIP-LCMV x $CCL5^{-/-}$ mice, we found a reduced T1D incidence in RIP-LCMV x $CXCR6^{gfp/gfp}$ and RIP-LCMV x $CX_3CR1^{gfp/gfp}$ mice in which the respective chemokine receptor genes have been disrupted by insertion of the green fluorescent protein (gfp) gene. This lower T1D incidence was reflected by a decreased insulitis. Our data indicate that both the CXCL16/CXCR6 and the CX3CL1/CX3CR1 axis might be important in the attraction of autoaggressive cells to the islets. Further, since we found a variable distribution of the individual chemokine receptors among autoaggressive T cells, a combinatorial inhibition of several chemokines rather than interfering with a single chemokine axis might be more successful as a T1D therapy.

2. Material and Methods

2.1. Virus and mice

The Armstrong stain of LCMV, clone 53b, was used for all experiments. LCMV was plaque purified three times on Vero cells (ATCC CCL-81), and stocks were prepared by a single passage on hamster kidney fibroblast cell line BHK-21 (ATCC CCL-10). Mice were infected intraperitoneally with 1x104 pfu LCMV. Generation and screening by PCR of RIP-LCMV-GP and RIP-LCMV-NP transgenic mice were as previously described [10, 11]. Transgenic CX3CR1gfp/gfp mice were generated by replacement of CX3CR1 gene with the cDNA encoding EGFP (Clontech). The EGFP gene replaces the first 390 bp of the second CX3CR1 exon, which encodes the crucial N-terminus of the receptor for CX3CL1-binding [14]. Transgenic CXCR6gfp/gfp mice were generated by replacement of the CXCR6 gene with the cDNA encoding EGFP [15]. Transgenic

CCL5-deficient mice have been generated by targeted disruption of the RANTES gene by replacing the promoter, the transcription initiation site, the initiation codon, and a portion of the coding region in exon 1 with a hygromycin-resistance cassette [16] and have been kindly provided by Matthias von Herrath, La Jolla Institute for Immunology, La Jolla, CA. RIP-LCMV-GP/NP x CX3CR1$^{gfp/+}$ and RIP-LCMV-GP/NP x CXCR6$^{gfp/+}$ were generated by crossing single-transgenic CX$_3$CR1$^{gfp/gfp}$ and CXCR6$^{gfp/gfp}$ mice to RIP-LCMV-GP/NP single transgenic mice. RIP-LCMV-GP/NP x CX3CR1$^{gfp/+}$ or RIP-LCMV-GP/NP x CXCR6$^{gfp/+}$ were further crossed to obtain RIP-LCMV-GP/NP x CX$_3$CR1$^{gfp/gfp}$ and RIP-LCMV-GP/NP x CXCR6$^{gfp/gfp}$ mice. RIP-LCMV-GP/NP x CX$_3$CR1$^{+/+}$ and RIP-LCMV-GP/NP x CXCR6$^{+/+}$ littermates were used as controls. RIP-LCMV-GP/NP x CCL5$^{-/-}$ were obtained by crossing single-transgenic CCL5$^{-/-}$ mice to RIP-LCMV-GP/NP single transgenic mice. The heterogenous lines were further crossed to generate homozygous RIP-LCMV-GP/NP x CCL5$^{-/-}$ and RIP-LCMV-GP/NP x CCL5$^{+/+}$ littermates. All animal experiments were approved by the local Ethics Animal Review Board RP Darmstadt, Germany (V54-19c 20/15 F143/02, F143/69).

2.2. Laser Capture Dissection (LCM)

Mouse pancreata were obtained on days 0 (uninfected), 1, 3, 7, 10, 14, and 28 post-infection. After dissection they were immediately transferred into cryogenic vials filled with Tissue-Tek O.C.T. (Sakura Finetek) and frozen in liquid nitrogen to preserve RNA integrity. Cryovials were stored at -80°C until cryostat sectioning. Membrane covered slides (1 mm, Zeiss) were UV treated at 254 nm for 30 minutes shortly before cryostat sectioning. Immediately prior to LCM, 3 µm frozen pancreatic sections were cut, dehydrated in ice-cold 100 % Ethanol for 3-5 minutes and washed in RNase-fee H2O for 10 seconds. Then, sections were stained with haematoxylin (Sigma) containing RNase Inhibitor (SUPERase In, Ambion) for 2 minutes, washed in RNase-fee H2O for 10 seconds, and fixed in 100% Ethanol for 10 seconds. The sections were air dried for 5 minutes and LCM was performed using an Axiovert 200M laser-dissection microscope (Zeiss) and pressure catapulting technique with a UV laser beam (PALM). Islet tissue was collected in 0.5 ml soft tubes (Biozym) containing RTL lysis buffer (Qiagen) with 1% β-mercaptoethanol and finally stored at -20°C until RNA extraction.

2.3. RNA extraction

RNA extraction was performed using a RNeasy Micro Kit (Qiagen) according to manufacturer's instructions. Total RNA quality was evaluated using RNA 6000 Nano Chips (Agilent Technologies) and Agilent 2100 Bioanalyzer with a RIN cut-off of >5. Total RNA (input: 20ng) amplification and cDNA labelling was done using standardized protocols (Ovation Pico WTA System V2 amplification kit and Encore Biotin Module labelling kit from NuGEN).

2.4. Microarrays

Microarray hybridization to GeneChip Mouse Gene 1.0 ST V1 arrays (Affymetrix), washing steps, and scanning of the microarrays were performed according to the Affymetrix protocol. Probe level normalization was conducted using the variance stabilization method by [17]. Probe set summarization was calculated using the median polish method [18] on the normalized data. For each probeset, a robust additive model was fitted across the arrays, considering the different sensitivity of the probe sets via the probe effect*. Differential expression:* Quality control and analysis of the microarray data have been analyzed with the transcriptome analysis console (TAC) version 4.0.3.14 (Applied Biosystems). Many of the genes on the microarray are not expressed or might have only a small variability across the samples. First, we used an expression intensity filter to reduce the dimension of the microarray data: We filtered the data with an intensity filter (the intensity of a gene should be above 100 in at least 0.5 percent of the samples, if the group size is equal) and a variance filter (the interquartile range of log2 intensities should be at least 0.3, if the group size is equal). The data discussed in this publication have been deposited in the NCBI Gene Expression Omnibus and are accessible through GEO series accession number GSE229287. (https://www.ncbi.nlm.nih.gov/geo/query/acc.cgi?acc=GSE229287)

2.5. Real-time PCR/Gene expression analysis

Expression of selected genes was evaluated by Real-Time qRT-PCR. Therefore, total RNA (input: 500pg-50ng) was amplified using Ovation Pico SL WTA System V2 amplification kit (NuGEN) following manufacturer's instructions. Reverse transcription was performed with M-MuLV reverse transcriptase (Promega). Real-time PCR was performed using TaqMan gene expression assays (Applied

Biosystem) with 100 ng cDNA for each reaction in duplicate. The following TaqMan probes were used: CCL5 (Mm01302427_m1), CCR5 (Mm01216171_m1), CXCL10 (Mm00445235_m1), CXCR3 (Mm00438259_m1), CXCL16 (Mm00469712_m1), CXCR6 (Mm00472858_m1), CX_3CL1 (Mm00436454_m1), CX_3CR1 (Mm00438354_m1), XCL1 (Mm00434772_m1), and XCR1 (Mm00442206_s1). Data were normalized using Gapdh housekeeping gene (4352339E), and subsequent analysis was performed using $2^{-\Delta\Delta Ct}$ method.

2.6. Immunohistochemistry

Tissue sections were fixed with either ethanol or 1:1 ethanol/acetone at -20°C for 15 minutes. Avidin/biotin blocking was performed before tissue sections were incubated with primary and biotinylated secondary antibodies. Color reaction was obtained with avidin peroxidase conjugate and diaminobenzidine-hydrogen peroxide (Vector laboratories). Primary antibodies: Rabbit anti-mouse CXCL10 (PeproTech); rabbit anti-mouse CXCR3 (Zymed); rabbit anti-mouse CX_3CL1 (Abcam), rabbit anti-mouse CX_3CR1 (Abcam), rabbit anti-mouse CXCL16 (Bioss), rabbit anti-GFP (Acris Antibodies); goat anti-mouse CCL5 (R&D Systems); Armenian hamster anti-mouse CCR5 (BioLegend); guinea pig anti-insulin (Dako). Secondary antibodies: Goat anti-guinea pig, goat anti-rabbit, and rabbit anti-goat (all biotinylated from Vector laboratories); biotinylated goat anti-armenian hamster (eBioscience). Images were acquired with an Axioscope 2 microscope (Zeiss).

2.7. Insulitis scoring

The degree of insulitis was scored according to the following system: Score 0: Very minor or no insulitis, only very few infiltrating cells; score 1: mild to moderate insulitis, 25-50% infiltrations, large parts with intact β-cells; score 2: considerable insulitis, 50-75% infiltrates, still some parts with intact β-cells; score 3: massive insulitis, 75-100% infiltrates, only few remaining β-cells producing insulin, islet scar.

2.8. RNAscope

Pancreata together with the pancreatic draining lymph nodes were dissected, immerged in buffered 4% paraformaldehyde, and incubated on a shaker overnight at room temperature. The following day, samples were dehydrated using Leica TP 1020 Tissue Processor and then embedded in paraffin. Tissue sections of 4 µm were cut and the ACDBio RNAscope 2.5 HD duplex manual assay kit (ACD/Bio-Techne, Minneapolis, MN) was used, following the manufacturer's protocol. The time of “target retrieval” and “protease plus” incubations was reduced to 11 minutes and 15 minutes, respectively. The different probes were detected in channel 1 (C1) through an enzymatic reaction via horseradish peroxidase (HRP) to develop a blue color and in channel 2 (C2) through an alkaline phosphatase reaction, developing a red color. The probes used were: CCL5 (Cat No. 469601-C2, red) and CCR5-blue (Cat No. 438651, blue); CXCL10 (Cat No. 408921-C2, red) and CXCR3 (Cat No. 402511, blue) CXCL16 (Cat. No. 466681-C2, red) and CXCR6 (Cat. No. 871991, blue); CX_3CL1 (Cat No. 426211, blue) and CX^3CR1 (Cat No. 314221-C2, red). Images were acquired using a Axioscope 2 microscope (Zeiss) with a 63x oil objective.

2.9. Flow Cytometry

Cells were isolated from the spleen or the pancreatic draining lymph nodes (PDLN) by squeezing the tissue through a 70 µm nylon cell strainer with a glass pestle in RPMI, followed by centrifugation and erythrocyte lysis with 0.83% NH4Cl. The resulted single-cell suspensions were stimulated overnight with 2 µg/ml LCMV peptides GP33 (CD8) and GP61 (CD4) in presence of Brefeldin A. The following antibodies were used for surface staining for (30 minutes at 4°C in the dark): V450-conjugated rat anti-mouse CD4 (BD Biosciences) and V500-conjugated rat anti-mouse CD8 (BioLegend), PE-conjugated rat anti-mouse CXCR3, PerCP-conjugated rat anti-mouse CXCR6 (BioLegend), and APC-conjugated rat anti-mouse CX3CR1 (R&D Systems). After fixation and permeabilization with PFA/saponin (10 min at RT), cells were stained for intracellular expression of IFN-γ (APC-conjugated rat anti-mouse IFN-γ, BD Biosciences) to quantify LCMV-GP specific T cells (30 minutes at 4°C in the dark). Samples were acquired using a FACSCanto II flow cytometer (BD Biosciences).

3. Results

3.1. Islet expression roadmap

To establish a roadmap for the gene expression in the islet microenvironment during T1D pathogenesis, we collected islet material from RIP-GP mice by laser-capture microdissection at several times after disease initiation through LCMV-infection. RNA was isolated from islet material collected from pancreas sections of uninfected mice and at days 1, 3, 7, 10, 14, and 28 after LCMV-infection (figure 1A). The isolated islet microenvironment contained both the (remaining) islet itself and infiltrating immune cells (figure 1B). RNA quality was tested using RNA 6000 Nano Chips (Agilent Technologies) and Agilent 2100 Bioanalyzer. RNA with a RIN cutoff of >5 has been used for cDNA generation and microarray hybridization to Affymetrix GeneChip Mouse Gene 1.0 ST V1 arrays. Volcano blots visualized that overall, more genes were upregulated than downregulated during experimental T1D development (figure 2A). These genes were grouped into clusters related to inflammation, effector T cell function, and β-cell function (see heatmaps & pathways in supplemental figures). Here, we focused on the expression kinetics of chemokine ligands and receptors. Almost all chemokine ligands and receptors were upregulated during T1D pathogenesis (figure 2B). The mean expression levels relative to the expression in uninfected RIP-GP mice are displayed in table 1 and a heatmap with a hierarchical clustering is available in the supplemental figures (suppl. Fig S1C). The expression kinetics followed a similar pattern for most chemokine ligands, with an expression peak around day 7-10 after infection. Chemokine receptor expression was slightly delayed suggesting cellular infiltration in response to the local chemokine expression (table 1). Interestingly, some chemokine ligands and receptors stayed elevated until day 28, reflecting the ongoing inflammatory process during chronic T1D. We further focused on four particular chemokine axes, namely CCL5/CCR1,3,5; CXCL10/CXCR3, CXCL16/CXCR6, and CX3CL1/CX3CR1 and confirmed their expression by quantitative real-time PCR (qPCR), RNAscope, and immunohistochemistry (figure 3). The RNA expression kinetics detected by qPCR followed a similar pattern as previously seen in gene array analysis (figure 3A). The expression of the selected chemokine axes was further analyzed by RNAscope duplex assays in pancreas sections of RIP-GP mice obtained at days

0, 10, and 28 after LCMV-infection (figure 3B). All four ligand/receptor pairs localized to the islet microenvironment and visualized the expression kinetics detected in the gene array data set. No or only marginal expression has been found in tissue sections of uninfected mice (figure 3B). The impressive upregulation of CCL5 at day 10 post-infection, as seen in the gene array data set, was nicely reflected in the RNAscope staining. Also, the slow increase but persistent nature of CX3CR1 and the early upregulation and persistence of CXCL16 was clearly visible (figure 3B). To further confirm the expression on the protein level, immunohistochemistry was performed with pancreas sections obtained at day 28 post-infection (figure 3C). We found that CXCL10 expression was predominantly localized to the β-cell region (figure 3C). This finding confirms earlier reports by us and others that β-cells themselves release CXCL10 during stress and/or inflammation [19-21]. In contrast, CCL5, CXCL16, and CX_3CL1 localized to the site of cellular infiltration (figure 3C). Similarly, the respective receptors CXCR3, CCR5, CXCR6, and CX_3CR1 have been found among infiltrating cells rather than on islet cells (figure 3C). Note that due to a lack of an appropriate antibody to CXCR6, we used RIP-GP x $CXCR6^{gfp/+}$ mice that were heterozygous for CXCR6 and GFP (see next paragraph). Visualization of cells expressing CXCR6/GFP was done by immunohistochemistry using an anti-GFP antibody (figure 3C).

3.2. Type 1 diabetes is reduced in CXCR6 and CX_3CR1 deficient mice

We have investigated the role of the CXCL10/CXCR3 axis on several occasions before and recognized its important role during the recruitment of T cells to the islets in different settings using CXCL10-deficient mice or neutralizing antibodies to CXCL10 [12, 13, 19]. Here we used transgenic mice deficient in CCL5, CXCR6, or CX_3CR1 and crossed them with two different RIP-LCMV mouse lines, the fast onset T1D line RIP-GP and the slow onset T1D line RIP-NP [11]. Whereas no significant differences were detected in presence or absence of CCL5 in both RIP-LCMV mouse lines, we found significant decreases in T1D incidence in absence of CXCR6 or CX_3CR1 (figure 4). Hereby the incidence in the fast-onset RIP-GP model was reduced from 88% to 59% and from 65% to 41% in CXCR6-deficient and CX_3CR1-deficient mice, respectively. Even more pronounced, in the slow-onset RIP-NP model, the T1D incidence significantly decreased from 65%

to 29% in RIP-NP x CXCR6$^{gfp/gfp}$ and from 70% to 27% RIP-NP x CX3CR1$^{gfp/gfp}$ mice, compared to the RIP-NP single transgenic littermates (figure 4).

3.3. Insulitis is reduced in CX3CR1 deficient mice

At day 28 after infection, pancreas sections of RIP-GP x CCL5$^{-/-}$, RIP-GP x CXCR6$^{gfp/gfp}$, and RIP-GP x CX3CR1$^{gfp/gfp}$ mice and their corresponding RIP-GP littermates were stained for insulin (figure 5a). Overall, the insulin staining confirmed the incidence data for the RIP-GP line (figure 4) in that mice with high blood glucose levels showed only small areas of insulin producing β-cells. However, due to the large variation of insulitis between islets of individual mice or different mice per experimental group, the representative pictures shown in figure 5a are far from conclusive. Therefore, we used these stained sections to score the degree of insulitis (see legend figure 5). This quantification revealed that the presence or absence of CCL5 in RIP-GP mice had no influence on the overall insulitis (figure 5b). In contrast, insulitis was slightly diminished in CXCR6-deficient and significantly reduced in CX_3CR1-deficient mice (figure 5b and c). The mean insulitis score in CX_3CR1-deficient mice was 1.7, which is a clear indication that many islets were still functional with large areas of insulin-producing β-cells and constitutes a considerable reduction when compared with RIP-GP littermates (mean score 2.6) (figure 5c). These data correspond well to the T1D incidence data that showed the most pronounced decline in CX_3CR1-deficient RIP-GP mice.

3.4. Chemokine receptors are differentially expressed on islet autoantigen-specific T cells

Our data demonstrate that some chemokines (CXCL10, CXCL16, and CX_3CL1) that are upregulated upon T1D initiation and remain chronically elevated influence onset and severity of T1D. A lack of one of these chemokines provides a partial protection from T1D. One reason for this only incomplete protective effect might be the redundancy of the chemokine network. Thus, we determined the frequencies of total and islet autoantigen-specific CD8 T cells bearing CXCR3, CXCR6, and/or CX_3CR1 by flow cytometry. Lymphocytes isolated from spleen or PDLN were stimulated with the immunodominant LCMV peptide GP33 in presence of Brefeldin A and then stained for the individual chemokine

receptors, CD8 and intracellular IFNγ. The overall frequency of chemokine receptor-positive CD8 T cells increased strongly between days 7 and 10 post-infection in the spleen. However, even after 14 days, 31% of total CD8 T cells did not show any surface expression of CXCR3, CXCR6, or CX_3CR1 (figure 6B). In contrast, the vast majority of islet autoantigen-specific CD8 T cells showed surface expression of at least one of the three chemokine receptors (figure 6B). Interestingly, by day 14 post-infection, about two third of all LCMV-specific CD8 T cells were CXCR6/CX_3CR1 double-positive (figure 6B). The chemokine receptor distribution in the PDLN was different from the one in the spleen (figure 6C). First, the majority of total CD8 T cells was negative for all three receptors. Second, the dominant population of islet autoantigen-specific CD8 T cells was CXCR3/CXCR6 double positive. Third, at day 14 after T1D initiation, more than half of LCMV-GP-specific CD8 T cells expressed CXCR3 confirming the importance of the CXCL10/CXCR3 axis. Concurrently, even 77% of all islet autoantigen-specific CD8 T cells were CXCR6 positive, which might explain why an interference with the CXCL16/CXCR6 axis is successful in reducing the incidence of T1D. Nevertheless, at day 14 post-infection substantial fractions of cells, 40%, 23%, and 65% were negative for CXCR3, CXCR6, and CX_3CR1, respectively. Throughout the observation time only 9–21 % of islet autoantigen-specific CD8 T cells expressed all three receptors.

4. Discussion

We provide here a complete gene expression profile of T1D as induced in the RIP-LCMV model. The use of laser-dissection microscopy allowed us to precisely follow the gene expression kinetics directly in the islet microenvironment. Remaining islet material as well as the clusters of immune cells around and in the islets have been used for RNA isolation. Expectedly, a whole plethora of genes were differentially expressed during the pathogenesis of T1D. Whereas most genes associated with islet cell function have been downregulated, the majority of genes associated with inflammation were acutely and/or chronically upregulated. Here, we focused on the expression kinetics of chemokines and their receptors since they play a dominant role in the trafficking of immune cells to the islets. We could confirm previous observations made by us and others that a multitude of chemokine ligands and receptors, such as the CXCL10/CXCR3

axis, are upregulated during T1D [12, 20-24]. In addition, several other chemokine axes caught our attention, and we, therefore, generated several lines of chemokine-deficient RIP-LCMV mouse lines, including RIP-LCMV x $CCL5^{-/-}$, RIP-LCMV x $CXCR6^{gfp/gfp}$, and RIP-LCMV x $CX_3CR1^{gfp/gfp}$ mice. The transgenic interference with the chemokine axes had a differential impact on the outcome of T1D. The absence of CCL5 seemed to have only a very minor effect on T1D incidence and onset in our model, although both CCL5 as well as CCR5 were prominently expressed in the islet microenvironment as demonstrated by gene array analysis and RNAscope. CCL5 is predominantly secreted by T cells and monocytes, but is expressed also by platelets, eosinophils, fibroblasts, endothelial, epithelial and endometrial cells [25]. CCL5 binds to three different receptors, CCR1, CCR3, and CCR5, with the highest affinity for CCR5, which is mainly expressed by T cells, but is also present on macrophages, DC, and eosinophils [26]. It has been shown previously that CCL5 might play a role in T1D. In patients with T1D, serum CCL5 increased during disease progress [27] and decreased CCL5 serum levels were associated with disease remission [28]. Treatment of NOD mice, that express CCL5 in the islets of Langerhans, with a neutralizing anti-CCR5 antibody caused an arrest of β-cell destruction and T1D progress. However, the general infiltration of the islet environment was not prevented [29]. In this context, our data are somewhat surprising, since it has been shown that the CCL5-deficient mice used for our study in general display both a reduced migration to the site of inflammation as well as a diminished T cell activation [16]. In addition, it has been demonstrated that LCMV-specific memory CD8 T cells are excellent producers of CCL5 upon restimulation [24]. Thus, it seems likely that the overwhelming flood of chemokines produced acutely after LCMV infection and chronically throughout the progress of chronic T1D render the CCL5/CCR5 chemokine axis somewhat redundant. In contrast, the CXCL16/CXCR6 axis seems to be more important for the pathogenesis of T1D. CXCL16 is produced by various cell types including epithelial cells, hepatocytes, neuronal, and glial cells, fibroblasts and cardiomyocytes and predominantly attracts activated T cells and NK T-cells, but also macrophages and DC bearing its receptor CXCR6 [30-32]. Although the expression of CXCL16 in the islet microenvironment, as detected by RNAscope, was not as prominent as CCL5, many CXCR6-positive cells were detected in the infiltration clusters. An

interference with the CXCL16/CXCR6 axis had a considerable effect on T1D onset and incidence in both the fast-onset RIP-GP and the slow-onset RIP-NP model. The CXCL16/CXCR6 axis has previously been demonstrated to play a role in inflammatory diseases such as experimental autoimmune encephalomyelitis (EAE) [33], psoriasis [34], liver fibrosis [35], and proliferative diabetic retinopathy [36]. CXCL16 is a chemokine that is membrane bound and is only released upon cleavage by A Disintegrin and Metalloproteinase 10 (ADAM10) or 17 (ADAM17) [37]. In this context it is interesting to note that in the β-cell toxin streptozotocin (STZ)-induced T1D model ADAM10 as well as soluble CXCL16 was found to be upregulated in diabetic mice [38]. Treatment of mice with the stilbenoid resveratrol resulted in a decrease in islet ADAM10 expression, CXCL16 cleavage, and T cell islet infiltration [38]. Our gene array analysis revealed that ADAM10 and ADAM17 were also slightly upregulated in the islets of RIP-GP mice. The maximal fold increase for ADAM10 and ADAM17 was 1.81 and 2.89, respectively, at day 10 after infection and their expression levels returned close to baseline level after 28 days (data not shown). Differential expression of CX_3CR1 and especially its ligand CX_3CL1 was not as strong as observed for the CXCL10/CXCR3, CCL5/CCR5, and CXCL10/CXCR6 axes. However, our RNAscope data confirmed previous observations that both CX_3CL1 and CX_3CR1 are expressed in the islet microenvironment. Importantly, CX_3CR1 deficient mice showed a significant decrease of T1D incidence and onset in the RIP-NP model and a strong tendency towards a similar beneficial effect in the RIP-GP model. Thus, CX_3CL1/CX_3CR1-dependent cell recruitment to the islet environment is required for efficient destruction of β-cells. During inflammation CX_3CL1 is expressed in monocytes, macrophages, fibroblasts, endothelial cells, and DC and attracts selectively cells expressing CX_3CR1, including cytotoxic effector lymphocytes, such as NK cells, CTLs, and γδ T-cells [39, 40]. CX_3CR1 has even been suggested as a marker for antigen-experienced CD8 T cell subsets [41]. However, CX_3CR1 has also been found on a subgroup of islet-resident CD11b+ DC [42]. During murine T1D the number of such CX_3CR1+ CD11b+ DC is increasing, most likely due to further recruitment from the circulation [42]. Interestingly, although not as prominent as CXCL10 expression, CX_3CR1 has been detected in the islet microenvironment in both pre-diabetic mice and T1D patients [22] indicating an active participation in the disease

pathogenesis. Interestingly, like CXCL16, also CX_3CL1 is initially membrane-bound and is released upon cleavage by ADAM10 or ADAM17 [37]. Thus, even though the upregulation of ADAM10 and 17 expression was rather low compared to the increase in expression levels of most chemokine ligand and their receptors, a therapeutic intervention might be considered to lower soluble CXCL16 and CX3CL1. Although our data confirmed previous observations made for the CXCL10/CXCR3 and the CX_3CL1/CX_3CR1 axes and demonstrated an important role of the CXCL16/CXCR6 axis in the pathogenesis of T1D, it is obvious that considerable fractions of chemokine ligand and/or receptor-deficient mice still develop T1D. One reason for this independence of the pathogenic process from particular chemokines in some mice might be the redundance of the chemokine network. Not only that many ligands bind to more than one receptor and vice versa, leukocytes and T cells in particular express a multitude of chemokine receptors simultaneously. Thus, deficiency or blockade of just one chemokine ligand/receptor axis might not result in a complete inhibition of cell migration. We found that substantial fractions of islet autoantigen-specific CD8 T cells carry at least two of the three receptors CXCR3, CXCR6, and CX_3CR1. Thus, it is no surprise that T1D is still attainable in some mice deficient for only one chemokine ligand or receptor. A simultaneous blockade of at least two axes would interfere with the migration of a larger fraction of islet autoantigen-specific CD8 T cells and might therefore be more successful in reducing disease progress and severity.

5. Conclusions

We provide here a differential gene expression profile of the islet microenvironment in diabetic RIP-GP mice. Focusing on the expression of chemokine ligand/receptor axes, we have confirmed previous findings by us and others [12, 20-24] and identified new candidates for possible therapeutic interventions. In particular, the CXCL16/CXCR6 and the CX_3CL1/CX_3CR1 axes seem to be important for an efficient destruction of β-cells and the development of T1D. However, rather than targeting just one of the chemokine ligand/receptor axes, one should consider a combination treatment aiming at concerted inactivation of several axes, such as a simultaneous administration of blocking agents directed against CXCL10/CXCR3, CXCL16/CXCR6 and CX_3CL1/CX_3CR1. In addition, one must carefully consider the time of treatment.

Whereas the disease initiation is clearly defined in the RIP-LCMV model, it is usually not known for T1D patients. Thus, a possible treatment might come too late during the disease progression. Although, we have demonstrated that many chemokine ligands and receptors are chronically elevated during the T1D progress, the expression peak in the islet environment was mostly at day 7-10 post-infection. Should pathogen infection really be an initiating factor in autoimmune diseases like T1D, as frequently suggested [43], the chemokine expression peak might occur long before diagnosis. However, in reset situations, such T cell depletion therapies with anti-CD3 antibodies, such as teplizumab [7], or with anti-thymocyte globulin [44] a de novo infiltration of the islets might be prevented by an interference with one or more chemokine axes. We have demonstrated this previously by blocking the CXCL10/CXCR3 axis with a neutralizing anti-CXCL10 antibody following an anti-CD3 therapy. Indeed, such a combination therapy was superior to the corresponding monotherapies [13]. A similar situation with a known starting point would be an islet or pancreas transplantation in which autoaggressive T cells can be prevented from entering the transplant from the beginning. Indeed, neutralization of CXCL10 reduced the rejection of transplanted islets in diabetic RIP-LCMV mice [19]. Thus, for future translational approaches, it will be important to consider combination therapies that might cover more than just one aspect of the disease pathogenesis and to carefully evaluate the time and duration of the treatment.

References

[1] M. A. Atkinson, G. S. Eisenbarth, A. W. Michels. Type 1 diabetes. Lancet, 2014;383:69-82.

[2] C. S. Frandsen, T. F. Dejgaard, S. Madsbad, J. J. Holst. Non-insulin pharmacological therapies for treating type 1 diabetes. Expert Opin Pharmacother, 2018;19:947-60.

[3] M. von Herrath, M. Peakman, B. Roep. Progress in immune-based therapies for type 1 diabetes. Clin Exp Immunol, 2013;172:186-202.

[4] B. E. Phillips, Y. Garciafigueroa, M. Trucco, N. Giannoukakis. Clinical Tolerogenic Dendritic Cells: Exploring Therapeutic Impact on Human Autoimmune Disease. Front Immunol, 2017;8:1279.

[5] H. Yu, R. Paiva, R. A. Flavell. Harnessing the power of regulatory T-cells to control autoimmune diabetes: overview and perspective. Immunology, 2018;153:161-70.

[6] K. C. Herold, S. E. Gitelman, M. R. Ehlers, P. A. Gottlieb, C. J. Greenbaum, W. Hagopian et al. Teplizumab (anti-CD3 mAb) treatment preserves C-peptide responses in patients with new-onset type 1 diabetes in a randomized controlled trial: metabolic and immunologic features at baseline identify a subgroup of responders. Diabetes, 2013;62:3766-74.

[7] A. L. Perdigoto, P. Preston-Hurlburt, P. Clark, S. A. Long, P. S. Linsley, K. M. Harris et al. Treatment of type 1 diabetes with teplizumab: clinical and immunological follow-up after 7 years from diagnosis. Diabetologia, 2019;62:655-64.

[8] N. Sherry, W. Hagopian, J. Ludvigsson, S. M. Jain, J. Wahlen, R. J. Ferry, Jr. et al. Teplizumab for treatment of type 1 diabetes (Protege study): 1-year results from a randomised, placebo-controlled trial. Lancet, 2011;378:487-97.

[9] R. Aronson, P. A. Gottlieb, J. S. Christiansen, T. W. Donner, E. Bosi, B. W. Bode et al. Lowdose otelixizumab anti-CD3 monoclonal antibody DEFEND-1 study: results of the randomized phase III study in recent-onset human type 1 diabetes. Diabetes Care, 2014;37:2746-54.

[10] M. B. A. Oldstone, M. Nerenberg, P. Southern, J. Price, H. Lewicki. Virus infection triggers insulin-dependent diabetes mellitus in a transgenic model: Role of anti-self (virus) immune response. Cell, 1991;65:319-31.

[11] M. G. von Herrath, J. Dockter, M. B. A. Oldstone. How virus induces a rapid or slow onset insulin-dependent diabetes mellitus in a transgenic model. Immunity, 1994;1:231-42.

[12] U. Christen, D. B. McGavern, A. D. Luster, M. G. von Herrath, M. B. Oldstone. Among CXCR3 chemokines, IFN-gamma-inducible protein of 10 kDa (CXC chemokine ligand (CXCL) 10) but not monokine induced by IFN-gamma (CXCL9) imprints a pattern for the subsequent development of autoimmune disease. J Immunol, 2003;171:6838-45.

[13] S. Lasch, P. Muller, M. Bayer, J. M. Pfeilschifter, A. D. Luster, E. Hintermann et al. Anti-CD3/anti-CXCL10 antibody combination therapy induces a persistent remission of type 1 diabetes in two mouse models. Diabetes, 2015;64:4198-212.

[14] S. Jung, J. Aliberti, P. Graemmel, M. J. Sunshine, G. W. Kreutzberg, A. Sher et al. Analysis of fractalkine receptor CX(3)CR1 function by targeted deletion and green fluorescent protein reporter gene insertion. Mol Cell Biol, 2000;20:4106-14.

[15] D. Unutmaz, W. Xiang, M. J. Sunshine, J. Campbell, E. Butcher, D. R. Littman. The primate lentiviral receptor Bonzo/STRL33 is coordinately regulated with CCR5 and its expression pattern is conserved between human and mouse. J Immunol, 2000;165:3284-92.

[16] Y. Makino, D. N. Cook, O. Smithies, O. Y. Hwang, E. G. Neilson, L. A. Turka et al. Impaired T cell function in RANTES-deficient mice. Clin Immunol, 2002;102:302-9.

[17] W. Huber, A. von Heydebreck, H. Sultmann, A. Poustka, M. Vingron. Variance stabilization applied to microarray data calibration and to the quantification of differential expression. Bioinformatics, 2002;18 Suppl 1:S96-104.

[18] J. W. Tukey. Exploratory Data Analysis. Addison-Wesley Publishig Company; 1977.

[19] C. Bender, S. Christen, K. Scholich, M. Bayer, J. M. Pfeilschifter, E. Hintermann et al. Islet-Expressed CXCL10 Promotes Autoimmune Destruction of Islet Isografts in Mice With Type 1 Diabetes. Diabetes, 2017;66:113-26.

[20] S. Frigerio, T. Junt, B. Lu, C. Gerard, U. Zumsteg, G. A. Hollander et al. beta cells are responsible for CXCR3-mediated T-cell infiltration in insulitis. Nat Med, 2002;8:1414-20.

[21] B. O. Roep, F. S. Kleijwegt, A. G. van Halteren, V. Bonato, U. Boggi, F. Vendrame et al. Islet inflammation and CXCL10 in recent-onset type 1 diabetes. Clin Exp Immunol, 2010;159:338-43.

[22] S. A. Sarkar, C. E. Lee, F. Victorino, T. T. Nguyen, J. A. Walters, A. Burrack et al. Expression and Regulation of Chemokines in Murine and Human Type 1 Diabetes. Diabetes, 2012.

[23] J. Eberlein, B. Davenport, T. T. Nguyen, F. Victorino, K. Jhun, V. van der Heide et al. Chemokine Signatures of Pathogen-Specific T Cells I: Effector T Cells. J Immunol, 2020;205:2169-87.

[24] B. Davenport, J. Eberlein, T. T. Nguyen, F. Victorino, V. van der Heide, M. Kuleshov et al. Chemokine Signatures of Pathogen-Specific T Cells II: Memory T Cells in Acute and Chronic Infection. J Immunol, 2020;205:2188-206.

[25] R. E. Marques, R. Guabiraba, R. C. Russo, M. M. Teixeira. Targeting CCL5 in inflammation. Expert Opin Ther Targets, 2013;17:1439-60.

[26] Z. Zeng, T. Lan, Y. Wei, X. Wei. CCL5/CCR5 axis in human diseases and related treatments. Genes Dis, 2022;9:12-27.

[27] Z. Jamali, M. Nazari, H. Khoramdelazad, E. Hakimizadeh, M. Mahmoodi, M. N. Karimabad et al. Expression of CC chemokines CCL2, CCL5, and CCL11 is associated with duration of disease and complications in type-1 diabetes: a study on Iranian diabetic patients. Clin Lab, 2013;59:993-1001.

[28] C. Pfleger, A. Kaas, L. Hansen, B. Alizadeh, P. Hougaard, R. Holl et al. Relation of circulating concentrations of chemokine receptor CCR5 ligands to C-peptide, proinsulin and HbA1c and disease progression in type 1 diabetes. Clin Immunol, 2008;128:57-65.

[29] C. Carvalho-Pinto, M. I. Garcia, L. Gomez, A. Ballesteros, A. Zaballos, J. M. Flores et al. Leukocyte attraction through the CCR5 receptor controls progress from insulitis to diabetes in non-obese diabetic mice. Eur J Immunol, 2004;34:548-57.

[30] C. H. Kim, E. J. Kunkel, J. Boisvert, B. Johnston, J. J. Campbell, M. C. Genovese et al. Bonzo/CXCR6 expression defines type 1-polarized T-cell subsets with extralymphoid tissue homing potential. J Clin Invest, 001;107:595-601.

[31] S. Tabata, N. Kadowaki, T. Kitawaki, T. Shimaoka, S. Yonehara, O. Yoshie et al. Distribution and kinetics of SR-PSOX/CXCL16 and CXCR6 expression on human dendritic cell subsets and CD4+ T cells. J Leukoc Biol, 2005;77:777-86.

[32] S. Paust, H. S. Gill, B. Z. Wang, M. P. Flynn, E. A. Moseman, B. Senman et al. Critical role for the chemokine receptor CXCR6 in NK cell-mediated antigen-specific memory of haptens and viruses. Nat Immunol, 2010;11:1127-35.

[33] R. A. O'Connor, X. Li, S. Blumerman, S. M. Anderton, R. J. Noelle, D. K. Dalton. Adjuvant immunotherapy of experimental autoimmune encephalomyelitis: immature myeloid cells expressing CXCL10 and CXCL16 attract CXCR3+CXCR6+ and myelin-specific T cells to the draining lymph nodes rather than the central nervous system. J Immunol, 2012;188:2093-101.

[34] C. Gunther, N. Carballido-Perrig, S. Kaesler, J. M. Carballido, T. Biedermann. CXCL16 and CXCR6 are upregulated in psoriasis and mediate cutaneous recruitment of human CD8+ T cells. J Invest Dermatol, 2012;132:626-34.

[35] A. Wehr, C. Baeck, F. Heymann, P. M. Niemietz, L. Hammerich, C. Martin et al. Chemokine receptor CXCR6-dependent hepatic NK T Cell accumulation promotes inflammation and liver fibrosis. J Immunol, 2013;190:5226-36.

[36] A. M. Abu El-Asrar, M. I. Nawaz, A. Ahmad, A. De Zutter, M. M. Siddiquei, M. Blanter et al. Evaluation of Proteoforms of the Transmembrane Chemokines CXCL16 and CX3CL1, Their Receptors, and Their Processing Metalloproteinases ADAM10 and ADAM17 in Proliferative Diabetic Retinopathy. Front Immunol, 2020;11:601639.

[37] A. Ludwig, C. Weber. Transmembrane chemokines: Versatile 'special agents' in vascular inflammation. Thromb Haemostasis, 2007;97:694-703.

[38] M. S. Abdel-Bakky, A. Alqasoumi, W. M. Altowayan, E. Amin, M. A. Darwish. Resveratrol Inhibited ADAM10 Mediated CXCL16-Cleavage and T-Cells Recruitment to Pancreatic beta-Cells in Type 1 Diabetes Mellitus in Mice. Pharmaceutics, 2022;14.

[39] B. A. Jones, M. Beamer, S. Ahmed. Fractalkine/CX3CL1: a potential new target for inflammatory diseases. Mol Interv, 2010;10:263-70.

[40] G. E. White, D. R. Greaves. Fractalkine: a survivor's guide: chemokines as antiapoptotic mediators. Arterioscler Thromb Vasc Biol, 2012;32:589-94.

[41] C. Gerlach, E. A. Moseman, S. M. Loughhead, D. Alvarez, A. J. Zwijnenburg, L. Waanders et al. The Chemokine Receptor CX3CR1 Defines Three Antigen-Experienced CD8 T Cell Subsets with Distinct Roles in Immune Surveillance and Homeostasis. Immunity, 2016;45:1270-84.

[42] N. Yin, J. Xu, F. Ginhoux, G. J. Randolph, M. Merad, Y. Ding et al. Functional specialization of islet dendritic cell subsets. J Immunol, 2012;188:4921-30.

[43] U. Christen. Pathogen infection and autoimmune disease. Clin Exp Immunol, 2019;195:10-4.

[44] G. Simon, M. Parker, V. Ramiya, C. Wasserfall, Y. Huang, D. Bresson et al. Murine antithymocyte globulin therapy alters disease progression in NOD mice by a time-dependent induction of immunoregulation. Diabetes, 2008;57:405-14.

Acknowledgments

Author Contributions:

C.B., P.M., and C.T. contributed equally to the study and share first authorship. They were involved in the design of the experiments, generated raw data, analyzed and interpretated data, and helped drafting the manuscript. J.H., M.H., S.L., M.B., E.H., and C.D. carried out the experiments and analyzed the data. J.M.P., F.T., A,L., and M.H., provided material or mice and helped designing the experiments and drafting the manuscript. U.C. designed the study, generated raw data, analyzed and interpreted data, and drafted the manuscript. All authors helped to critically revise the intellectual content of the manuscript and approved the final submission. U.C. is the guarantors of this work and takes responsibility for the contents of the article.

Funding:

This study was funded by a grant of the German Research Foundation (DFG) to U.C., a fellowship of the Else Kröner-Fresenius Foundation (EKFS), Research Training Group Translational Research Innovation - Pharma (TRIP) to P.M., and Goethe University Frankfurt.

Conflict of interests:

The authors have no conflict of interest in context of this manuscript

Figure Legends

Figure 1: Laser dissection – (A) Pancreas tissue was obtained from RIP-GP mice before and at different times after infection with LCMV. Times used were: day 1: immediate effects of virus infection; day 3: peak of virus titer; day 7: peak of T cell response; day 10: the first mice display diabetic blood glucose levels (i.e. >300 mg/dl); day 14: the majority of mice is diabetic; day 28: chronic T1D with most islets destroyed. – (B) Representative pictures of laser dissections of islet microenvironments at days 1 and 10 after LCMV-infection. Note that the islet microenvironment contains both the islets themselves as well as infiltrating leukocytes.

Figure 2: Differential gene expression – (A) Volcano blots of gene expression detected in the islet microenvironment at days 1, 3, 7, 10, 14, and 28 after LCMV-infection in comparison to those of uninfected mice as obtained after the analysis of the GeneChip Mouse Gene 1.0 ST V1 array data. All genes up- or downregulated by less than 2-fold or exhibited a p-values of >0.05 are displayed in gray. Note that considerably more genes are upregulated (green) than downregulated (red) between days 7 and 14. – (B) Volcano blots of gene expression of chemokine ligands and receptors in the islet microenvironment of LCMV-infected mice at days 1, 3, 7, 10, 14, and 28 in comparison to uninfected mice. The chemokine axes CCL5/CCR5, CXCL10/CXCR3, CXCL16/CXCR6, and CX_3CL1/CX_3CR1 are highlighted in color. Note that starting at day 7 post-infection the vast majority of chemokine ligands and receptors are upregulated and remain highly expressed during the chronic phase of T1D.

Figure 3: Chemokine ligand and receptor expression – (A) The expression of the selected chemokine axes CCL5/CCR5, CXCL10/CXCR3, CXCL16/CXCR6, and CX3CL1/CX3CR1 has been confirmed by quantitative real-time PCR of the same islet microenvironment RNA that has been used for gene array analysis. – (B) RNAscope duplex assays for CCL5/CCR5, CXCL10/CXCR3, CXCL16/CXCR6, and CX_3CL1/CX_3CR1 of tissue sections of pancreata of RIP-GP mice obtained at days 0, 10, and 28 after LCMV-infection. Note that the colors for CX_3CL1 and CX_3CR1 are different from the other chemokine ligand/receptor pairs. – (C) Immunohistochemistry for CCL5/CCR5, CXCL10/CXCR3, CXCL16/CXCR6, and

CX_3CL1/CX_3CR1 protein expression. Note that due to the lack of an appropriate antibody, the expression of CXCR6 was demonstrated in CXCR-GFP heterozygous mice using an anti-GFP antibody (see material and methods).

Figure 4: T1D incidence is decreased in some chemokine axis deficient mice – RIP-GP (fast onset T1D) and RIP-NP (slow onset T1D) mice have been crossed with mice deficient for CCL5, CXCR6, or CX_3CR1. The mice were infected with LCMV, and blood glucose was monitored for 3 (RIP-GP) or 6 months (RIP-NP). Note the significant decrease in T1D incidence in CXCR6-deficient RIP-GP and -NP mice, as well as in CX*3*CR1-deficient RIP-NP mice. The absence of CCL5 had no effect on T1D onset and incidence in both RIP-GP and -NP mice. Statistical evaluation of the data was by the log-rank (Mantel-Cox) test using GraphPad Prism 8.4.3. software.

Figure 5: Insulitis is reduced in some chemokine axis deficient mice - RIP-GP mice have been crossed with mice deficient for CCL5, CXCR6, or CX_3CR1 and were infected with LCMV. - (A) Representative pictures of pancreas tissue sections obtained at day 28 after infection stained for insulin. – (B) Insulitis was scored as follows: Score 0: Very minor or no insulitis, only very few infiltrating cells; score 1: mild to moderate insulitis, 25-50% infiltrations, large parts with intact β-cells; score 2: considerable insulitis, 50-75% infiltrates, still some parts with intact β-cells; score 3: massive insulitis, 75-100% infiltrates, only few remaining β-cells producing insulin, islet scar. Data were from 3-6 mice per group with a total number of 30-84 islets scored. – (C) Mean insulitis score per mouse. Note that CX_3CR1-deficient RIP-GP mice showed a significantly diminished insulitis compared to normal RIP-GP mice.

Figure 6: Chemokine receptor surface expression on CD8 T cells - RIP-GP mice were infected with LCMV. At days 0 (uninfected), 7, 10 and, 14 after infection lymphocytes have been isolated from spleen and pancreatic draining lymph node (PDLN) and were assessed for surface expression of CXCR3 (R3), CXCR6 (R6), and CX_3CR1 (R1). In order to identify islet autoantigen-specific CD8 T cells, the isolated lymphocytes have been stimulated overnight with the immunodominant LCMV-GP epitope GP33 in presence of Brefeldin A and were stained for intracellular IFNγ. – (A) Gating strategy: Total and RIP-GP-specific CD8 T cells

(IFNγ+) have been gated into CX_3CR1-positive and CX_3CR1-negative cells. These events have then been further gated into CXCR3- and/or CXCR6-positive cells. As displayed on the right side for CX_3CR1 single positive (R1), CX_3CR1/CXCR3 (R1R3) and CX_3CR1/CXCR6 (R1R6) double positive, and CX_3CR1/CXCR3/CXCR6 (R1R3R6) triple positive cells. – (B, C) Pie chart of chemokine receptor distribution among total and islet autoantigen (RIP-GP)-specific CD8 T cells in spleen (B) and PDLN (C). Note that virtually no autoantigen-specific CD8 T cells can be detected in uninfected mice. Further, note the profound differences between spleen and PDLN on the one hand and between total and islet-autoantigen-specific CD8 T cells.

Bender et al. – Figure 1

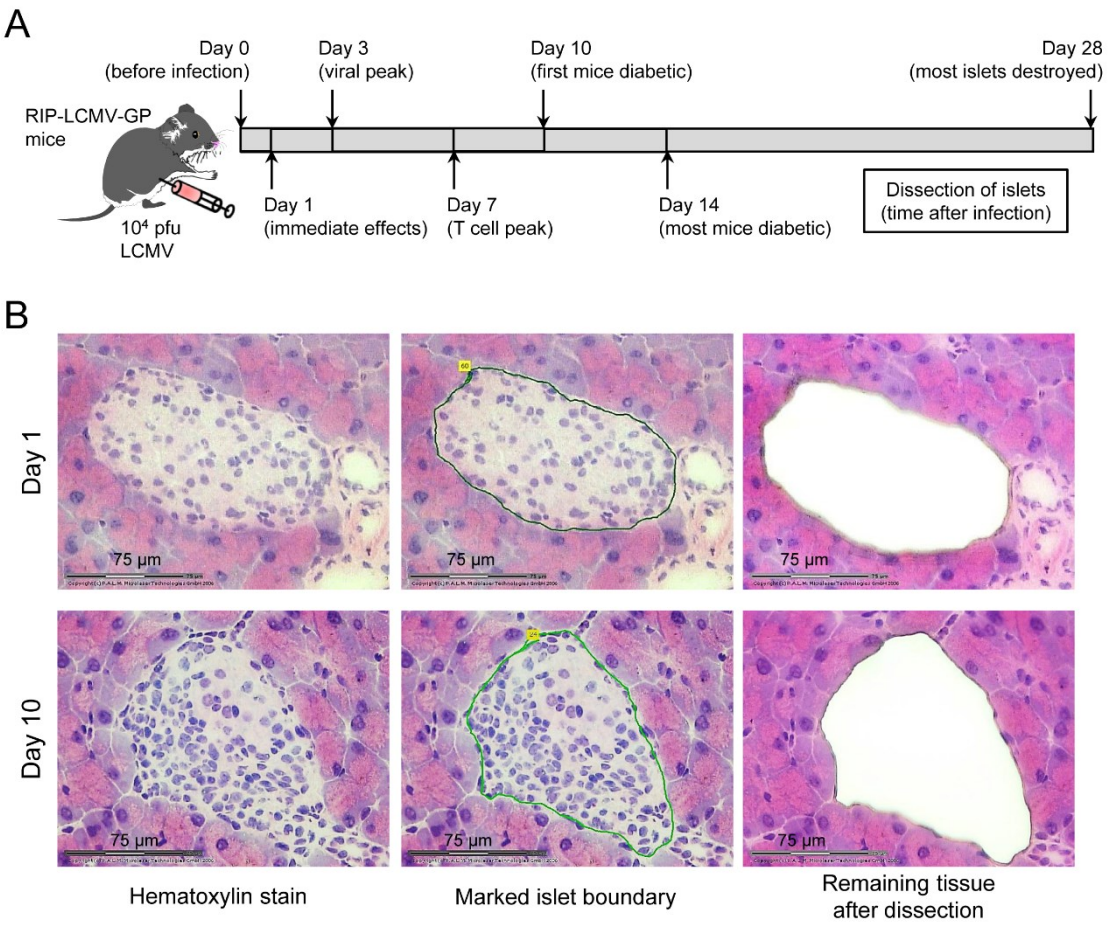

Bender et al. – Figure 2

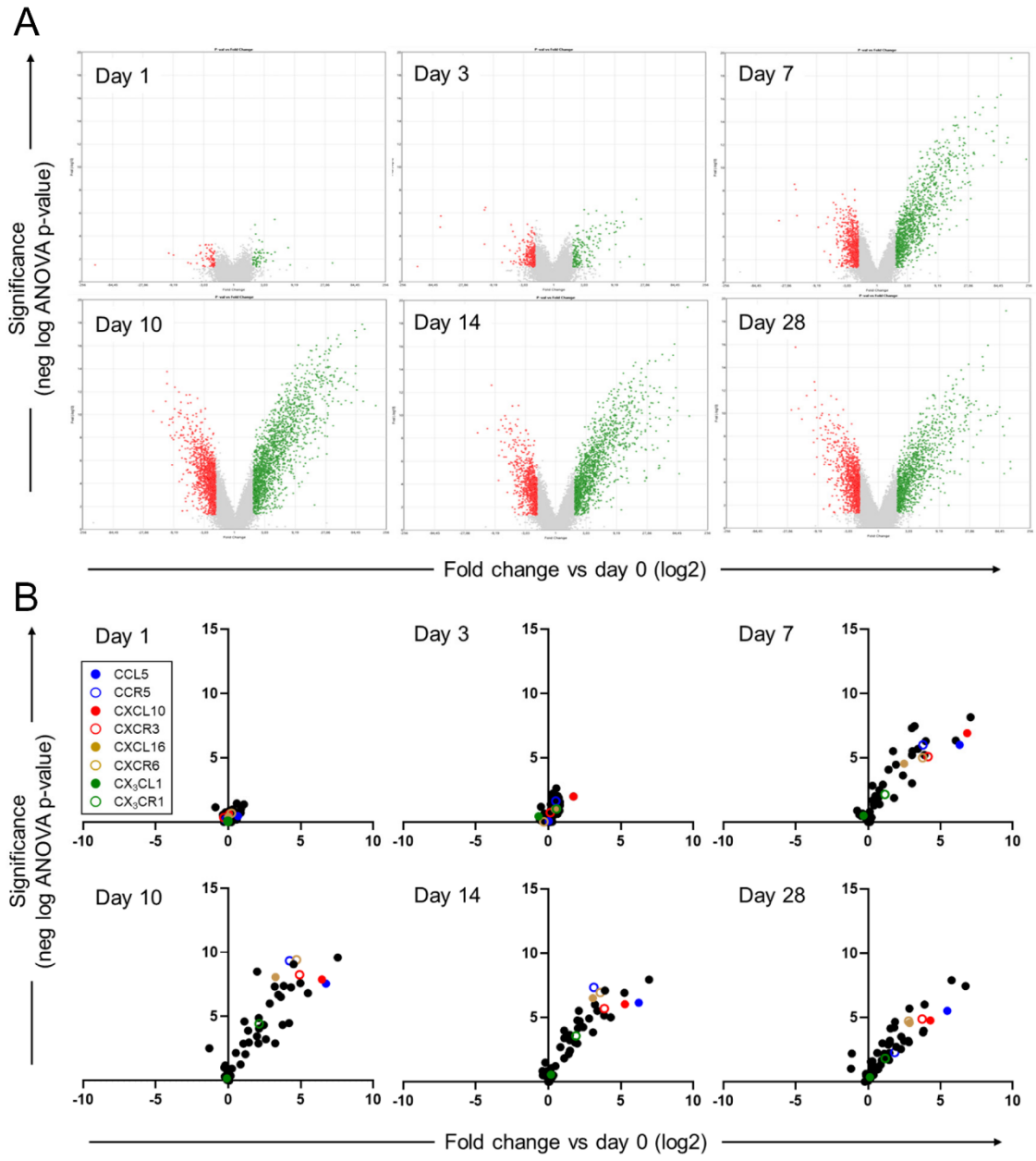

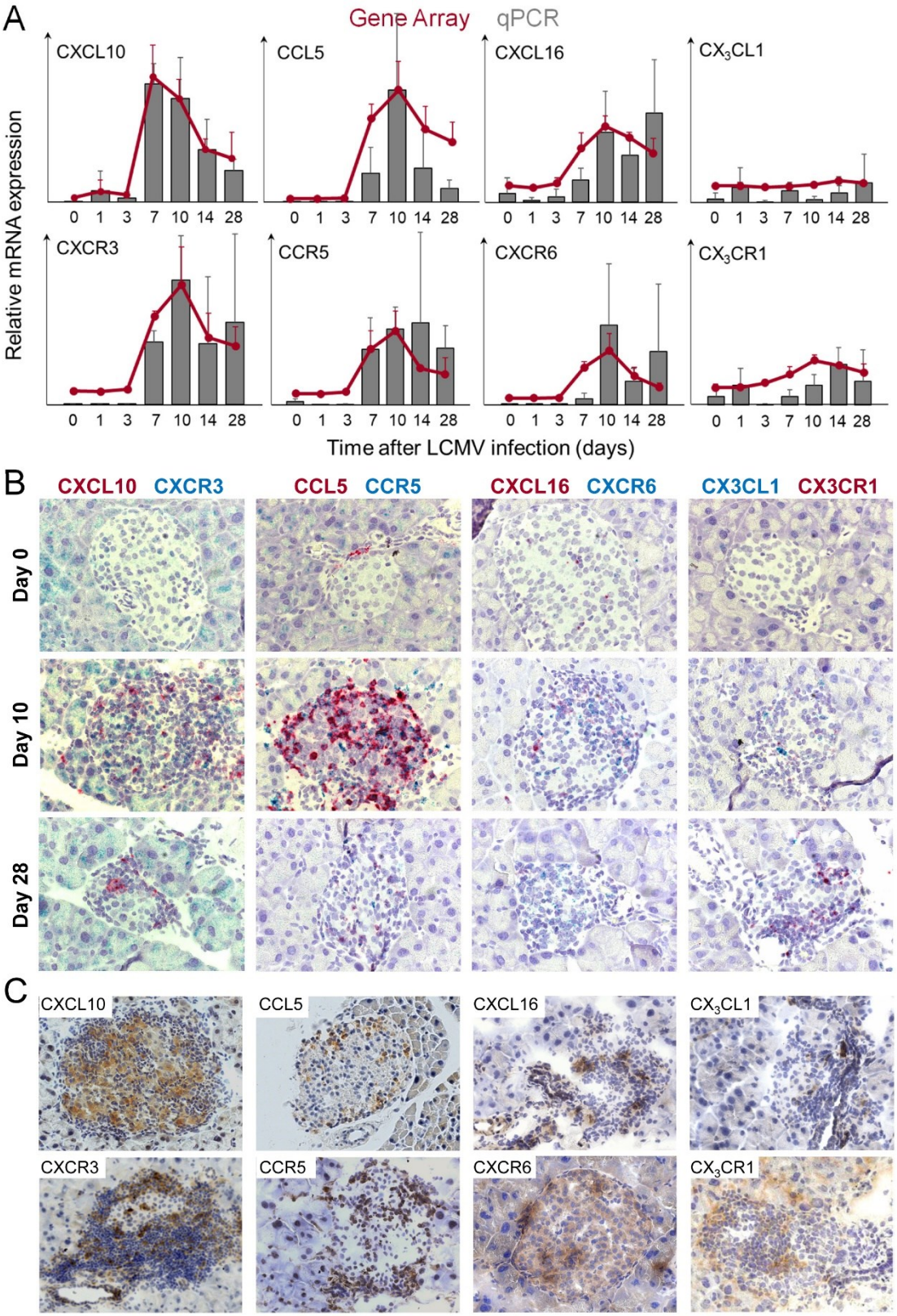
A
Gene Array
qPCR
Relative mRNA expression
CXCL10
CCL5
CXCL16
CX3CL1
CXCR3
CCR5
CXCR6
CX3CR1
0 1 3 7 10 14 28
Time after LCMV infection (days)
B
CXCL10 CXCR3
CCL5 CCR5
CXCL16 CXCR6
CX3CL1 CX3CR1
Day 0
Day 10
Day 28
C
CXCL10
CCL5
CXCL16
CX3CL1
CXCR3
CCR5
CXCR6
CX3CR1

Bender et al. – Figure 4

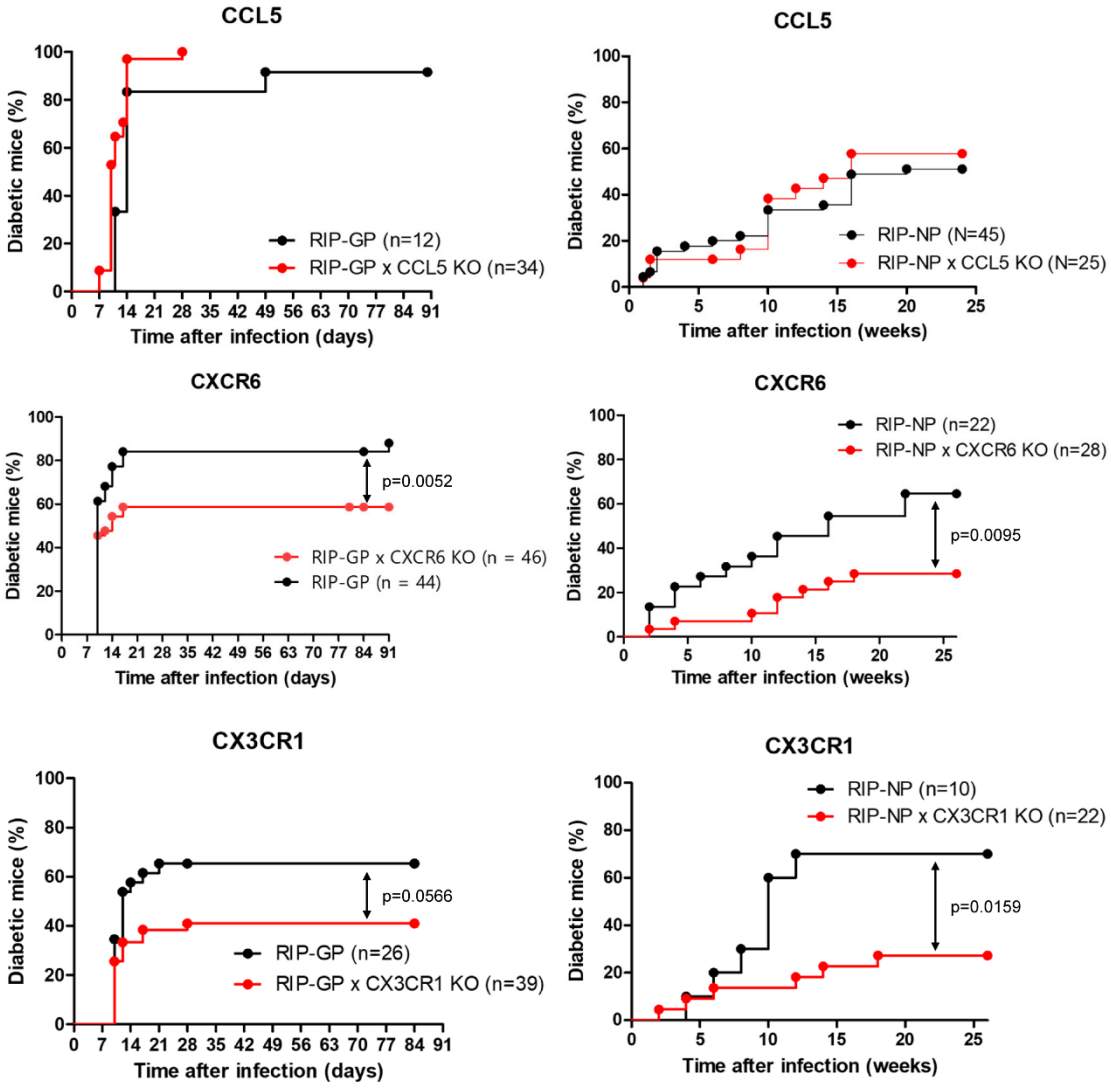

Bender et al. – Figure 5

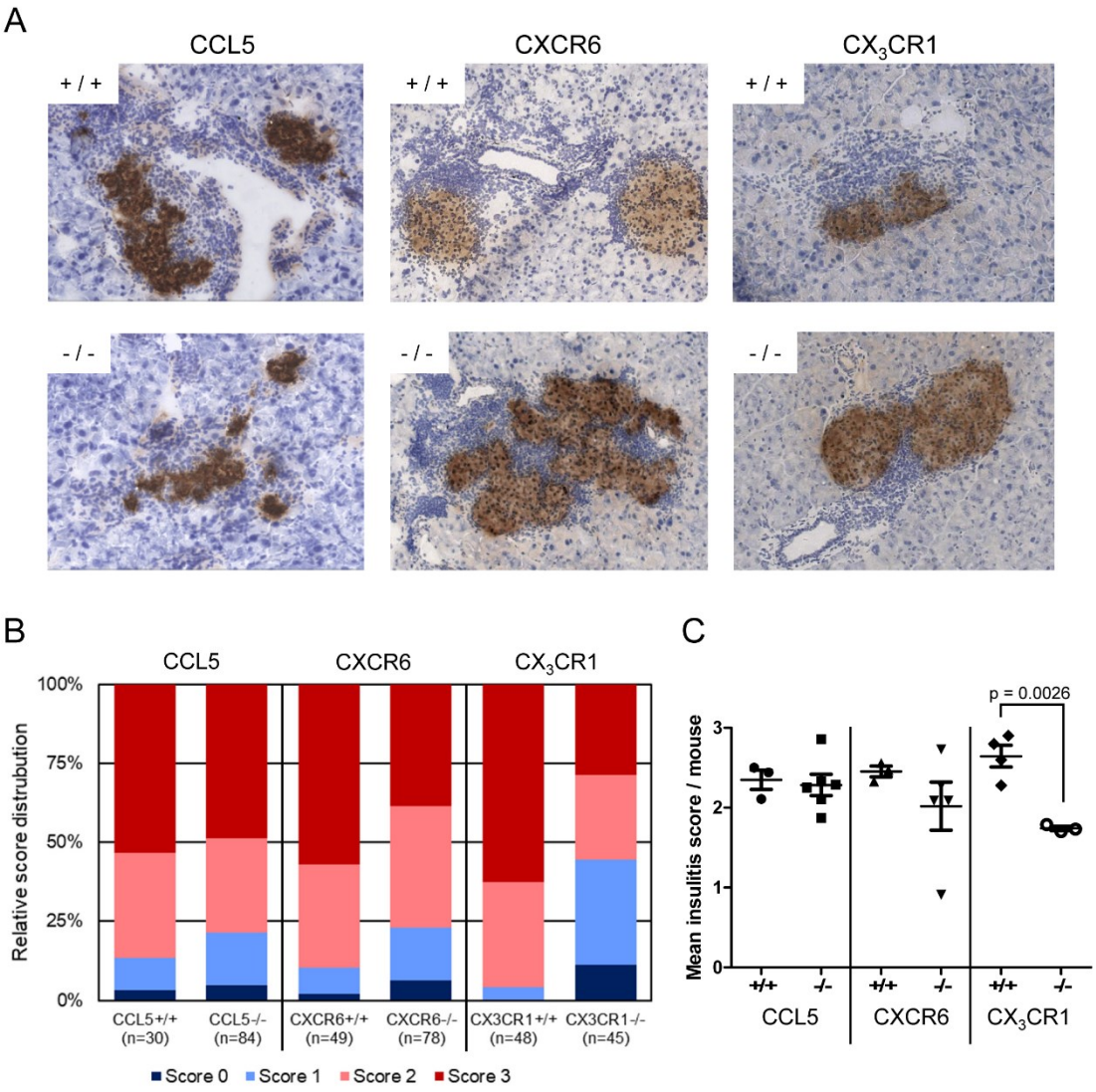

Bender et al. – Figure 6

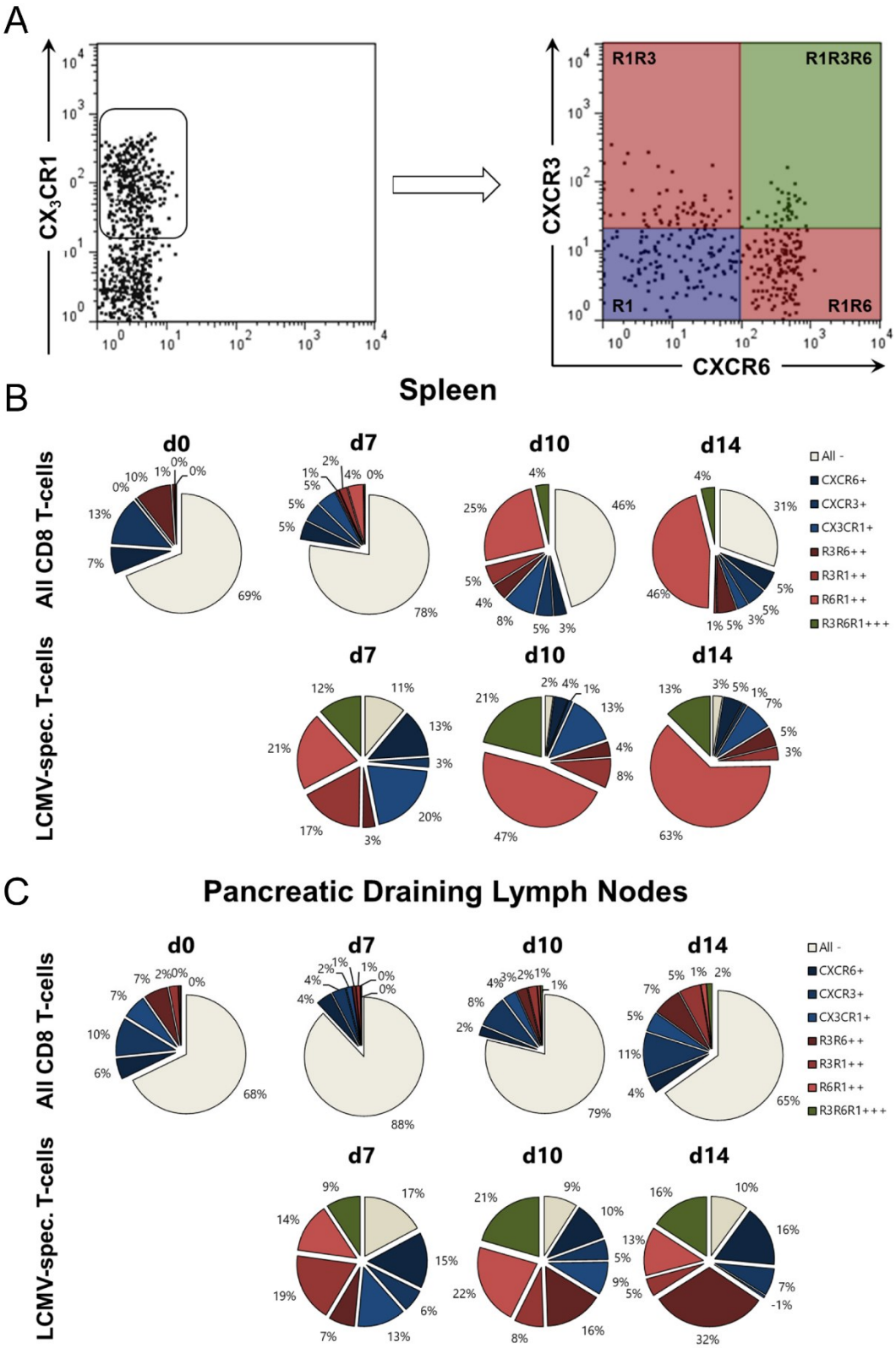

Table 1: Fold change in gene expression levels of chemokine ligands and receptors vs. Day 0

Ligands

	Day 1	Day 3	Day 7	Day 10	Day 14	Day 28
CCL1	1,5	1,33	8,26	14,24	4,77	2,94
CCL2	1,34	1,75	15,82	12,34	7,05	5,63
CCL3	1,81	1,02	66,84	44,99	19,82	13,98
CCL4	1,03	1,46	9,28	7,22	4,46	2,61
CCL5	1,59	1,02	80,5	106,86	75,74	44,61
CCL6	-1,27	1,03	1,62	2,7	2,8	1,92
CCL7	1,12	1,33	8,22	4,38	2,14	1,55
CCL8	1,83	-1,07	10,88	31,23	37,99	54,68
CCL9	1,09	1,18	1,56	3,93	4,28	2,73
CCL11	1,06	1,07	3,81	4,29	3,97	2,77
CCL12	1,25	1,66	14,8	10,93	8,48	7,12
CCL17	1,52	1,57	1,72	9,47	3,59	2,17
CCL19	2,11	-1,23	5,35	13,4	14,41	14,3
CCL20	1,17	1,17	1,1	1,12	1,27	1,57
CCL22	-1,07	1,37	1,73	18,26	9,34	4,89
CCL24	1,13	1,14	-1,04	-1,16	-1	-1,16
CCL25	1,07	1,26	-1,09	-1,05	1,18	-1,09
CCL26	-1	1,43	1,11	-1,14	-1,03	1,2
CCL27	-1,03	-1,28	-1,53	-1,2	-1,01	1,23
CCL28	1,13	1,2	-1,69	-2,49	-1,31	-2,18
CXCL1	1,02	1,2	1,32	1,03	1,12	1,19
CXCL2	-1,06	1,12	1,25	1,19	1,12	1,02
CXCL3	-1,02	1,44	1,03	-1,05	-1,04	1,13
CXCL5	-1,03	1,07	1,04	-1,13	-1,05	1,26
CXCL9	1,47	1,56	135,15	187,24	123,76	106,68
CXCL10	1,03	3,32	115,11	87,84	38,75	19,71
CXCL11	-1,04	1,17	3,31	3,98	2,45	2,82
CXCL12	1,04	-1,15	1,57	2,17	2,78	2,84

Fold change vs. Day 0
<2
2 - 5
5 - 10
10 - 20
20 - 50
50 - 100
>100

Receptors

	Day 1	Day 3	Day 7	Day 10	Day 14	Day 28
CCR1	-1,08	1,33	1,41	1,81	1,16	1,35
CCR2	-1,3	-1,06	8,38	20,15	10,39	7,26
CCR3	-1,17	1,15	-1,1	1,01	1,04	1,02
CCR4	-1,01	1,19	1,07	1,02	1,14	1,24
CCR5	-1,12	1,44	13,83	18,77	8,83	3,58
CCR6	1,19	1,05	1,16	1,03	1,8	1,99
CCR7	1,08	1,13	1,12	6,01	4	4,81
CCR8	-1,12	-1,2	-1,08	2,26	2,64	2,18
CCR9	-1,15	1,12	1,31	4,25	2,17	1,83
CCR10	1,34	1,76	1,19	-1,18	1,21	1,3
CXCR1	-1	1,18	1,08	-1,04	-1,03	1,07
CXCR2	1,14	1,1	1,14	-1,02	1,04	1,02
CXCR3	-1,24	1,1	17,72	30,41	14,58	13,43
CXCR4	-1,13	1,71	3,46	5,48	5,27	6,86
CXCR5	-1,24	1,19	-1,01	2,07	2,81	3,51
CXCR6	1,16	-1,24	13,65	26,22	11,94	7,03

10.5 Schriftliche Erklärung

Ich erkläre ehrenwörtlich, dass ich die dem Fachbereich Medizin der Johann Wolfgang Goethe-Universität Frankfurt am Main zur Promotionsprüfung eingereichte Dissertation mit dem Titel

Elucidating the Role of the XCL1/XCR1 Chemokine Axis in Type 1 Diabetes Pathogenesis: Implications for Novel Therapeutic Interventions

Am Zentrum der Pharmakologie, im Institut für Allgemeine Pharmakologie und Toxikologie unter Betreuung und Anleitung von Prof. Dr. Urs Christen ohne sonstige Hilfe selbst durchgeführt und bei der Abfassung der Arbeit keine anderen als die in der Dissertation angeführten Hilfsmittel benutzt habe. Darüber hinaus versichere ich, nicht die Hilfe einer kommerziellen Promotionsvermittlung in Anspruch genommen zu haben.

Ich habe bisher an keiner in- oder ausländischen Universität ein Gesuch um Zulassung zur Promotion eingereicht*. Die vorliegende Arbeit wurde bisher nicht als Dissertation eingereicht.

Vorliegende Ergebnisse der Arbeit wurden (oder werden) in folgendem Publikationsorgan veröffentlicht:

Tondello C., Bender C., Puppe D., Blickberndt E. M., Golden G. J., Bayer M., Buchmann G., Pfeilschifter J. M., Bachmann M., Hintermann E., Brandes R. B., Betts M. R., Kroczek R. A., Christen U. *Submitted, 2023.* "The XCL1/XCR1 axis is activated in patients with type 1 diabetes and its disruption tips the T cell balance and ablates β-cell damage in a mouse model"

Bender C., Müller P., **Tondello C.**, Horn J., Holdener M., Lasch S., Bayer M., Pfeilschifter J. M., Tacke F., Ludwig A., Hansmann M. L., Döring C., Hintermann E., Christen U. *Submitted, 2023.* "Gene-expression profiling of laser-dissected islets and studies in deficient mice reveal chemokines as differential driving force of type 1 diabetes"

_____ _____

(Ort, Datum) (Unterschrift)

*) im Falle des Nichtzutreffens entfernen